GEAR ERROR INDUCED IMPACT IN A MULTIPLE TAKE-OFF TEXTILE DRIVE SYSTEM OPERATING UNDER LIGHT LOADING

by

DAVID TRUEMAN, B.Tech. (Loughborough)

A Doctoral Thesis

Submitted in partial fulfilment of the requirements

for the award of

Doctor of Philosophy of the Loughborough University of Technology

June, 1974.

Joint Supervisors: PROFESSOR B. DOWNS, M.Eng.(Liverpool), C.Eng., M.I.Mech.E.
Department of Mechanical Engineering.

DR. W. BERGWERK, B.Sc., D.I.C., Ph.D.(London), C.Eng., M.I.Mech.E., F.T.I.
Platt International Limited.

ACKNOWLEDGEMENTS

The author wishes to thank Professor B. Downs for his valued guidance and for his constructive criticisms and suggestions offered throughout the research.

He is indebted to Platt International Ltd. for providing equipment for the experimental work and technical information relating to their commercial products; he thanks in particular Dr. W. Bergwerk; he also thanks Mr. F. Greenwood and Mr. H. Scowcroft for their cooperation throughout the work.

It gives him pleasure to acknowledge the practical assistance provided by Mr. P. Norton, Mr. J. Burton, Mr. K. Topley and others of the departmental technical staff at Loughborough; his thanks are also due to Mr. R. Vitols for many helpful discussions and to Mrs. M. Pugsley for typing the thesis.

Finally, the author gratefully acknowledges the financial assistance provided by Platt International Ltd. in support of this research.

STATEMENT OF RESPONSIBILITY FOR THE WORK SUBMITTED

The author carried out the research on which this thesis is based between September, 1970, and December, 1973. The work represents original contributions with the following exceptions.

The theory set out in Section 5.2 is reproduced with a minor correction from reference R25. The modelling set out in Sections 5.3.1 and 5.3.2 is based on original work of Professor Downs including a preliminary computer program which formed the basis for the extensive development by the author outlined in Section 5.4.

The technique described in Section 8.3.1 embodying automatic gear error compensation was first suggested by Professor B. Downs who also suggested and supervised the undergraduate project of R. W. Grundy which forms the basis for Section 8.4.

ABSTRACT

A combined theoretical and experimental investigation is made into the causes of premature gear failures which had occurred in the complex and lighly loaded gear trains of an industrial textile machine. A comprehensive review of previous relevant work identifies the problem as one of torsional vibratory impact excited by gear transmission errors.

An extension of the dynamic stiffness method is developed for the analysis of forced vibration response due to relative displacement, harmonic excitation imparted by transmission error components. The technique is then applied to a generalised mathematical model of the complete machine in which typical production distributions of gear error magnitude and relative phasing are inserted. Gear tooth dynamic loads are computed at every mesh for a number of different machine configurations over the operating speed range. The influence of selected inertia, flexibility and damping elements is demonstrated.

A novel technique employing magnetic drums is devised and evaluated for the direct measurement of relative motions in a meshed pair of oscillating gears. Automatic compensation is provided for transmission error and mounting eccentricity. A further direct technique is reported for the detection of tooth impacts and is based on the change in electrical resistance between meshing teeth as the contact pressure varies.

Measurements in a multi-gearbox experimental rig demonstrated that the gears described non-linear motions, involving excursions through the backlash and heavy impacts on both drive and reverse faces.

Theoretical predictions of dynamic loading distribution within machines show reasonable compatibility with patterns of gear failure recorded in service, even though the analysis does not allow for system non-linearities.

Machine design considerations are examined in retrospect from a dynamics standpoint. Past and present designs are appraised and possible alternatives to these are briefly discussed.

Finally, the salient factors identified in the investigation are summarised and recommendations made for future work.

CONTENTS

Page No.

Page No.

LIST OF SYMBOLS

A	random number between 0.0 and 1.0
B	random number between 0.0 and 1.0
D	damping coefficient; diameter
DA, DB, DC	subsystem critical damping coefficients, defined in Table 5.1.
D_1 - D_{11}	damping coefficients defined in Figure 5.4.
E	Young's Modulus
e	base of natural logarithm
F	flexibility
$\bar{F}$	dynamic flexibility
F_1 - F_{12}	flexibilities defined in Figure 5.4.
FD_1, FD_{10}, FD_{11}	damping coefficients defined in Figure 5.4.
G	modulus of rigidity
g	acceleration due to gravity
i	integer
J	polar moment of inertia
J_1 - J_{11}	polar moments of inertia defined in Figure 5.4.

j	complex operator = $\sqrt{-1}$; integer
K	stiffness
$\bar{K}$	dynamic stiffness
L	length
M	mass
n	integer
P	force
T	torque
T_D	dynamic torque
t	time
x	displacement
⊕	angular displacement amplitude
θ	angular displacement
ρ	material density
ø	phase angle
ω	angular frequency
ω_n	natural (angular) frequency

Computer program input variables are defined in Appendix B.

LIST OF ILLUSTRATIONS

Fig. 6.11 Effect of drawroll damping on dynamic loading levels at 2355 r.p.m; drawroll damping coefficient = 2.90 lbf.in.sec/rad.

Fig. 6.12 Effect of drawroll damping on dynamic loading levels at 2355 r.p.m; drawroll damping coefficient = 14.5 lbf.in.sec/rad.

Fig. 6.13 10 box Type A/Type C machine

Fig. 6.14 10 box Type A/Type C system

Fig. 6.15 10 box Type A/Type C system

Fig. 6.16 10 box Type A/Type C system

Fig. 6.17 10 Box Type B/Type E machine

Fig. 6.18 10 box Type B/Type E machine

Fig. 6.19 10 Box Type A/Type C system

Fig. 6.20 10 Box Type A/Type C system

Fig. 6.21 Average distribution of dynamic loading in 4 box system at 1500 r.p.m.

Fig. 6.22 Average distribution of dynamic loading in 4 box system at 1800 r.p.m.

Fig. 6.23 Average distribution of dynamic loading in 4 box system at 1900 r.p.m.

Fig. 6.24 Average distribution of dynamic loading in 4 box system at 2000 r.p.m.

Fig. 6.25 Average distribution of dynamic loading in 4 box system at 2100 r.p.m.

Fig. 6.26 Average distribution of dynamic loading in 4 box system at 2200 r.p.m.

1. INTRODUCTION

Gear tooth loading is an important design parameter since its knowledge enables the designer to assess the reliability, in terms of wear performance, of a proposed gearing configuration.

It is generally well known that, in practice, manufacturing imperfections and tooth flexibility produce dynamic loads which are greater than the mean transmitted loads. Despite a considerable amount of research over the last 25 years, it remains difficult to estimate, with accuracy, the actual loads occurring in complex gearing systems.

The semi-empirical methods of Buckingham (1)* and Tuplin (2) were introduced around 1950 and although neither has been conclusively validated by experimental measurements, they still enjoy a wide acceptance by designers. The main reason for this is that more recent analyses, although technically superior, are of such complexity that they do not easily lend themselves to design calculations.

In recent years, the availability of electronic instrumentation has stimulated experimental studies of gearing behaviour and these have, in general, provided more useful information. There is remarkable agreement between independent researchers that maximum dynamic loads do not exceed three times the applied load. This suggests that a safety factor of 3 or above would provide adequate protection in respect of dynamic behaviour.

On this basis, the gearing in textile drawtwister machines is considerably over-designed since gears of approximately 1 in. face width are employed to transmit torques of the order of 5 lbf.in.

* A more detailed review of the literature is given in Section 4.

In practice, however, premature gear failures have occurred in such machines on a scale sufficient to warrant further research.

The work described in this thesis aims at providing an understanding of the behaviour of certain gear trains in this particular machine. It is hoped that the investigation will serve as a case study thus enabling designers to adopt a similar approach to other dynamics problems within the same class of machinery. The work differs from virtually all other research work on gearing in that the whole of a gear drive system involving very many gear meshes is examined as a total entity.

2. DRAWTWISTER FUNCTION AND DESIGN

2.1 The Manufacture of Continuous Synthetic Yarns

Continuous filament yarns such as nylon and 'terylene' are produced from solid polymer by hot extrusion through a plate containing fine orifices, known as a spinneret. Several filaments are then combined together into a single thread. In this form the yarn has very little resistance to extension owing to the random orientation of its molecular chains.

In order to develop satisfactory load/extension properties, it is necessary to stretch, or draw, the yarn plastically to about 3 to 5 times its original length thereby preferentially orientating the molecular structure. It is also necessary to insert a degree of twist so that the constituent filaments become satisfactorily united as a single thread. These two operations are performed by the appropriately named drawtwister machine after which the yarn is ready for finishing processes.

Further details on the manufacture of man-made fibres may be obtained from the literature (3).

2.2 Drawing and Twisting Processes

Drawing is the more important of the two processes and the requirements for drawing, imposed by the properties of the various types of polymer fibre, largely determine the basic design of the drawtwister. Two of the commonest groups of fibres are polyamides, such as nylon, and polyesters, for example, 'terylene' and 'dacron'.

2. DRAWTWISTER FUNCTION AND DESIGN

2.1 The Manufacture of Continuous Synthetic Yarns

Continuous filament yarns such as nylon and 'terylene' are produced from solid polymer by hot extrusion through a plate containing fine orifices, known as a spinneret. Several filaments are then combined together into a single thread. In this form the yarn has very little resistance to extension owing to the random orientation of its molecular chains.

In order to develop satisfactory load/extension properties, it is necessary to stretch, or draw, the yarn plastically to about 3 to 5 times its original length thereby preferentially orientating the molecular structure. It is also necessary to insert a degree of twist so that the constituent filaments become satisfactorily united as a single thread. These two operations are performed by the appropriately named drawtwister machine after which the yarn is ready for finishing processes.

Further details on the manufacture of man-made fibres may be obtained from the literature (3).

2.2 Drawing and Twisting Processes

Drawing is the more important of the two processes and the requirements for drawing, imposed by the properties of the various types of polymer fibre, largely determine the basic design of the drawtwister. Two of the commonest groups of fibres are polyamides, such as nylon, and polyesters, for example, 'terylene' and 'dacron'.

Figure 2.1 shows a typical thread path arrangement employed for drawtwisting polyamide yarns. Drawing takes place between the drawroll and feedroll according to the relative surface speeds of these elements; the surface speed ratio of the former to the latter being defined as the draw ratio. Twisting occurs because the yarn is collected on the spindle package by winding it around its own axis of approach and hence the amount of twist is determined by the spindle speed and the take up speed (or 'drawspeed').

The physical properties of polyester yarns are such that a more elaborate arrangement, shown in Figure 2.2, is required for drawing. In particular, it is necessary to provide yarn heating in order to achieve a stable draw point*. This is accomplished by means of a hot plate and a heated upper drawroll. A degree of 'cold' drawing may be arranged to take place between the feedroll and upper drawroll but this is normally a small contribution to the overall draw ratio.

Commercial drawtwisters are essentially machines which operate simultaneously on a large number of threadlines in the same manner as described above. A typical design would incorporate 120 yarn positions in a double sided configuration, that is, 60 on each side of the machine. It will be seen later, however, that a modular construction allows for considerable flexibility in respect of size. Figures 2.3 and 2.4 show polyamide and polyester drawtwisters, respectively, in normal production service. Further details on commercial drawtwister designs may be obtained from a review article by Hoineman (4).

* The draw point is the physical location where the fibre diameter is suddenly reduced by plastic flow.

2.3 Platt Light to Medium Drawtwisters (MDT. Range)

The Platt MDT. range of drawtwisters process yarns in the range 15 - 300 denier*. Drawing torques, which are of considerable interest in this research, are low throughout the range being only about 5 lbf.in. for the heavier yarns.

2.3.1 General Layout

The general layout of all MDT. models is as shown in Figures 2.5 and 2.6 except that the polyester type also incorporates an upper set of drawboxes. In essence, each machine has a gearing headstock with main output shafts driving feedroll, drawbox and spindle systems. One version of the headstock drive arrangement is shown in Figure 2.7. A hydraulic and electrical systems cabinet was provided at the "tail" end of earlier machines (as illustrated in Figure 2.5) but more recent practice has incorporated these systems in an enlarged headstock cabinet.

Spindles are driven in banks of four by continuous flat tapes and individual, foot operated, spindle brakes are provided. Of particular importance in this research is the drawroll drive system which comprises a number of drawboxes coupled 'end-on-end' down the length of the machine.

2.3.2 Drawbox Assembly

Each drawbox houses 12 drawroll cartridges and the drawrolls are driven in pairs, from a central layshaft, by the helical gearing arrangement shown in Figure 2.8 which utilises four left hand and two right hand layshaft gears. The construction of a drawbox is shown in Figure 2.9 and a view of the complete assembly is given in Figure 2.10.

* the denier value is defined as the mass in grammes of a 9000 yard length of yarn.

Motion is transferred from the main shaft to one drawshaft through a crossed helical gear mesh and then to a second drawshaft through a 1 : 1 parallel helical mesh. A phosphor bronze intermediate gear meshed with two steel gears provides a satisfactory bearing combination for the high sliding characteristics of the crossed axis mesh. The "two-over-one" configuration also ensures that drawrolls on both sides of the machine rotate in the same sense when viewed by an operative.

Lubrication is by means of natural circulation and oil guides are arranged to direct a continuous flow into the mesh.

2.3.3 Drawroll Cartridge

The drawroll cartridge, or pod, illustrated in Figures 2.11 and 2.12 is designed as an interchangeable unit and is readily replaceable in the drawboxes. Two ball bearings support the drawshaft and the 5.0 in. diameter drawroll is of case hardened steel with hard chrome plate surface.

2.3.4 Polyamide Machines in the MDT. Range

2.3.4.1 Type A

This was the first of the MDT. range to enter production service, being first installed early in 1962. It had a single 40 H.P., 1450 r.p.m., A.C. motor for the standard 120 spindle version giving a maximum rated drawspeed of 4000 ft/min, corresponding to 3050 r.p.m. of the 5 inch diameter drawrolls. A 144 position machine was optional. The drawbox drive employed 29 tooth layshaft gears and 20 tooth pod gears, all being rigidly mounted on their shafts. Current practice is to use rubber bushes in the gear drawshaft connection to provide torsional flexibility*; details of these are

* Unless specifically stated to the contrary, all reference to drawshaft gears assumes that these are of the solid (i.e. keyed) variety.

given later (Section 3.3.9).

It was proposed to introduce a polyamide machine, with better performance than Type A, to be known as Type E. This model was never manufactured on a commercial scale and, after further design and development, it became Type B.

2.3.4.2 Type B

The Type B machine is generally similar to the Type A but employs a 60 H.P., 1450 r.p.m. main motor to provide improved performance and yarn handling capability. For example: it is available in sizes up to 156 spindles; it can produce much heavier yarn packages; it has a higher maximum spindle speed and has a greater range of drawratios although its maximum drawspeed is the same as that of Type A. By means of an improved headstock arrangement, employing two 30 H.P. D.C. motors with servo control, it is also available in a version with programmable spindle speeds. Rubber bushed drawshaft gears were fitted as standard at the outset and the layshaft gear size reduced to 25 teeth.

2.3.5 Polyester Machines in the MDT. Range

2.3.5.1 Type C

The Type C machine was the first polyester model of the range. Apart from the upper drawbox system and yarn heating apparatus, the machine has similar design features to the Type A and, indeed, many components are interchangeable between the two. Operating speeds and yarn handling capabilities are also similar.

2.3.5.2 Type D

Type D was designed along the lines of Type C but with a capability for producing much larger yarn packages and, in general, a greater flexibility of operation. It was the first MDT drawtwister featuring a single cabinet for headstock gearing, hydraulics and electrical systems.

2.3.5.3 Type E

The Type D machine was not manufactured on as large a scale as the Type C before it was further improved to become Type E , the polyester counterpart of the Type B.

2.3.6 Drawbox Gearing Data

Drawbox gear data for the various MDT drawtwisters may be obtained from Table 2.1.

TABLE 2.1 DRAWBOX GEAR DATA

	TYPES A, C and D		TYPES B AND E	
	LAYSHAFT GEARS	DRAWSHAFT GEARS	LAYSHAFT GEARS	DRAWSHAFT GEARS
Pitch circle diameter, (in)	3.4177	2.3570	2.9463	2.3570
Number of teeth	29	20	25	20
Normal diametral pitch	12	12	12	12
Normal pressure angle (degrees)	20	20	20	20
Helix angle (degrees)	45	45	45	45
Axial face width	1.0625	.8125 or 1.000	1.0625	.8125
Material	EN.24	Phosphor Bronze / EN.24	EN.24	Phosphor Bronze / EN.24
Drawshaft gear mounting	-	Keyed (some bushed* 1969 onwards)	-	Flexible Rubber Bushes

* Details of the rubber bushed gear drive are given in Section 3.3.9.

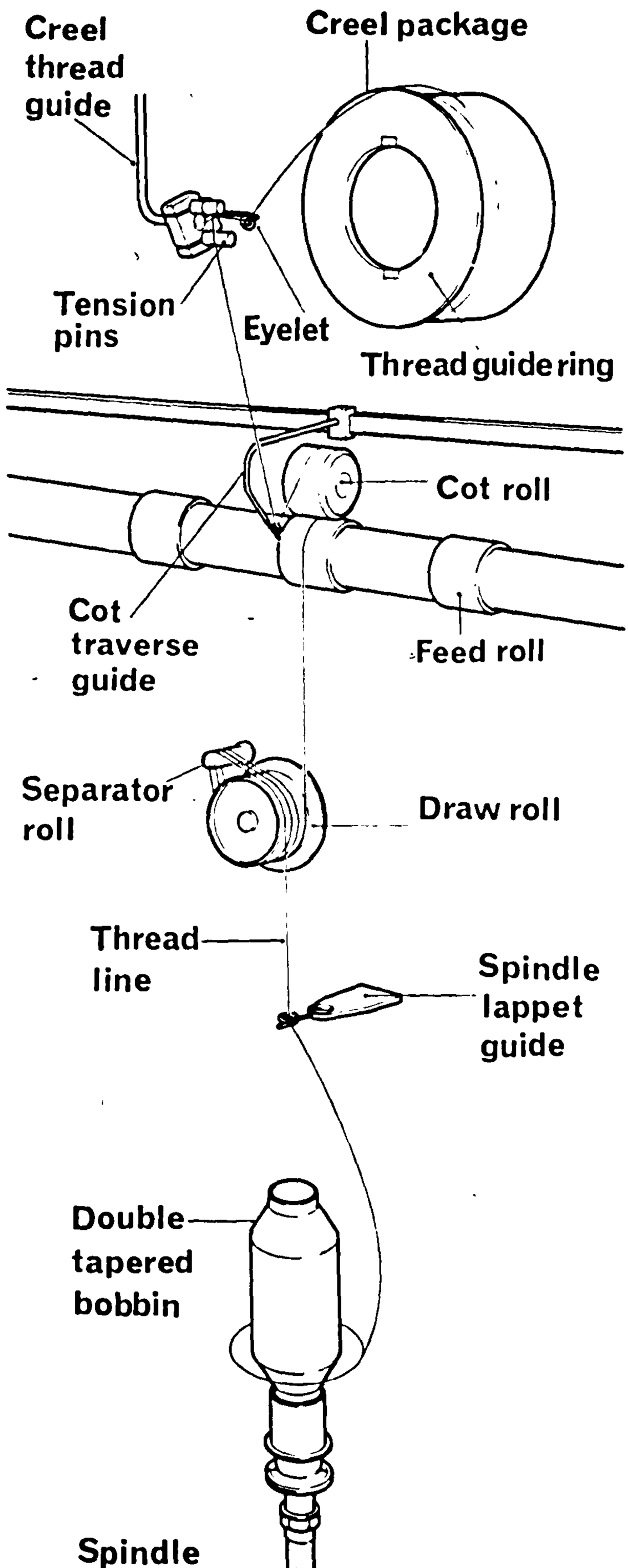

FIG. 2.1 Thread Path Arrangement for the Drawtwisting of Polyamide Yarns

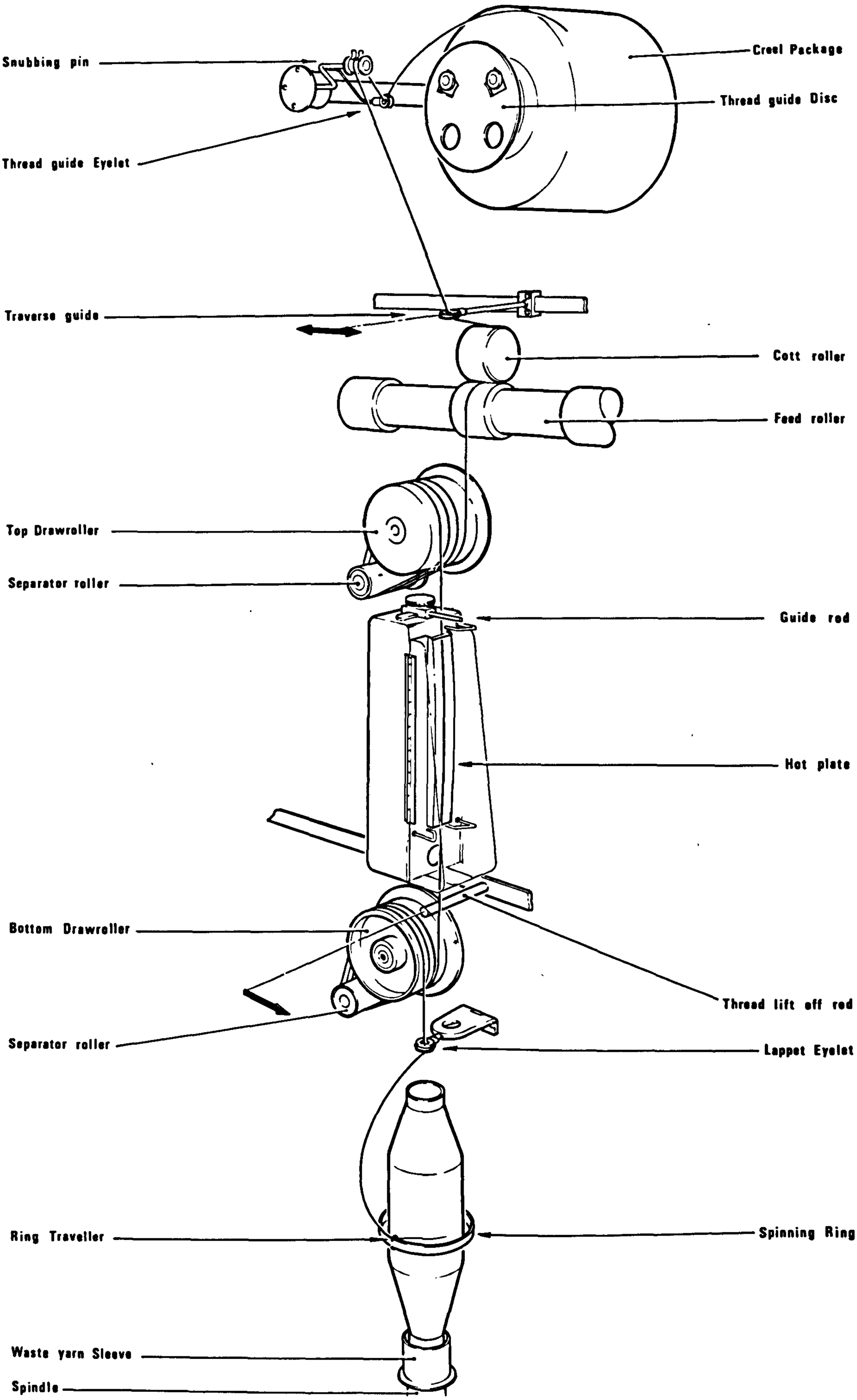

FIG. 2.2 Thread Path Arrangement for the Drawtwisting of Polyester Yarns

Figure 2.3 Polyamide Drawtwister

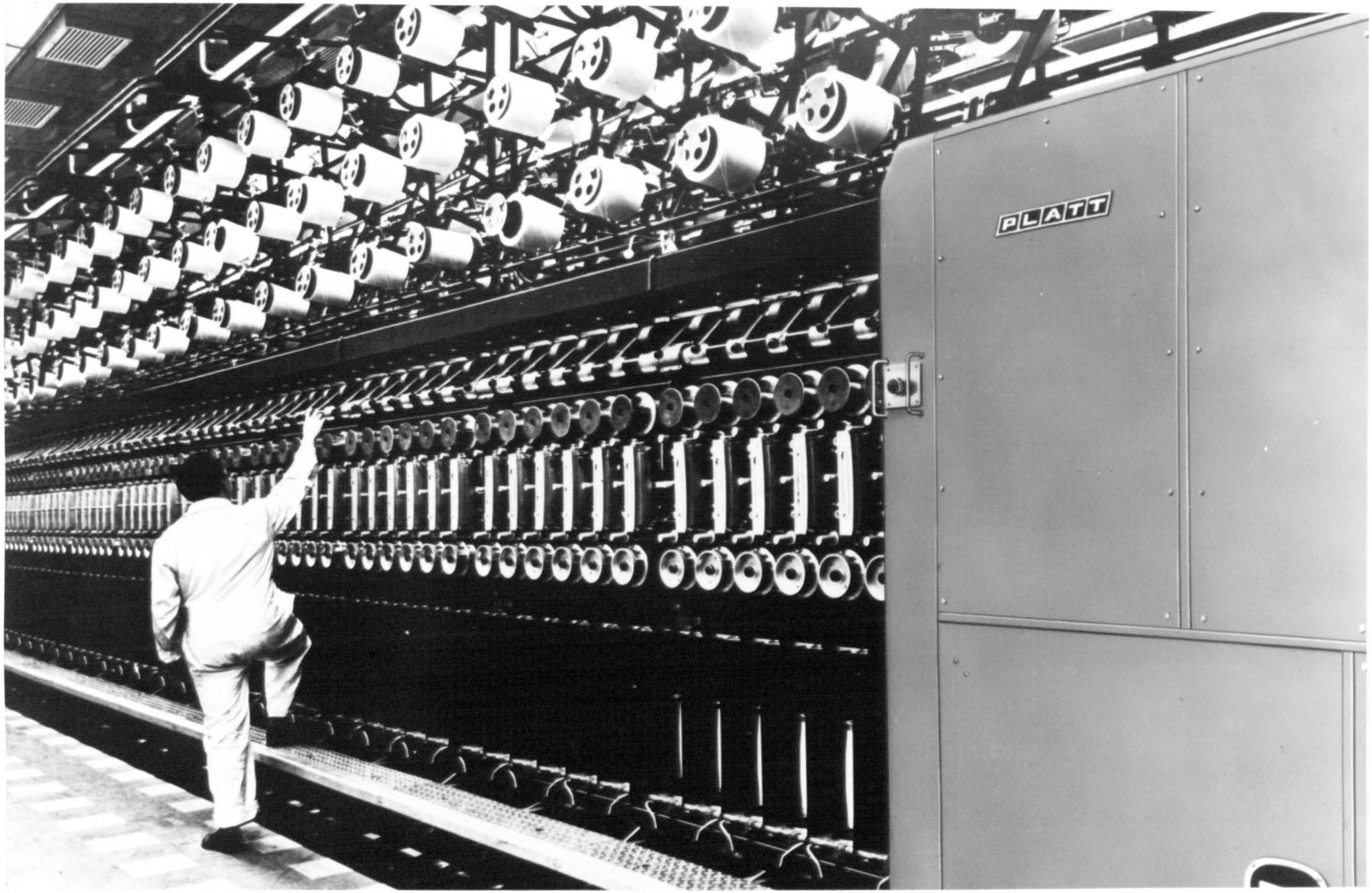

Figure 2.4 Polyester Drawtwister

① Headstock assembly
② Gearing cabinet
③ Feedrolls (on each side of m/c)
④ Creel packages
⑤ Main drive motor
⑥ Drawbox and drawrolls
⑦ Flexible coupling
⑧ Spindle package (drawn yarn)
⑨ Tape shaft (spindle drive)
⑩ Support frame
⑪ Hydraulic & electrical systems

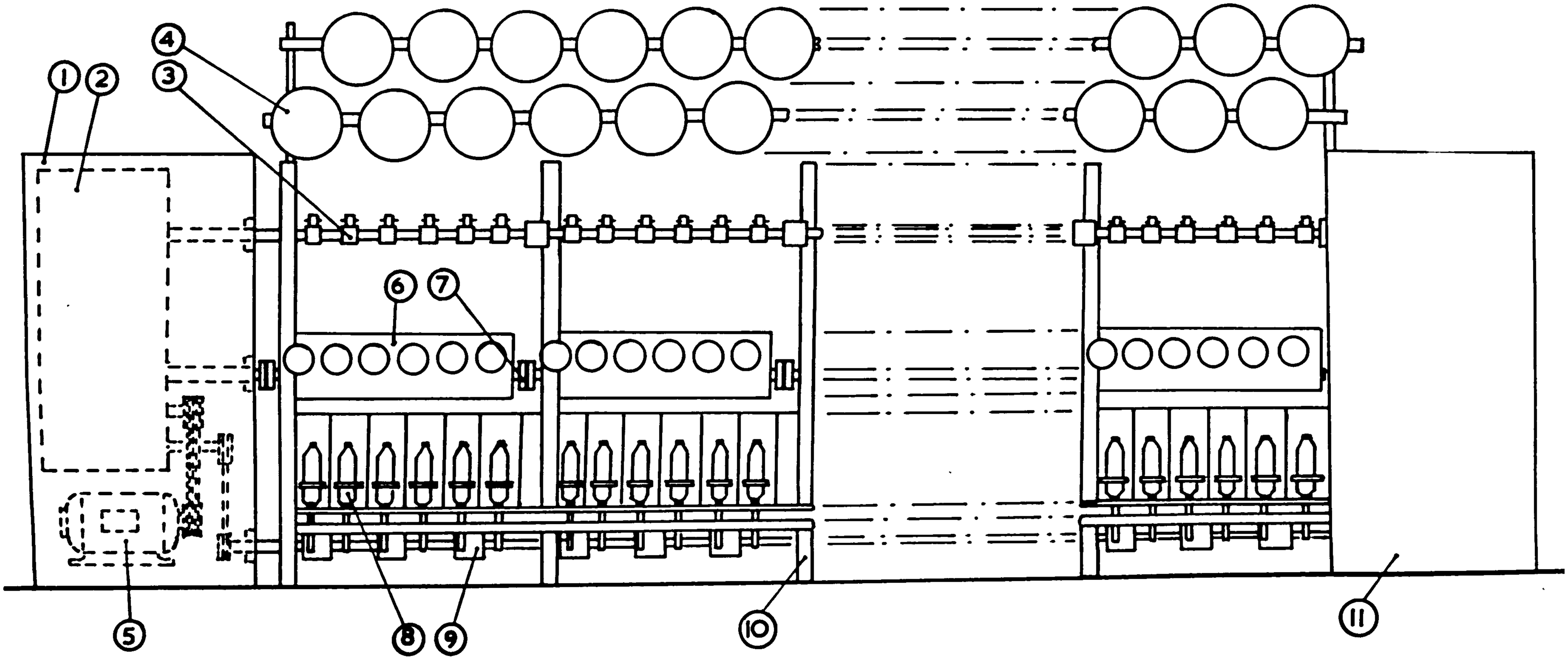

FIGURE 2.5 SCHEMATIC FRONT ELEVATION OF A POLYAMIDE DRAWTWISTER

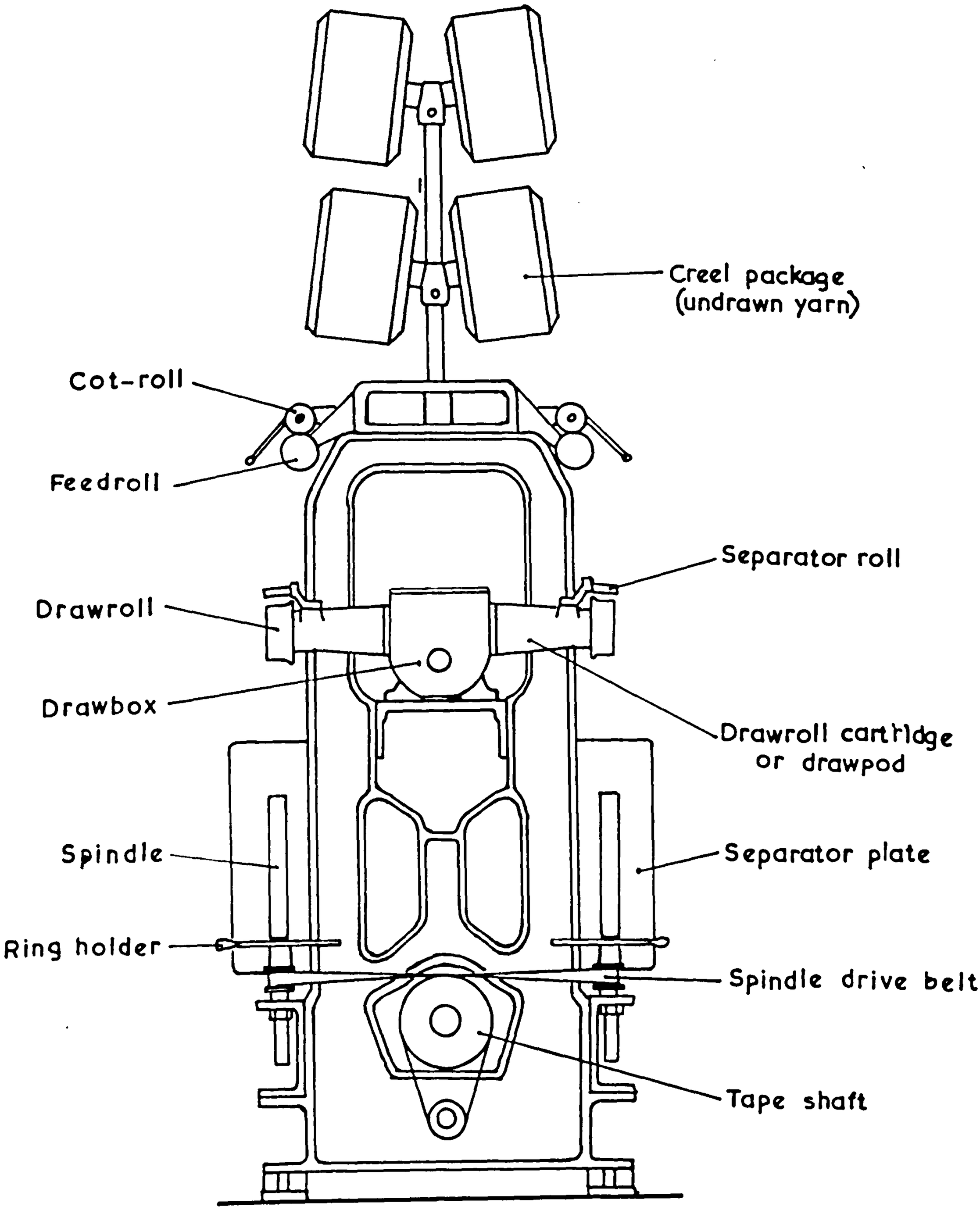

FIGURE 2.6. SCHEMATIC END ELEVATION OF A POLYAMIDE DRAWTWISTER

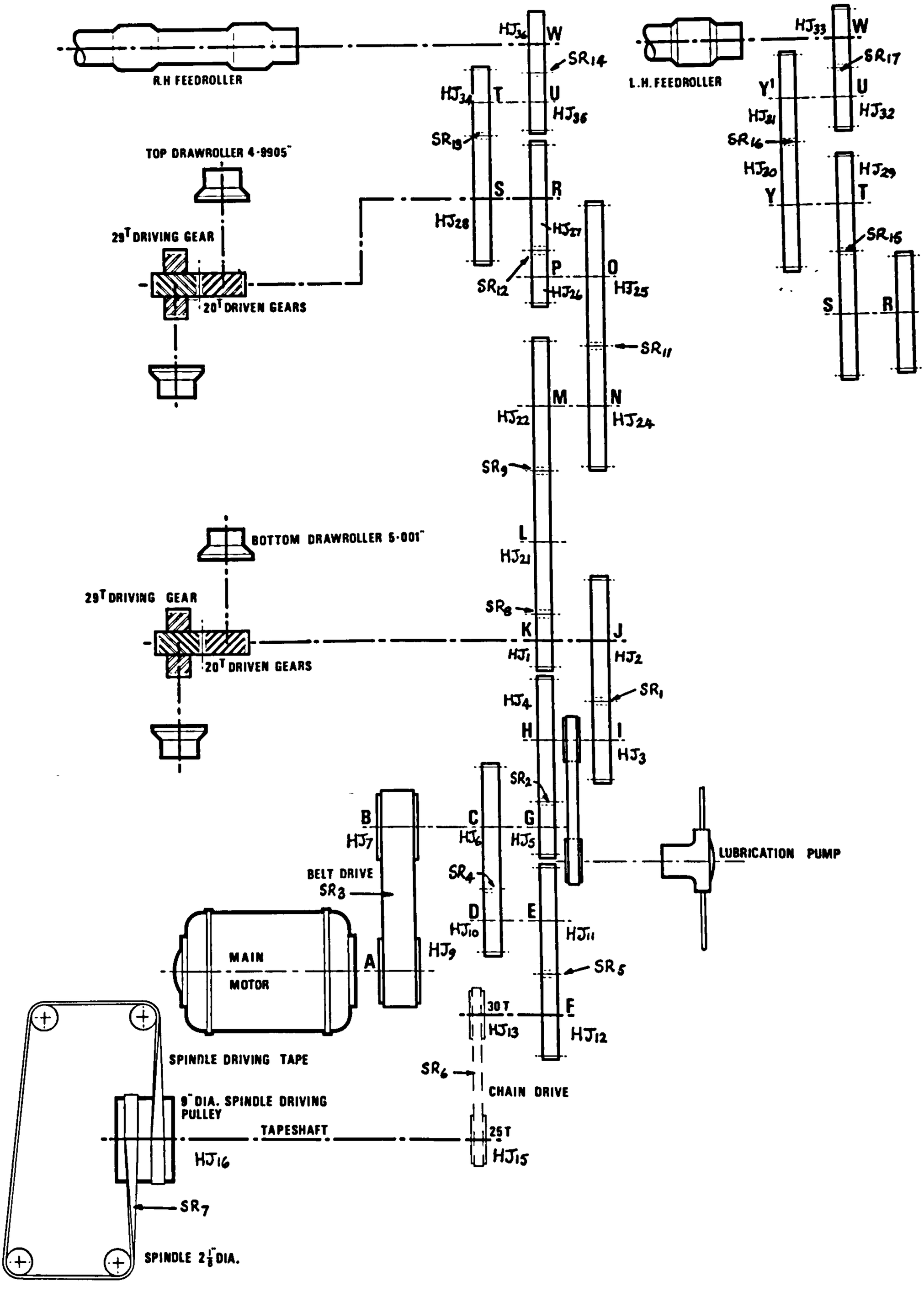

FIG. 2.7 Type C Headstock Gearing Arrangement

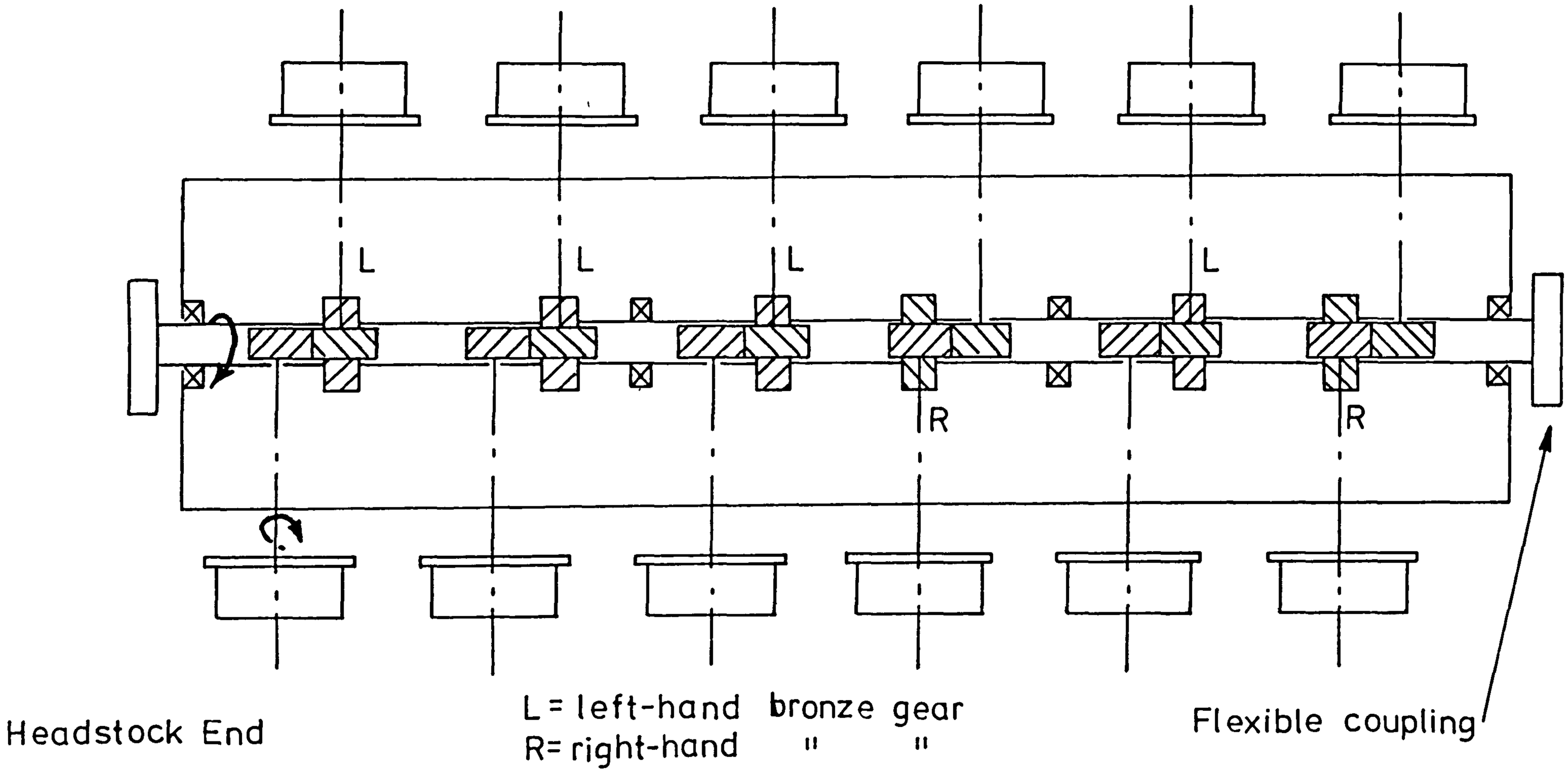

FIG. 2.8 Schematic Layout of Drawbox Gearing

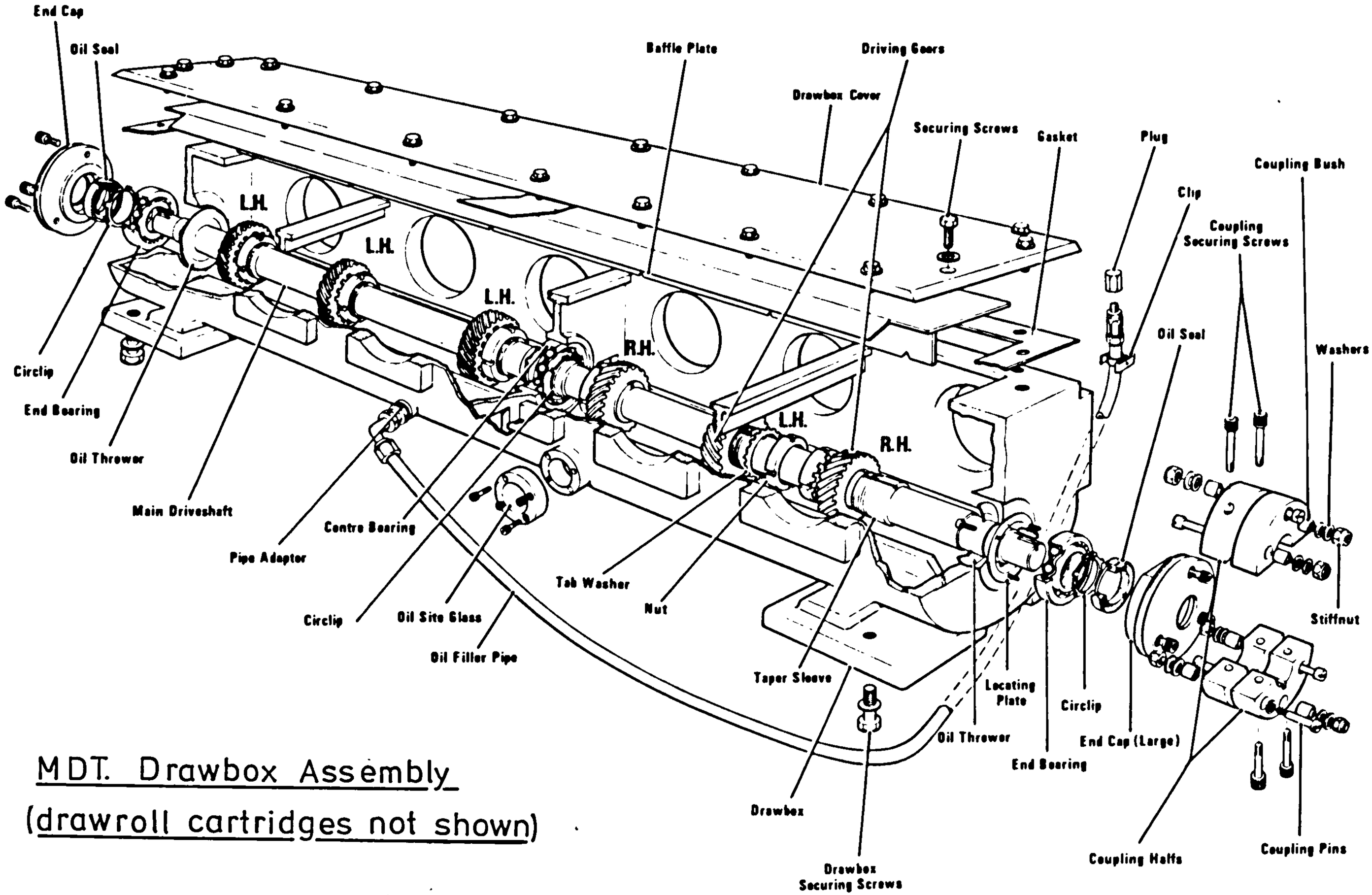

FIG. 2.9 MDT. Drawbox Assembly
(drawroll cartridges not shown)

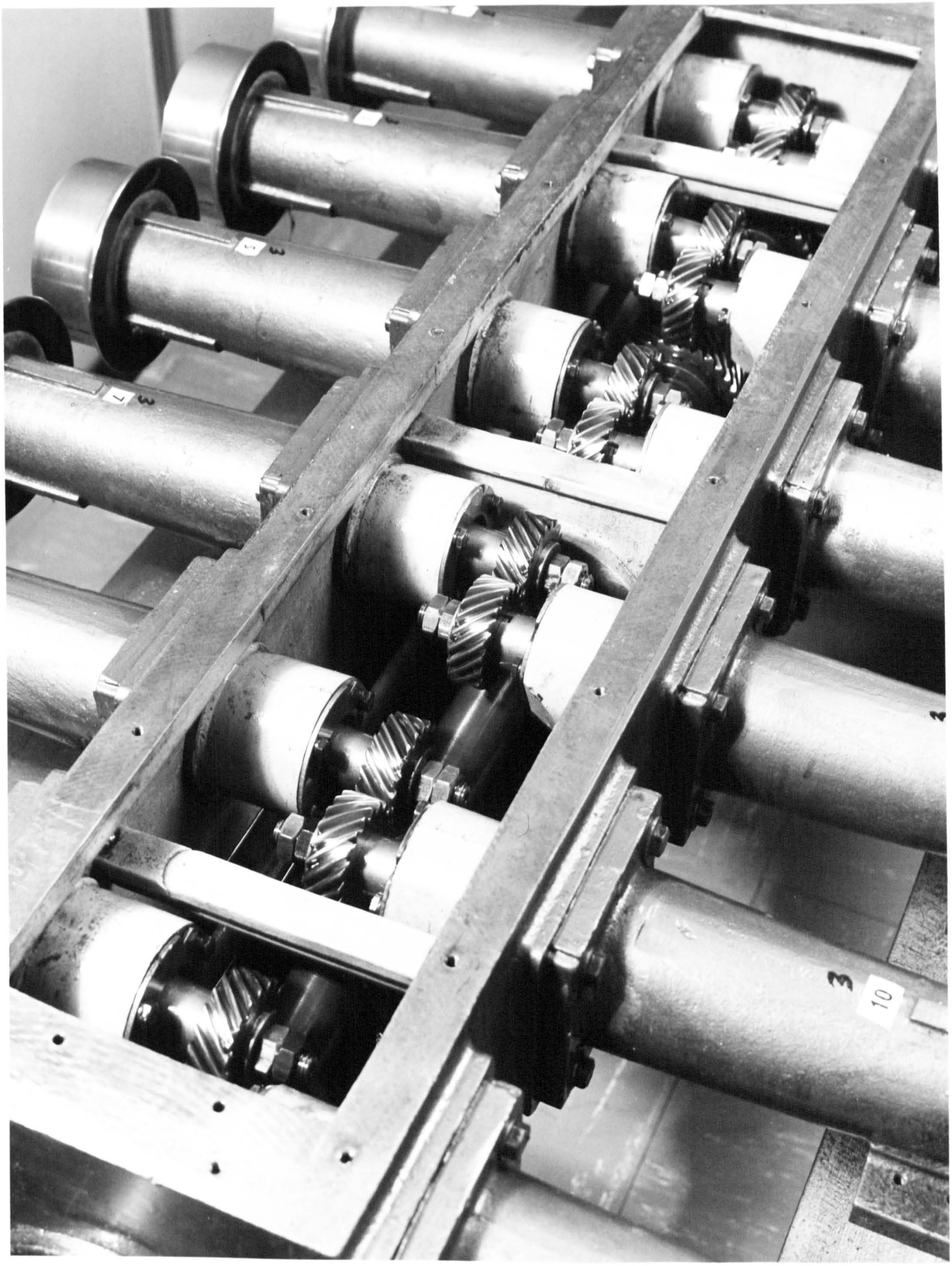

FIG. 2.10 General View of MDT. Drawbox (cover removed)

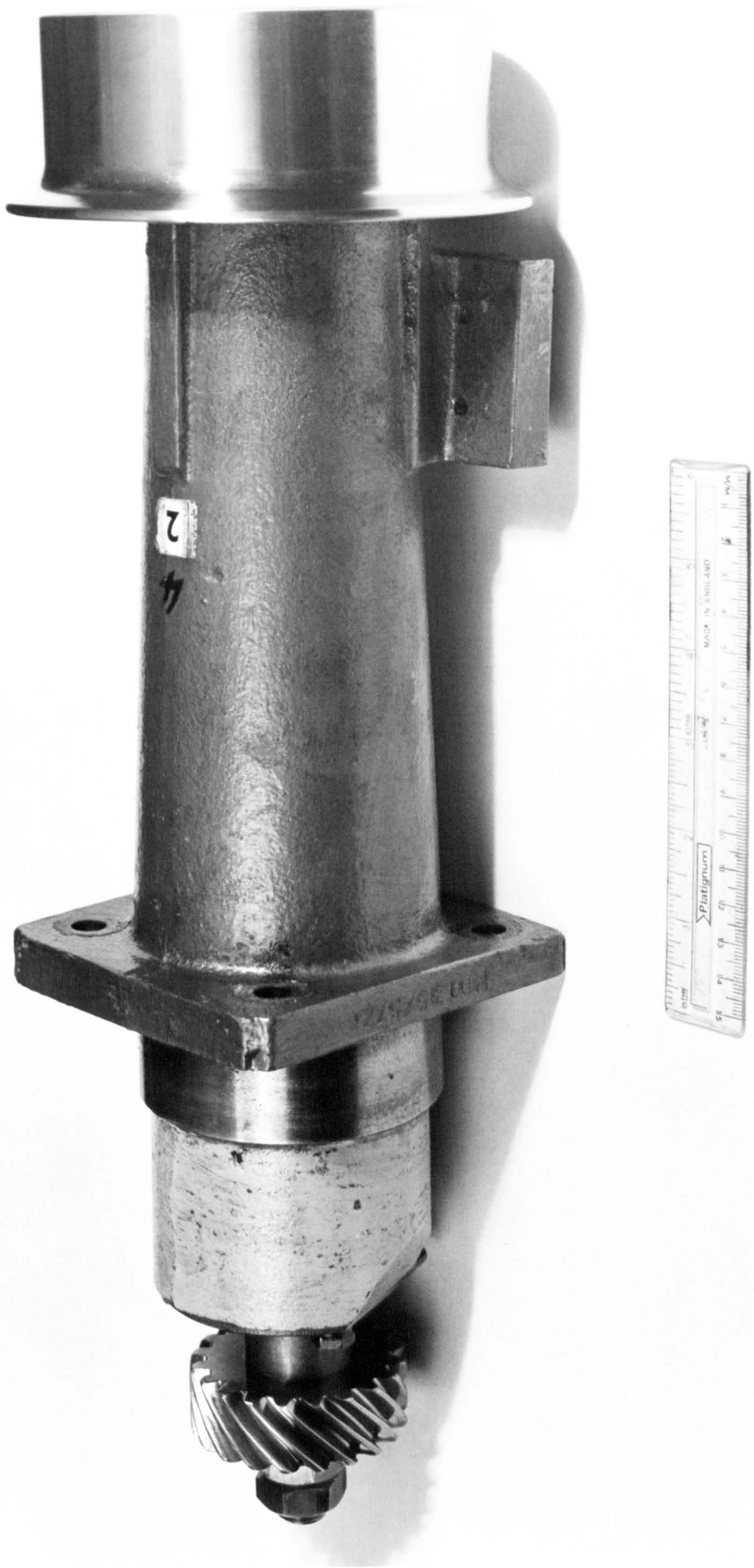

FIG. 2.11 Drawroll Cartridge or Drawpod

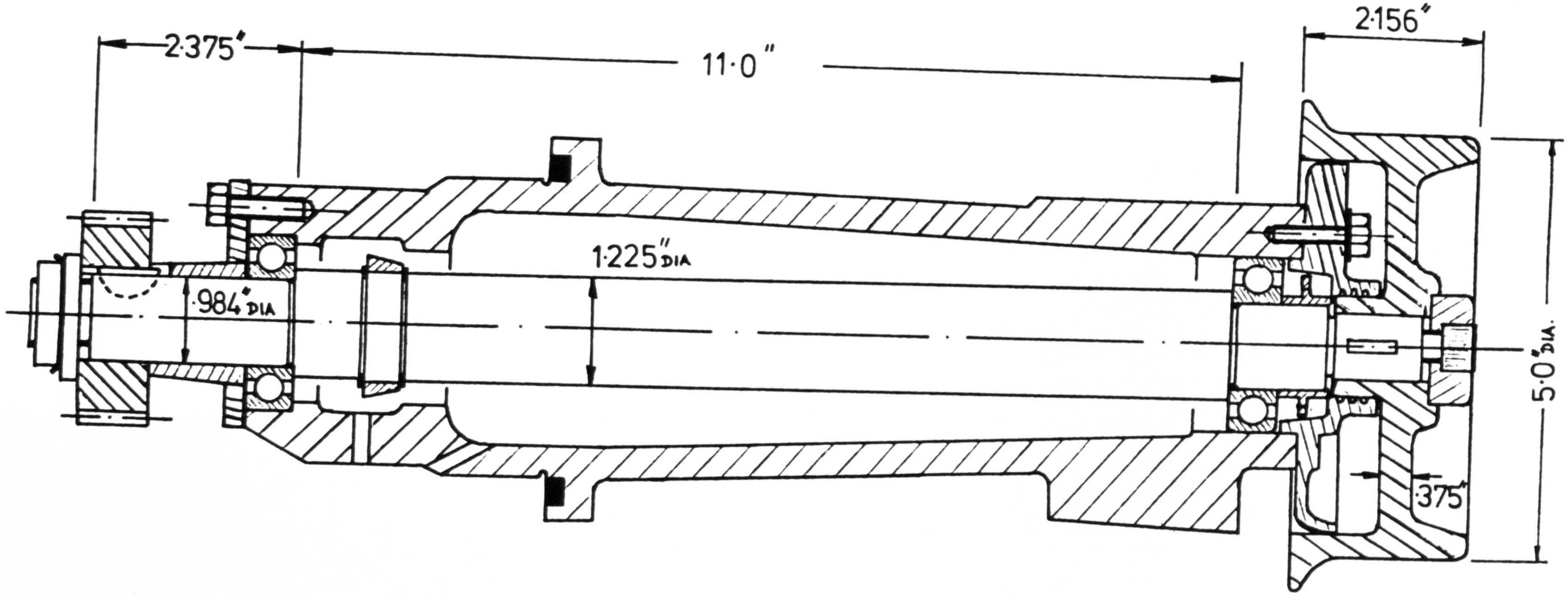

FIG. 2.12 Drawroll Cartridge Assembly

3. DRAWBOX GEAR PROBLEM 1961 - 1970

3.1 Historical Outline

Premature replacement of gears in drawboxes has been intermittently experienced over several years in drawboxes using the "two over one" helical gear arrangement (described in 2.3.2), the earliest replacement occurring in boxes using a steel/bronze/bronze material combination. The failure mode was diagnosed as severe pitting of the bronze gear teeth characterised by a cyclic damage pattern observed around the gear periphery. Wear from both crossed helical and parallel helical contacts was in evidence and for either type the wear was progressively transferred from the normal contact face to the non-contact, or trailing face, through 180 degrees of rotation. Relative locations of teeth with severest pitting damage are depicted in Figure 3.1. This characteristic wear pattern has always been identified whenever gear failures have occurred on any significant scale.

The prototype MDT (polyamide) machine was delivered to a nylon manufacturer in March, 1961. It had a steel/bronze/bronze drawbox gear arrangement and after a few months a problem involving gear pitting became apparent. The machine was withdrawn and, after being completely rebuilt with a steel/bronze/steel configuration, it was

* Draw-winder machines are similar to drawtwisters except that the yarn is fed normal to the axis of the collection package and hence there is no inserted twist.

installed at another company as the first Type A machine. Satisfactory performance of this machine led to a further batch of nine machines and ultimately to seventy five, being supplied to this company.

In the early sixties, process limitations were such that actual drawspeeds were normally only about half the specified maximum of 4000 ft/min. (3050 r.p.m. of drawshaft). Generally the machines gave satisfactory performance at these speeds. However, gear failures were reported at a number of installations from time to time. These were thought to be associated with insufficient accuracy in manufacture and assembly and, indeed, some alleviation was obtained when offending drawboxes were rebuilt to tighter tolerances.

As operating speeds were progressively increased production methods and standards were regularly reviewed and improved in an attempt to combat a growing number of bronze gear failures. In the period 1966-1967, machines were being run regularly at drawspeeds up to 3000 ft/min. resulting in failures on a considerable scale. Typical examples of gear damage are illustrated in Figures 3.2-3.5. At this time, gears were manufactured and assembled to the highest levels of precision and, since the cost of further improvement was prohibitive, the design of a satisfactory drive modification became a question of some urgency.

It had become clear that failures were the result of dynamic effects and a large programme of research and development was initiated to examine methods of reducing gear tooth dynamic loads. The influence of various system parameters, such as shaft stiffness and drawroll inertia, were investigated together with more radical modifications involving non-metallic and composite gears.

Arising from this work came a design of particular merit, which employed considerable torsional resilience between cartridge gear and drawshaft. (Further details of this design are given in Section 3.3.9). After small scale tests had proved satisfactory*, a full size machine, incorporating modified gears, was put on trial at a polyester installation early in 1969. Some initial problems with the flexible element were quickly overcome and this design modification is now considered to be a satisfactory solution to the problem.

Machines fitted with flexibly mounted gears have now been operating under production conditions for almost five years, often at yarn delivery speeds in excess of the rated maximum of 4000 ft/min. No gear failures have been reported during this time and, therefore, the drawbox problem is considered solved, if not completely understood. It is the purpose of the research described in this thesis to provide a greater understanding of the original problem.

A large volume of documentary evidence on the gear problem is contained in internal reports of Platt International Ltd. The remainder of Section 3 is devoted to the examination and discussion of these reports.

* As a side benefit, drawbox acoustic noise levels were considerably reduced by the bushed gears. A reduction of 14 dB(A) has been quoted for a single box operating at 4000 ft/min (R23) (Section 3.3.15).

3.2 Investigations in the Period 1962-1967

The reports from 1962 to 1967 give details of the gear failure problem. Dynamic loading considerations had not been seriously suggested as a factor in this period.

3.2.1 MORRIS (1962 (R1))

This report gives details of damage to bronze gears in high speed draw-winder machines and is the first discriminating evidence of gear damage occurring within Platt machines. The "two-over-one" helical gear arrangement was used in this machine but the material combination was steel-bronze-bronze (as opposed to steel-bronze-steel in the MDT range). It was found that tooth failure of the bronze gears was initiated by severe pitting and the characteristic wear pattern described in Section 3.1 was first observed.

Examination of drawshaft assemblies revealed evidence of considerable overheating and a number of instances of excessive play between gear keyway and key and slack gear spacing sleeves; the latter allowing an axial gear play of .043" in one severe case.

Several examples of machine damage illustrate the severity of the problem. One machine had run for 5 months at a delivery speed of 1600 ft/min (the rated maximum was 4000 ft/min) and 3 months at 2400 ft/min producing a large number of pitted gears. Another machine had run at 2400 ft/min for $2\frac{1}{2}$ months and, on inspection, 80% of the bronze gears were found to be excessively worn.

The report describes a number of checks and tests carried out as a result of performance in service. All drawbox components were found to be within reasonable commercial limits for the class of duty except, in a few cases, the gear keyway fit. Tests on individual gearboxes revealed no trouble after over 1000 hours running at speeds up to 4000 ft/min and the maximum box temperature recorded was only 33°C. Visual observation of the lubrication through transparent panels by means of a stroboscope confirmed oil presence at tooth faces at all times. Power tests showed that the heaviest yarns (250 denier) imposed a torque of only 3.5 lbf.in. on drawshaft gears at 2300 r.p.m. (3060 ft/min).

The writer stated that, in February, 1960, Professor W. A. Tuplin, who has published widely on gear dynamics, had agreed with drawbox design with regard to lubrication, materials and gear fastening. This supported his own conclusion, from tests carried out, that,working under normal conditions, the gears should operate satisfactorily.

3.2.2 PRIEST (1962 (R2))

Further details of the draw-winder gear failures are given in this report together with examples of machine behaviour at various speeds. Again the writer noted looseness of sleeves, evidence of overheating, and a pitting distribution on alternate tooth flanks around the gear periphery. He also observed that excessive gearbox acoustic noise had drawn attention to boxes where gear failures were imminent.

Oscillograph recordings showed severe oscillation of drawroll shafts over a number of positions in the machine (positions unspecified in report). A further oscillation was detected in the feedroll system but no relationship between the two could be established.

3.2.3 NEEDHAM (1962 (R3))

The pitting pattern described earlier (Section 3.1) was again noted in this laboratory report, the pitting being caused by material breakdown just below the surface. This caused cracks and eventually pits to a depth of .008" in a specimen bronze gear. Chemical analysis showed that the bronze conformed to specification and it was concluded that only marginal improvement in gear life could be obtained by changing the alloy composition.

3.2.4 TUPLIN (1963 (R4))

An assessment was made of the accuracy of Platt helical gears after examining production methods, machines and inspection procedures. Measurements were carried out on a gear selected at random from a production batch. The gear selected showed remarkably small pitch errors and was found to comply very nearly with the highest grades of precision specified in any British Standard.

It was concluded that procedures in manufacture, inspection and working tolerances were satisfactory and that changes in production were unnecessary.

3.2.5 TUPLIN (1964 (R5))

The writer commented on a pitted gear which had run for 660 hours from new. He observed that the type and distribution of the pitting was greater than could be expected with the apparent loading conditions.

3.2.6 ASHTON (1964 (R6))

Running tests on a single Type A drawbox are reported. The box was run almost continuously, for over 1200 hours, at various speeds but mainly in the region of 4000 to 5000 r.p.m. (drawroll speed). No evidence of even slight gear damage was found though a measured noise level of 96 dB (weighting not specified) at 5000 r.p.m. was considered high.

Axial movements of drawroll shaft and layshaft were measured during running and found to vary up to .005" for the former and up to .006" for the latter. Details of the measurement technique are not given.

The eccentricity of layshaft gears as assembled was measured and found to vary between .001" and .0035" whilst that for drawroll gears varied from .0005" to .0085".

Observation of lubricant flow, using a perspex lid, suggested that the lubrication system was effective even at speeds in excess of the rated maximum. Morris (Section 3.2.1) had earlier reached the same conclusion from his own independent tests.

3.2.7 SCOWCROFT (1967 (R7))

This report describes an investigation into a complaint by a customer that attempts to operate Type A drawtwisters at delivery speeds in the region of 1000 m/min. (3280 ft/min) had resulted in drawboxes overheating and large scale gear failures.

Production methods and tolerances were checked and several cases of significant drawshaft gear eccentricity were found, the chief causes being:-

(i) the faces of gear spacer sleeves were not sufficiently parallel.

(ii) badly fitting keys.

and (iii) lack of finesse on the part of fitters.-

It was decided to reduce drawroll gear eccentricity, as assembled, to not more than .001" total indicated reading at the pitch circle diameter. A special jig was made, similar to a Parkson gear tester but which could check the gears against a master in situ.

The offending machines, with drawroll gears reassembled to the eccentricity tolerance of .001", proved satisfactory after 250 hours of trials at various speeds up to 1000 m/min. The eccentricity tolerance and inspection procedure were adopted as standard production practice.

3.3 Investigations and Design Proposals, 1968-1969

3.3.1 TUPLIN (1968 (R9))

The writer was uncertain about the actual cause of the gear problem but thought it might be due to solid debris in the lubricant combined with dimensional inaccuracies of the crossed helical mesh. He thought (wrongly) that the failure mode was scuffing and reasoned that, since loads imposed by yarns were very low, the actual tooth loads might include a substantial contribution from dynamic effects.

On the basis that dynamic load is proportional to the square root of the effective mass of the lighter impacting bodies, the possibility of reducing the effective mass of drawroll gears was examined. It was recommended that drawroll shaft flexibility be increased, by reducing its diameter, in order to decouple the gear from the high drawroll inertia. Two designs for drawroll cartridge assemblies incorporating $\frac{1}{4}$ inch diameter shafts were presented.

3.3.2 HALL (P.E.R.A.) (1968 (R10))

P.E.R.A. investigating gear damage in Type D drawboxes, noted the characteristic once per revolution gear wear pattern and suggested that this might be caused by unbalanced drawroll shaft assemblies. It was found that drawrolls were produced from drawn bar and that only the ends were machined, leaving the shafts unmachined over the greater part of their length and thus producing considerable unbalance in some cases.

Simple tests were carried out on a single drawbox rig fitted with only one pair of drawroll cartridges. The effect of unbalanced drawshaft on box input torque was measured by means of a torque transducer over a range of running speeds. A resonance condition was detected at about 3000 r.p.m. (drawshaft speed) at which input torque and acoustic noise increased sharply. The torque traces were observed to contain a once per revolution frequency component in all cases and vibration levels were significantly reduced when balanced shafts were substituted. It was noted that the unbalanced shaft tested was a particularly bad one and probably not representative of production shafts.

Believing (wrongly) that gear failures in service had only occurred at drawroll speeds of about 3000 r.p.m., it was concluded that the resonance detected during tests, excited by shaft imbalance, was probably the cause of the problem.

3.3.3 TUPLIN (1968 (R11))

From an examination of bronze gears showing premature wear, the writer estimated that tooth dynamic loads were probably of the order of 100 times as great as the normal transmitted loads. He reiterated a previous contention (Section 3.3.1) that dynamic load could be reduced by minimising the inertia of components rigidly attached to the gears and proposed that standard drawshafts be reduced to a diameter of $\frac{1}{4}$ inch over as great a length as possible.

3.3.4 LABORATORY REPORT (1968 (R12))

Bronze gears returned from Contract X were found to exhibit the same once per revolution pitting pattern identified previously (Sections 3.2.1, 3.2.2, 3.2.3, 3.3.2). This pattern had been observed on all worn bronze gears examined by the laboratory since 1962. Microscopic observation of the teeth identified a series of subsurface cracks which tended towards the surface. Various alloys had been tried without success and it was suggested that the problem was one of excessive loading rather than of material composition.

3.3.5 SCOWCROFT (1968 (R13))

After noting the familiar wear pattern on each of a number of gears returned from service in Poland, the writer discusses the following possible causes:-

(i) dynamic unbalance of drawroll shaft assembly due to one or more components.

(ii) gear manufacturing errors, for example, pitch circle eccentric to bore.

(iii) eccentricity of gears on assembly.

It was thought that (i) and (iii) were the most probable causes of the problem.

3.3.6 WHITELEY (1968 (R14))

Drawbox lubrication is discussed in relation to gear

wear and the writer notes that worn gears have exhibited much pitting but relatively little scuffing. He reasoned that, since the pitting mechanism is thought to be associated with the presence of lubrication whereas scuffing results from its absence or breakdown, the lubrication system was probably adequate.

Measurements of layshaft input torque were made, by means of a strain gauge, in a single box rig. Pulses at once per revolution of drawroll speed were detected together with a higher frequency which was thought to be tooth meshing frequency.

A short gearbox with a single layshaft gear and a pair of drawroll cartridges was built to investigate the dynamic behaviour of the two-over-one gear configuration. The layshaft and steel gear drawshaft were fitted with strain gauges and slip rings and provision was made for fitting brake bands to the drawrolls to simulate yarn tension. The effects of the following factors were to be investigated:-

1. yarn tension
2. gear backlash
3. gear eccentricity
4. non-metallic gears
5. imbalance of drawshaft assembly.

3.3.7 LEE (1968 (R15))

Dynamic loads were computed for the drawbox crossed helical mesh by the Buckingham method* for a layshaft speed of 2400 r.p.m. and an assumed maximum adjacent tooth pitch error of .0005".

* Buckingham's theory for dynamic load is discussed in Section 4.1.

For a 250 denier drawn yarn, the crossed helical transmitted force was estimated at 3.3 lbf. and the dynamic increment force computed to be 130 lbf., giving a total dynamic loading of 133.3 lbf.* compared to a limiting load for wear of 45 lbf.

On the basis of these figures, it was concluded that nothing could be done with the existing gear arrangement to give a satisfactory fatigue life. Further calculations suggested that some improvement might be effected by redesigning the gears to a $14\frac{1}{2}$ degree pressure angle and reducing adjacent pitch errors.

* This value for dynamic load appears to be in error. Accepting, for the present, the values for speed and maximum adjacent pitch error, the figure for dynamic load is high because the writer has not made the allowance, provided in Buckingham's theory, for the effect of high speed. Consideration of this yields an effective pitch error of .0001" which would produce a dynamic load of only 8 lbf. Returning now to the writer's data, however, the layshaft speed of 2400 r.p.m. is considered unrealistically high since premature gear failures have occurred at about half of this speed, i.e. around 1200 r.p.m. (layshaft). Furthermore, measurements by Tuplin (R4) gave maximum adjacent pitch errors of only .0002". Inserting these two values into Buckingham's equations gives a dynamic load of 35 lbf. which is within the limiting load for wear, calculated to be 45 lbf.

3.3.8 WHITELEY (1968 (R16))

This is a progress report on experimental work carried out with the two-position gearbox rig described in (R14) (Section 3.3.6).

Measurements of dynamic torque in the instrumented drawshaft revealed a lightly damped torsional resonance at a frequency of 830 Hz, corresponding to tooth meshing frequency for the running speed of 2500 r.p.m. This frequency was in good agreement with the computed fundamental torsional frequency of the shaft assembly taking into account that the shaft had been modified to provide satisfactory strain gauge sensitivity (details of the modification not specified). Calculations for a standard shaft suggested that the resonance would normally occur at about 1000 Hz or a drawroll speed of around 3000 r.p.m.

Apart from the tooth frequency vibration of amplitude 8 lbf.in., the drawshaft record at 2500 r.p.m. also shows a superimposed torque fluctuation of $\pm$ 12 lbf.in.at once per revolution. By increasing the backlash from .020" to .050"* the low frequency torque characteristic was changed to once per two drawroll revolutions at the same speed of 2500 r.p.m. The tooth frequency vibration remained unchanged by this modification.

Gears of the following thermoplastic materials were tested in a full drawbox:-

1. high density polyurethane,
2. delrin,
3. nylatron G.S.
4. monocast nylon
5. nylon 6

* The radius at which backlash was measured was not specified; the production tolerance of .005" - .030" refers to measurements at a radius of $2\frac{1}{2}$", i.e. the drawroll diameter.

Both thermoplastic and composite gears were found to be significantly quieter than standard gears and experimentation was to continue.

3.3.9 SCOWCROFT (1968 (R17))

A brief review of the drawroll drive problem from 1961 is given followed by discussion on the possibility of using gears made, entirely or in part, from resilient materials. It is argued that thermoplastic gears and those with metal to non-metal interfaces in shear are unsatisfactory and an alternative design is proposed.

This is shown in Figure 3.6. Two small rubber bushes are inserted into diametrically opposed positions of the gear to locate steel drive pins protruding from a modified spacer bush which would be rigidly keyed to the drawshaft. The gear was thus permitted to rotate on the shaft, the only torsional restraint being provided by the 2 rubber bushes. To facilitate easy movement of the gear, oilways were to be machined around the shaft periphery and axial restraint was provided by the end washer.

In single box tests, rubber bushed gears were found to be noticeably quieter than the standard keyed gears. On inspection, after about 1000 hours of high speed running, there was no evidence of tooth wear, shaft fretting or bush damage. Tests were to continue.

(For production reasons, the bushed gear assembly was eventually modified as shown in Figures 3.7 and 3.8. The spacer bush became a gear support bush and the pin/rubber bush arrangement was reversed).

3.3.10 SCOWCROFT (1968 (R18))

Progress of the continuing experiments with bushed gears is reported. One gearbox had been run for over 2000 hours at drawroll delivery speeds up to 7000 ft/min. Another two boxes, coupled together, had logged over 1600 hours at up to 6000 ft/min. All gears and bushing arrangements were found to be in good condition on inspection.

3.3.11 MAKEHAM (1969 (R19))

The writer measured the surface texture of drawbox gears, finished by both shaving and grinding processes, using a piezo electric pickup. Both processes were found to produce finishes within precision classes A1 and A2 of British Standard BS 436 (1940) (5) but ground gears had fewer large surface irregularities than shaved gears. Measurements on a 20 tooth steel gear which had run for about 3000 hours indicated that the steel surface did not improve when meshing with the (softer) bronze gear.

3.3.12 WAUGH (1969 (R20))

This report describes further experiments with the two position drawbox rig mentioned earlier (Sections 3.3.6 and 3.3.8). A variety of gear and drawroll combinations were investigated at three running speeds by means of strain gauges fitted to the intermediate drawshaft. An average torque reduction of 24% was recorded when 4" diameter drawrolls, of 50% mass reduction, were used with the standard gear arrangement. Comparisons between various non-metallic and composite gears were inconclusive owing to severe vibration from a poorly seated shaft bearing.

A resonant frequency of 900 Hz was detected in the modified instrumented drawshaft in an otherwise standard arrangement. The fundamental torsional mode frequency computed by an approximate method was 870 Hz.

A full box of composite gears with polyurethane inserts was run for 2500 hours at 4000 ft/min but inspection revealed two cases where the interface bond had failed. Moulded polyurethane gears failed quickly when subjected to start/stop tests. This was due in part to the presence of air holes in the castings.

Further work was to be carried out with bonding agents for the composite gears and with machined polyurethane gears, which had performed satisfactorily in preliminary tests.

3.3.13 MAKEHAM (1969 (R21))

Measurements of drawroll rotary displacement are reported for MDT. drawboxes fitted with both solid and rubber bushed gears. The effect of backlash and drawroll inertia were observed for various running speeds.

3.3.14 MAKEHAM (1969 (R22))

The receptance technique (6) was used to compute the first two natural frequencies of a drawroll pair for a variety of shaft diameters and drawroll inertias. Distributed shaft inertia was considered but gear tooth flexibility was ignored. The frequency spreads for the first and second torsional modes were 250 to 280 Hz and 1000 to 1200 Hz respectively, depending on the various combinations of drawshaft diameter and drawroll inertia.

3.3.15 MAKEHAM (1969 (R23))

Acoustic noise measurements are reported for several MDT. drawbox configurations. These show solid gear assemblies to be considerably noisier than rubber bushed units. For example, the overall noise levels at one metre from a single box, running at 4000 ft/min, were 98 dB(A) for the former and 84 dB(A) for the latter.

3.4 The N.E.L. Investigation (R24)

Between October, 1969, and November, 1970, the National Engineering Laboratory carried out a theoretical and experimental investigation into the cause of MDT. drawtwister gear failures. They also collected some useful data on machine behaviour in production service.

3.4.1 Theoretical Work

3.4.1.1 Torsional Vibration Analysis

First mode frequencies of 1110 Hz and 1150 Hz were calculated for standard bronze and steel drawshaft assemblies respectively, whilst a frequency of 1180 Hz* is quoted for a pair considered coupled by the parallel axis gear mesh (it is not specified whether tooth flexibility has been considered). Critical frequencies of 260 and 1480 Hz were calculated for rubber bushed gear drawshafts but it is not clear which modes they correspond to.

* This corresponds to the second torsional vibration mode; the fundamental frequency of between 250 and 280 Hz referred to in Section 3.3.14, was not identified.

By representing the machine headstock as a single inertia, layshaft system critical speeds for a variety of machine configurations have been computed (theoretical method and data are not specified in the report). Critical operating zones have thus been identified and tabulated for all production machines including MDT. 6N and MDT. 6P.

3.4.1.2 Gearing Dynamic Loads

A dynamic load of 57 lbf. was calculated by Tuplin's method (version not specified) for a drawroll speed of 4350 r.p.m.

3.4.2 Experimental Programme

Large scale measurements were carried out on a nine box experimental drawtwister of Type A configuration. Strain gauges were attached to 15 positions in the total layshaft system and also to 3 pairs of drawroll shafts* but only 5 torque signals could be monitored simultaneously. Non-contacting inductive probes were employed to measure dynamic axial displacements of the three gears at a particular mesh.

The following arrangements were investigated in the experimental machine, operating at layshaft speeds from 300 to 3500 r.p.m. in steps of 200 r.p.m.:-

* Note:- In order to connect wiring to the strain gauges, layshafts were bored out to a diameter of about $\frac{5}{8}$ in. and drawshafts to about $\frac{1}{4}$ in. diameter. These changes represent reductions in polar second moment of area of 3% for a layshaft diameter of 1.5 in., but only .17% and .4% for drawshaft sectional diameters of 1.225 in. and .98 in. (see Figure 2.12).

(1) standard arrangement including solid gears.

(2) (a) reduced diameter shafts (2 boxes only)

(b) reduced diameter shafts and solid box couplings (2 boxes only).

(3) rubber bushed gears.

(4) machine loaded with nylon yarn as in production service for (1) and (3) above.

In an attempt to calibrate drawshaft strain gauge readings to provide gear dynamic loads, a drawroll cartridge assembly was set up. A vibration exciter was employed to insert torsional vibrations at the stationary gear whilst shaft strains were recorded by means of a strain gauge. The dynamic magnification factors determined in this way were (mistakenly) used to calculate gear tooth loads from the strain records obtained during machine running tests. Gear loads were determined for different operating speeds on the basis of this "calibration".

3.4.3 Experimental Results

3.4.3.1 Solid Gear Drive System

Specimen drawshaft strain records show clear pulses at rotational frequency with superimposed higher frequencies. The magnitude of the dynamic strains was generally greater in the case of the bronze gear shaft, however, the report provides no scaling factors and thus does not allow shaft torques to be estimated. The report noted that the vibration amplitudes were particularly pronounced at layshaft speeds of 1100 and 2200 r.p.m. where frequency components of 1050 and 1100 Hz were observed for bronze and steel gear assemblies respectively.

Significant axial vibrations of drawroll and layshaft gears were observed in the layshaft speed ranges of 1200 to 1400 r.p.m., 1700 to 1800 r.p.m. and 2000 to 2400 r.p.m. These normally occurred at drawshaft rotational frequency with superimposed higher frequencies but examples at layshaft rotational frequency were found.

Layshaft strain records were again observed to show fluctuations at drawroll frequency, particularly at 1190 r.p.m. (layshaft). At this speed, phase changes of 180 degrees were detected across the couplings between boxes 1 and 2 and 7 and 8. Further pronounced phase changes occurred at 1800 r.p.m. and it was thought that the two speeds corresponded to the third and fourth torsional criticals of the layshaft system and these, together with the drawshaft resonance, were believed to be the cause of the gear failure problem.

A maximum bronze gear dynamic load of about 350 lbf.in. was estimated and this occurred at a delivery speed of 3980 ft/min. The dynamic load at 3080 ft/min was estimated to be 185 lbf.in.

3.4.3.2 Modified Solid Drive System

Reduced diameter drawshafts (diameter unspecified) and solid couplings were used in an attempt to detune the drawshaft and layshaft resonances within the machine operating range. The results did not justify the modification as a practicable remedy.

3.4.3.3 Rubber Bushed Gear Drive System

Although a drawshaft resonance was identified in the region of 1400 to 1600 r.p.m. layshaft speed, depending on the actual rubber bushes used, the general levels of shaft dynamic torques were considerably reduced compared to the results for the solid gear system. A maximum bronze gear dynamic load of 80 lbf.in. was esimated based on measured shaft torque. Inspection of bronze gears, after testing, revealed marking, but no pitting, on front and reverse tooth faces from both crossed and parallel-axis contacts.

3.4.3.4 Yarn Production Conditions

The tests described above were carried out without yarn being processed, that is, under no applied load. To examine the effect of yarn loading on solid and bushed gear drives, a number of machine positions were arranged to process nylon filaments. For both gear types, a marginal shaft torque increase was detected when operating away from resonant speeds but at resonance the yarn produced a significant reduction in drawshaft vibration levels.

3.4.4 Other Experimental Work

3.4.4.1 Single Box Tests

Further experiments were carried out in a single box rig fitted with strain gauges on the layshaft and drawshafts. Drawshaft resonances were again detected, for both solid and bushed gears, at the same respective speeds as noted in the nine box machine.

3.4.4.2 Component Tests

Rubber bush load/deflection relationships were obtained under both static and dynamic conditions. These showed pronounced hysteresis characteristics and bush stiffness was found to vary considerably even within the same rubber type.

A number of measurements were also made of rotating component imbalance and gear mounting eccentricity.

3.4.5 Machine Performance in Service

A number of records of machines histories involving gear damage and replacement are predicted. On contract X damage occurred at drawspeeds in the range of 600-700 m/min. On contract Y damage occurred at 700 m/min and also at around 1000 m/min.

3.4.6 Conclusions

It is concluded that the critical speed of the layshaft-drawshaft assembly were the cause of the gearing problem and that although considerable improvement was afforded by the incorporation of bushed gears, there could be no absolute guarantee that this solution to the problem would be effective in all conceivable circumstances.

3.5 Delineation of a Framework for Research

Power measurements (R1) have revealed that the heaviest denier yarns processed in the MDT. range impose a drawshaft torque of only about 3.5 lbf.in. Taking note that the bronze helical gear drives two drawrolls, the normal loads transmitted by this gear probably never exceed 10 lbf.in., even when allowance is made for windage and bearing friction effects. For average denier yarns in the range, say 120 denier, the normal loads will probably be nearer 5 lbf.in. Since the bronze gear material has been verified to be satisfactory (R3),(R12), it is clear that premature failures, of the type shown in Figure 3.2, have been caused by dynamic loading effects. From pitting damage observed on specimen gears, Professor Tuplin (R11) has estimated that dynamic loads are probably of the order of 100 times as great as normal applied loads.

A considerable number of reports have noted the existence of a cyclic pitting pattern on bronze gears examined before the complete failure of teeth (R1),(R2),(R3),(R10),(R12),(R13),(R18).

The author has confirmed that this characteristic wear occurred in all [redacted] machines fitted with solid drawshaft gears, i.e. types A, C and D. [redacted]. Figure 3.9 shows photographs of both flanks of every tooth on a pitted gear obtained from the polyester installation. It clearly demonstrates the shifting of damage from contact to non-contact faces through 180 degrees of rotation, and pitting occurring at both helical (full face wear) and crossed helical (diagonal wear band) contacts can be observed.

A wear pattern of this kind is consistent with torsional oscillation of the parallel axis gear pair at drawshaft rotational

frequency. Thus the gears, in drive contact at one angular position, lose contact and traverse the tooth clearance and engage in reverse contact most heavily at 180 degrees from the original heavy drive point. That layshaft and drawshaft torque fluctuations have been detected at drawroll rotational frequency is evidence of this behaviour (R14),(R16),(R24).

The only excitation which could induce and sustain the motions described above is the fundamental component of static transmission error* at the parallel helical mesh. This may be caused by errors in gear manufacture, such as tooth pitch errors and eccentricity of assembly, although other sources are possible. Some alleviation of machine trouble has been effected by reduction of gear eccentricity (R7) thus demonstrating the significance of this factor. In respect of manufacturing errors, it has been reported (R4),(R19) that the accuracy of drawbox gears compares well with the highest levels of precision specified by British Standards.

Disturbing levels of shaft imbalance were suggested by P.E.R.A. (R10) as being the source of gear damage. In so far as rotary imbalance could produce shaft flexure and hence an eccentric gear effect, such a mechanism is possible.

The author's investigations have revealed, however, that since 1967 high precision production techniques have been employed resulting in insignificant shaft imbalance.

* Static transmission error, sometimes called velocity ratio error, is defined as the departure from uniform rotary motion of the driven gear when the driving gear is rotated slowly and with uniform motion.

The gear failure problem commenced well before this exercise and remained even after the dynamic balancing of drawrolls and box couplings was introduced as standard practice early in 1968.

A number of investigations (R16),(R20),(R22),(R24) have identified resonances of drawshaft assemblies induced by tooth meshing effects. The suggestion that these are the cause of gear failure is inconsistent on two counts. Firstly, the shaft frequencies are incompatible with the gear damage pattern of once per revolution and, secondly, gear failures have occurred at operating speeds where drawshaft resonances cannot be strongly excited. Experiments to detune drawshaft system resonances by means of reduced diameter shafts (R24) have proved inconclusive.

Only one attempt has been made to determine gear tooth dynamic loads by experiment (R24) (Section 3.4.2). The dynamic response of a stationary drawroll assembly was measured by strain gauges whilst torsional vibrations were applied to the gear by means of a vibration exciter. This "calibration" was employed to determine actual gear torques for shaft strain readings recorded during running tests. Such an approach is basically unsound because damping due, for example, to lubricant in the gear mesh and air drag on the drawroll is a function of rotational speed and is, therefore, not properly accounted for in a stationary calibration. Furthermore, the possibility of sub-system vibration allows the existence of drawshaft strains at instants when separation effects have reduced tooth loads to zero. Thus, it is likely that only careful direct measurements at the meshing gears can provide accurate information on tooth loads.

A number of questions relating to practical aspects of the gear problem are not resolved by the various investigations. For example, detailed correlations between MDT. drawtwister running histories and corresponding failures are sparse and only one report (R24) presents evidence of gear failure distributions within machines. Such questions are discussed in Section 10 in the light of further investigation.

The research described in this thesis is aimed primarily at achieving a fuller understanding of factors underlying the gear failure problem.

The inability to reproduce comparable failure severity in single box tests (R1),(R6) to that experienced in service, coupled with the detection of layshaft vibration modes by N.E.L. (R24) have suggested that the problem is associated with the dynamic characteristics of the total machine. This, in turn, suggests the possibility that all parallel helical gear pairs contribute periodic disturbances to the total system and hence the dynamic loads at any particular gear mesh. A multiple excitation concept is therefore pursued in the theoretical analysis which computes total system response to relative displacement excitations provided by all gear pair transmission errors.

To examine the validity of assumptions underlying the theoretical analysis, direct experimental techniques are developed. These aim at providing information on drawshaft gear torsional motions of which tooth impacts are clearly an important feature.

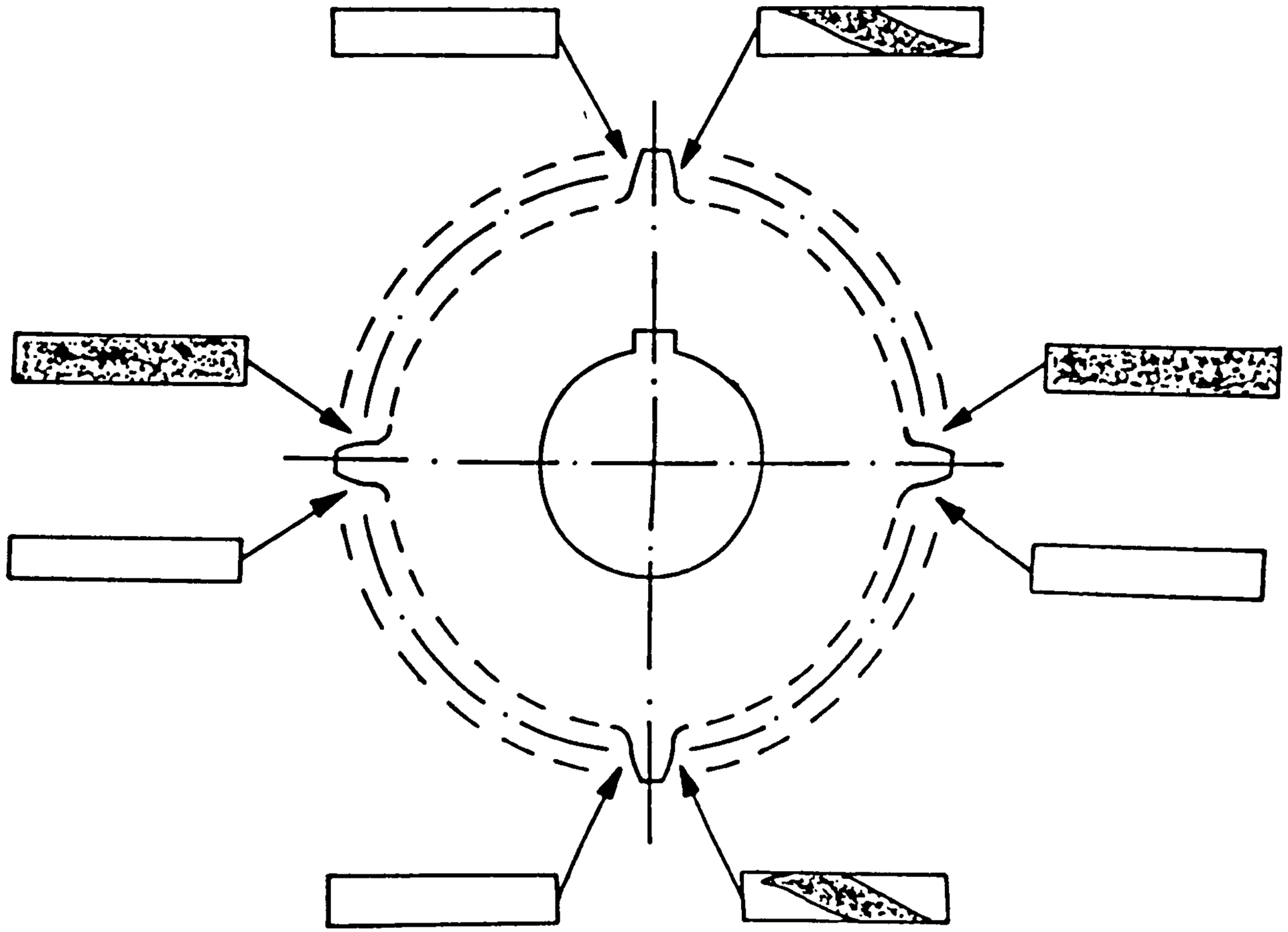

FIGURE 3.1 DISTRIBUTION OF PITTING DAMAGE ON BRONZE GEARS

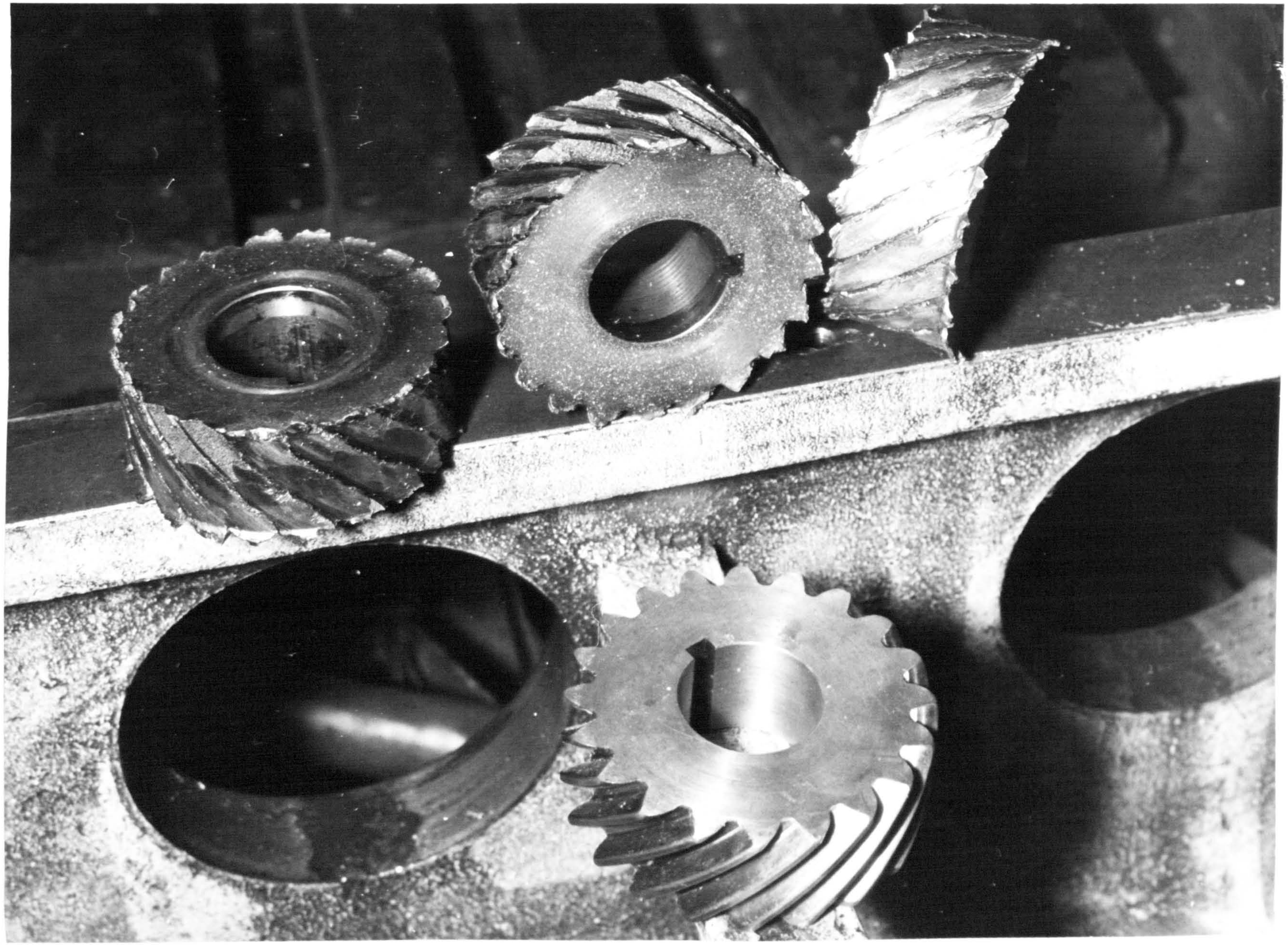

Figure 3.2 Failed Bronze Drawbox Gears

Figure 3.3 Drawbox Debris produced by Gear Damage

FIG. 3.4 Worn Layshaft and Drawshaft Gears

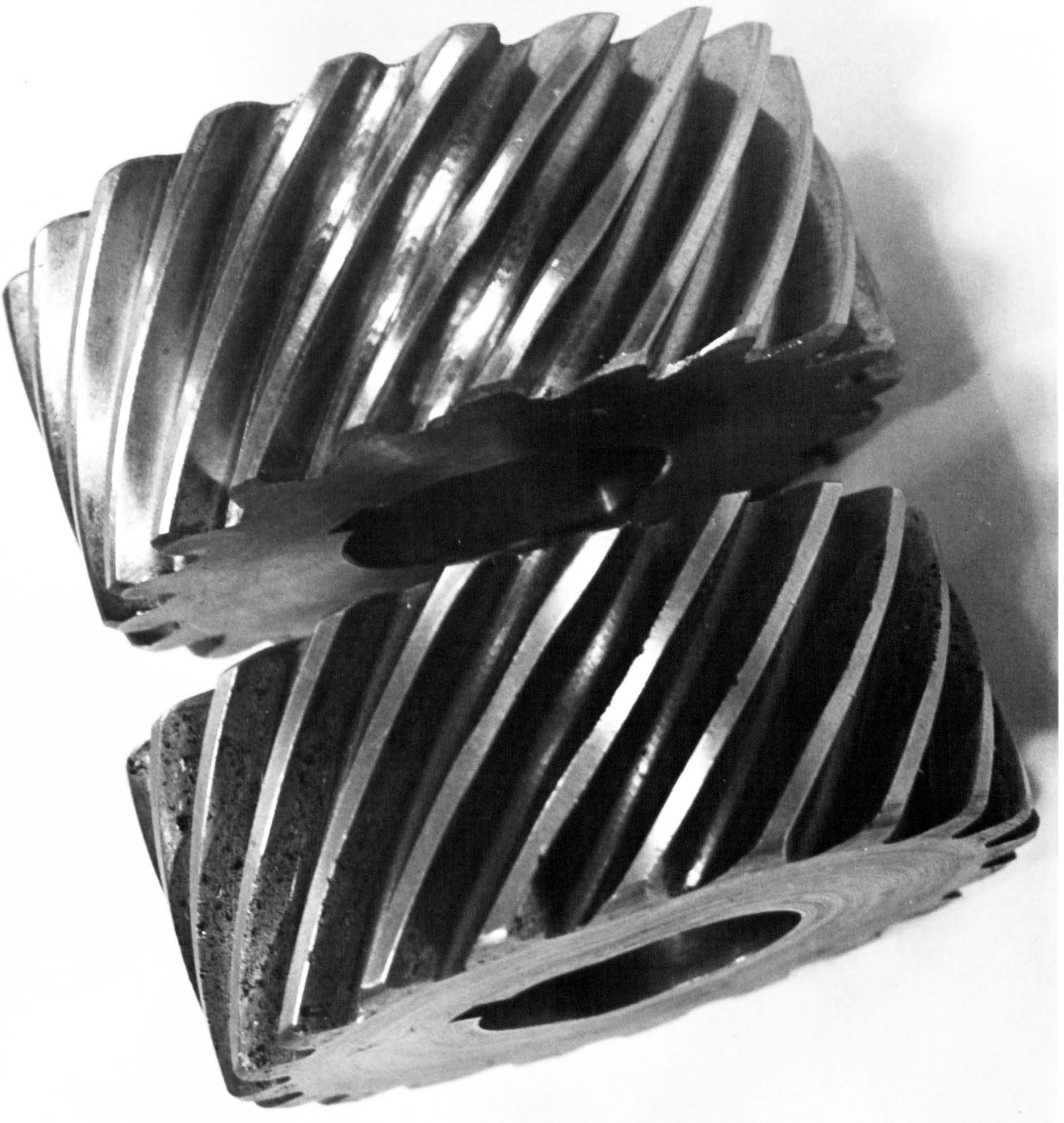

FIG. 3.5 Comparison of Pitted and New Bronze Gears

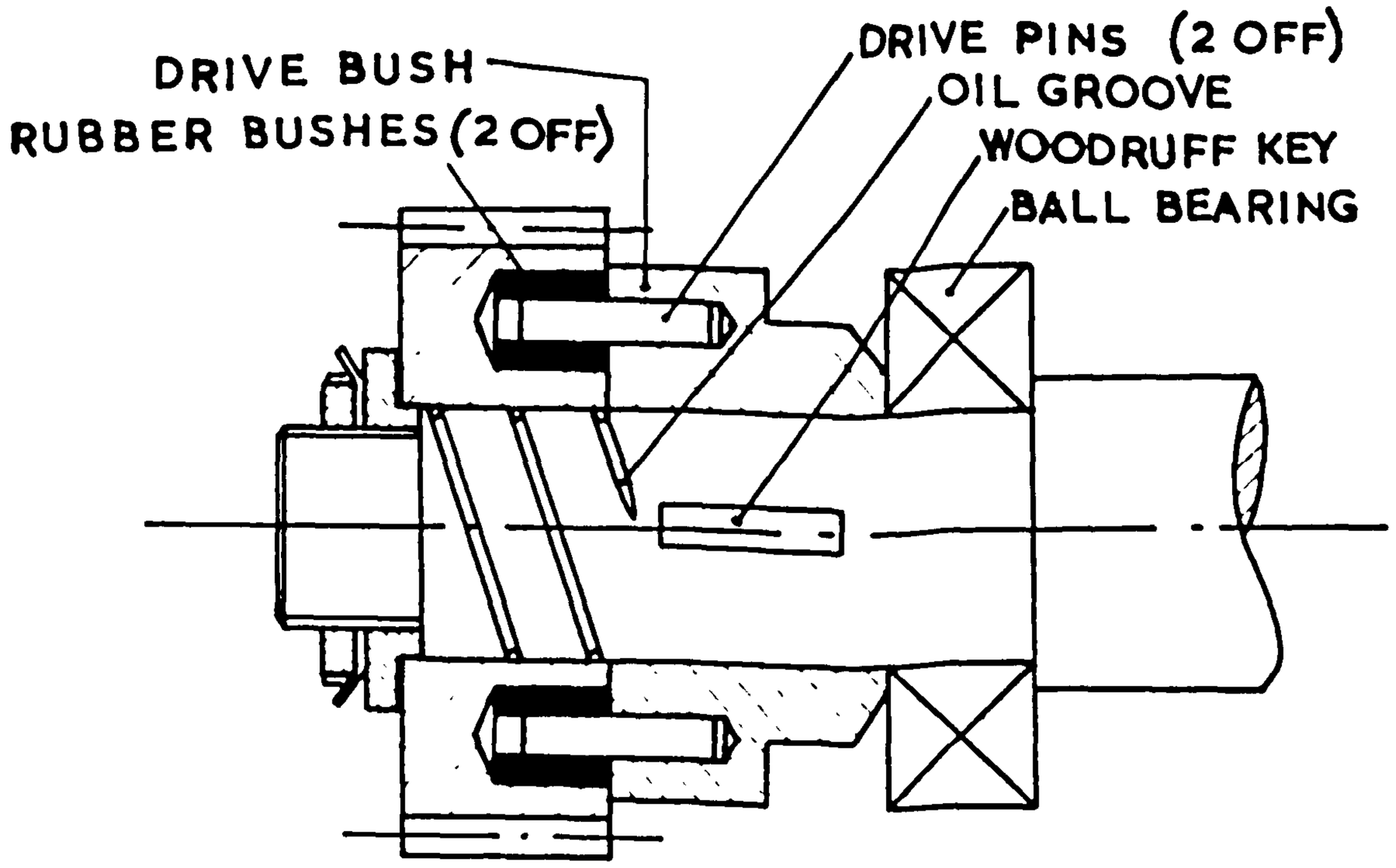

FIG. 3.6. TORSIONALLY FLEXIBLE DRIVE PROPOSED BY SCOWCROFT (R 17)

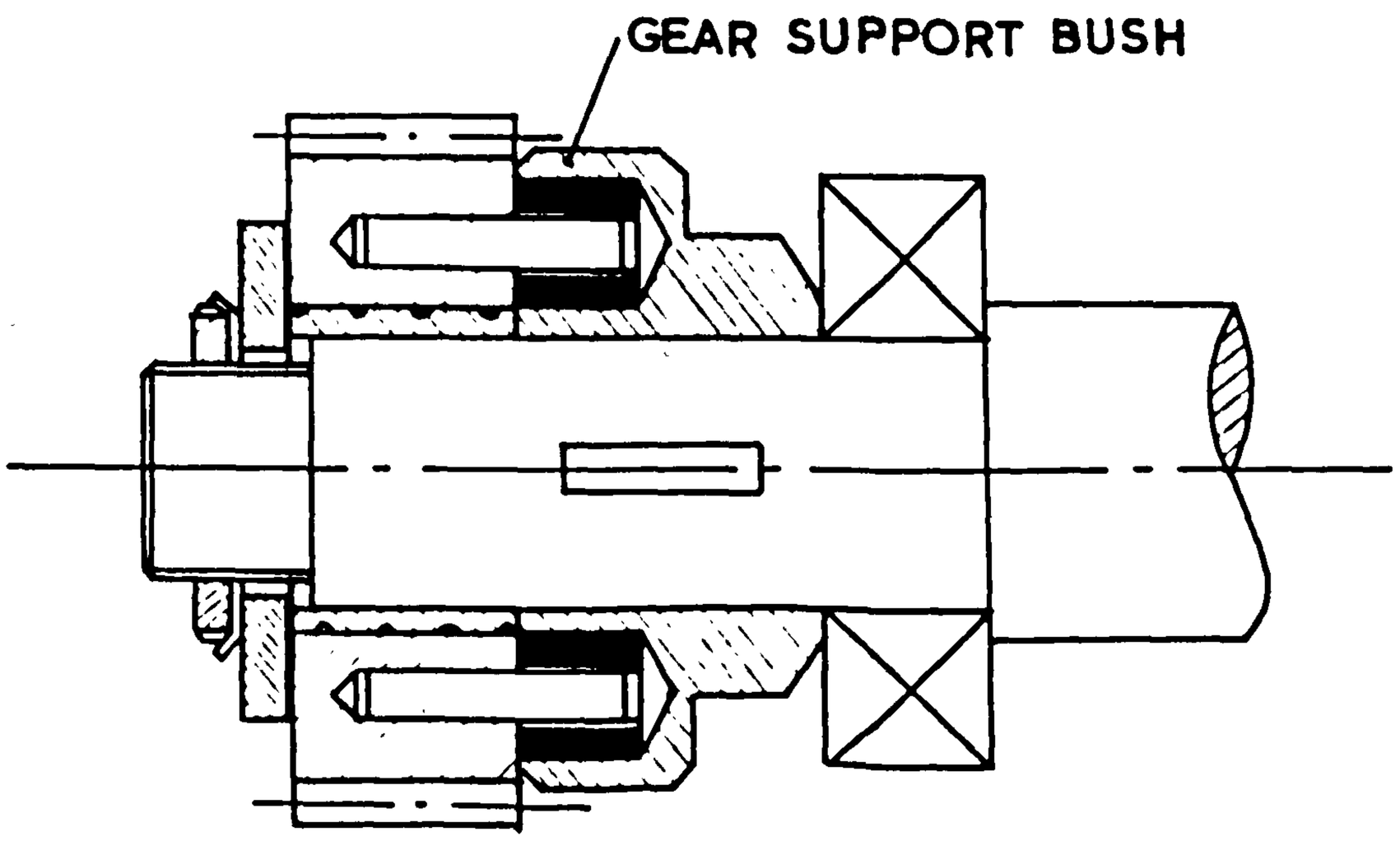

FIG. 3.7. TORSIONALLY FLEXIBLE DRIVE ADOPTED FOR MANUFACTURE

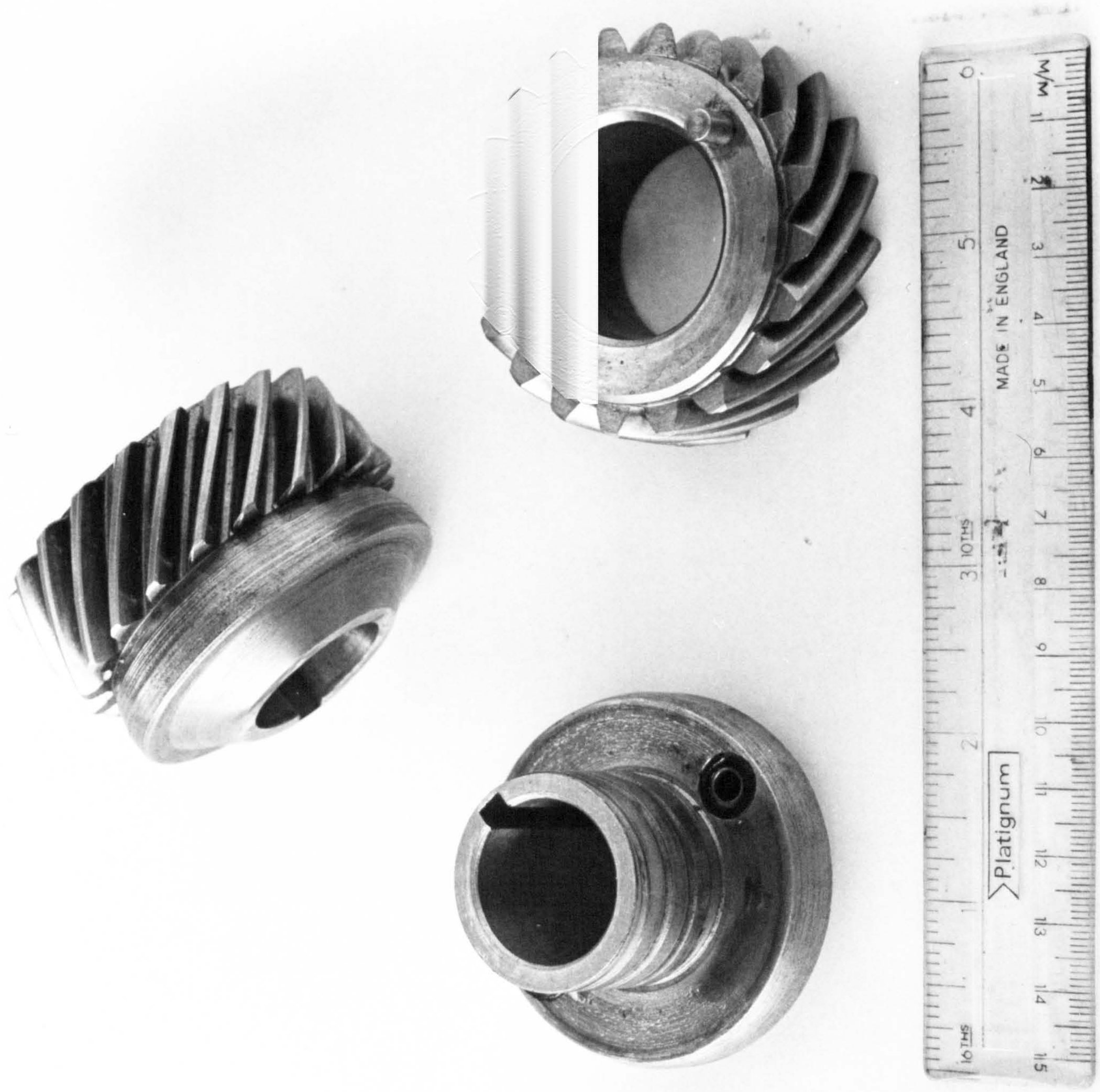

FIG. 3.8 Rubber Bushed Drawshaft Gears

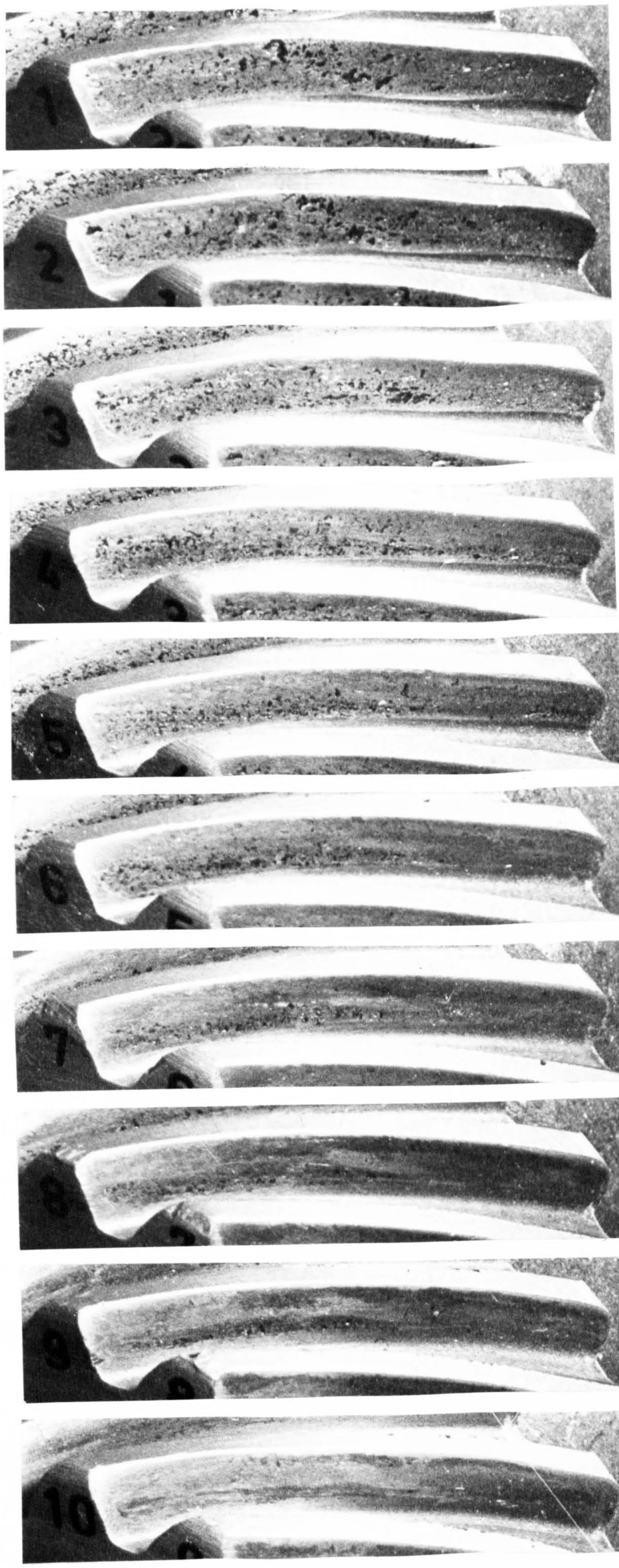

(a) Side 1, tooth numbers 1 - 10

Figure 3.9 Photographs of Pitting Damage on all Teeth of a Selected Bronze Gear

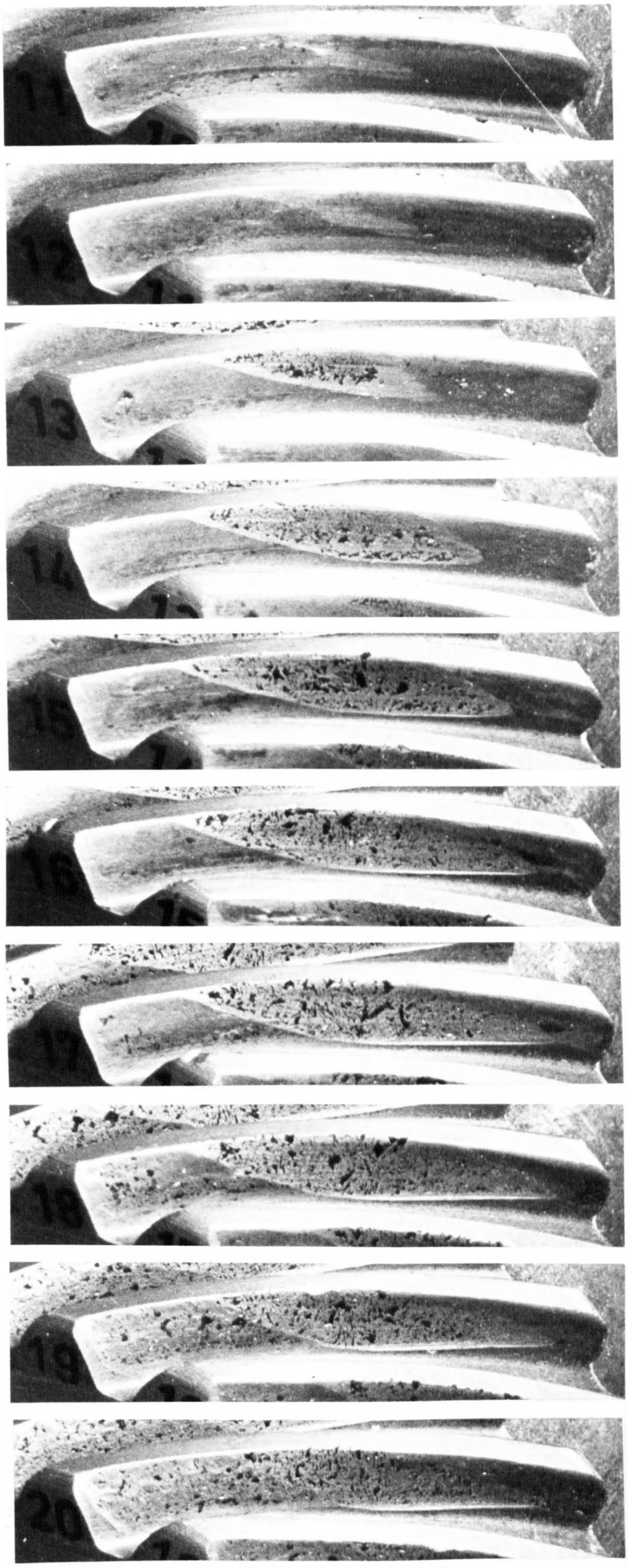

Fig. 3.9(b) Side 1, tooth numbers 11 - 20

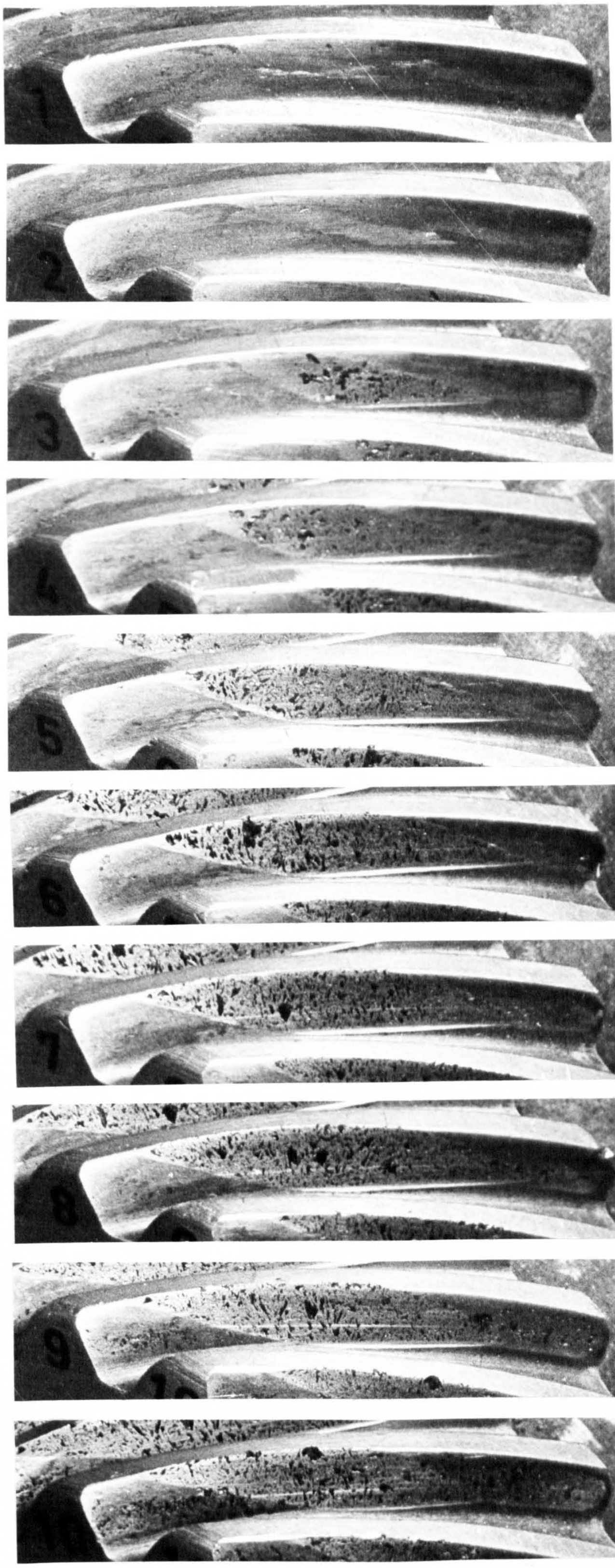

Fig. 3.9(c) Side 2, tooth numbers 1 - 10

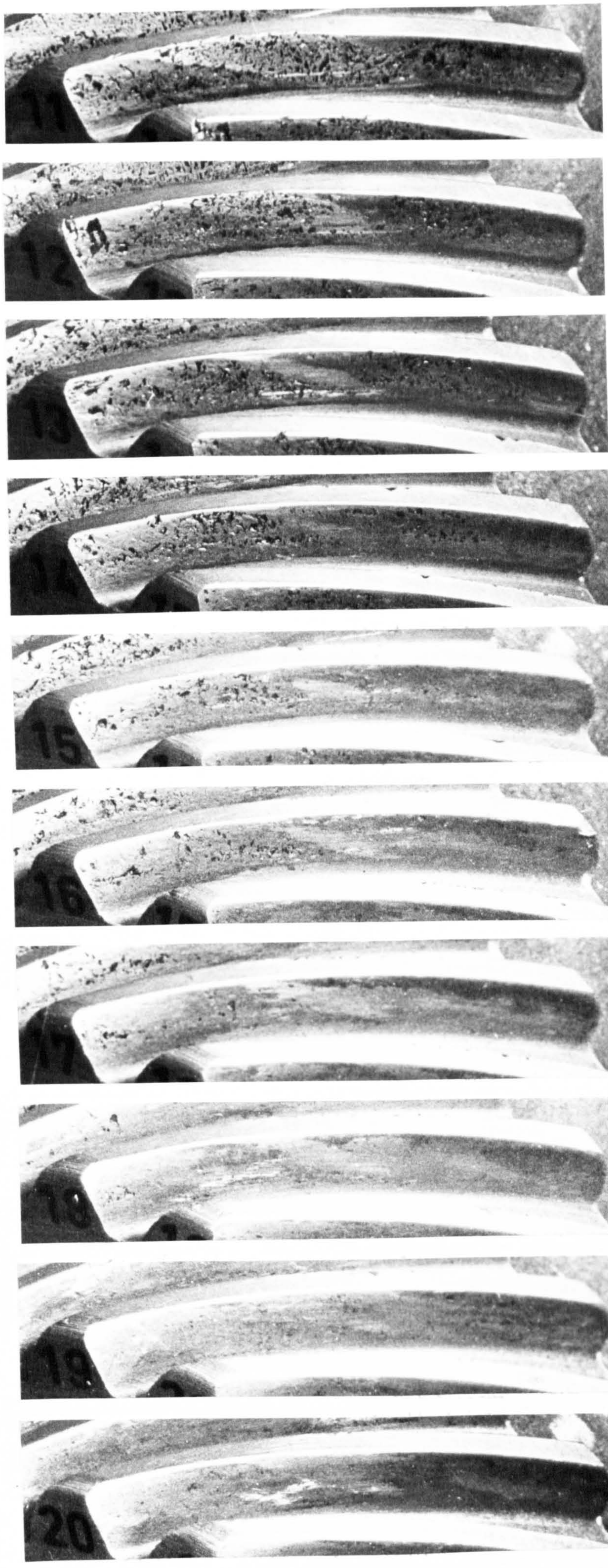

Fig. 3.9(d) Side 2, tooth numbers 11 - 20

4. LITERATURE SURVEY

4.1 Theoretical Literature

Perhaps the earliest theoretical analysis of gear tooth dynamic loading of any present importance was carried out by the American Society of Mechanical Engineers Special Committee, in 1931 (7), and subsequently developed by Buckingham, 1949 (1), who was a member of that committee. The analysis is based on a study of extensive experimental data and examines the transient behaviour produced by tooth to tooth imperfections. It was realised that tooth stiffness and the effective inertias of the gearwheels would influence the dynamic load but the tooth errors were regarded as sudden discontinuities in the velocity ratio. Thus the approach assumes the motion immediately prior to the tooth error to be uniform and that the resulting dynamic load is attenuated before the engagement of the next pair of teeth. Tuplin, 1950 (2), 1953 (8), 1958 (9), and Reswick, 1954 (10), have also developed methods of this kind, the latter considering separately the cases of light and heavy applied loads.

Strauch, 1953 (11), was probably the first to consider dynamic loading from a vibrational standpoint. He considered an isolated gear pair to be a single degree of freedom system (i.e. two inertias connected by tooth stiffness) and analysed the forced response due to a periodic variation of transmission error. Unfortunately, the analysis fails to maintain continuity of velocity between single and double tooth contact and Harris (12) has subsequently presented corrected results.

In 1956, Utagawa and Nakada (13) analysed the motions of a pair of involute spur gears by treating the single and double contacts separately. They assumed constant values for damping and tooth stiffness in each case and produced results similar in form to those of Strauch. Utagawa, 1958 (14), has separately published a similar analysis.

Zeman, 1957 (15), considered gear pair transient response to four forms of sinusoidal error and compared his results to those of Buckingham, Tuplin and Reswick. He also obtained a steady state solution for a continuous sinusoidal error and examined the effect of damping.

In 1958, Harris (12) published generalised equations of motion of an isolated gear pair without manufacturing errors. He first examined transmission error under low speed conditions and discussed in detail the effects of tooth profile modification first introduced by Walker (16) in 1938 and 1940. The simplified analysis identified three possible types of vibratory motion which could occur due to variation in tooth stiffness and deflection during the meshing cycle:

type (1) forced linear vibrations due to periodic transmission error,

type (2) a self-excited motion governed by Mathieu's equation which could become unstable in certain frequency ranges,

type (3) a non-linear vibration, with tooth separation, occurring at primary resonance and also at subharmonic orders of this.

The forced linear vibration case has also been studied by Johnson, 1958 (17), using receptance techniques (6). He showed that tooth dynamic load peaks are to be expected whenever a component of the transmission error curve resonates with a natural frequency of the gearing system. Examination of the error curve suggested that the most important components are at tooth meshing frequency and submultiples of this. He notes, without analysis, that tooth separation and the resulting non-linearity would produce a change of resonant frequencies and the possibility of resonance at submultiples of the velocity ratio error components.

Kohler, 1959 (18), has reviewed in detail many of the major contributions to gear dynamic loading theory in the period 1929 to 1958. He derives a generalised equation of motion for a gear pair and progressively introduces simplifying assumptions to arrive at a forced linear case which may be solved for any particular harmonic component of the transmission error function.

The theoretical analysis of Harris has been extended by Munro, 1962 (19), whose simplified equation includes many important features of the real gear pair system. In particular, tooth separation and thus non-linear vibration is allowed for. By ignoring damping, solutions of the forced non-linear equation of motion were obtained but solutions with damping considered required the use of an analogue computer. A paper by Gregory, Harris and Munro, 1963 (20), based on Munro's doctoral research, examines the torsional motions of a pair of spur gears but is primarily concerned with their non-linear behaviour due to tooth separation.

Oeppen, 1964 (21), has analysed the simplified equation, previously studied by Harris and Munro, but considered the more

general case of motions right across the backlash region. Results, derived from a mechanical analogue, suggested that running gears with little backlash could permit dangerous motions involving heavy contacts on both driving and non-driving tooth faces.

Following the work of Strauch and Harris, Bollinger and Harker, 1967 (22), have analysed the vibrational behaviour of a pair of gears without manufacturing error, whose only excitation was that due to the variation of tooth stiffness at meshing frequency. The Mathieu type equation of motion with damping and forcing terms was solved by means of an analogue computer and the results demonstrate the possibility of instability at twice the natural frequency apart from resonances at the natural frequency and a less severe one at half of this frequency. The existence of instability was shown to be a function of tooth stiffness variation and damping. A similar study involving the forced, damped Mathieu equation had earlier been reported by Böhm in 1958 (23).

In 1967, Opitz (24) simulated the dynamic behaviour of spur and helical gear pairs by means of an analogue computer. He considered excitation produced by manufacturing errors and by tooth stiffness variation throughout the path of contact. He demonstrated the influence of system variables and external disturbances on the tooth dynamic load and, for a particular configuration, compared his results with those obtained using other theoretical methods.

Although many standard methods exist for the analysis of natural characteristics of branched torsional systems (25),(26), few investigators have considered the forced vibration response in multi degree of freedom, torsional systems due to gear transmission errors. Yates, 1955 (27), has done so by employing an electrical analogy to model a marine branched system and derived solutions using

circuit theory. Tordion, 1963 (28), has applied mechanical impedance methods to the problem of gear error induced vibration. For a given applied loading, he derives an expression for critical tooth error amplitudes above which tooth separation will occur.

4.2 Experimental Literature

The A.S.M.E. Special Committee, 1931 (7), were probably the first investigators to employ the concept of a testing machine to investigate the dynamic behaviour of gears. They used a back-to-back rig with locked-in torque and the gears were electrically insulated from the machine frame so that an electric current could be passed across the tooth mesh when the gears were in contact. Earphones were connected into the circuit allowing loss of contact to be detected as an audible "click" by a listener. This approach was largely unsuccessful except for low speed tests and a second technique employing a complex mechanical linkage was also used to indicate torsional disturbances of the test gears.

More recently, strain gauges have been a particularly popular tool for the detection of tooth strains and hence the estimation of dynamic loads. Altia, 1956 (29),(30), was one of the first to use the technique for gearing studies, employing a gauge as an extensometer on one tooth of a test gear. The instrumented tooth was meshed with four different teeth of the mating gear and four sets of tooth deflections recorded for a variety of running speeds and applied loads. Mercury slip rings were used in the lead arrangement and the records were calibrated by static tests using known loads.

Utagawa, 1956 (31), 1958 (14), estimated dynamic loads from strain gauge measurements of tooth strain in a power circulating machine. He employed relatively flexible elements to decouple the gear pair from the rest of the machine. The active gauge was attached to the unloaded face of a tooth near the root fillet and three dummy gauges connected to the side of the gear. The influence of parameters such as tooth stiffness, tooth errors and contact ratio were investigated and the results show that the actual behaviour of the heavily loaded isolated gear pair was in reasonable agreement with that predicted by linear vibration theory. Richardson, 1958 (32), again using strain gauges, has independently reached the same conclusion.

Harris, 1956 (33), 1958 (12), has measured dynamic tooth stresses photoelastically, following the much earlier pioneering work of Heymans and Kimball, 1924 (34). He used test gears of Columbia Resin 39 in a power circulating machine. A spark technique assisted photography of the photoelastic stress patterns. Because it was impractical to photograph continuously, about 100 exposures were taken at intervals of a few seconds by careful synchronisation so that a succession of about 10 teeth were pictured. No appreciable non-linear vibration was detected during the experiments and it was concluded that the damping in the rig was too high for such motions. Harris also obtained continuous records of static transmission error in loaded gears. Two identical discs concentrically mounted on the test gears carried steel tapes which were led off vertically under tension provided by counterweights. Relative movement of the tapes was detected by a mirror arrangement supported from the two tapes. Over short arcs, the combined gear errors were repeatable to 5×10^{-5} in.

A large number of measurements of dynamic tooth forces have been reported by Niemann and Rettig, 1957 (35), 1958 (36), using an inductance extensometer near the tip of a particular tooth. The tooth was carried by a disc attached to one gear and the measuring system employed a 20 KHz carrier frequency. Static displacements were also measured by an inductive transducer. The authors found that the natural vibrations (at tooth meshing frequency) became more evident as the applied load decreased and as the tooth error and gear mass increased but that dynamic loads arose even with perfect gears. The maximum value for the ratio of dynamic load to applied load was 2.8 for an estimated damping ratio of 0.13 to 0.15.

Kohler, 1959 (18), 1960 (37), has measured dynamic deflections of spur gears using strain gauges and also an inductive technique similar to that of Niemann and Rettig. His rig was a power circulator and the test gears were decoupled torsionally from the rest of the machine. He also employed a slight modification of Harris' method for the continuous recording of static transmission error. The error curves were found to be continuous functions whose main harmonic components, apart from those associated with rotational period, were those of tooth interval period and its integral submultiples. Forced resonances were usually detected whenever the gear speed was such that one of these components produced a frequency coinciding with the natural frequency of the gear pair. Magnification factors of about 20 were found for small amplitude resonances but for larger amplitudes tooth separation effects prevented dynamic loads from exceeding 3 x transmitted load. The mean value of damping ratio for the rig was estimated to be about 0.025.

An experimental rig with low damping (.02 of critical) was specially built by Munro (19) in order to encourage and study non-linear gear vibrations. His high precision spur test gears were profile corrected to give nominally zero transmission error at a design load of 2000 lbf per inch face width and the gears were connected to the rest of the power circulating rig by flexible torsion rods. Continuous records of both static and dynamic transmission error were provided by an optical technique employing perspex radial gratings having 500 lines per revolution. An annular light source illuminated one of the gratings and the transmitted light was focussed concentrically onto the second grating by means of a pair of mutually perpendicular mirrors and a lens. The set-up was such that the intensity of light transmitted through the second grating during rotation varied in direct proportion to the transmission error. The method applies only to gears of 1 : 1 ratio. Munro's results confirmed that non-linear motions occurred in practice and added weight to Harris' prediction that even with perfect gears, operating at their design load, tooth separation and high dynamic loads could occur. Details of Munro's experimental work are also reported in papers by Gregory, Harris and Munro, 1963 (38), 1964 (39).

Wood, 1960 (40), and Wood and Hunt, 1964 (41), have reported investigations into the excitation of resonant vibrations in simple spur and helical gear systems. Static transmission error was measured by means of a mechanical linkage whilst resistance strain gauges attached to the gear shafts were used for the determination of dynamic torques. The authors reported a detuning of resonance usually, but not always, at light applied loads and they judged tooth separation to be responsible. It was also observed that damping varied considerably from mode to mode (.004 to .042 of critical). In relation to excitation,

it was concluded that transmission errors were the primary source of disturbance in spur gears but with helical gears a prominent factor was the variation in length of contact.

In 1963, Tordion (28) reported experiments with a back-to-back rig having gears which were dynamically isolated from the rest of the system. He employed etched foil strain gauges at the roots of eight consecutive teeth; gauge numbers 1, 3, 5 and 7 making up one bridge whilst numbers 2, 4, 6 and 8 made up a second. During contact of any particular tooth in an instrumented set, the remaining three gauges acted as dummies and hence the arrangement allowed the recording of load cycles on eight consecutive teeth.

Tordion and Gerardin, 1967 (42), have devised a technique for the measurement of dynamic transmission error in gears. Miniature accelerometers are employed to detect torsional acceleration of a gear pair. The signals are fed to an analogue computer and rotary transmission error is determined on the basis of a linear model.

In 1967, Opitz (24) reported dynamic experiments with spur and helical gears using strain gauges for the measurement of tooth strains. He observed that actual gear system resonances often occurred about 20% below the computed critical speeds and reasoned that this was due to the lowering of mean tooth stiffness by the zero contribution during periods of tooth separation.

More recently, Pratt, 1971 (43), has reported measurements of helical gear motions by means of seismic torsional vibration transducers on each of the meshing gear shafts. The transducer output signals are scaled to cater for the gear ratio and then combined to provide a picture of the gear mesh behaviour.

4.3 Discussion of Literature in Relation to this Research

4.3.1 General

It has been established by investigations reported in Section 3 that drawtwister bronze gear failures were produced by tooth dynamic loads. A number of the main contributions to knowledge in the field of dynamic loading have been summarised and it is now appropriate to briefly consider these works in relation to real geared systems exemplified by the drawtwister machine.

Almost all of the researches described earlier have focussed attention on an isolated spur gear pair which, being the simplest possible system, is particularly amenable to theoretical analysis. The vibration approaches relate dynamic loads to resonances within the one degree of freedom system comprising two gear inertias connected by a tooth mesh flexibility (which is not constant). Since the natural frequency of such a system is generally very high*, only excitations at tooth meshing frequency and higher harmonics are considered to provide system disturbance in practical speed ranges. This approach has created a bias for experimental investigations to be carried out with isolated gear pairs in order to substantiate the simplified theoretical analyses. In general, reasonable correlation has been achieved between predicted and observed dynamic behaviour although the inability to manufacture a completely isolated gear pair has produced some unexpected results (19), (21).

* Gear pair natural frequencies are often of the order of several thousand Hz.

In practice it will generally be found that gearing applications are much more complicated. In the case of a drawtwister machine, it would be difficult to achieve satisfactory mathematical modelling without considering a system of several hundred degrees of freedom. For such a complex system, the resonant frequencies are much lower than those of the comparatively simple systems studied by earlier investigators. Low frequency excitation of these real systems becomes highly relevant and higher frequency excitation, for example, tooth meshing frequency, less so. It must be emphasised that resonance constraint by damping is frequency dependent and that low frequency behaviour is notoriously difficult to control.

A second important factor in multiple gear mesh arrangements is the possibility of excitation at more than one gear mesh. The author has been unable to locate any previous theoretical treatment of this topic.

Independent experimental work (18), (35), (36), (19), (39), (24) is in remarkable agreement that maximum dynamic tooth forces are between 2 and 3 times the nominal transmitted load. Investigations into drawbox gear problems (R11),(R24) have suggested that magnification factors of order 100 times are involved in the destruction of bronze gears. An explanation for this considerable discrepancy is discussed in Section 11.3.

4.3.2 Non-Vibrational Analyses of Dynamic Loading

The semi-empirical analyses of Buckingham (1), Tuplin (2),(8),(9) and Reswick (10) all examine the transient response to isolated tooth errors. Motion is considered to be uniform before the insertion of an error function leads to dynamic loads. All resulting transient motion is assumed to subside before the next tooth contact.

These methods were the earliest attempts to calculate dynamic loads based on gear errors and, although experimental measurements (18),(24) have not verified any of them, they have gained some degree of acceptance by design engineers. This is mainly due to the relative ease with which the methods may be applied to gearing design calculations compared to the more sophisticated vibrational approaches discussed in the next section.

The treatment of isolated tooth errors may be reasonably justified in the case of slow running gears with large individual tooth errors, however, in modern gearing, speeds are generally high and individual tooth errors are normally quite small and almost identical. The dynamic effects of isolated errors thus become relatively unimportant compared to those induced by small but periodic functions and thus the problem is, in essence, one of vibration.

The methods of Buckingham and Tuplin have been applied to the drawbox gear problem (R15),(R24) (sections 3.3.7 and 3.4.1). It will be noted, however, that the gear damage pattern of once per revolution clearly involves oscillatory motions of greater time period than tooth meshing period and hence the isolated error assumption is not appropriate in this case.

4.3.3 Vibrational Analyses of Dynamic Loading

The vibrational analyses examine the forced torsional vibration response in a gear pair induced by tooth manufacturing errors and/or the non-linear variation in tooth contact stiffness. The latter is particularly important in heavily loaded precision gears where deflections under load are significant compared to zero load transmission errors. For lightly loaded gears, such as those found in the trains of a drawtwister, manufacturing errors assume a greater

importance.

Experimental measurements (31),(14),(32) have shown that, in general, heavily loaded gears behave as predicted by linear theory. More recent investigations (19),(21),(40) have found that non-linear effects such as tooth separation are often associated with light or moderate applied loads.

Although only a single degree of freedom is generally considered in the vibrating system, the inclusion of damping and non-linear stiffness elements yields an equation of motion of great complexity. In the case of the most exact mathematical models (19),(21) solution has only been possible with the aid of analogue techniques. It is clear, therefore, that a complex arrangement, such as the drawroll drive system, would require greatly simplified analytical modelling to facilitate solution. An analogue computer of unusually great capacity would be necessary to perform a non-linear study of the total system.

4.3.4 Measurement Techniques in Gearing Dynamics

The study of tooth contact/separation behaviour through changes in mesh electrical resistance was first employed by the A.S.M.E. Special Committee (7). Although their tests were, in the main, unsuccessful, the basic concept is a useful one and has been applied by the author to drawbox dynamic measurements (Section 8.2).

By far the most popular techniques have been resistance strain gauges and inductive transducers which have been used extensively to measure tooth dynamic loads. Because of the practical difficulties involved, these have, in general, only been applied to a single tooth at any one time and consequently only one

meshing cycle could be observed during rotation*. This is a serious limitation for there is no guarantee that the instrumented tooth behaviour is representative of that occurring on all of the gear teeth. Indeed, the bronze gear wear pattern described in Section 3 suggests that, during certain periods, some teeth may carry very high dynamic loads whilst others carry none at all through not making contact at any time during rotation. In torsional vibration studies, it is therefore more important to either instrument every tooth or observe the motions of the complete gear continuously during rotation.

Harris (12),(33) was one of the first to appreciate the drawbacks of individual tooth measurements, which he was able to overcome, to a certain extent, using dynamic photoelasticity. Although this technique provided records of about 10 consecutive teeth, these were obtained at intervals of a few seconds and hence during different revolutions. This could cause some difficulty in identifying short duration transients due, for example, to system non-linearities. Whilst the technique is useful in special test rig environments, it is not suitable as a measurement tool in gear boxes under normal operating conditions.

Munro (19),(38),(39) achieved notable success with an optical method for dynamic transmission error measurement. He reports, however, that considerable precision is required in setting up, and that the apparatus is susceptable to vibration. The chief limitation of the method, so far as drawbox studies are concerned, is its inability to distinguish between genuine gear motions at once per revolution and eccentricity of the optical gratings.

* The method employed by Tordion(28) is an exception.

The techniques described by Tordion and Gerardin (42) and Pratt (43) are limited by the physical requirement to attach vibration transducers directly onto the gears. Where the gears are directly attached to a shaft by means of a keyed or splined connection, the transducers may instead be mounted on the gear shafts, however, in the case of flexibly mounted gears (e.g. rubber bushed drawshaft gears) this simplification is not possible.

5. THEORETICAL ANALYSIS

5.1 Introduction

From a consideration of previous theoretical work, it is apparent that a greatly simplified model is required to analyse the complex drawtwister system. In the analysis to be described in this Section, considerable simplification is effected by ignoring all non-linear behaviour; thus, a linear theory is applied which assumes the maintenance of tooth contact at all times.

Tooth separation occurs whenever the dynamic tooth force exceeds the combined load resistance due to yarn tension, bearing friction, windage and system inertia forces. It is not surprising, therefore, that previous researches (19),(21), (40) have found that loss of contact has been more prevalent in lightly loaded systems. The application of a linear analysis is reasonable since by comparing computed vibratory loads with transmitted loads it should, at least, be possible to establish when contact would be lost. Furthermore, it is logical to suppose that those gearing stations having high vibratory forces during tooth contact also suffer the greatest impact loads after tooth separation and motion through the backlash.

The theory to be developed in this Section is based on the dynamic stiffness method, a brief summary of which appears in Appendix A.

5.2 Treatment of Relative Displacement Excitation by the Dynamic Stiffness Method

5.2.1 Assumptions

The following assumptions are made initially:-

(1) Only torsional vibration modes are considered.

(2) Bearings give rigid radial and axial support.

(3) Tooth mass is ignored.

(4) Damping is considered to be viscous in character.

(5) Tooth contact is maintained at all times and all non-linear elements are ignored.

5.2.2 Derivation

Although the theory developed (R25) is quite general, the derivation is related to the isolated drawshaft gear mesh shown schematically in Figure 5.1. The modelling of this assembly, in terms of spring, inertia and damping elements, is shown in Figure 5.2. The steel and bronze gear inertias (shown as J_C and J_E) are separated by tooth mesh flexibility F_D and the static transmission error function is considered to be inserted between J_C and J_E. Points X and Y (Figure 5.2) may be regarded as physical locations at the roots of a pair of meshing teeth so that the steel and bronze gears move with points X and Y respectively.

The dynamic stiffness method studies the response in a vibrating system due to a single harmonic excitation force (or torque) and, therefore, it cannot be directly applied to excitation by relative harmonic displacements. An adaptation is possible by the introduction of vibratory torques $T_X e^{j\omega t}$ and $T_Y e^{j\omega t}$ at

X and Y respectively. These give rise to motions θ_X and θ_Y which may be analysed by the dynamic stiffness method and related to relative displacement excitation and tooth deflection.

Consider, first, the behaviour of the system shown in Figure 5.2 when a harmonic motion $\theta_X = \Theta_X e^{j(\omega t + \phi_X)}$ occurs at point X, where Θ_X is an unknown amplitude and ϕ_X is an unknown phase angle. Referring to the dynamic stiffness analysis diagram, given in Figure 5.3, and denoting torsional dynamic stiffness by vector $\bar{K}$ and torsional dynamic flexibility by vector $\bar{F}$, we can write:

$$\bar{K}_{17} = j\omega D_G$$

$$\bar{K}_{16} = -\omega^2 J_G$$

$$\bar{K}_{15} = \bar{K}_{17} + \bar{K}_{16}$$

$$\bar{K}_{14} = \frac{\bar{K}_{15} - Z \tan\left(\frac{\omega L}{c}\right)}{1 + \frac{\bar{K}_{15}}{Z} \tan\left(\frac{\omega L}{c}\right)}$$

(where $Z = \omega J \sqrt{G\rho}$ and $C = \sqrt{G/\rho}$

and J = polar second moment of area of shaft

G = modulus of rigidity of shaft material

ρ = density of shaft material

L = length of shaft.

This equation takes account of both flexibility and distributed inertia of a shaft. The derivation is given elsewhere (46).)

$$\bar{K}_{12} = \bar{K}_{14} - \omega^2 J_E$$

$$\bar{F}_{12} = {}^{1}/_{\bar{K}_{12}}$$

$$\bar{K}_T(\text{tooth dynamic stiffness}) = {}^{1}/_{F_D} + j\omega D_D$$

$$\bar{F}_T = {}^{1}/_{\bar{K}_T}$$

$$\bar{F}_4 = \bar{F}_T + \bar{F}_{12}$$

$$\text{and } \bar{K}_4 = {}^{1}/_{\bar{F}_4}$$

The displacement function θ_X is compatible with a vibratory torque, at the tooth mesh, given by

$$T_D = \bar{K}_4 \cdot \theta_X \qquad (5.1)$$

We now consider the system behaviour when a displacement function $\theta_Y = \Theta_Y e^{j(\omega t + \phi_Y)}$ occurs at point Y, where Θ_Y is an unknown amplitude and ϕ_Y is an unknown phase angle. The analysis diagram is identical to that for excitation at X (Figure 5.3) except that:

J_E and J_C exchange places

B and F exchange places

J_G and J_A exchange places

D_G and D_A exchange places

As before, the motion θ_Y at point Y is compatible with a mesh dynamic torque $T_D^{\cdot}$ given by:

$$T_D^{\cdot} = \bar{K}_4^{\cdot} \theta_Y \qquad (5.2)$$

where $\bar{K}_4$ is the dynamic stiffness at station 4 (Figure 5.3) for the system element exchanges noted above. Obviously there can only be one transmitted vibratory torque induced by harmonic variations in velocity ratio and, because displacements θ_X and θ_Y occur on opposite sides of the mesh flexibility,

$$T_D' = - T_D \qquad (5.3)$$

The angular twist θ_D due to combined tooth deflection under vibratory torque T_D is given by

$$\theta_D = T_D \cdot \bar{F}_T \qquad (5.4)$$

Finally, it is known that

$$\begin{bmatrix}\text{Relative gear}\\ \text{deflection}\end{bmatrix} = \begin{bmatrix}\text{Static transmission}\\ \text{error}\end{bmatrix} + \begin{bmatrix}\text{Deflection}\\ \text{due to}\\ \text{dynamic load}\end{bmatrix} + \begin{bmatrix}\text{Deflection due}\\ \text{to applied load}\\ \text{and (variable)}\\ \text{tooth flexibility}\\ (\theta_L)\end{bmatrix}$$

$$\text{or} \quad (\theta_X - \theta_Y) = \theta_E + \theta_D + \theta_L \qquad (5.5)$$

Combining equations (5.1) - (5.5) gives:

$$\frac{T_D}{\bar{K}_4} + \frac{T_D}{\bar{K}_4'} = \theta_E + T_D \cdot \bar{F}_T + \theta_L$$

and after simple manipulation:

$$T_D = \frac{(\theta_E + \theta_L)}{\bar{F}_4 + \bar{F}_4' - \bar{F}_T}$$

More generally, dynamic tooth load T_D may be expressed as:

$$T_D = \frac{\dot{\theta}_E + \dot{\theta}_L}{\bar{F}_{R1} + \bar{F}_{R2} - \bar{F}_T} \qquad (5.6)$$

where $\bar{F}_{R1}$ is the dynamic flexibility of the part of the system seen outwards from the tooth root of one gear,

$\bar{F}_{R2}$ is the dynamic flexibility of the part of the system seen outwards from the tooth root of the other gear.

5.3 Modelling of Drawtwister

5.3.1 Further Assumptions

The following further assumptions are now introduced in relation to the particular application:

(6) Variable tooth stiffness effects do not contribute any excitation to the system. This assumption is reasonable since drawbox gears are lightly loaded in all operating conditions. Equation 5.6 becomes:-

$$T_D = \frac{\dot{\theta}_E}{\bar{F}_{R1} + \bar{F}_{R2} - \bar{F}_T} \qquad (5.6a)$$

(7) All excitation occurs at the parallel helical gear mesh.

(8) Only excitation at the fundamental period of gear rotation is considered.

(7) and (8) are consistent with the bronze gear wear pattern - reported in Section 3.

(9) The actual dynamic load at a particular gear mesh depends not only on that generated by the errors at that mesh but also on contributions from all other mesh stations. Thus the dynamic torque T_D derived from equation (5.6a) creates vibratory torques at all other gearing stations which the dynamic stiffness method calculates by feeding T_D to both ends of the machine via all other drawshaft gear mesh stations. The actual gear dynamic loads for each gear pair are given by the vector summation of all contributions. Hence in a machine with NBM boxes, each helical gear pair will transmit dynamic loads which have 1 direct contribution from local gear errors together with (6 x NBM) - 1 contributions from gear errors in the rest of the machine.

A further assumption is implicit in this approach, i.e.

(10) that the principle of superposition holds throughout the system.

5.3.2 Drawbox Model

Figure 5.4 shows the layout of all inertias and spring elements considered in the mathematical idealisation of a single drawbox. The inertia values of layshaft sections are considered to be lumped at the layshaft gear stations but allowance is made for inertia distribution and diameter steps in the drawshaft. Damping elements have been omitted from Figure 5.4 for clarity and are discussed later (Section 5.5.3).

To calculate dynamic torques at a particular gear mesh (induced by transmission errors at that mesh) using equation (5.6a) requires a knowledge of system dynamic flexibility with respect to

tooth roots of both steel and bronze drawshaft gears. This will depend not only on the mesh position within the drawbox but also on the position of the drawbox within the total machine. Thus, six pairs of dynamic stiffness analysis diagrams are required for the six gearing stations within a box together with a further pair of diagrams for the transference of dynamic stiffness both ways across each box. In practice, however, the diagrams have much in common and it is only necessary to reproduce four of these as shown in Figures 5.5 - 5.8; the full range of transmission paths being accounted for in the computer program described later.

5.3.3 Headstock Model

For any particular MDT. machine, it is necessary to evaluate the dynamic stiffness of the headstock including those systems, such as feedrolls and spindles, driven by the headstock. This value is then considered to be attached at the appropriate position in drawbox number 1.

5.3.3.1 Type C [redacted] Headstock

A schematic layout of the type C headstock arrangement is shown in Figure 2.7. The upper drawboxes have been modelled in the same way as the lower boxes except that no excitation functions have been inserted since no gear problem has ever been associated with the much slower running upper boxes.

In the absence of accurate information on the various belt and shaft stiffnesses, the headstock model has been simplified by ignoring all spring elements. Thus, all speed reduction ratios due to gearing and belting pairs are accounted for in computing equivalent inertias of the headstock, spindle and feedroll assemblies

with respect to drawroll rotational speed.

The total dynamic stiffness of the headstock and associated assemblies will depend on the various shaft speed ratios and hence on the operating spindle speed, drawratio and delivery speed. It will also depend on the yarn package inertia which, of course, varies continuously during commercial operation.

5.3.3.2 Type A Headstock

The type A headstock has been modelled in the same way as the type C, using the appropriate design drawings, except that upper drawboxes are excluded.

5.3.3.3 Type B and Type E

The type B and E headstocks are considered to be the same as those of type A and type C respectively*.

* This is not strictly correct in practice for both type B and type E machines can employ two independent D.C. motors in machine options incorporating programmable spindle speeds. Theoretical results discussed in Section 6 suggest, however, that such a refinement in the headstock would not significantly influence the drawbox system dynamic behaviour.

5.4 Main Computer Program

The analytical method described in the foregoing sections requires such a high volume of calculation that solution is best handled by digital computer. The theroetical results presented in this thesis were obtained by means of the Loughborough University ICL 1904A computing system. The author's main program is listed in Appendix C and a brief outline of the more important steps in calculation is now given.

For a machine configuration selected for computer analysis, the operating conditions, such as spindle speed, drawratio and delivery speed, are supplied as input data followed by the values for the various inertia, flexibility and damping elements. A list of input data relating to machine parameters is given in Appendix B.

After reading all input data from punched cards, the program determines the dynamic stiffness of the headstock system* for attachment to box number 1. This is facilitated by means of three subroutines which cover the following drive arrangements:-

1. Polyamide machine headstock (type A and type B)
2. Polyester machine headstock (type C and type E)
3. An A.C. motor and variable speed unit driving a simple drawbox system.

It is convenient to proceed from gear mesh position 1 in box number 1 (the position nearest to the headstock/drive unit) to

* or the drive unit, when a simplified experimental rig is being analysed - see Section 7.

position 6 in the last box. For any particular gear mesh, it is necessary to compute the two dynamic flexibilities at the tooth roots, taking account of the total system. Mesh transmission error amplitude and phasing are assigned on the basis of uniform probability distribution and then the (direct) tooth dynamic torque may be derived using equation (5.6a). The indirect vibratory torques induced at the other five meshes in the same box are calculated by tracing dynamic torque flow to the ends of the box.

After computing the shaft deflection at the driven end of the drawbox together with all dynamic stiffnesses in the next box, at this end, the induced torques at the mesh stations in this box may be found. The procedure is repeated until position 1 in box 1 is reached whereupon attention is focussed on the drawboxes on the "tail" side of the box in which excitation is being considered, thus providing all mesh induced torques up to position 6 in the last box (number NBM). The one direct dynamic load and the (6 x NBM) - 1 induced dynamic loads are added vectorially to all values previously computed for the respective gear stations.

The dynamic flexibilities and transmission error amplitude and phasing are then determined for the next excitation mesh considered and another series of dynamic torques computed, leading to a further updating of the stored values. When each gear station has been considered as an excitation source, the procedure is terminated and the modulus of each resultant vector gives the overall dynamic torque for the appropriate mesh.

On an ICL 1904A computing system, the main program run time is about 21 minutes when all dynamic loads are computed for a 10 box machine operating from 1000 to 4000 r.p.m. in steps of 50 r.p.m. The program requires a core area of about 20 K.

Natural frequency analysis is particularly straightforward with the dynamic stiffness approach and required only a simple modification to the main program. The total system dynamic stiffness is plotted against machine speed to reveal critical speeds whenever the overall dynamic stiffness is zero.

5.5 Summary of Computer Program Functions

A number of FORTRAN computer programs and subroutines have been developed by the author for various aspects of the theoretical study. These are now briefly summarised.

5.5.1 Programs for the Computation of Machine Behaviour

MAIN PROGRAMS

"DT TOTAL ANALYSIS" (program statements are listed in Appendix C) - Computes dynamic loads at every helical gear mesh in a drawbox system, due to transmission error excitation at all meshes. Two series of random numbers are generated to assign typical production variations in error magnitude and phasing throughout the theoretical model.

SUBROUTINE "CROSSBOX" (Appendix D) - Computes the dynamic stiffness values, in any drawbox, with respect to either the machine headstock end or the "tail" end. The left hand and right hand total dynamic stiffnesses for any box are also calculated to facilitate the transfer of attention throughout the system.

SUBROUTINE "BOXTORK" (Appendix E) - Computes the dynamic torques at all helical gear mesh stations in a particular box, due to the action of a vibratory torque applied at either end of the layshaft.

SUBROUTINE "MDT. 2 DRIVE" (Appendix F) - Computes the headstock dynamic stiffness for polyamide machines. This is "attached" to box number 1 in the main program.

SUBROUTINE "MDT. 3 DRIVE" (Appendix G) - Computes the headstock dynamic stiffness for polyester machines. This is "attached" to box number 1 in the main program.

SUBROUTINE "VS DRIVE" (Appendix H) - Computes the drive system dynamic stiffness of the experimental rig for attachment to box number 1 in the main program. (The rig is described in Section 7).

SUBROUTINE "GEAR DATA" (Appendix I) - Computes the inertia values of gears used in drawtwister headstocks. The main gear variables are:- size, material and design. "GEAR DATA" is used in conjunction with "MDT.2 DRIVE" and "MDT. 3 DRIVE".

5.5.2 Programs for the Manipulation and Graph Plotting of Output Data

PROGRAM "SPEEDPLOT" (Appendix J) - Plots dynamic torques through any specified speed range for all mesh positions within a total machine or experimental rig.

PROGRAM "HISTOPLOT" (Appendix K) - Plots a histogram of dynamic torques throughout a machine (or rig) for any specified speed.

PROGRAM "HISTOLIMIT PLUS" (Appendix L) - For any number of "theoretical" machines operating at the same or different speeds the program plots, in histogram form,

(a) the maximum and minimum dynamic loads occurring anywhere within the total machine,

and

(b) the average dynamic loads at every particular station within the total machine.

5.6 Discussion of Machine Parameters

5.6.1 Gear Mesh Transmission Error

The general form of the transmission error curve is:

$$\theta_E = \sum_n \textcircled{\#}_n \cos(n\omega t + \phi_n) \qquad (5.7)$$

$$n = 1,2,3....$$

or, in complex form:

$$\theta_E = \sum_n \textcircled{\#}_n e^{j(n\omega t + \dot{\phi}_n)} \qquad (5.7a)$$

$$n = 1,2,3....$$

where $\textcircled{\#}_n$ is the error component amplitude and ϕ_n is a phase angle.

In this research, interest centres on the fundamental error at a period of one revolution. Measurements (R4) of pitch error have given a typical amplitude of .0005 in. For a pair of meshing gears, the worst case will be where these amplitudes are fully cumulative,

i.e. Maximum pitch error amplitude = 2 x .0005 in. = .001 in.

Further measurements (R24) have identified maximum gear mounting eccentricities of .003 in. Again, the worst case will be when the eccentricities are fully additive giving a combined error in concentricity of .006 in. The effect of this radial displacement is to close the mesh by .006 in. For two 20 degree pressure angle, 45 degree helix angle gears, this gives a relative rotation of:

$$\frac{.006}{\sin 45^\circ} \cdot \sin 20^\circ = .00145 \text{ in.}$$

The possible maximum equivalent pitch error amplitude =

.001 in. + .00145 in. = .00245 in.

or $\frac{.00245 \times 2}{2.357 \text{ in}}$ = .0021 radians.

A chance pair of gears could be produced such that no significant transmission error would exist. On the other hand, when all errors are fully cumulative, an error amplitude of .0021 radians could occur. Most gear pairs will be somewhere between these limits and, because the equivalent error is the sum of several contributions, it is assumed that a random distribution with uniform probability governs both amplitude and relative phasing of gear pair transmission error (Michalec (47) and Welbourn (48) have suggested that individual errors follow a Gaussion probability).

For the fundamental of transmission error, equation 5.7(a) may be written:

$$\theta_{E1} = \textcircled{\pm}_1 \cdot e^{j\phi_1} \cdot e^{j\omega t} \qquad (5.8)$$

In the computer program,error magnitude and phasing are accounted for by introducing two random numbers A and B, which can lie anywhere between zero and unity, and putting

$$\textcircled{\pm}_1 = \text{ERR} \times \text{A radians}$$

where ERR is the maximum error amplitude (.0021 radians) and

$$\phi_1 = 2\pi \times \text{B radians.}$$

In this way, production distributions may be taken into account by introducing new random numbers A and B for each helical gear mesh. Before inserting θ_{E_1} (eq. 5.8) into equation 5.6(a) the factor $e^{j\omega t}$, which is common to all excitations, is omitted and the remaining expression is rearranged to the more convenient form:

$$\theta_{E1} = (ERR \times A)\cos(2\pi B) + j(ERR \times A)\sin(2\pi B) \qquad (5.9)$$

5.6.2 Tooth Contact Flexibility

One of the first theoretical studies of static load/deflection relationships in helical gear teeth was due to Merritt, 1942 (49), who considered the teeth to comprise a large number of independent thin slices operating in parallel. A more rigorous treatment was given by Weber and Banaschek, 1950 (51), following the work of Weber, 1949 (50), on spur gear tooth flexibility. Again, the complex helical tooth geometry was simplified by the consideration of thin slices. More recently, Seager, 1967 (52), and Niemann and Baethge, 1970 (74), have reported more complete studies of tooth flexibility in helical gears.

Seager's analysis has been used to derive the drawshaft mesh flexibility of 6.5×10^{-7} rads/lbf.in. used for theoretical computation in this thesis. It should be noted that this is only a typical value of a quantity which varies throughout the tooth meshing cycle. Even ignoring tooth separation effects, the flexibility will vary with time depending on the phase of engagement and the tooth overlap ratio. Mesh flexibility becomes infinite whenever separation occurs and clearly the time averaged flexibility will depend on the proportions of time spent in normal engagement and separation.

In the absence of relevant published information, the flexibility of a drawbox crossed helical mesh was assumed to be the same as that for a parallel axis mesh, i.e. 6.5×10^{-7} radians/lbf.in.

5.6.3 Damping

5.6.3.1 General

Damping is a general term relating to all those factors which dissipate energy from a vibrating system to the surroundings. The presence of damping prevents the theoretical concept of constant amplitude free vibrations from occurring in practice, that is, a constant amplitude oscillation cannot exist unless a continuous excitation replenishes energy dissipated by damping. Damping is particularly important at resonance for its presence is all that limits amplitude growth and hence dynamic stresses.

Torsional systems are generally only lightly damped although three main sources may exist.

Viscous damping is proportional to velocity and energy dissipated by this mechanism is proportional to frequency and the second power of displacement. It is particularly amenable to modelling by theoretical methods and occurs in practice when relative motion takes place across a fluid film such as in film lubricated journal bearings.

Hysteresis damping occurs because no material is perfectly elastic even at low stresses. Thus, during a cycle of loading, a hysteresis loop is formed in the stress/strain diagram and this represents energy absorbed by the material. Material hysteresis is very complex (53) and depends on material, temperature, vibration amplitude, material heat treatments, previous stress history and other factors. Hysteresis damping is often modelled by means of an "equivalent" viscous damping coefficient (54).

Coulomb (or solid friction) damping is proportional to normal applied load and is independent of both frequency and vibration amplitude. Dissipated energy is proportional to normal load and vibration amplitude. Coulomb damping occurs at the interface of sliding surfaces, for example, in keyed or splined shaft connections, sleeve bearings and in heavily loaded gear teeth. An "equivalent" viscous damping coefficient is sometimes employed to facilitate linear theoretical analysis.

Other sources include impactive damping, which dissipates energy by the generation of shock waves in solid or fluid media, and windage loss.

5.6.3.2 Damping in the Drawtwister System

The following are considered to be the most likely sources of damping in the gear-train system:

1. Drawrolls - due to the threadline* and windage provided by surface boundary layer drag.
2. All shafting - due to hysteresis loss.
3. All bearings - due to both hysteresis and coulomb damping.
4. All gear and drawroll mountings - due to coulomb damping.
5. All gear meshes - due to viscous oil shear between teeth, impact, tooth hysteresis and windage.
6. Rubber bushed gears - as for (5) above, plus significant damping due to bush hysteresis.
7. Drawbox Couplings - due to bush hysteresis and air windage. (Standard type)

* Evidence of threadline damping is given in Section 3.4.3.4.

In the theoretical analysis, damping is considered to be viscous in type and lumped at or between inertia stations as shown in Figures 5.5 - 5.8. To provide some basis for the allocation of system damping coefficients, critical damping coefficients were computed for fundamental mode vibrations of various sub-systems. The results are quoted in Table 5.1. The theoretical damping considered at any particular system location can be related to sub-system critical damping. Such an approach is somewhat arbitrary and crude, the only justification being that, without some approximation, it would not be possible to analyse real damped systems.

Some guidance to typical damping ratios may be obtained from the literature. Table 5.2 gives a summary of estimates made by investigators in relation to particular test rigs*. After an extensive study of damping in geared systems, Ashfield, 1969 (55), concluded that such estimates could easily be in error by over 100%. Until knowledge of system damping is greatly increased, however, the quoted values are useful in setting typical orders of magnitude.

Using published estimates as a guide, the following lumped damping coefficients are assumed to model those occurring in standard practice:-

1. at both helical and crossed helical gear meshes - .025 DA
2. at all drawrolls - .010 DB
3. due to box coupling bushes - 0.10 DC
4. at all layshaft gears and box couplings - 0.0001 DC
5. due to rubber bushes in bushed gear units - 1.0 DA

* In addition, reference (27) presents a discussion of damping in a practical application - a marine geared system.

TABLE 5.1

CRITICAL DAMPING COEFFICIENTS FOR DRAWBOX SUBSYSTEMS

	Vibrating System and Mode	Theoretical Critical Damping Coefficient
Case A	Gear connected to drawshaft flexibility and oscillating about a node at the drawroll end.	DA = 25 lbf.in. sec/rad.
Case B	Drawroll and drawshaft with drawroll oscillating about node at gear end.	DB = 145 lbf.in. sec/rad.
Case C	Layshaft with half coupling inertias fitted to each end - first torsional vibration mode	DC = 312 lbf.in. sec/rad.

TABLE 5.2

ESTIMATED DAMPING RATIOS

FOR EXPERIMENTAL GEAR RIGS

Investigator(s)	Estimated Damping Ratio (= $\frac{\text{actual damping}}{\text{critical damping}}$)
Niemann and Rettig (35)(36)	0.13 - 0.15
Kohler (18)	0.025
Munro (19)	0.020
Wood and Hunt (41)	0.004 - 0.042
Oeppen (21)	0.036

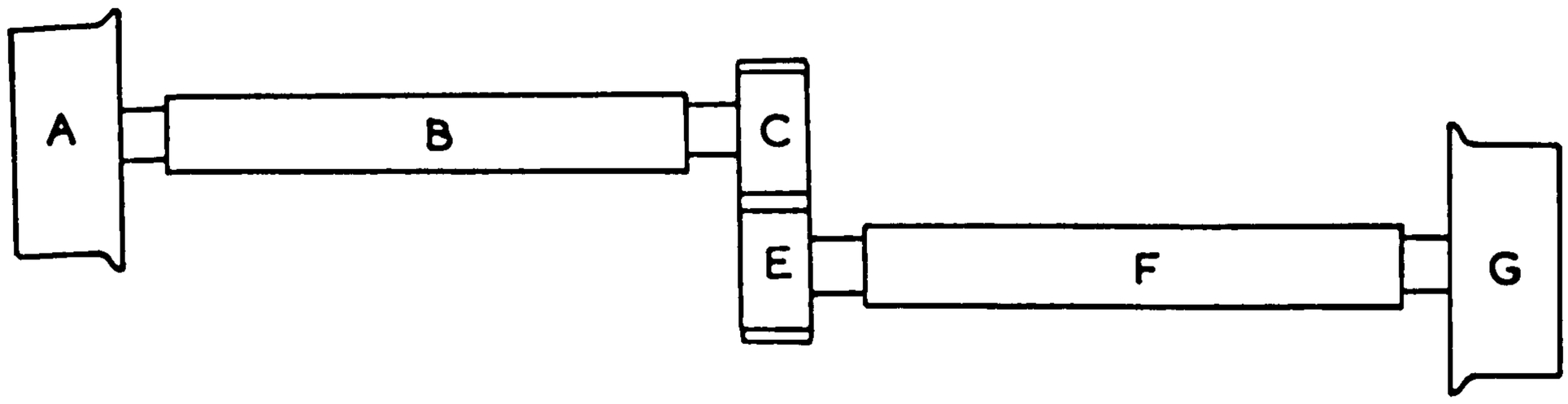

FIG. 5.1 ISOLATED DRAWROLL PAIR

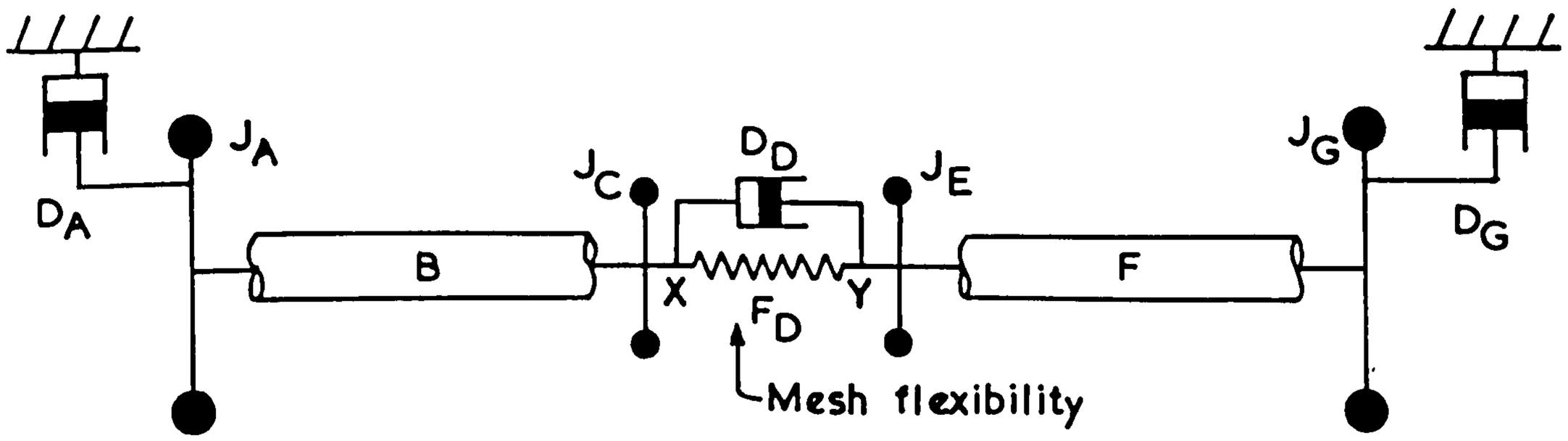

FIG.5.2 SYMBOLIC LAYOUT OF BASIC ELEMENTS FOR DRAWROLL PAIR

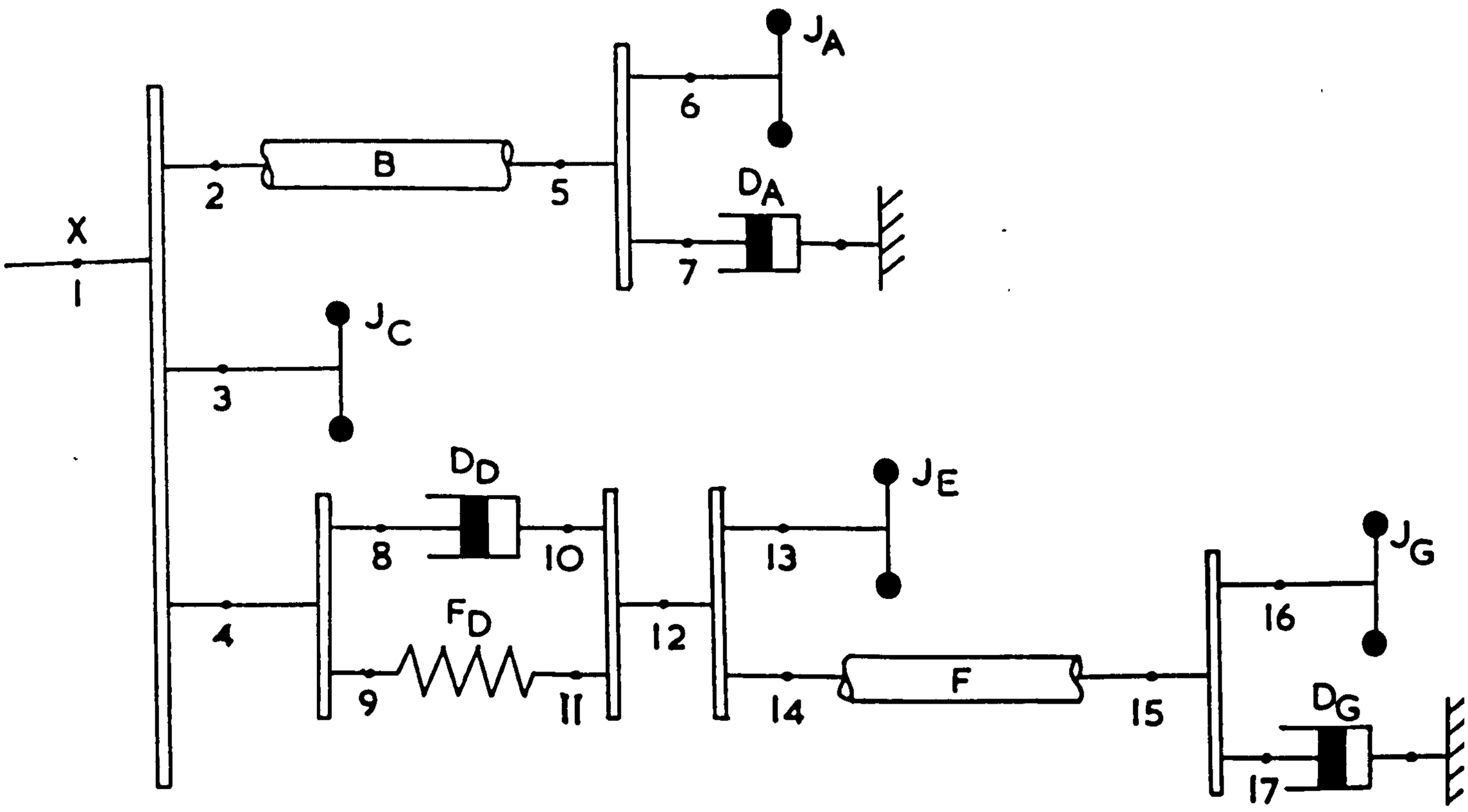

FIG. 5.3 DYNAMIC STIFFNESS ANALYSIS DIAGRAM FOR DRAWROLL PAIR EXCITED AT POINT 'X'

INERTIAS

J_1, J_8	half box coupling
$J_2 - J_7$	layshaft gear + shaft section
J_9	bronze drawshaft gear
J_{10}	steel " gear
J_{11}	drawroll

FLEXIBILITIES

F_1	box coupling
$F_2 - F_8$	layshaft sections
F_{10}	crossed helical mesh
F_{11}	parallel " mesh
F_{12}	drawshaft

DAMPERS

FD_1	box coupling
FD_{10}	crossed helical mesh
FD_{11}	parallel " "
$D_1 - D_{11}$	associated with inertias $J_1 - J_{11}$ (but not shown)

NOTE all drawroll pair branches are identical

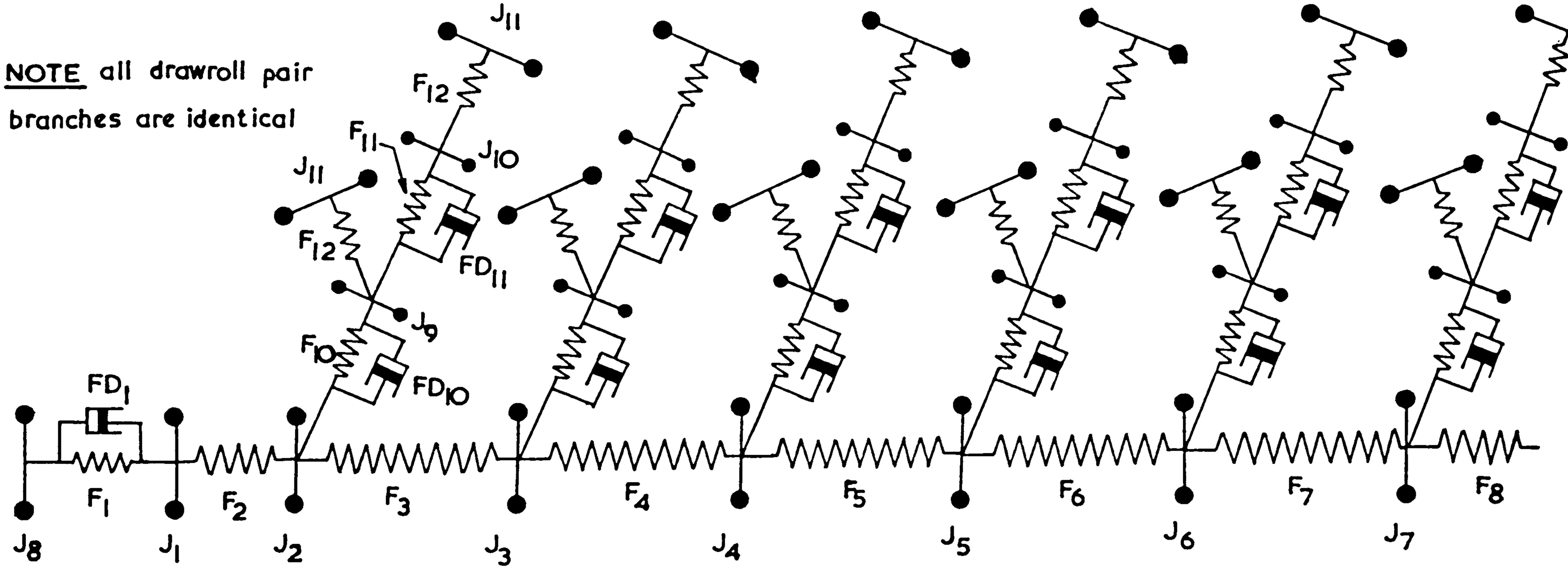

FIGURE 5.4 SYMBOLIC LAYOUT OF BASIC ELEMENTS FOR ONE DRAWBOX

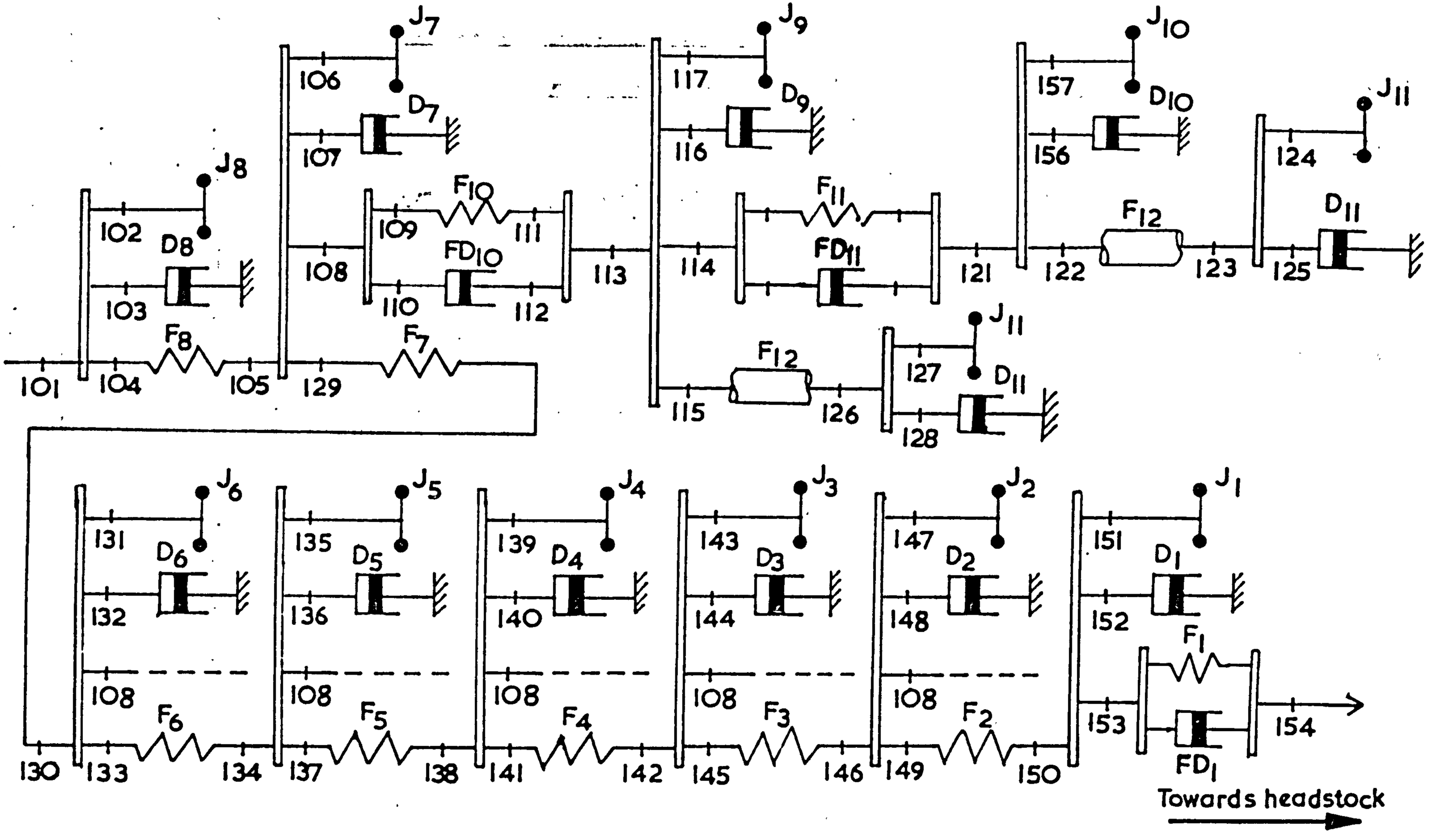

FIGURE 5.5 DYNAMIC STIFFNESS ANALYSIS DIAGRAM FOR TRANSFER ACROSS A COMPLETE DRAWBOX

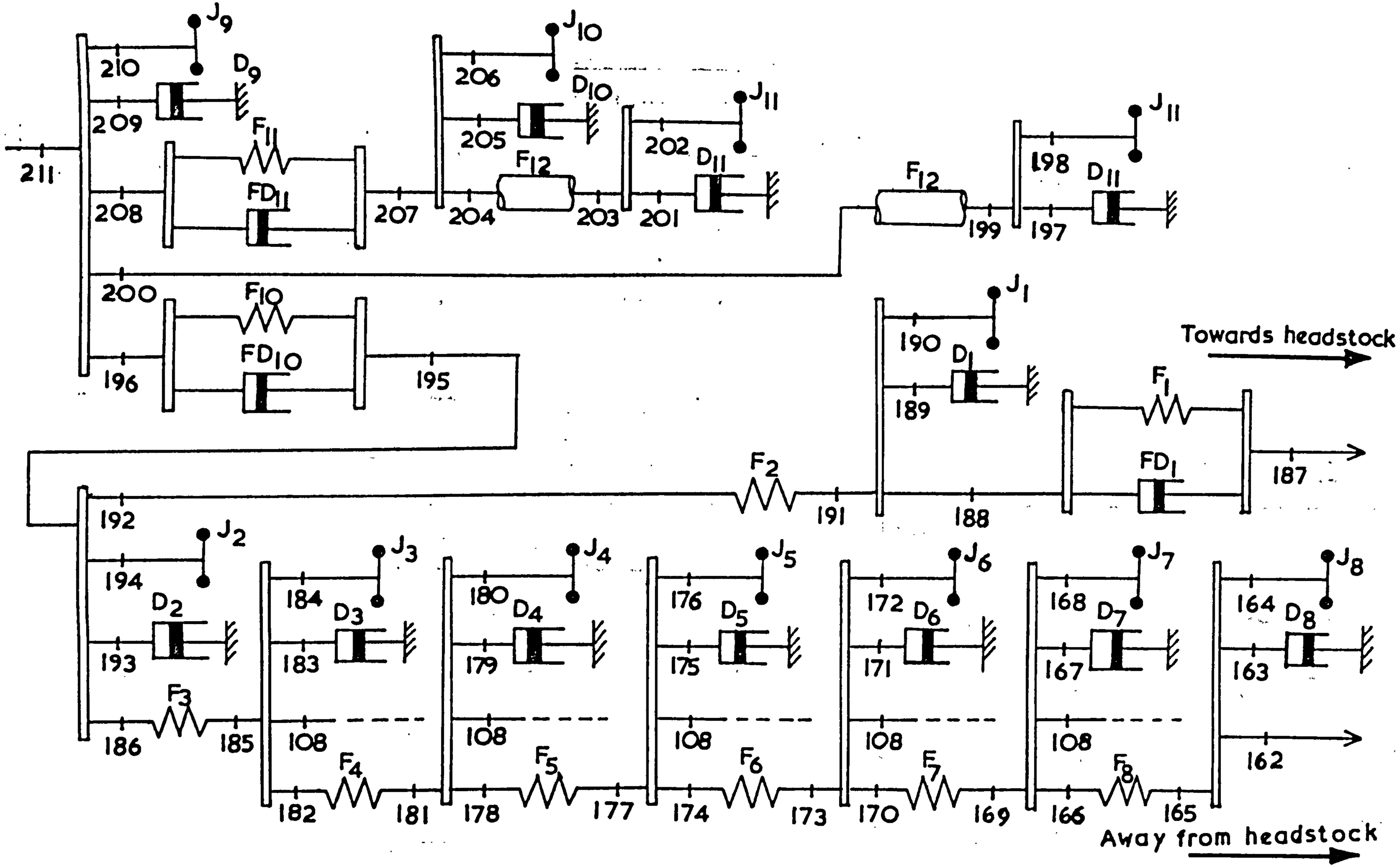

FIG. 5.6. DYNAMIC STIFFNESS ANALYSIS DIAGRAM FOR EXCITATION AT TOOTH ROOT OF BRONZE GEAR No. 1 IN ANY DRAWBOX

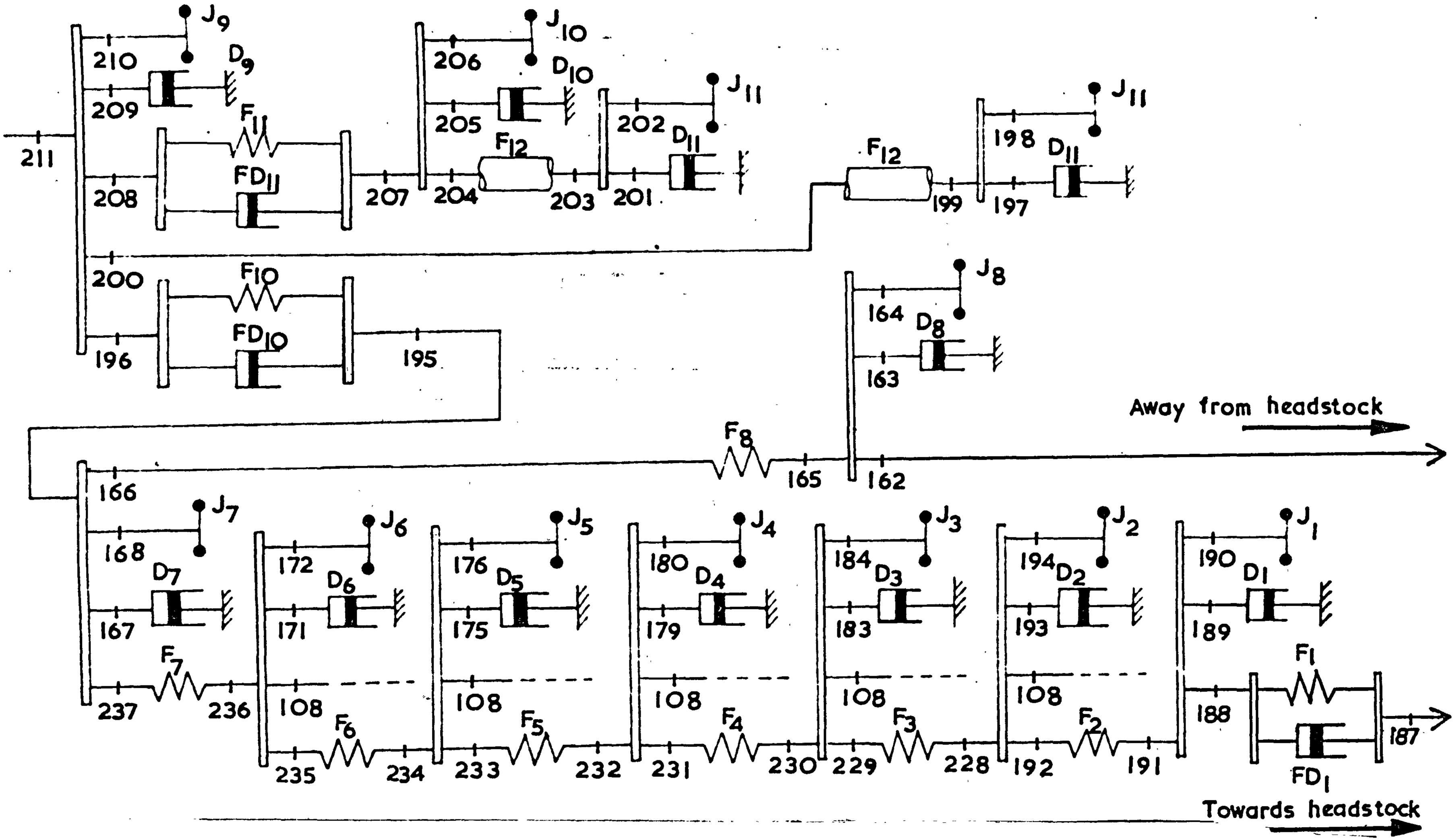

FIG. 5.7 DYNAMIC STIFFNESS ANALYSIS DIAGRAM FOR TOOTH ROOT EXCITATION OF BRONZE GEAR NO. 6 IN ANY DRAWBOX

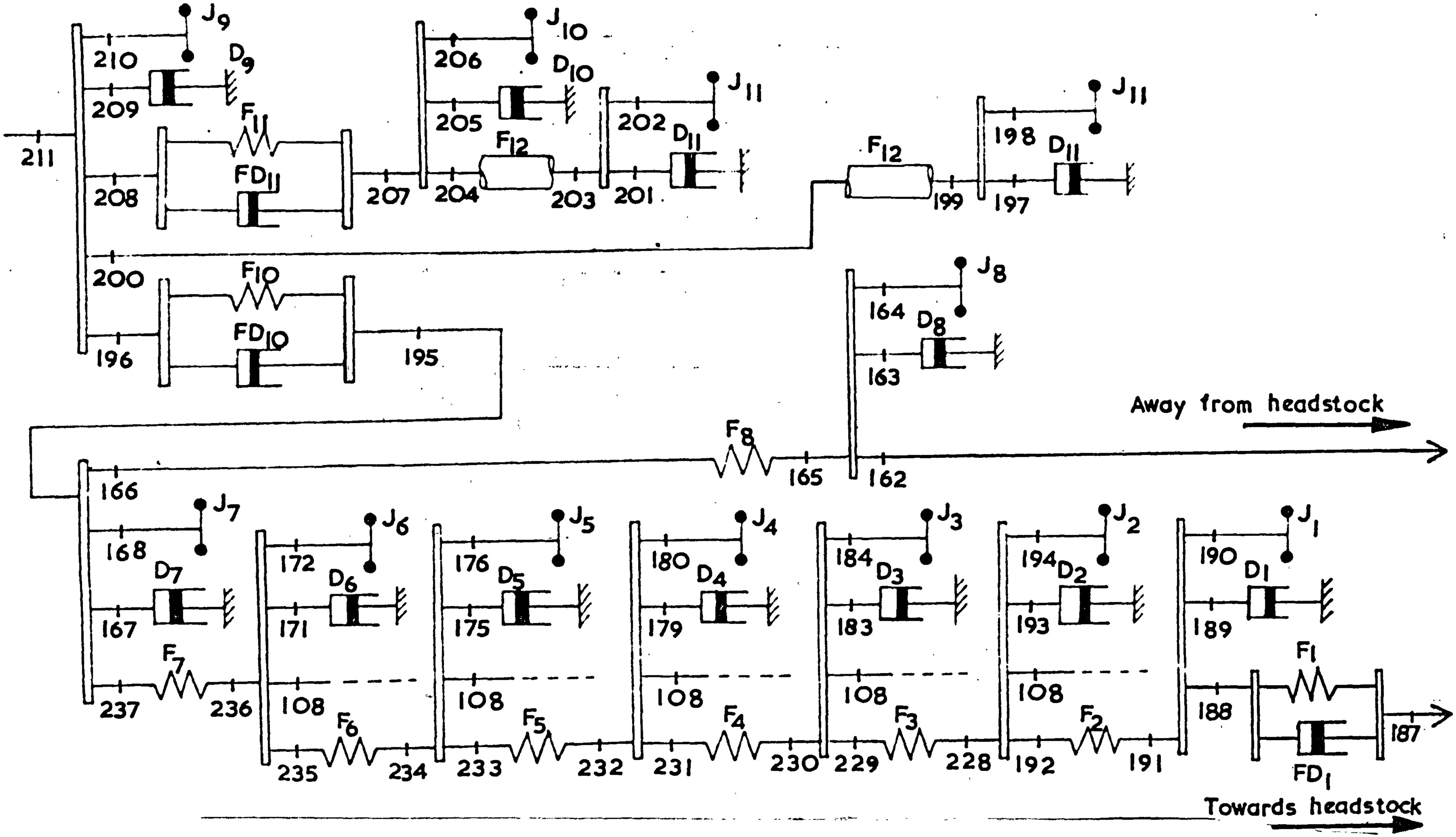

FIG. 5.7 DYNAMIC STIFFNESS ANALYSIS DIAGRAM FOR TOOTH ROOT EXCITATION OF BRONZE GEAR NO. 6 IN ANY DRAWBOX

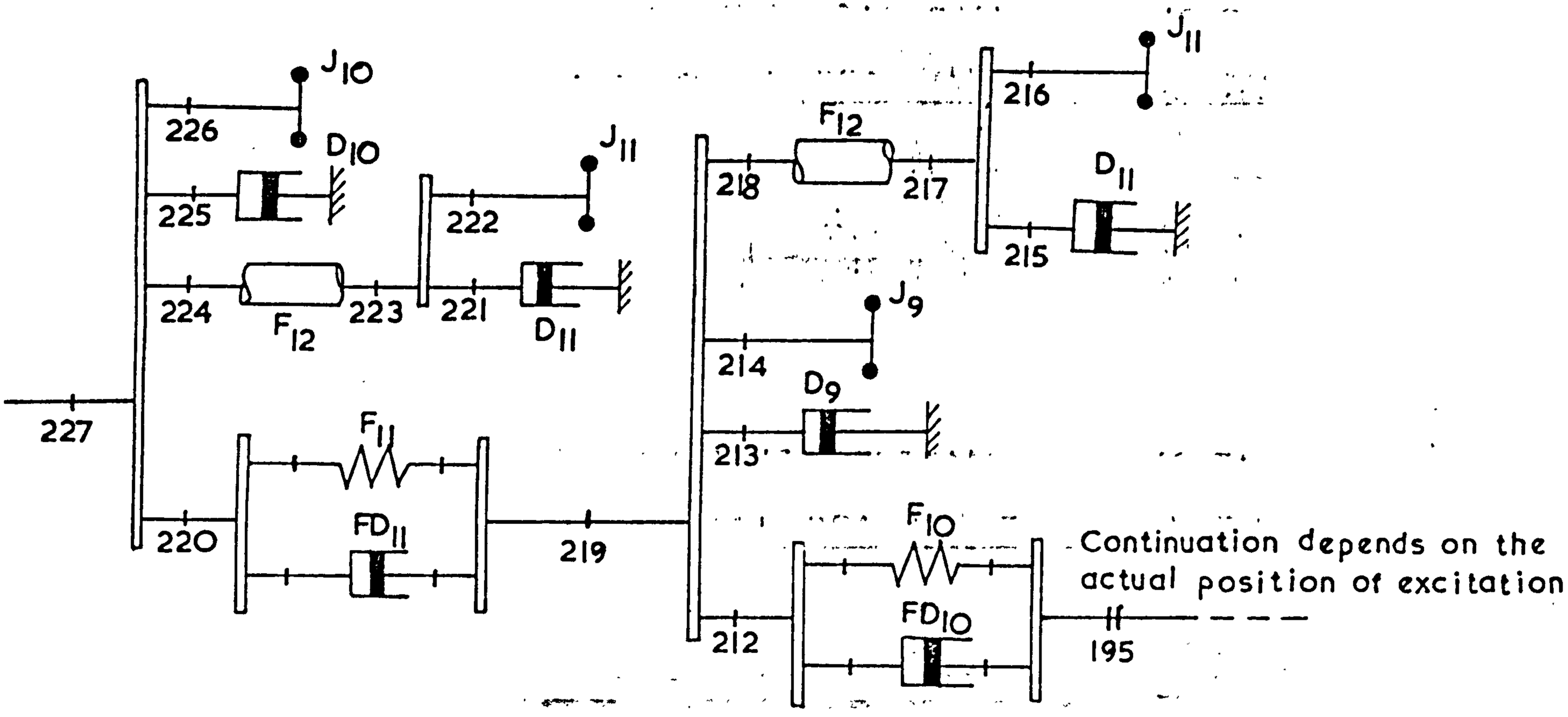

FIGURE 5.8 DYNAMIC STIFFNESS ANALYSIS DIAGRAM FOR EXCITATION AT THE TOOTH ROOT OF ANY STEEL DRAWSHAFT GEAR WITHIN A BOX

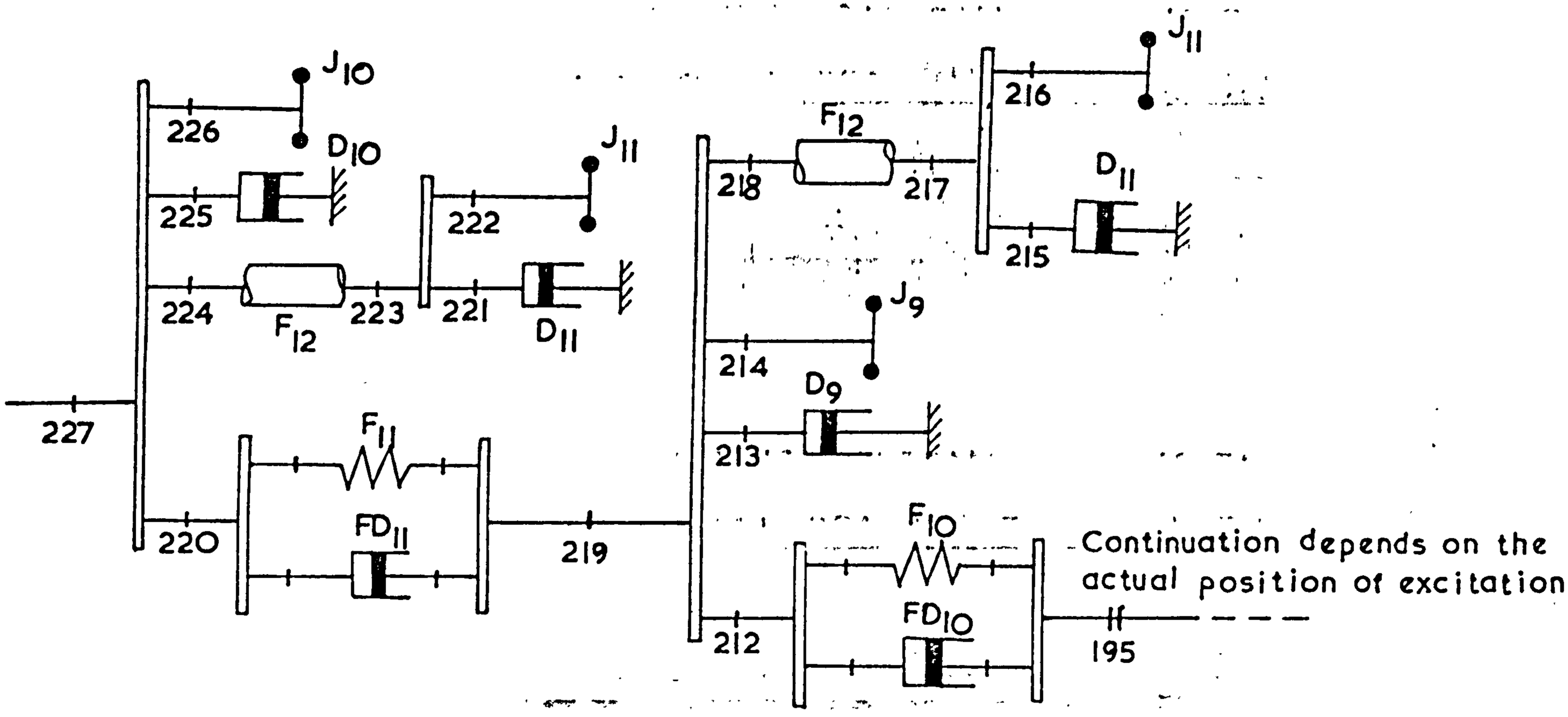

FIGURE 5.8 DYNAMIC STIFFNESS ANALYSIS DIAGRAM FOR EXCITATION AT THE TOOTH ROOT OF ANY STEEL DRAWSHAFT GEAR WITHIN A BOX

6. THEORETICAL RESULTS

6.1 Introduction

The theoretical method outlined in the previous section has been applied to a number of machine configurations. Several hundred graphical records have been produced in all and a small sample of these is presented, and briefly discussed, in this section. For standard machine arrangements, the damping values used are as given in Section 5.6.3.2 and all other data required for computation are given in Appendix B. Unless otherwise stated, all results and discussion relate to 10 box machines of standard construction.

6.2 TYPE A and TYPE C Drawtwisters with Solid Gears

Computed results showed that the dynamic response of the TYPE C gearing system was almost identical to that of the TYPE A despite the presence of upper drawboxes and a modified headstock. Consequently, all results presented in this section are considered to relate equally to each type of drawtwister.

Figure 6.1 depicts the typical forced response behaviour of all helical meshes in box number 10* of a 10 box machine. The curves for each mesh are similar in shape and highlight very severe dynamic load peaks, particularly at about 2450 and 3400 r.p.m., where loads are of the order of 10,000 lbf.in. The latter peak would not have been encountered in practice since operating speeds did not exceed 1000 m/min (about 2500 r.p.m.) before the phasing out of solidly

* boxes are numbered in sequence starting with number 1 at the headstock end of the machine.

mounted gears in the period 1969-1972. Interest therefore centres on the range 1000-2500 r.p.m. Within this range, gear failures have been reported occurring at around 1200 r.p.m. (R1),(R2), 1700-1800 r.p.m. (R1),(R2),(R24) and 2260-2500 r.p.m. (R7),(R24)*.

A delivery speed of 3080 ft/min. (2355 r.p.m. drawroll) was thought to produce the greatest number of failures in installations where this speed had not been exceeded. Figures 6.2 and 6.3 show typical histograms of dynamic loading distribution at this speed. The difference between these two diagrams is due entirely to differences in the random numbers which were employed to represent gear error amplitude and phase relationships, for two otherwise identical theoretical machines, operating at the same speed. Figure 6.4 shows the maximum and minimum torque limits derived from 10 such theoretical machines based on production distributions of gear errors. A wide variation is observed, for example, in box 10 where dynamic torques vary from 60 lbf.in. to about 3000 lbf.in. according to the distribution of gear errors, including phasing, throughout the system. These results suggest the possibility that both "good" and "bad" machines may be produced by what appear to be identical manufacturing techniques.

An average loading distribution taken from 10 systems operating at 2355 r.p.m. is given in Figure 6.5. The general shape is that of a third layshaft system resonance having nodal points at the first, fifth and ninth flexible couplings, counting from the headstock.

* It should be remembered that the MDT. 2 and MDT. 3 models employ charge gears in the headstock to vary the delivery speed and, therefore, only a finite number of possible operating speeds exists.

Peak amplitudes are reduced as the headstock is approached due to its high inertia dominance. In general, loading distributions at this speed were similar in shape to Figure 6.5, however, certain transmission error combinations produced departures from this general rule. Examples are given in Figures 6.6, 6.7 and 6.8 which illustrate unexpected peaks in boxes 4,5 and 9 respectively. These results suggest that, in practice, the worst boxes in terms of severe dynamic loading, are not governed solely by modal considerations. Furthermore, it seems likely that "rogue" boxes can occur within a machine owing to error combinations and, indeed, the behaviour in a particular drawbox might, in some cases, be more influenced by remote gear meshes than those within that drawbox*.

A typical mesh loading distribution at 1750 r.p.m. is shown in Figure 6.9. Peak amplitudes are generally lower than those occurring at 2355 r.p.m. but, nevertheless, loads of this magnitude could certainly account for premature failures reported in the region of 1700-1800 r.p.m.

Although Figure 6.1 illustrates a significant peak at 1200 r.p.m. this could not have accounted for many gear failures in practice, especially since 1965, for machines were normally operated in excess of this speed.

In general, the dynamic loading distributions discussed in the foregoing show a characteristic shape for a given speed. This suggests that, in practice, gear failures occurring in any machine would not be randomly distributed but would form a definite pattern according to.

* Subsequent investigation, reported in Section 10.4, has revealed evidence of this behaviour.

the loading distributions, although some masking effect would be expected from multiple speed running. At the time these results were computed only one previous investigation (R24) had uncovered evidence of failure distributions and this was considered insufficient for meaningful comparisons. Discussion of this topic is therefore delayed until Section 10 where further evidence of machine performance in service is presented.

6.3 Influence of Machine Operating Variables

6.3.1 Draw Ratio

A lowering of the draw ratio increases the feedroll speed with respect to the drawroll speed and therefore modifies the dynamic stiffness attached to box number 1. It was found, however, that a variation in draw ratio within the limits of the performance specification (1.0 to 6.0) produced no significant change in the drawbox system response. The influence of cold draw ratios (from 1.0 to 3.0) in polyester machines was, similarly, found to be negligible.

6.3.2 Spindle Speed

Spindle speed is independent of drawroll speed and may be set to a large number of values in the range 5000 to 12,000 r.p.m. Computed results showed machine dynamic behaviour to be insensitive to any changes within this range.

6.3.3 Spindle Package Inertia

Total system inertia varies continuously through production as yarn is fed to the spindle package. The maximum yarn inertia at each spindle was calculated on the basis of a 6 lb. cylinder rotating with an effective diameter of 3 in. (Minimum yarn inertia is zero - at the start of production). Again it was found that machine behaviour was independent of this operating variable.

6.4 Influence of Damping

The influence of damping at various locations was determined using the approach outlined in Section 5.6.3.

6.4.1 Damping at the Gear Meshes

Tooth vibratory loads were found to be almost completely insensitive to damping at the gear meshes. No significant response variations were obtained for damping ratios in the range 0.01 to 1.0 related to sub-system critical damping (DA in Table 5.1). This result suggests that the tooth contact is too stiff to permit effective damping between the gears.

6.4.2 Damping at the Drawrolls

The influence of drawroll damping on tooth loading is shown in Figure 6.10* which relates to drawroll pair number 1 in box 10. The four damping coefficients represent damping ratios of

* It should be noted that torque values were computed for speed increments of 50 r.p.m. and the coordinate points so produced joined by straight lines.

.01, .015, .02 and .03 with respect to critical damping factor DB (Table 5.1). It is readily apparent from the diagram that damping at the drawrolls exerts a strong influence over mesh dynamic loading. The effect of drawroll damping on the distribution of dynamic loading in a complete machine is illustrated by Figures 6.11 and 6.12.

6.4.3 Damping at the Inter-Box Couplings

Figure 6.13 demonstrates the effect of coupling damping on the dynamic behaviour at mesh 1 in box 10. The three damping values used correspond to damping ratios of .01, .10 and 1.0 in relation to critical damping factor DC (Table 5.1). The influence of damping at this location is clearly significant although less so than damping at the drawrolls. It is important to note that damping at the box couplings will exert an influence over vibratory torque transfers down the layshaft system and thereby influence the ability of a mesh to be loaded by the behaviour at remote gear pairs.

6.5 Influence of System Parameters

6.5.1 Drawroll Shaft Diameter

The chief effect of drawshaft diameter reduction is to increase flexibility and thereby to depress system critical speeds. Figure 6.14 shows the dynamic loading behaviour in box number 10 of an MDT. 2/3 system incorporating drawshafts reduced to $\frac{1}{2}$ in. diameter over the 11 in. length normally at 1.225 in. diameter (see Figure 2.12). Whilst considerable alleviation in tooth loading is readily apparent, the predicted behaviour is still not satisfactory and further reduction in diameter would be impractical in respect of lateral

deflection considerations.

6.5.2 Drawroll Inertia

The speeds at which severe dynamic torques occur are elevated or depressed according to whether drawroll inertia is reduced or increased respectively. Typical response curves are given in Figure 6.15 for an inertia reduction of 50%. Again, although significant tooth load reductions were observed in computed results, no single inertia value was sufficient to give satisfactory performance over the wide operating region through which drawtwisters are operated in service.

6.5.3 Box Coupling Flexibility

Increasing the box coupling flexibility serves to depress the vibratory load peaks in the speed (or frequency) domain until, in the machine operating zone, each box is effectively decoupled from the rest of the system and hence the behaviour of each box is similar. Computed results (Figure 6.16) show that this condition is achieved, to a reasonable degree, when the coupling flexibility is increased by a multiple factor of about 100. Although this modification appears to represent a simple remedy to the gear failure problem, initial caution should be adopted since the "solution" is only valid in terms of the mathematical model employed. Further work, beyond the scope of this investigation, would be required to examine the suitability of this modification in practice.

6.6 TYPE B and TYPE E

The headstock system models employed for type A and type C machines have been applied, without modification, to type B and type E respectively. This is justified since variations in headstock features (section 6.2) and operating variables (section 6.3) have produced no significant changes in drawbox gearing response.

Figure 6.17 shows the dynamic torque curves for the meshes in the last box of a 10 box type B/type E drawtwister. (No appreciable difference was observed between the results for ~~four~~ type B and type E). A gradual increase in dynamic loading is illustrated together with a peak at 1650-1700 r.p.m. Up to 3060 r.p.m., corresponding to the maximum rated delivery of 4000 ft/min, the mesh load in this box is nowhere greater than 60 lbf.in. In comparing this figure with those derived for other machine configurations, it is suggested that the numerical values should not be taken too literally but rather they should be used to illustrate trends in behaviour.

Total drawbox system loading at 1700 r.p.m. is illustrated in Figure 6.18 which demonstrates that maximum activity occurs in box number 9. This predicted torque distribution is in good agreement with subjective noise tests carried out on a 10 box Type B/Type E machine.

These results clearly demonstrate an improvement in dynamic performance of Type B/Type E when compared to the corresponding results for the original Type A and Type C systems.

6.7 Type A or Type C with Bushed Gear Conversion

The effect of incorporating rubber bushed gears in an otherwise unchanged type A/type C configuration is illustrated in Figure 6.19. The curves are similar in shape to those for Type B/type E (Figure 6.17) except that a slight displacement along the speed axis is evidenced. Again, the rubber bushed gearing modification produces substantially improved dynamic behaviour over the original solid gear drives.

In the theoretical model, it is considered that rubber bushes would contribute both high flexibility and damping to the system*. Attempts were made to distinguish between these contributions by examining the effects of each separately. Figure 6.20 shows a typical graph portraying the influence of flexibility only, that is, bush damping has been completely ignored. Beyond a peak at 1650 r.p.m. the vibratory torque level decreases with increasing speed. Thus, the result suggests that careful selection of the rubber bush, or alternative flexible element, could yield even better dynamic behaviour. A more general, and less conventional, conclusion is that high damping is not necessarily a desirable goal in the design for satisfactory vibration behaviour.

* Numerical values for these quantities are presented in Appendix B and the theoretical representation of damping is discussed in Section 5.5.3.2.

6.8 Critical Speeds

A summary of selected critical speeds, based on once per drawroll revolution effects, is given in Table 6.1. In investigations of the kind reported in this thesis, a knowledge of theoretical critical speeds is useful but of limited value compared to the forced response diagrams discussed earlier. Comparisons between response graphs and critical speed figures reveal some correspondence; for example, the dynamic load behaviour in the region of 2400 r.p.m. for MDT. 2/3 (Figures 6.1 and 6.5) is clearly influenced by the third torsional critical speed of the layshaft system.

6.9 Theoretical Results for Experimental Rig

The results to be discussed relate to the four box experimental rig described in Section 7.

6.9.1 Rig Incorporating Standard Couplings

Computed results for the rig model highlight only one critical speed* (2070 r.p.m.) in the range 0 - 4000 r.p.m.

Figures 6.21 - 6.28 illustrate dynamic loading distributions throughout the rig for drawroll speeds in the range 1500 - 2500 r.p.m. The curves are similar in shape and show resemblance to a first torsional mode shape. These loading patterns may be compared to measured distributions of tooth impact activity reported in Section 9.2.3.

* Critical speeds are based on drawroll rotational frequency.

6.9.2 Rig Incorporating Highly Flexible Box Couplings

Increasing the coupling flexibility by a multiple factor of 290 yields the following critical speeds* in the range 0 - 4000 r.p.m:-

1. 177 r.p.m.
2. 394 r.p.m.
3. 584 r.p.m.
4. 727 r.p.m.

That these values are so low suggests that, in the practical operating zone, the boxes are effectively dynamically decoupled from each other. The influence of highly flexible couplings is discussed in Sections 9.3.4 and 9.4. in the light of the experimental investigation.

* Critical speeds are based on drawroll rotational frequency.

TABLE 6.1 SUMMARY OF CRITICAL SPEEDS

MACHINE	CRITICAL SPEEDS				
	1	2	3	4	5
Standard type A with Solid Gears	473	1413	2332	3215	4052
Standard type C with Solid Gears	476	1422	2346	3233	4065
Type B	618	1440	1760	1884	1940
Type E	622	1444	1763	1885	1941
Type C with Bushed Gears	460	1109	1396	1520	1580
Standard Type A with ½" Diameter Drawshafts	475	1318	1925	2310	2545
Standard Type A with Drawroll Inertia Reduced by 50%	621	1856	3069	4245	5371
Standard Type A with Coupling Flexibility increased by 100 times	95	283	464	637	795
Standard Type C with Coupling Flexibility increased by 100 times	103	283	465	637	796

NOTES:-

1. Only the first 5 critical speeds are given for each machine configuration.
2. Critical speeds are related to drawroll speed.
3. In all cases, the machine configurations have 10 drawboxes.

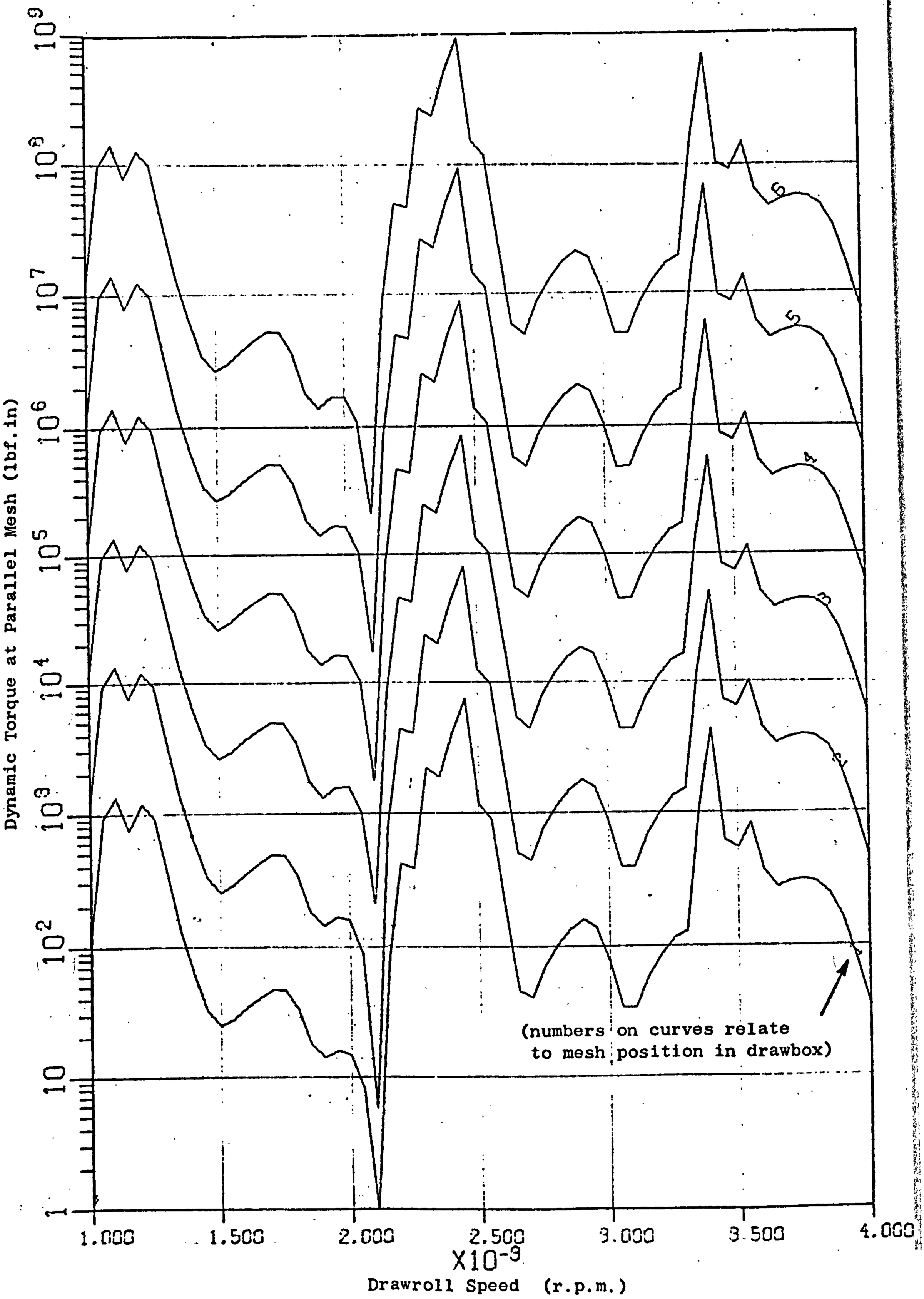

FIG. 6.1 Variation of Gear Dynamic Load with Speed
a 10 box Type A/Type C machine.
(curves separated by a factor of 10)

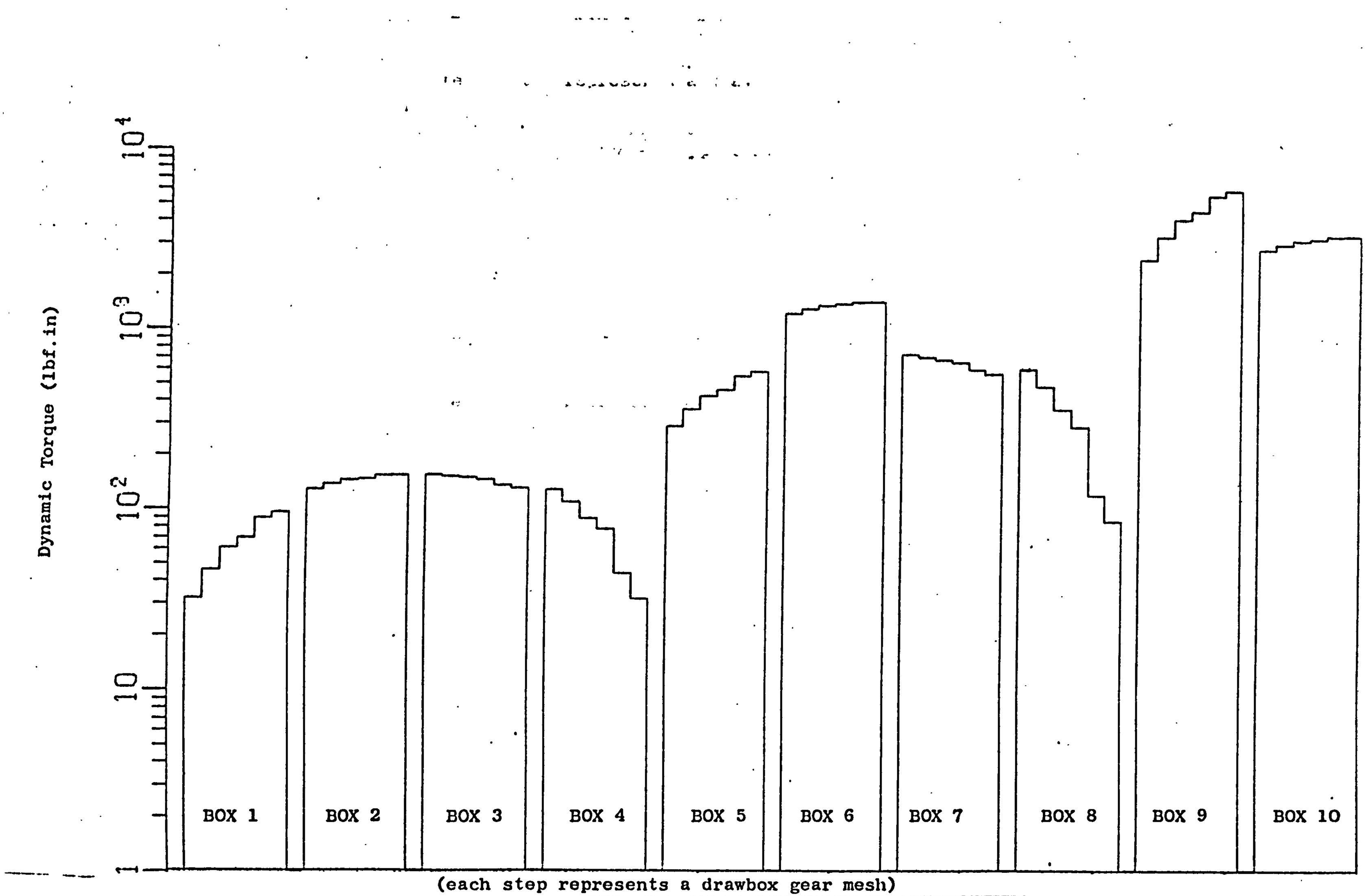

FIG. 6.2 Typical Dynamic Loading Distribution in a 10 box Type A/Type C machine at 2355 r.p.m.

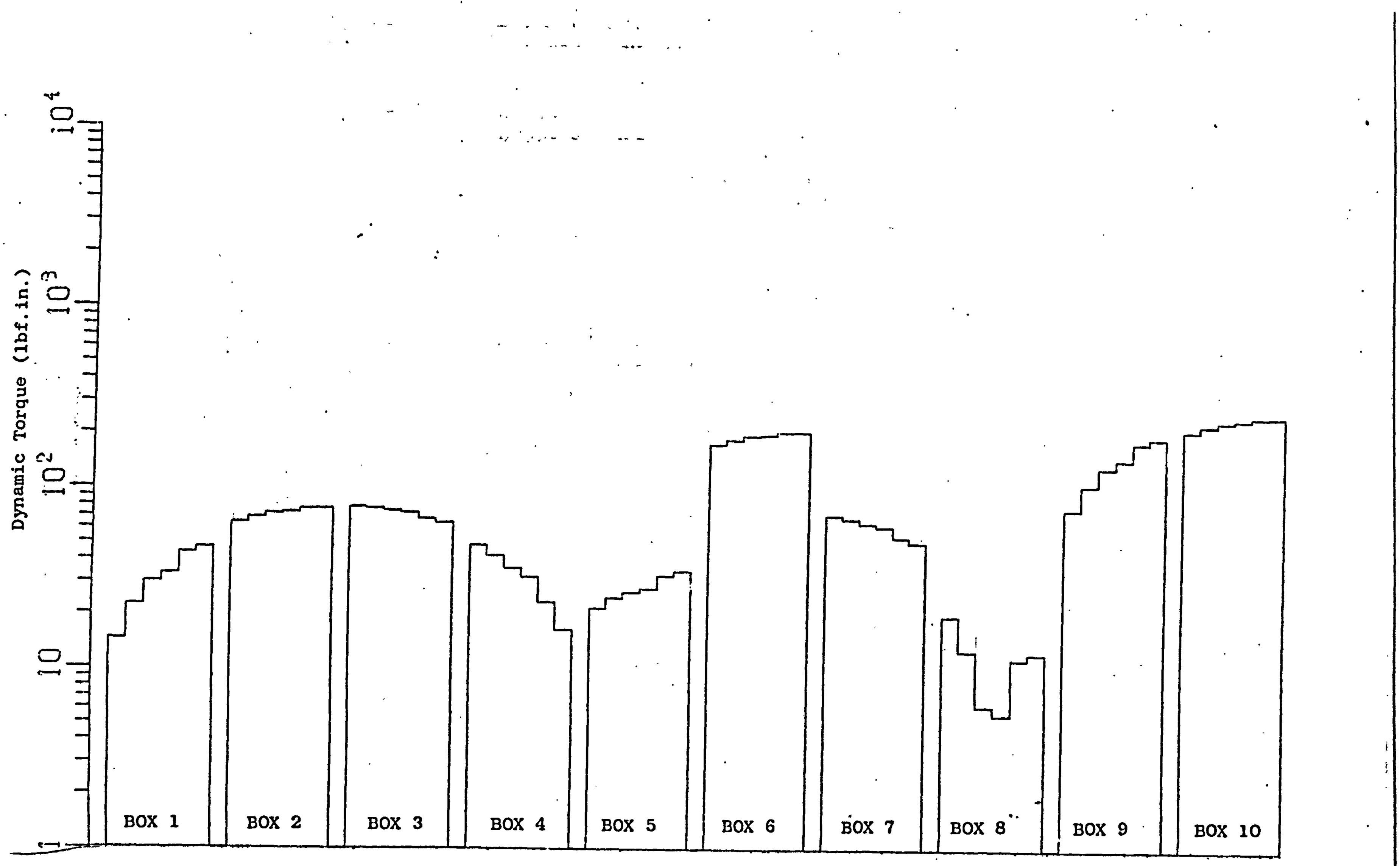

FIG. 6.3 Typical Dynamic Loading Distribution in a 10 Box Type A/Type C Machine at 2355 r.p.m.

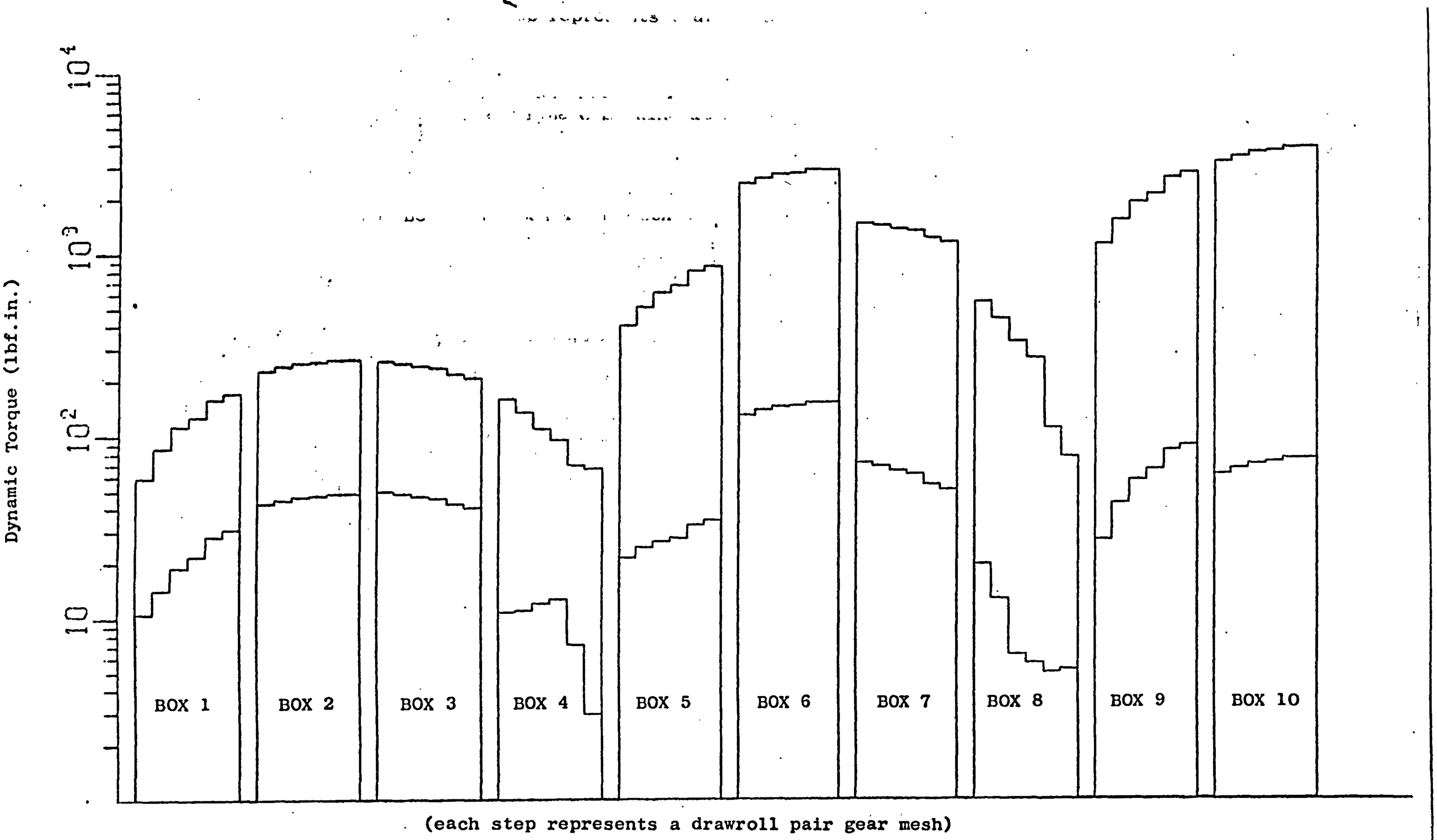

FIG. 6.4 Maximum and Minimum Dynamic Torque Limits for a 10 Box Type A/Type C machine at a Drawroll Speed of 2355 r.p.m.

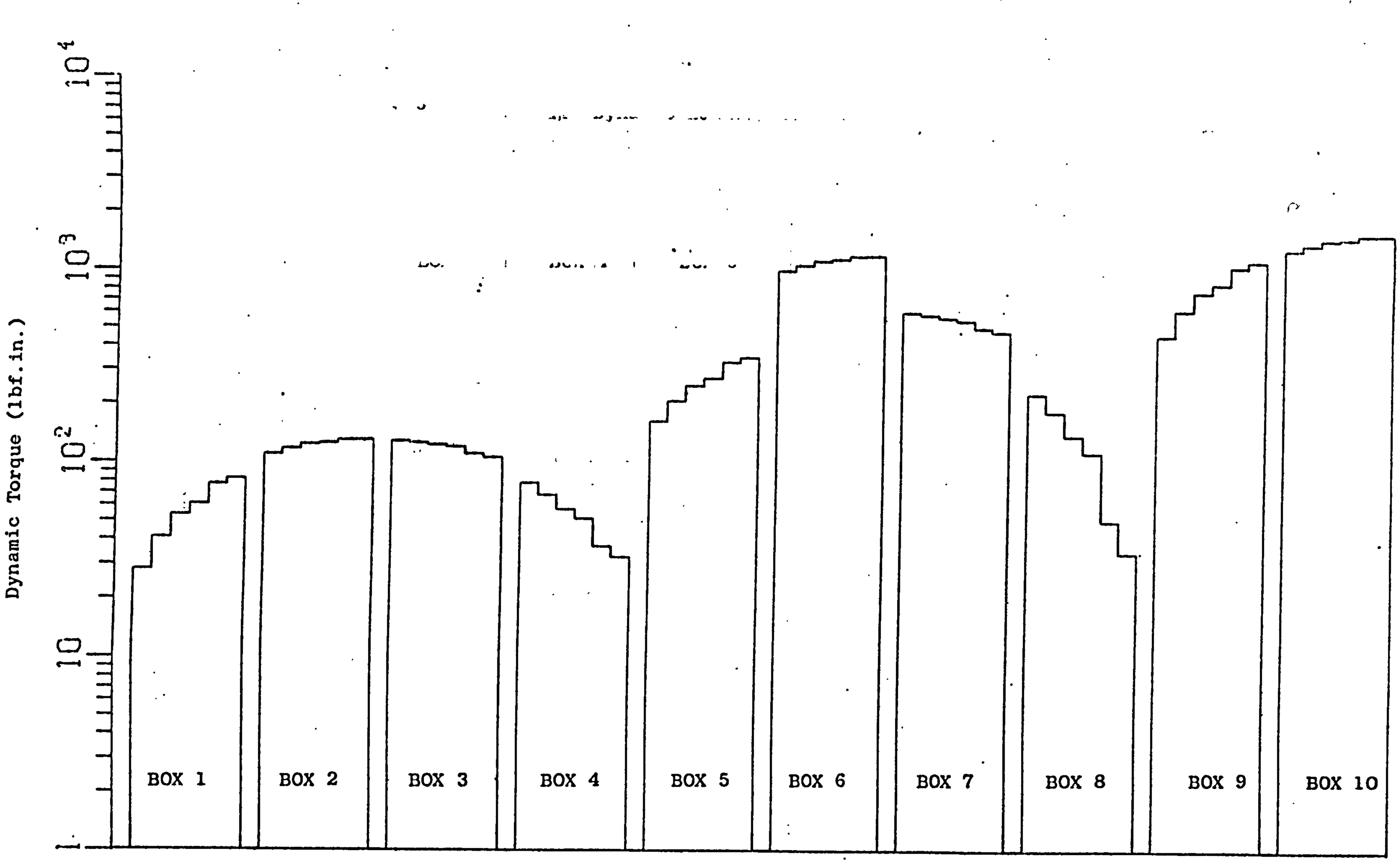

FIG. 6.5 Average Dynamic Loading Distribution in a 10 Box Type A/Type C Machine at 2355 r.p.m.

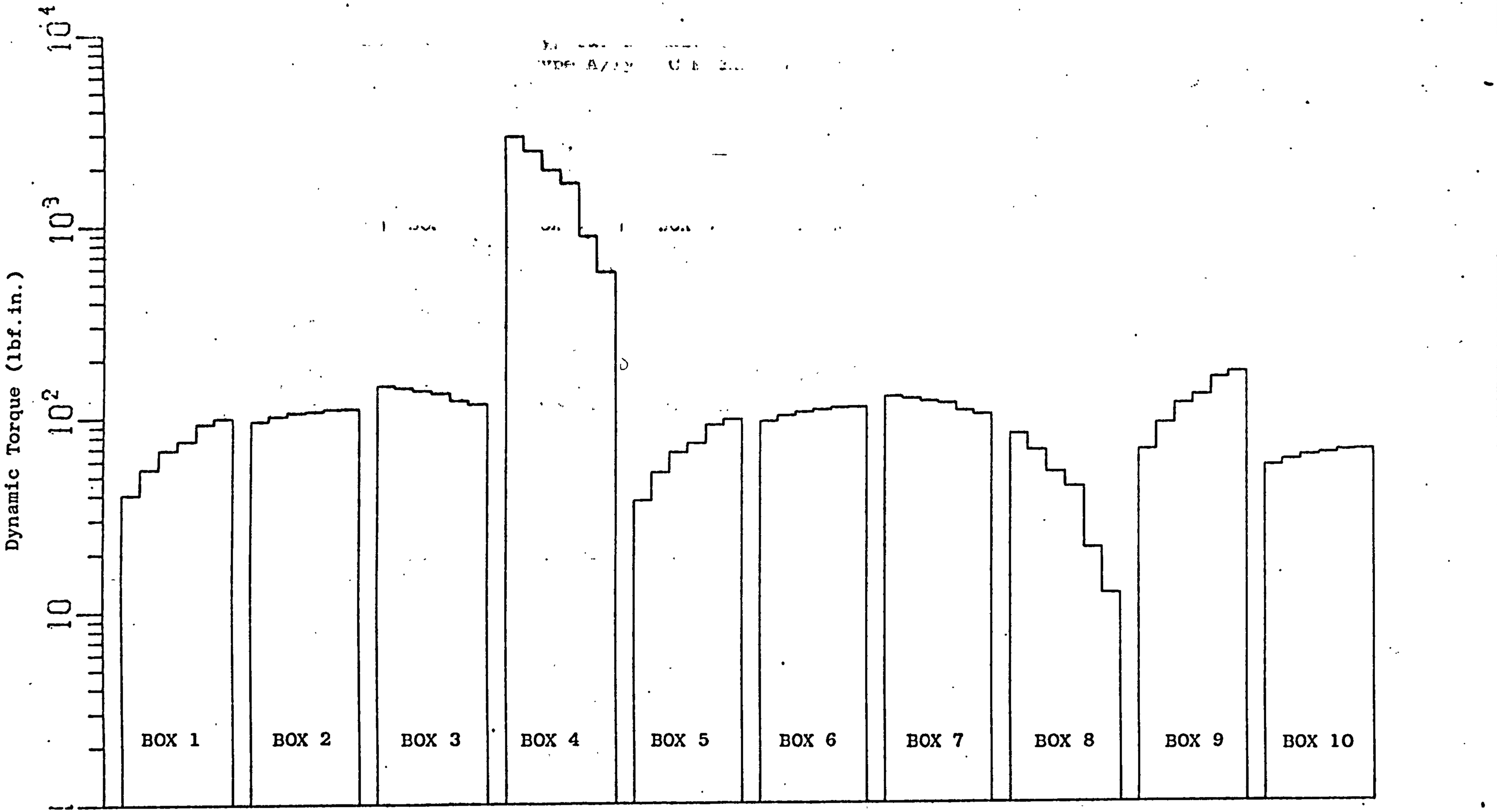

FIG. 6.6 Typical Dynamic Loading Distribution in a 10 Box Type A/Type C Machine at 2355 r.p.m.

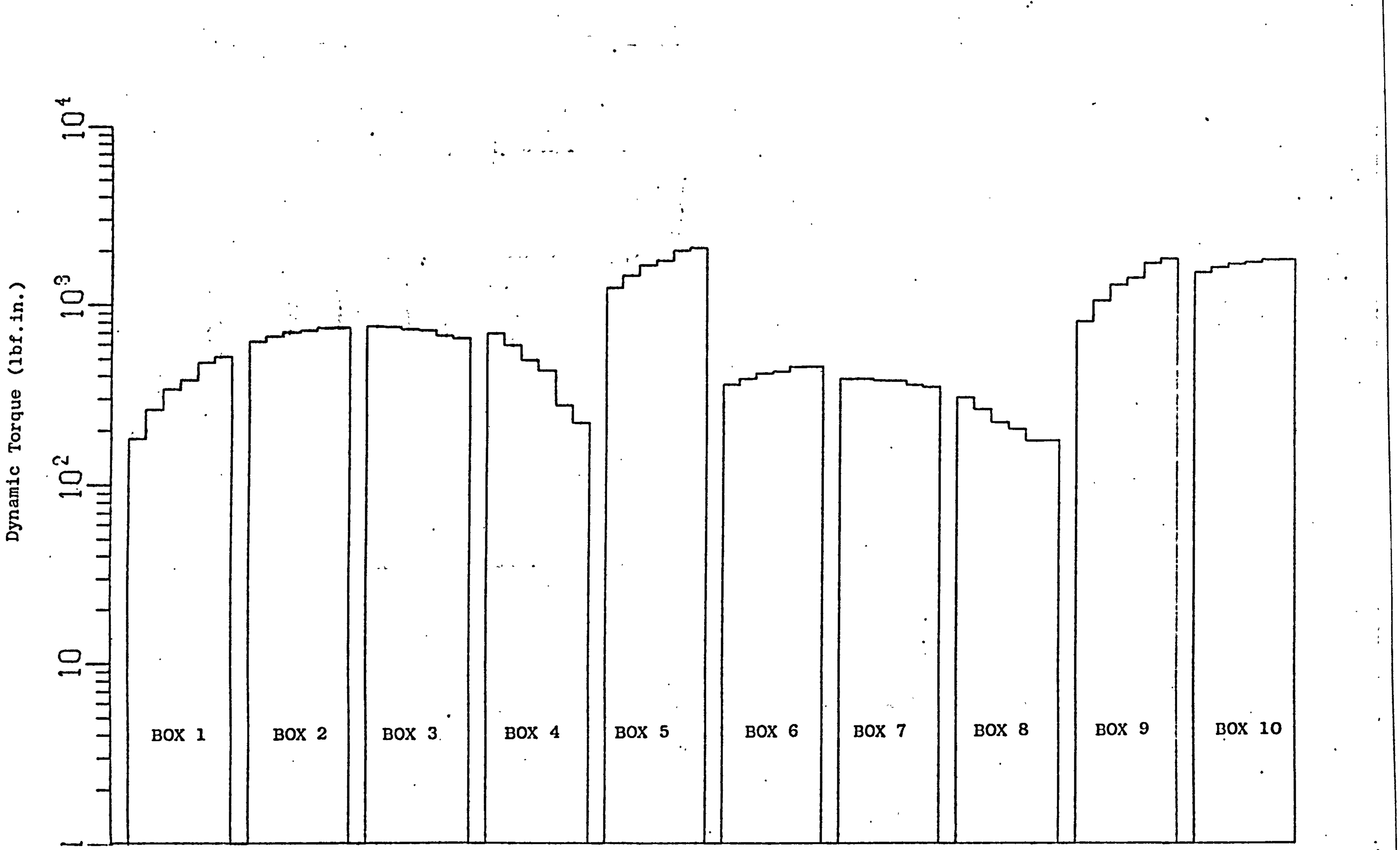

FIG. 6.7 Typical Dynamic Loading Distribution in a 10 Box Type A/Type C Machine at 2355 r.p.m.

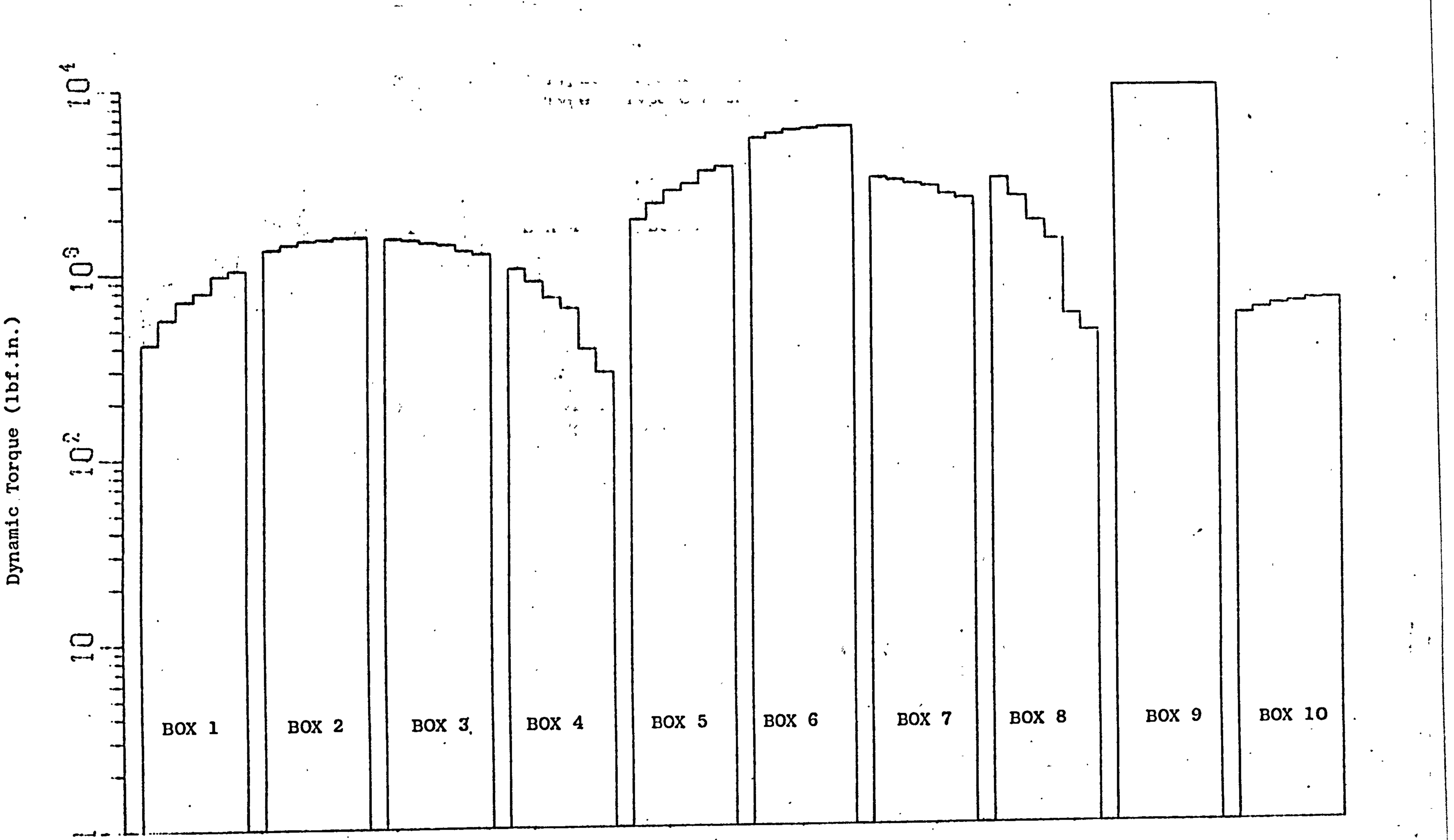

FIG. 6.8 Typical Dynamic Loading Distribution in a 10 box Type A/Type C machine at 2355 r.p.m.

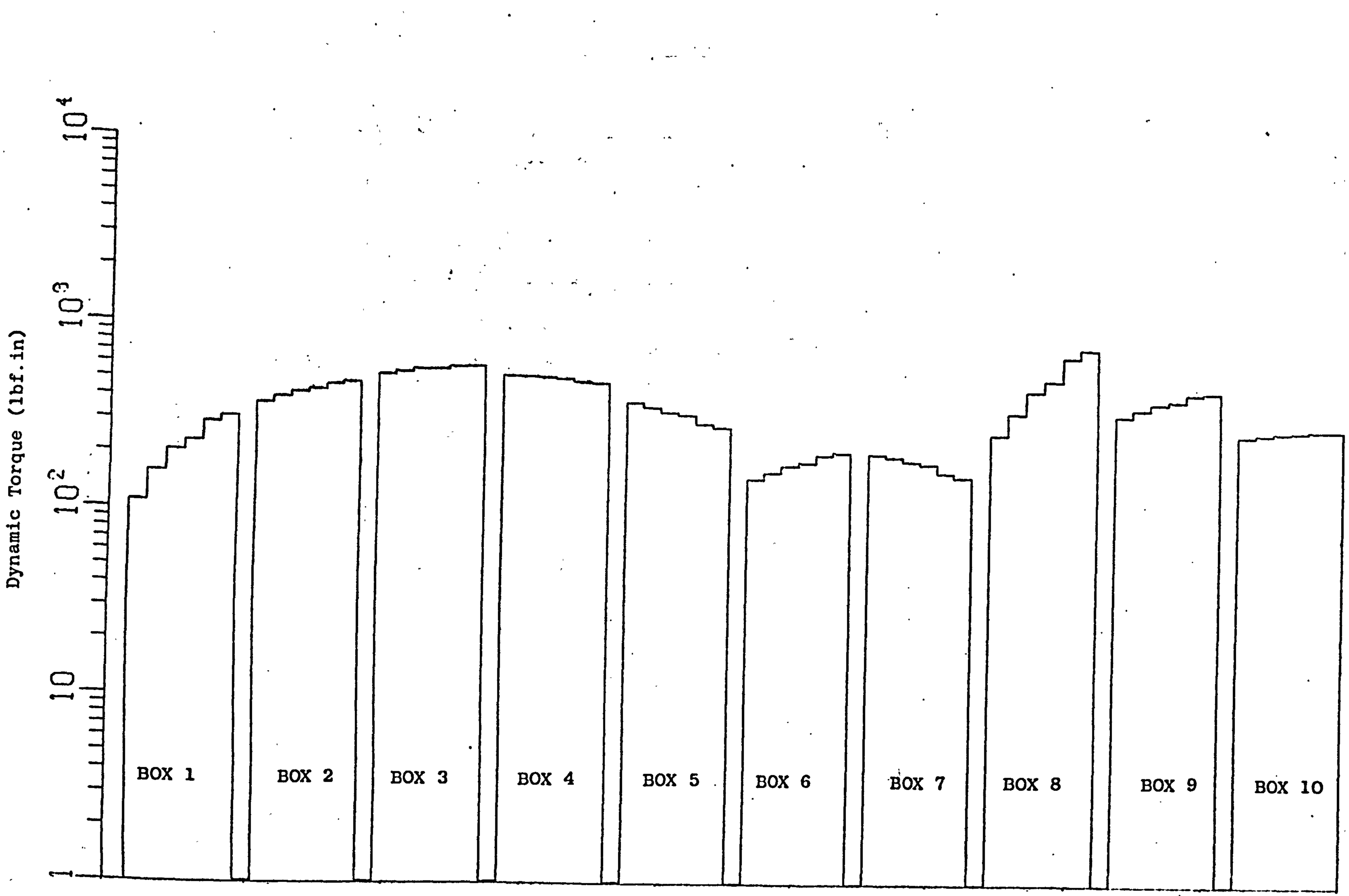

FIG. 6.9 Typical Dynamic Loading Distribution in a 10 Box Type A/Type C Machine at 1750 r.p.m.

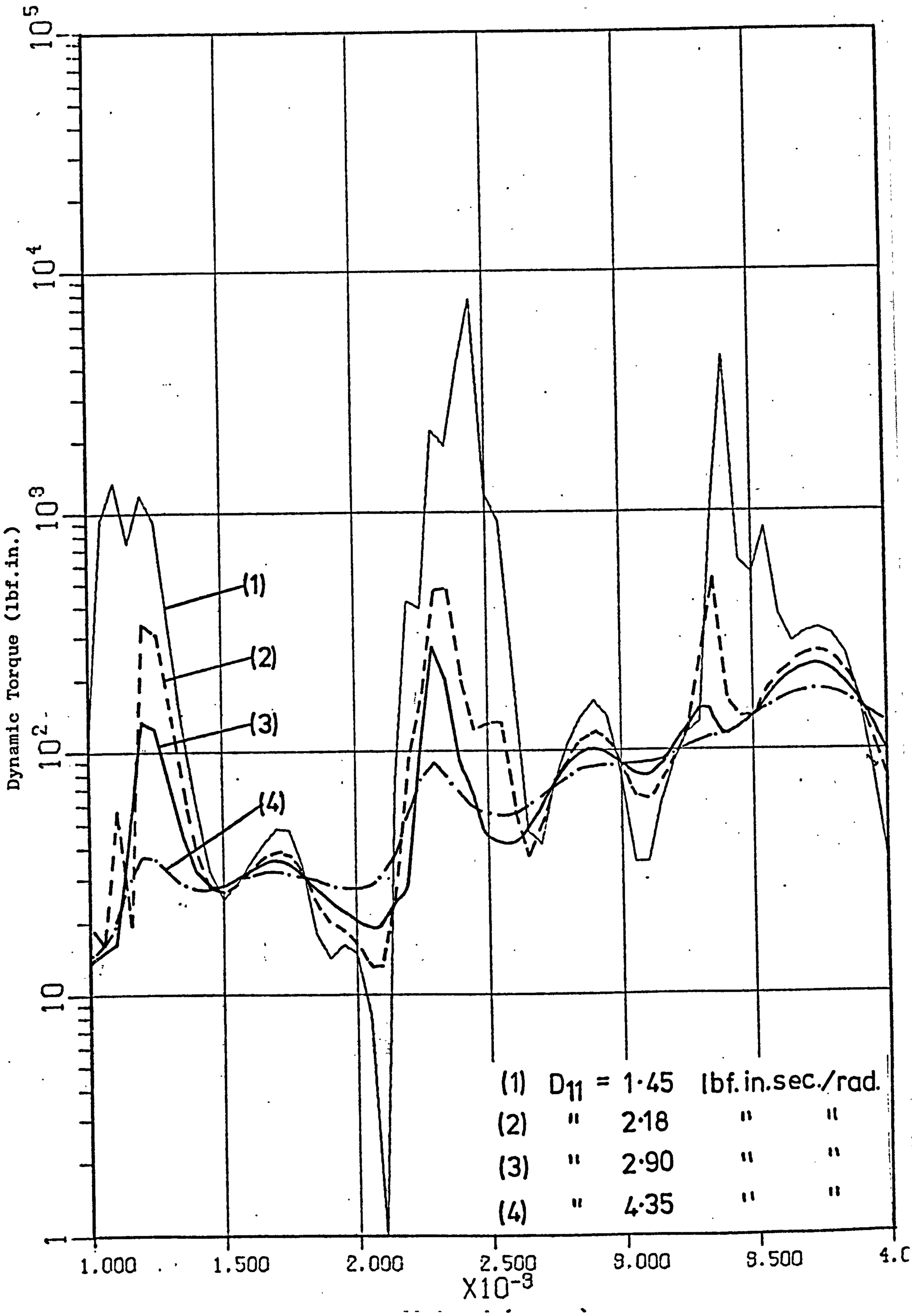

FIG. 6.10 Effect of Damping at Drawrolls in a 10 Box Type A/Type C Machine; behaviour shown for Mesh No. 1, Box 10.

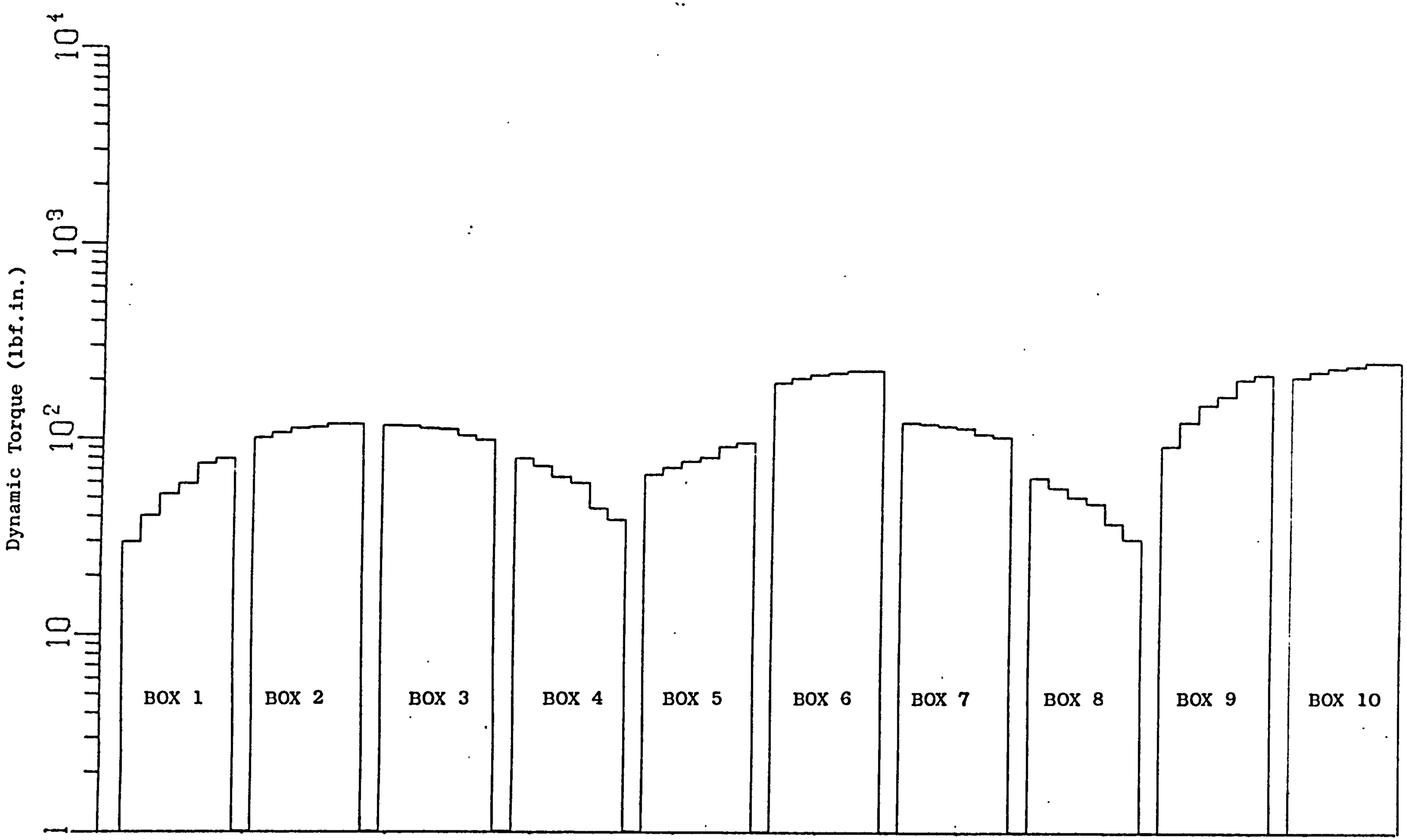

FIG. 6.11 Effect of Drawroll Damping on Dynamic Loading Levels at 2355 r.p.m.; Drawroll Damping Coefficient = 2.90 lbf.in.sec/rad.

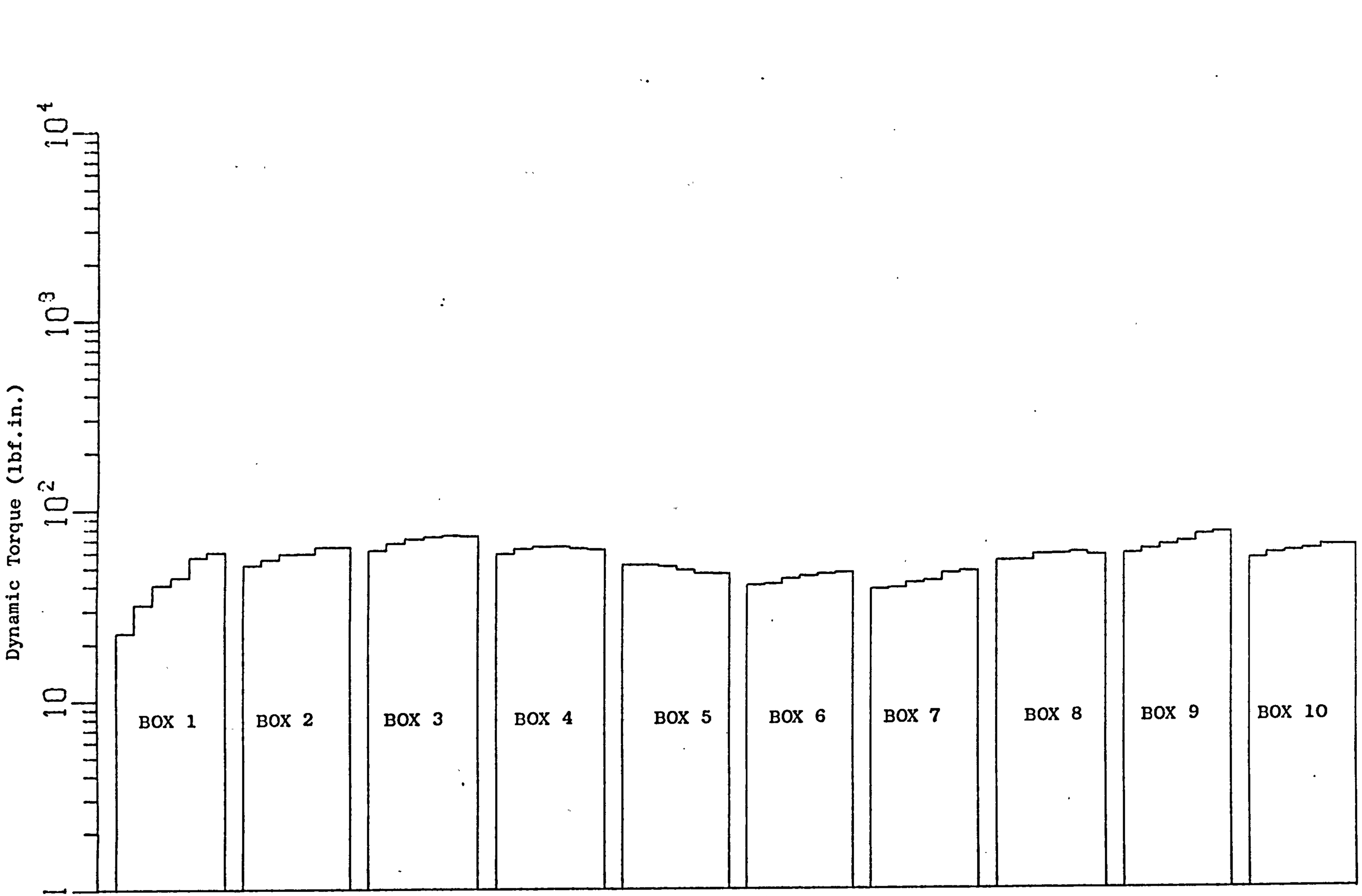

FIG. 6.12 Effect of Drawroll Damping on Dynamic Loading Levels at 2355 r.p.m.; Drawroll Damping Coefficient = 14.5 lbf.in.sec/rad.

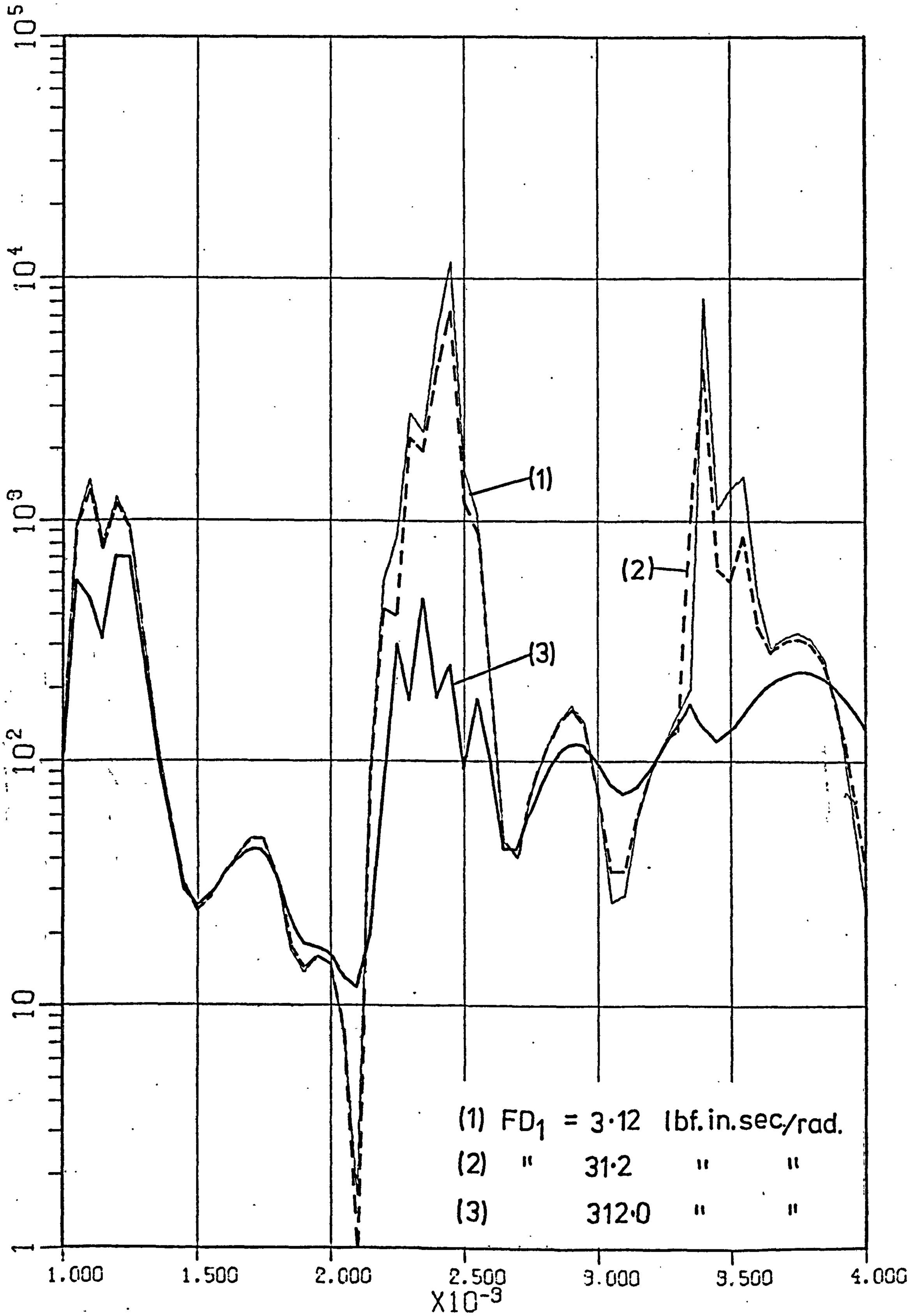

FIG. 6.13 Effect of Damping at Box Couplings in a 10 Box Type A/Type C Machine; behaviour shown for Mesh No. 1, Box 10.

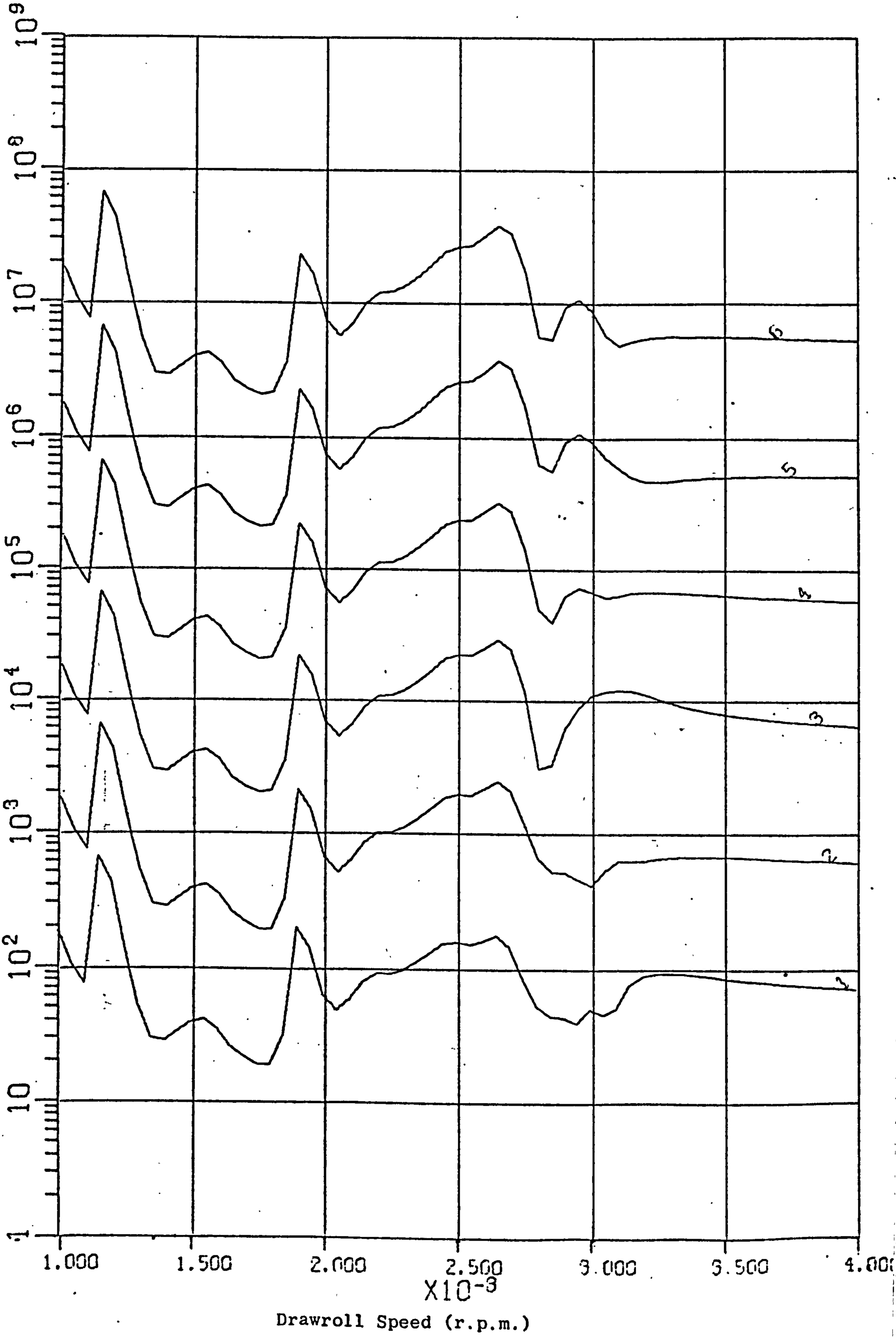

FIG. 6.14 Variation of Dynamic Load with Speed in Box 10 of a 10 Box Type A/Type C Machine incorporating ½ inch Diameter Drawshafts.

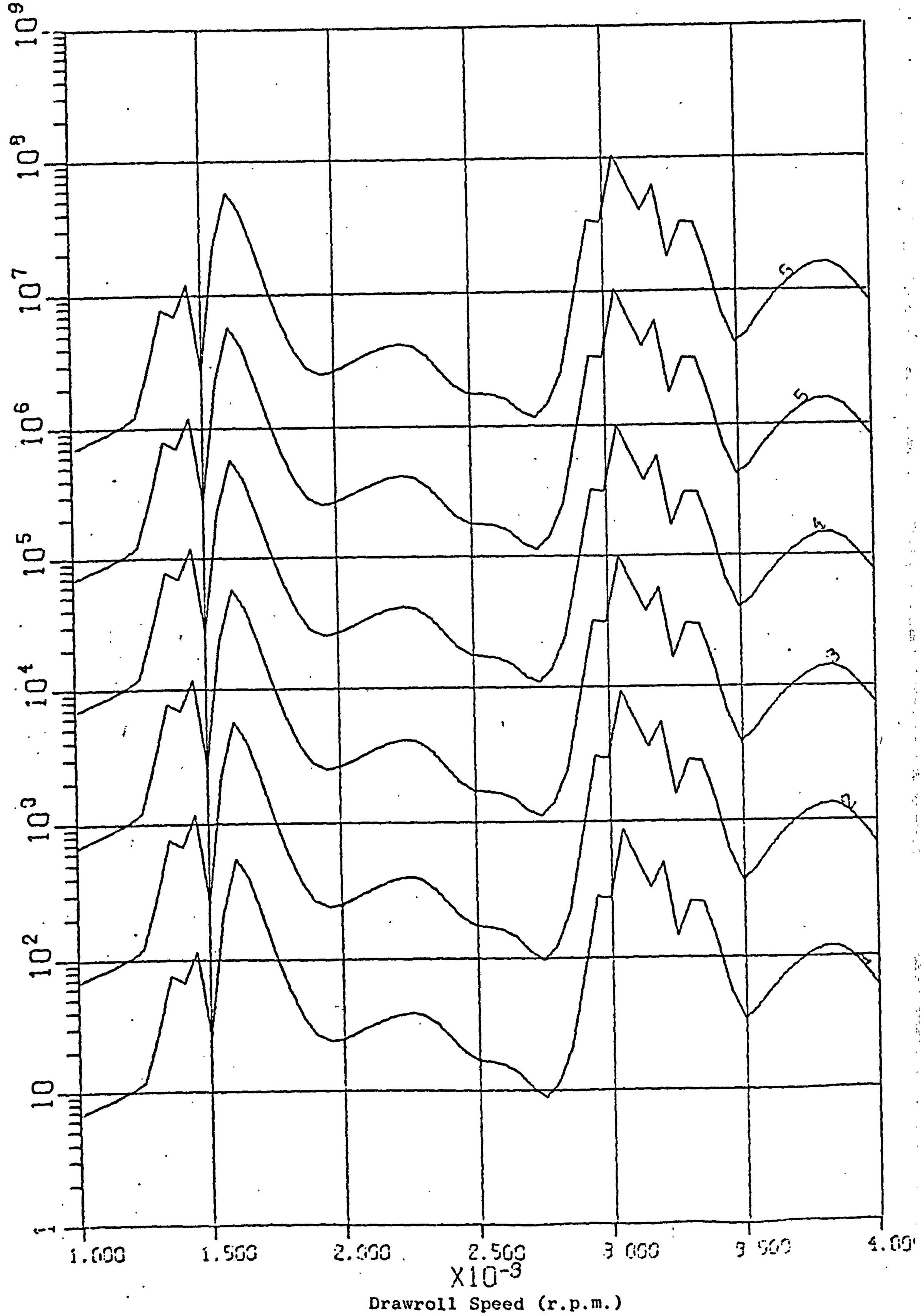

FIG. 6.15 Variation of Dynamic Load with Speed in Box 10 of a 10 Box Type A/Type C machine incorporating Drawrolls reduced in Inertia by 50%.

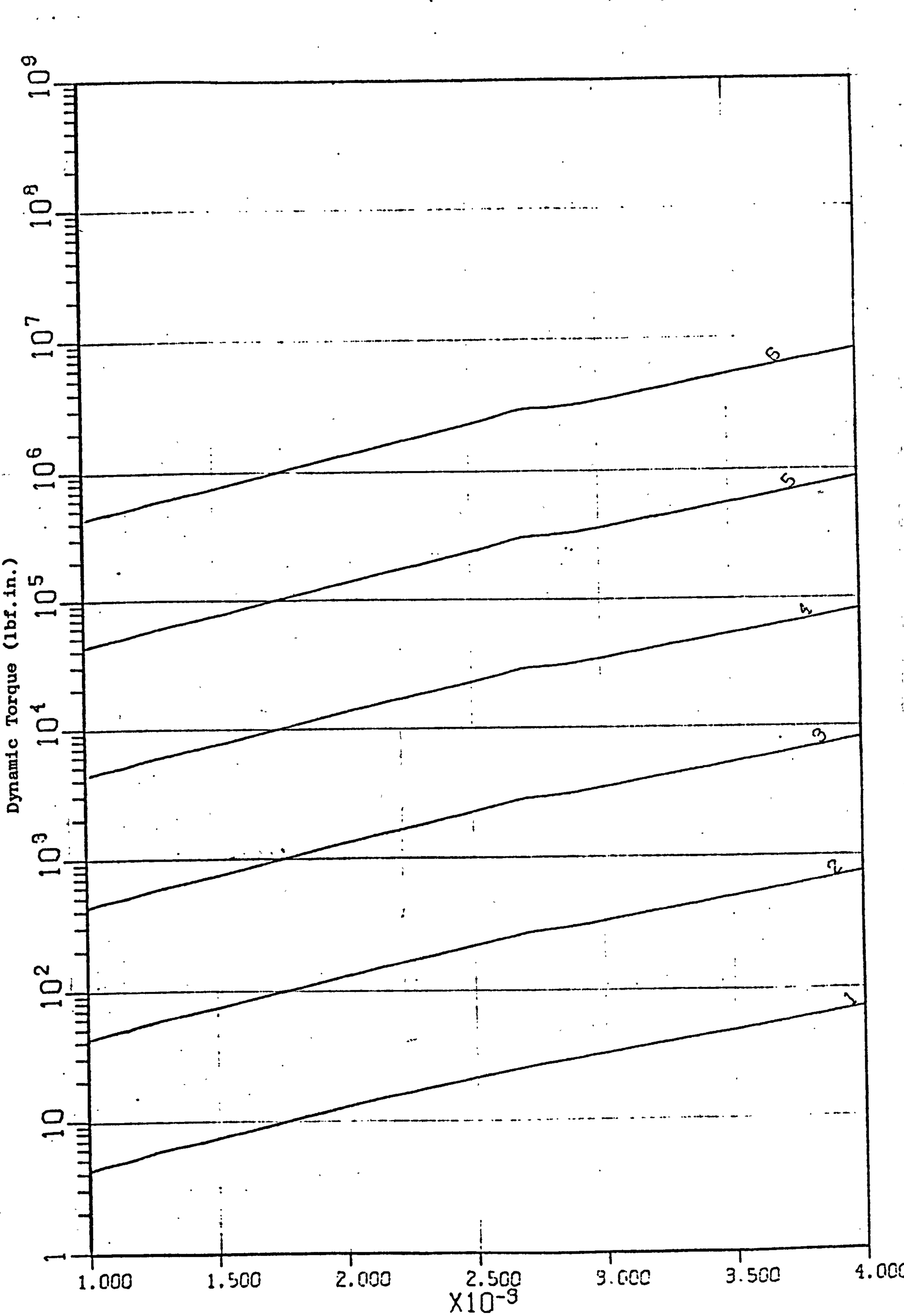

FIG. 6.16 Variation of Dynamic Load with Speed in Box 10 of a 10 Box Type A/Type C machine with Layshaft Coupling Flexibility increased by a Factor of 100.

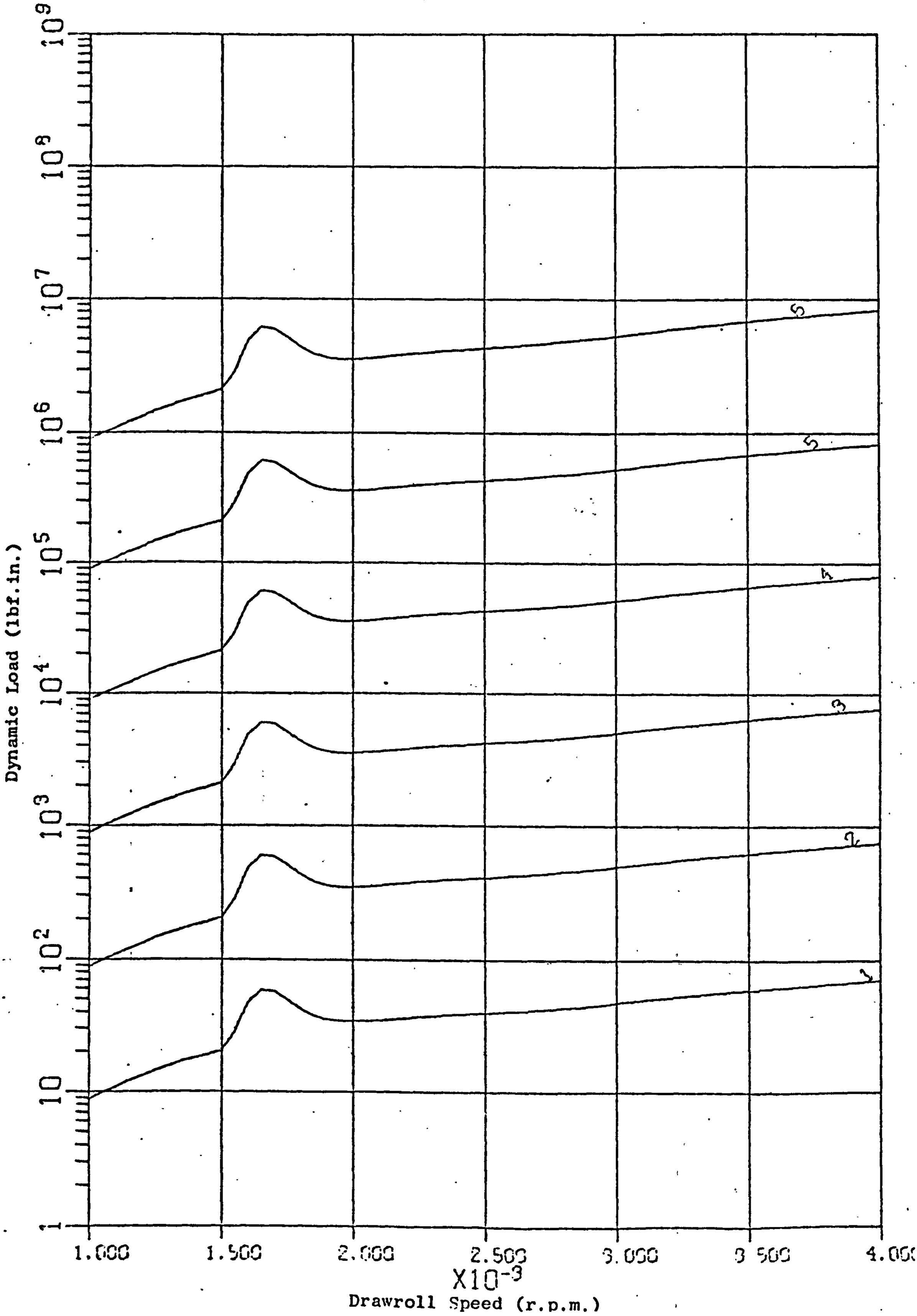

FIG. 6.17

Variation of Dynamic Loading with Speed in Box 10 of a 10 Box Type B/type E Machine.

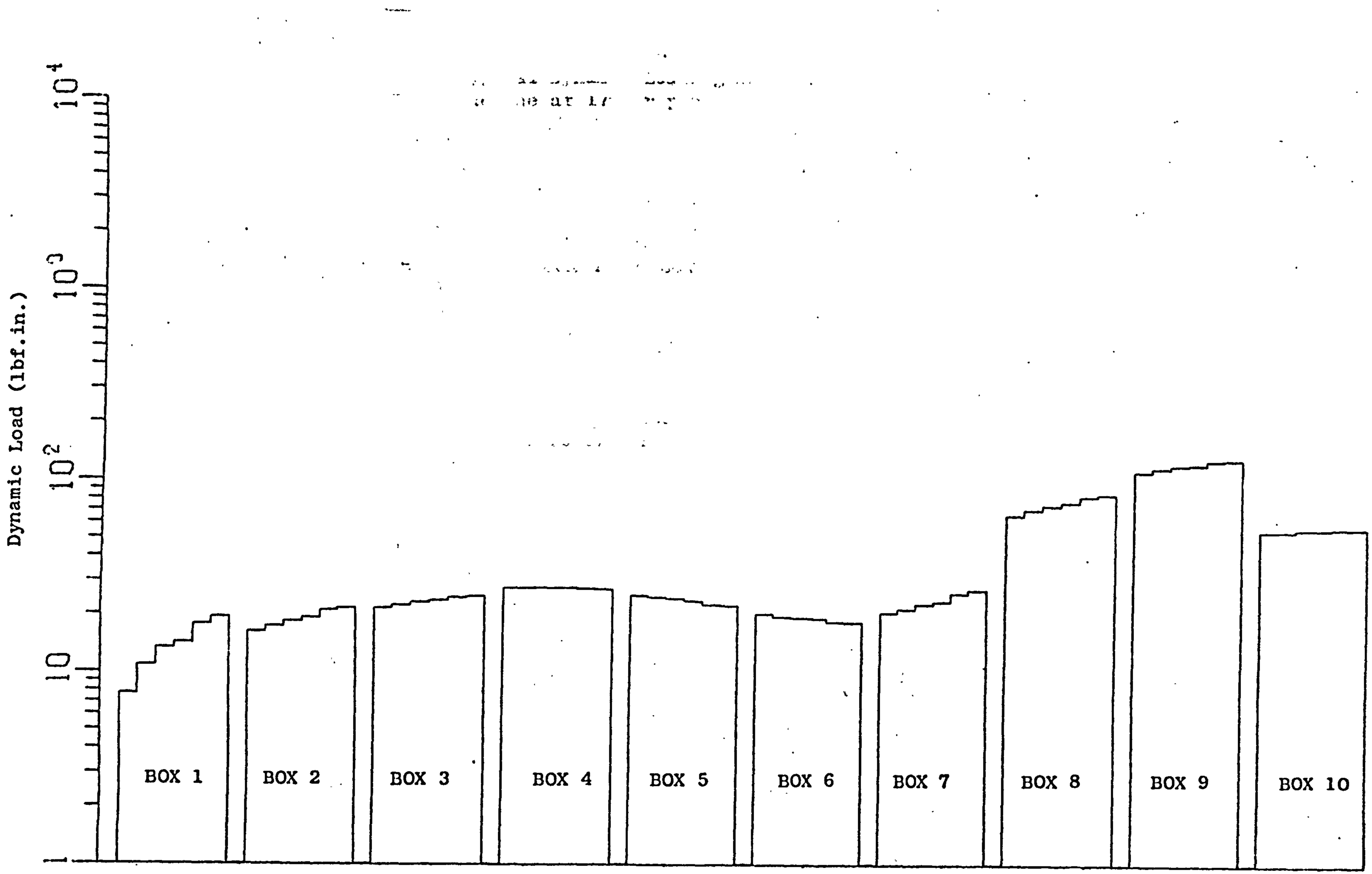

FIG. 6.18 Typical Dynamic Loading Distribution in a 10 Box Type B/Type E machine at 1700 r.p.m.

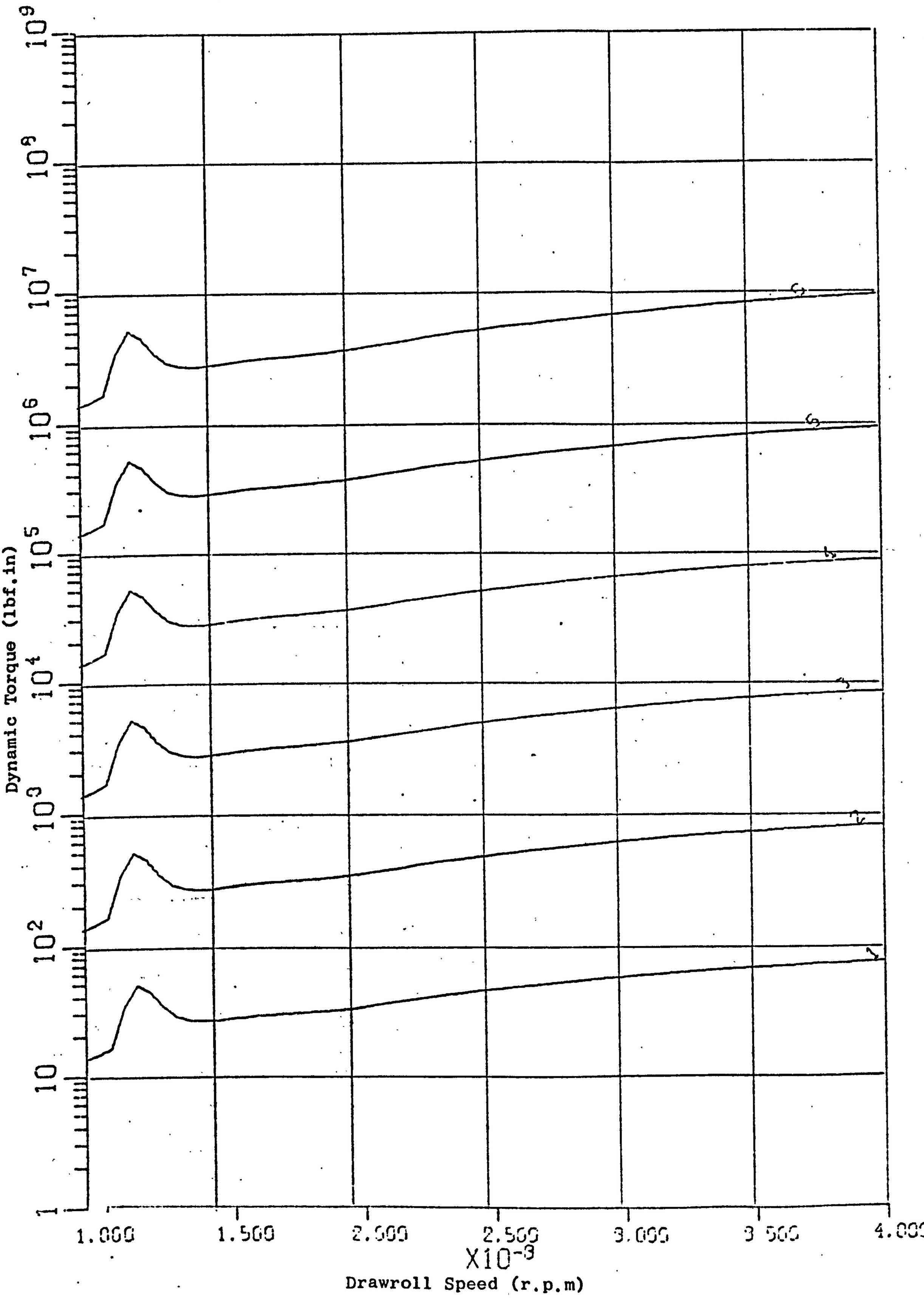

FIG. 6.19 Variation of Dynamic Load with Speed in Box 10 of a 10 Box Type A/Type C System incorporating Rubber Bushed Gears.

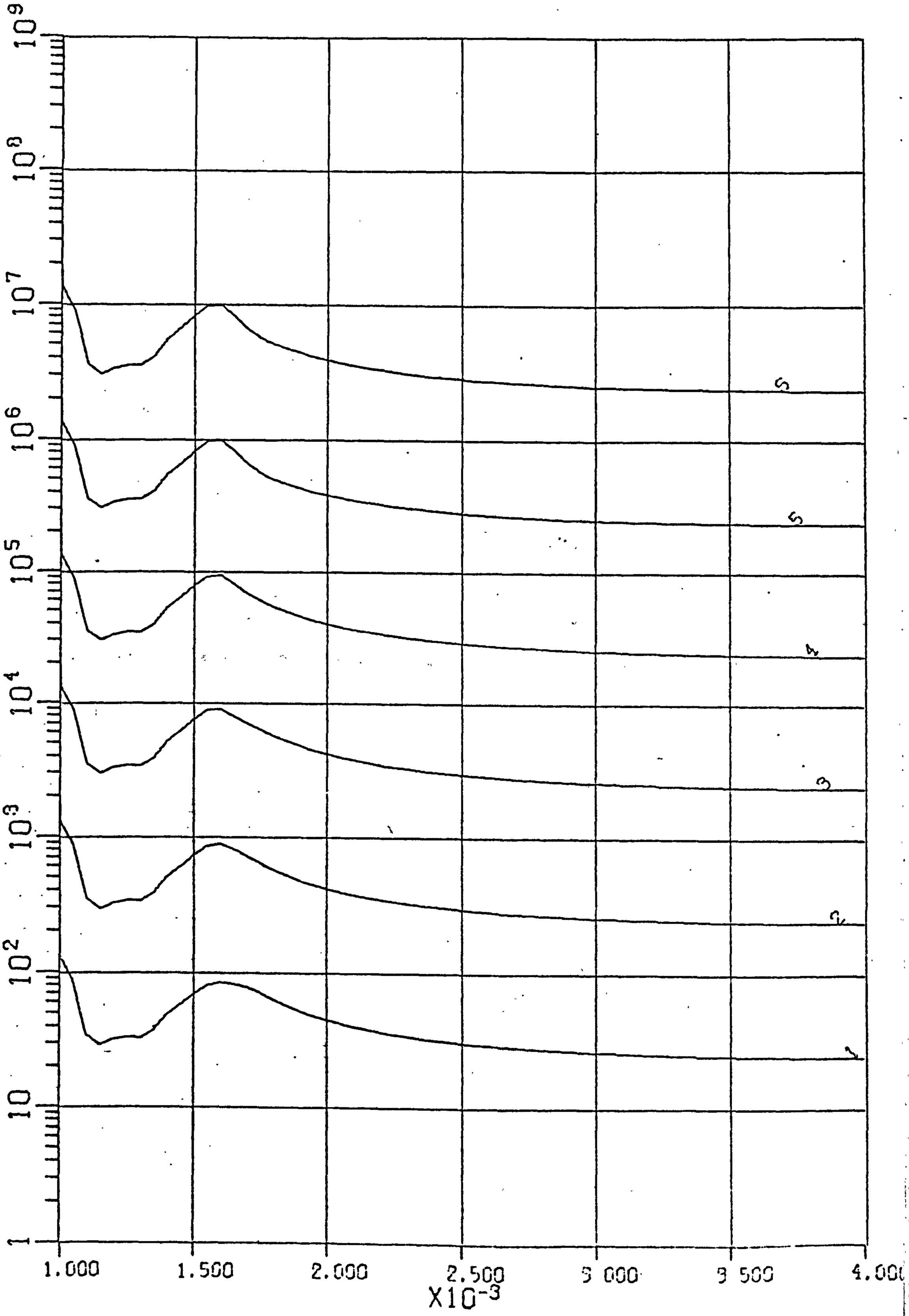

FIG. 6.20 Variation of Dynamic Load with Speed in Box 10 of a 10 Box Type A/Type C System with Bushed Gears having Zero Damping

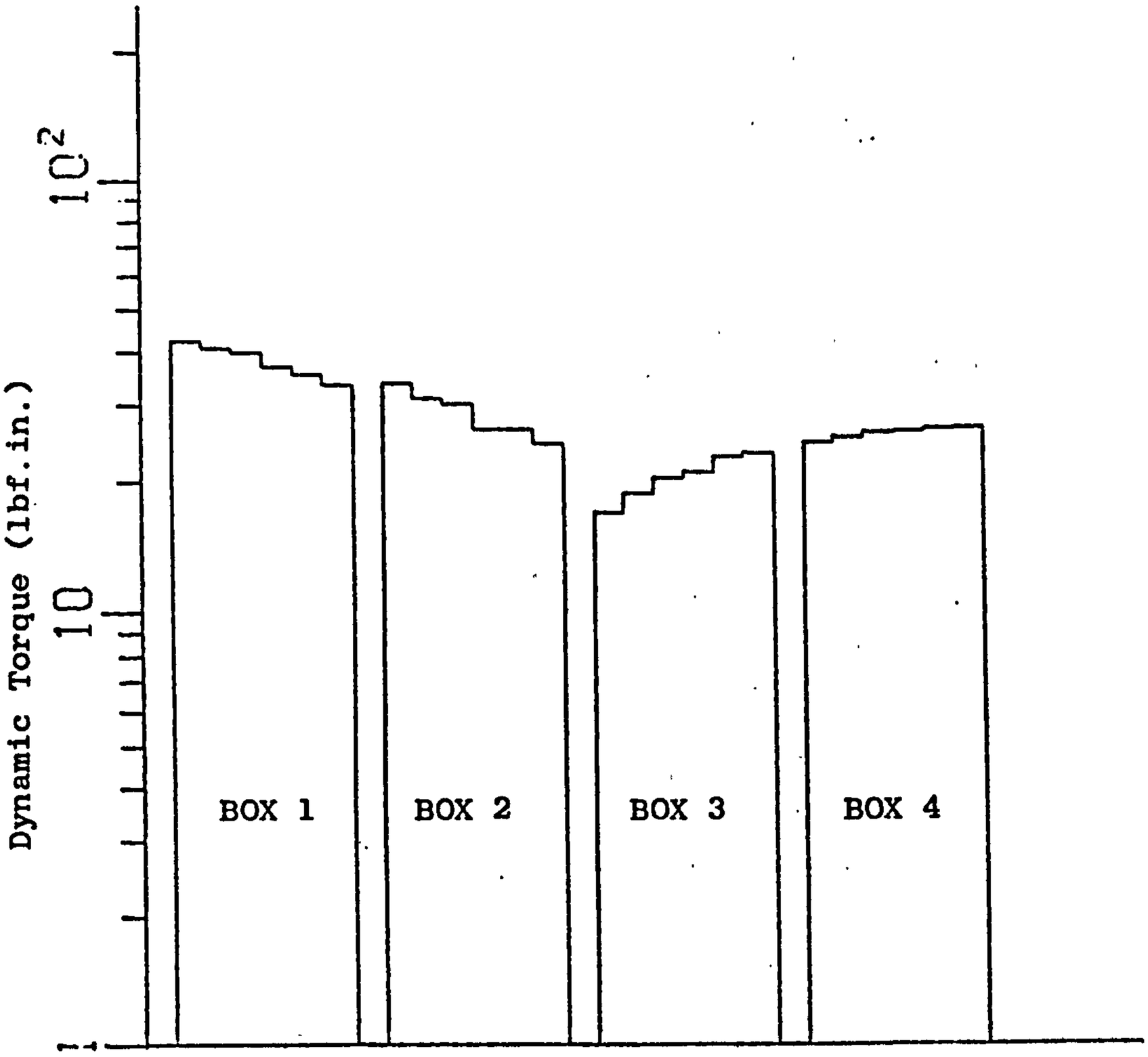

FIG. 6.21 Average Distribution of Dynamic Loading in 4 Box System at 1500 r.p.m.

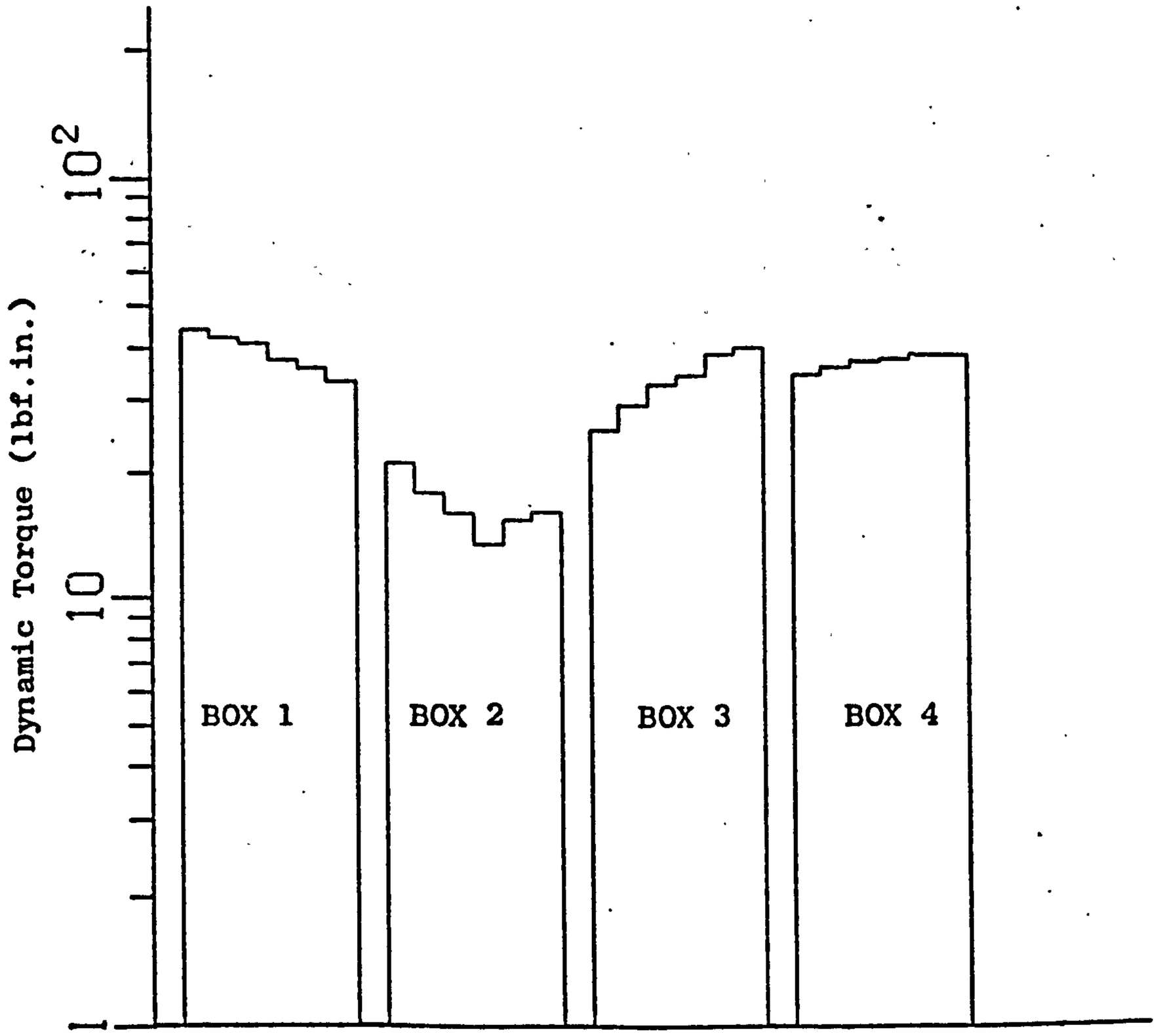

FIG. 6.22 Average Distribution of Dynamic Loading in 4 Box System at 1800 r.p.m.

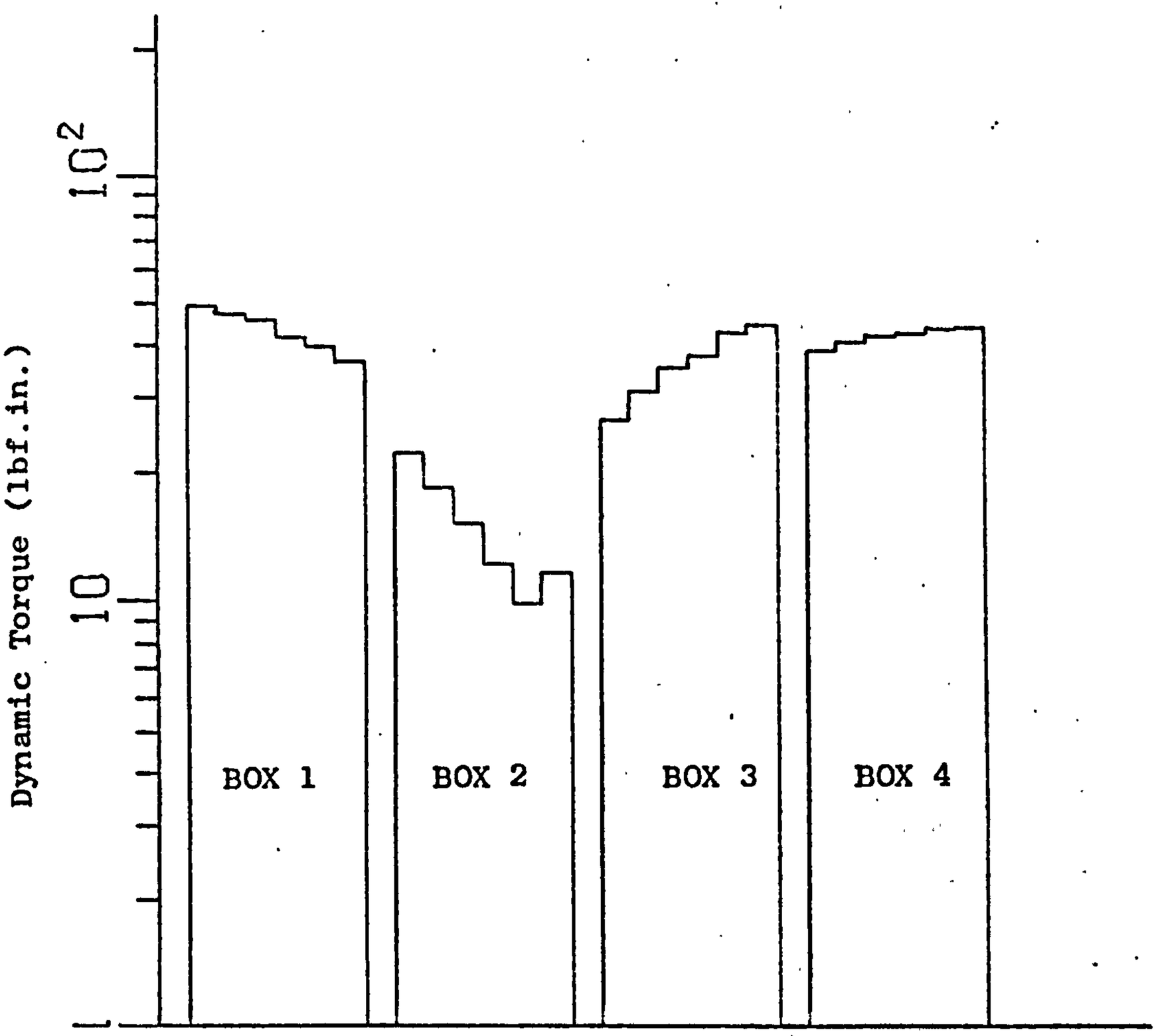

FIG. 6.23 Average Distribution of Dynamic Loading in 4 Box System at 1900 r.p.m.

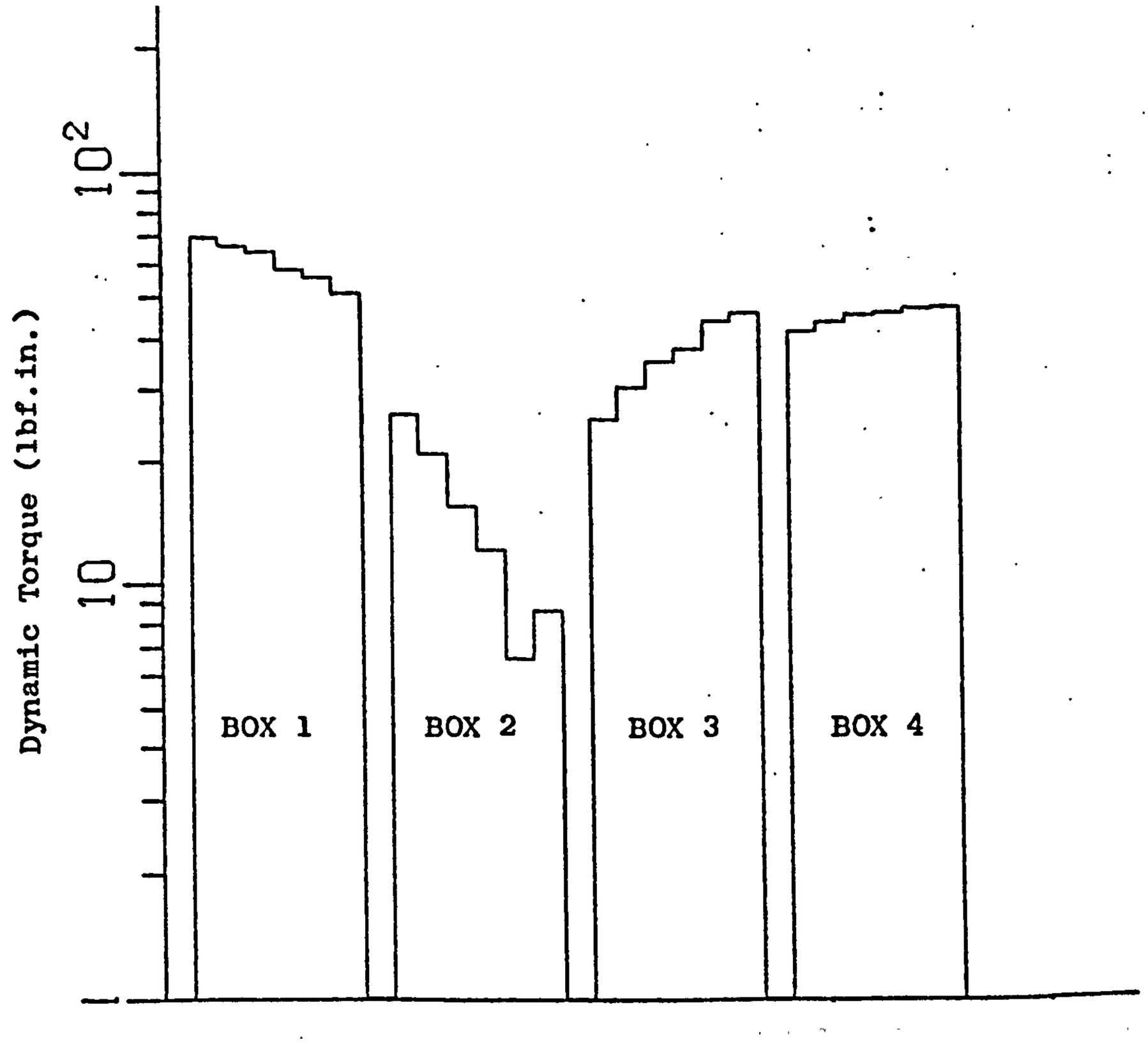

FIG. 6.24 Average Distribution of Dynamic Loading in 4 Box System at 2000 r.p.m.

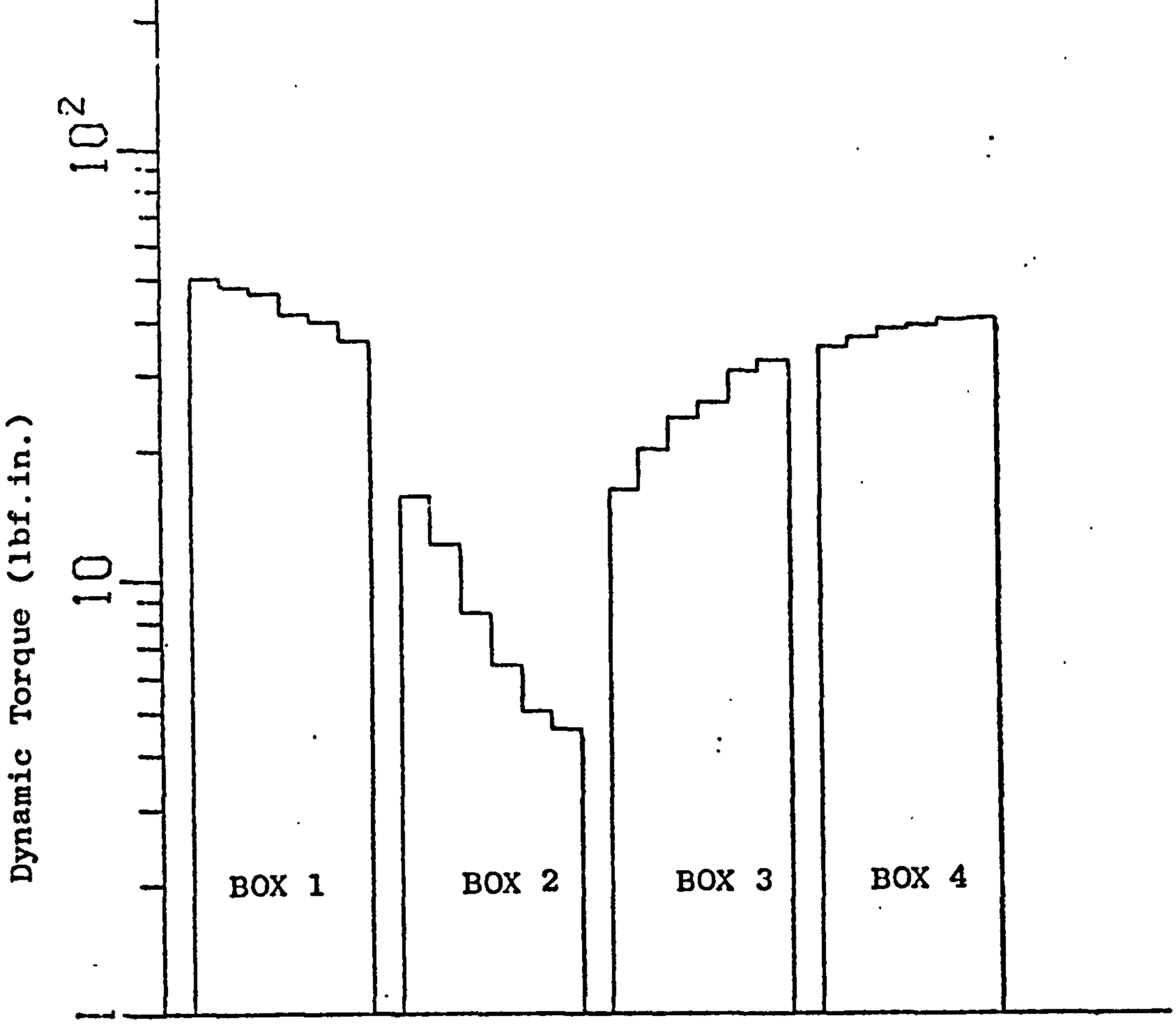

FIG. 6.25 Average Distribution of Dynamic Loading in 4 Box System at 2100 r.p.m.

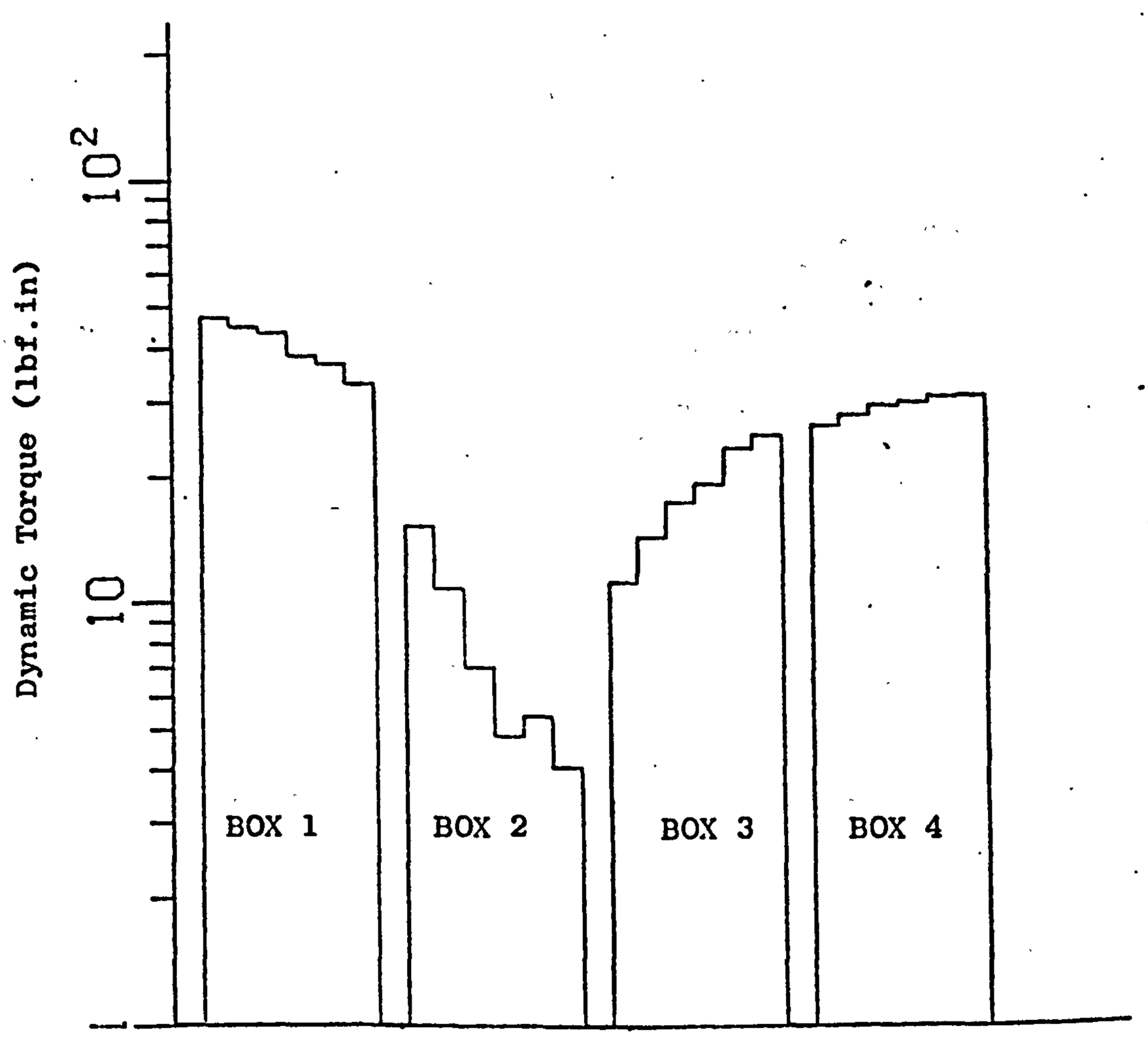

FIG. 6.26 Average Distribution of Dynamic Loading in 4 Box System at 2200 r.p.m.

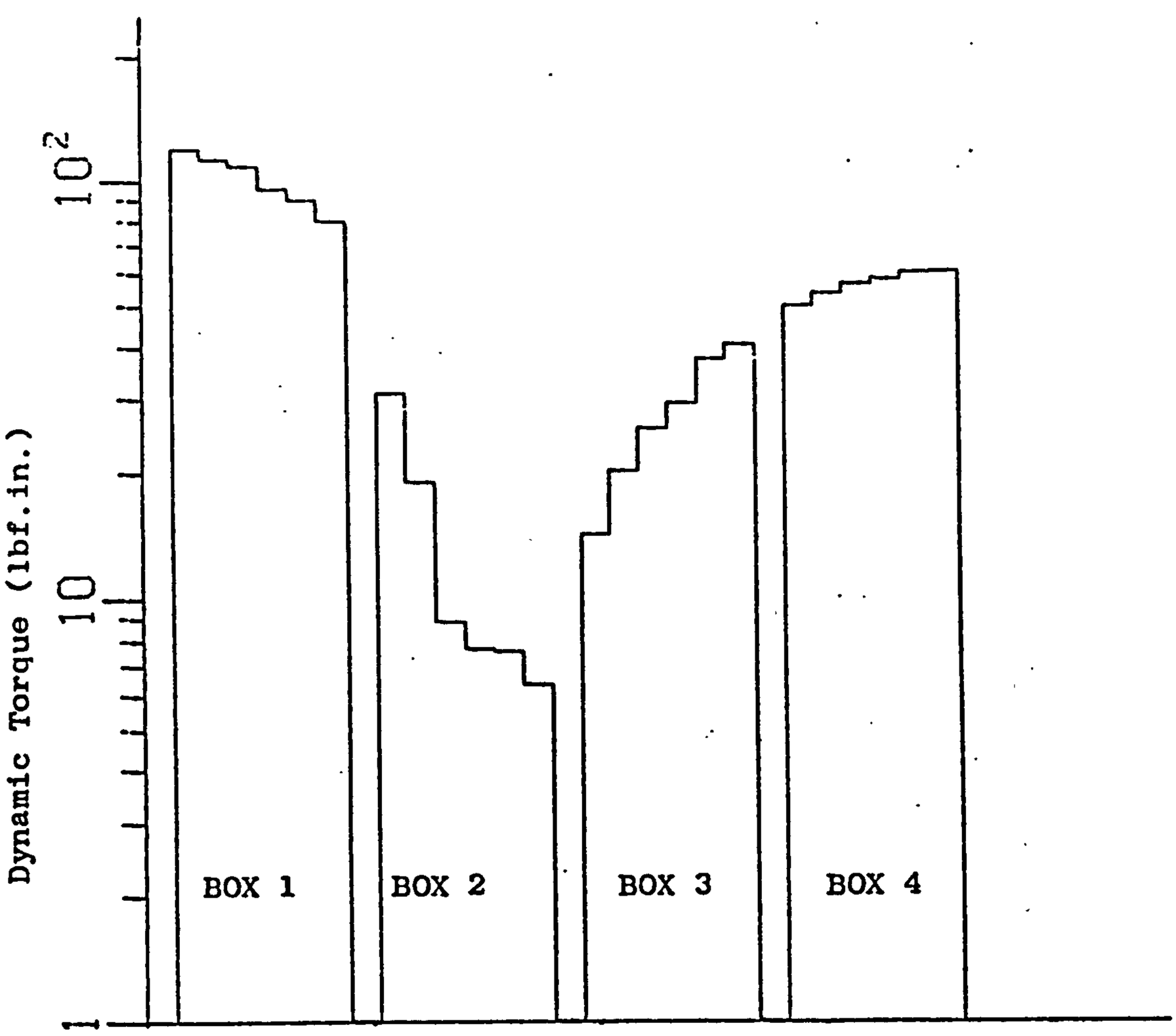

FIG. 6.27 Average Distribution of Dynamic Loading in 4 Box System at 2400 r.p.m.

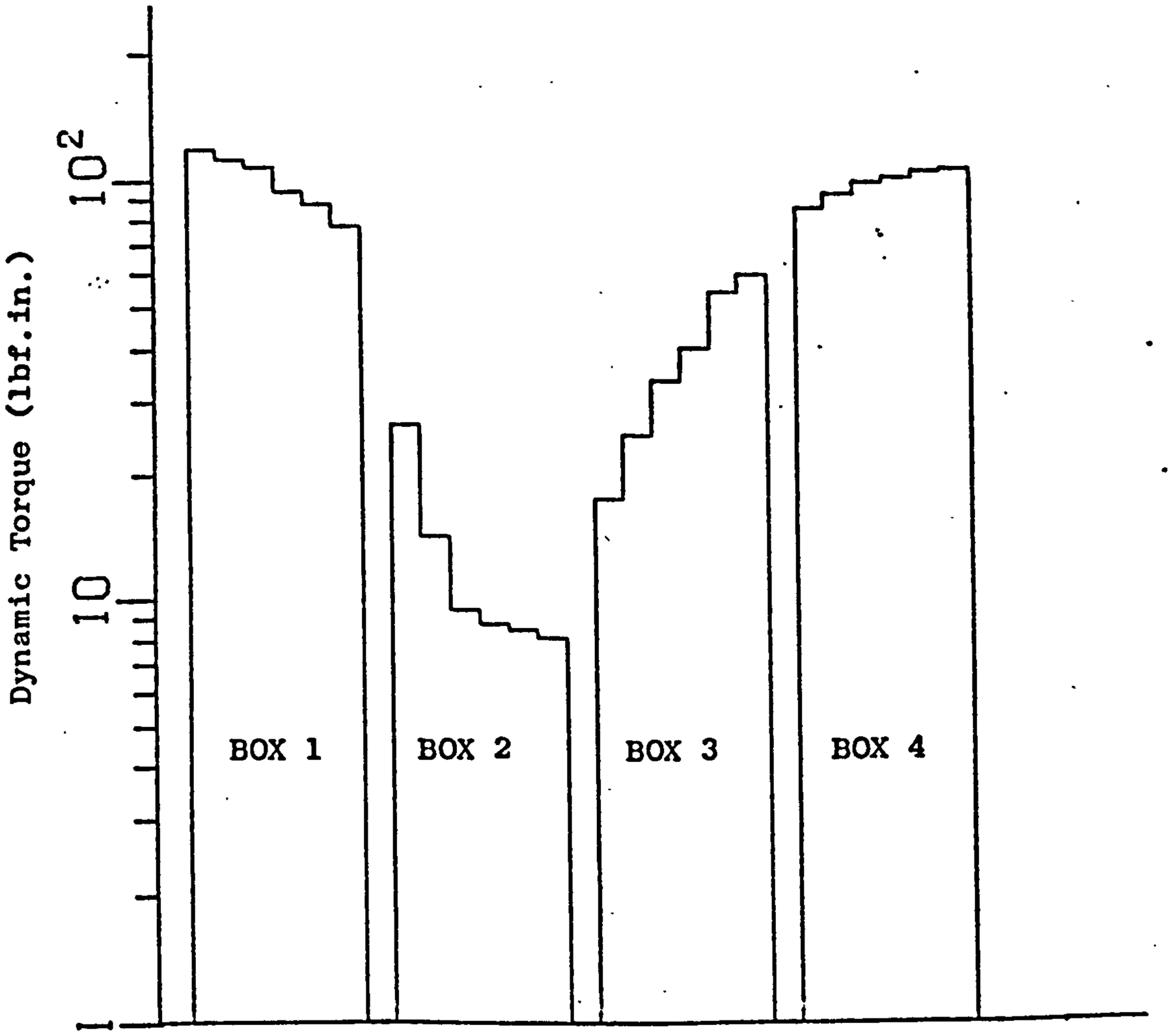

FIG. 6.28 Average Distribution of Dynamic Loading in 4 Box System at 2500 r.p.m.

7. EXPERIMENTAL RIG

7.1 General

The main reason for erecting an experimental rig was to observe drawbox system behaviour under controlled conditions and thus to establish the validity of assumptions underlying the theoretical analysis. Experimental observations could also be useful in themselves in producing evidence of dynamic behaviour in a gearing system more complex than is generally the subject of such studies. The immediate importance of a test rig would be associated with development of measurement techniques capable of application to practical gearbox environments. It was intended that such techniques could then be applied to drawtwister machines operating under normal service conditions.

7.2 Requirements of an Experimental Rig

7.2.1 General Construction

It was important that the rig should comprise at least two end-coupled drawboxes with variable speed running capability. A further requirement was that all boxes should be of the same type, manufactured by standard production methods to normal tolerances and fitted with solid cartridge gears. It was not considered necessary to provide a yarn processing capability and thus feedroll and spindle systems were not required.

7.2.2 Dynamic Characteristics

Within the speed range, at least one layshaft system resonance should be possible based on linear theory and an excitation frequency equal to the first order of drawroll rotation.

7.2.3 Speed Range

Drawroll speed should be infinitely variable, preferably up to the maximum rated delivery of 4000 ft/min. (3060 r.p.m.), however, a speed of 2500 r.p.m. would be adequate since this speed was not exceeded in the period up to 1969 when the phasing out of solid gears commenced.

7.3 Description of Test Rig

An experimental rig, incorporating four drawboxes, was erected and is shown in Figure 7.1.

The support frame was fabricated from 6" x 3" section channel and 15" x 6" I-section beams. All surfaces locating box machined feet were ground flat whilst the weight of all four boxes was taken by the frame. Each box was mounted on four $2\frac{1}{2}$ in. diameter bosses each with a $\frac{5}{8}$ in. centre hole allowing a bolted joint with the support frame. Adjacent layshafts were aligned radially to .001" and parallel to .002" in 8" length.

Power was provided by means of a 10 H.P. 3 phase motor (nominally 1450 r.p.m.) which was coupled to a Kopp Variator, type A2OFS, variable speed unit, with a speed ratio of $^{1}/3$ to 3 times input speed. Performance figures, obtained by the two Wattmeter method, indicated that a drawroll speed of almost 3000 r.p.m. could be achieved before

the Kopp Unit became overloaded.

Initially, the drive system was mounted directly onto the support frame; however, it induced considerable flexural vibrations within the frame assembly due to imbalance. The drive was therefore located semi-independently on a solid timber block fitted with a slotted base plate, and secured, within guides, to the frame. This arrangement produced substantial reduction in the frame vibrations. The drive arrangement is shown in Figure 7.2.

Unfortunately, the drawboxes available for this rig were not all of the same kind. The two nearest to the drive were of Type A type whilst the others were of Type C construction*. Also, the gears in the latter were brand new stock, whereas those in the former had completed an unknown period of duty prior to erection of the rig. That these gears displayed only light wear suggested that the previous run time was not substantial, perhaps amounting to only a few hundred hours.

The gearboxes were lubricated with a recommended gear oil, Shell Macoma 68.

* The Type C drawshafts are approximately 1" longer.

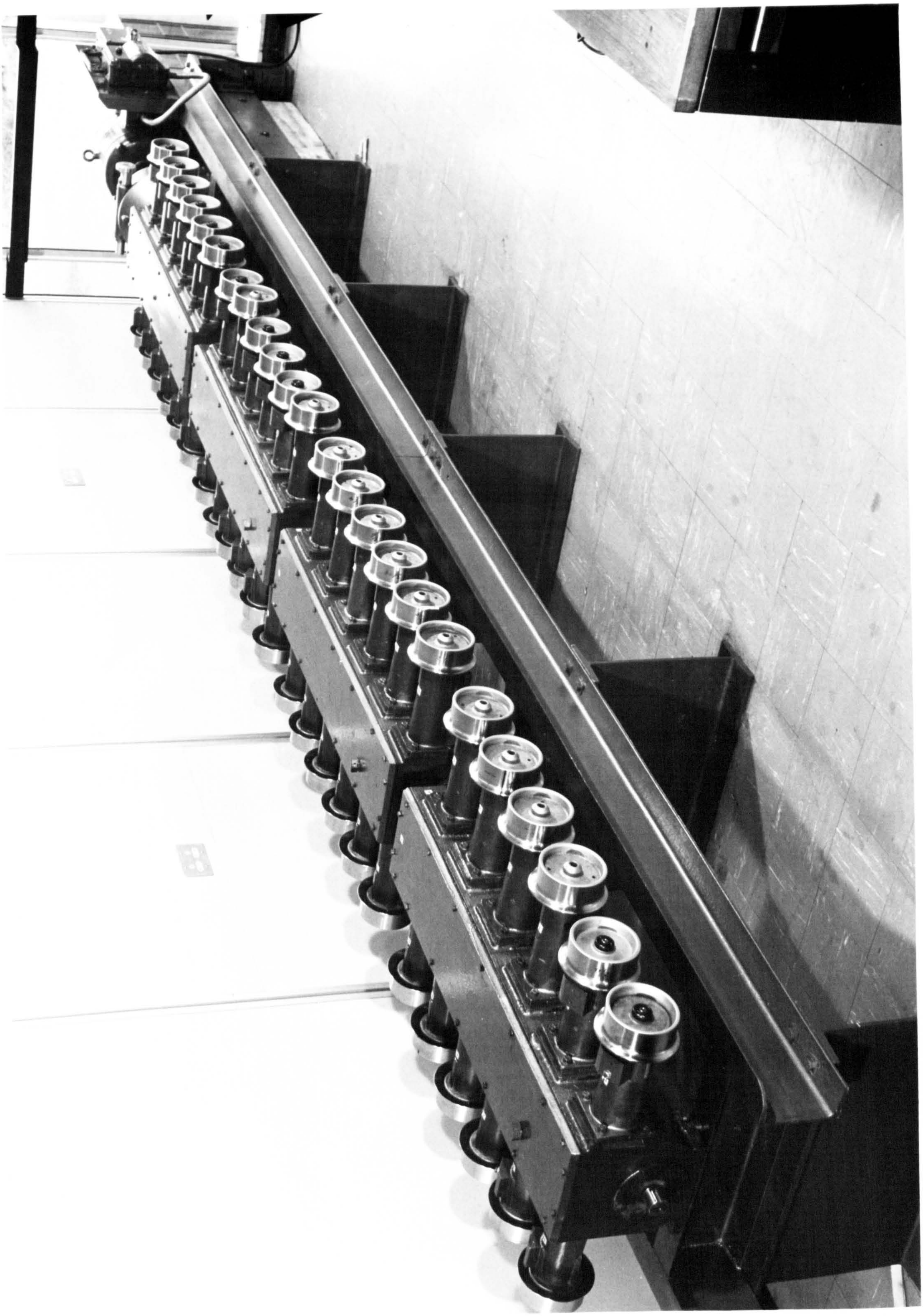

FIG. 7.1 The Multi-box Experimental Rig_

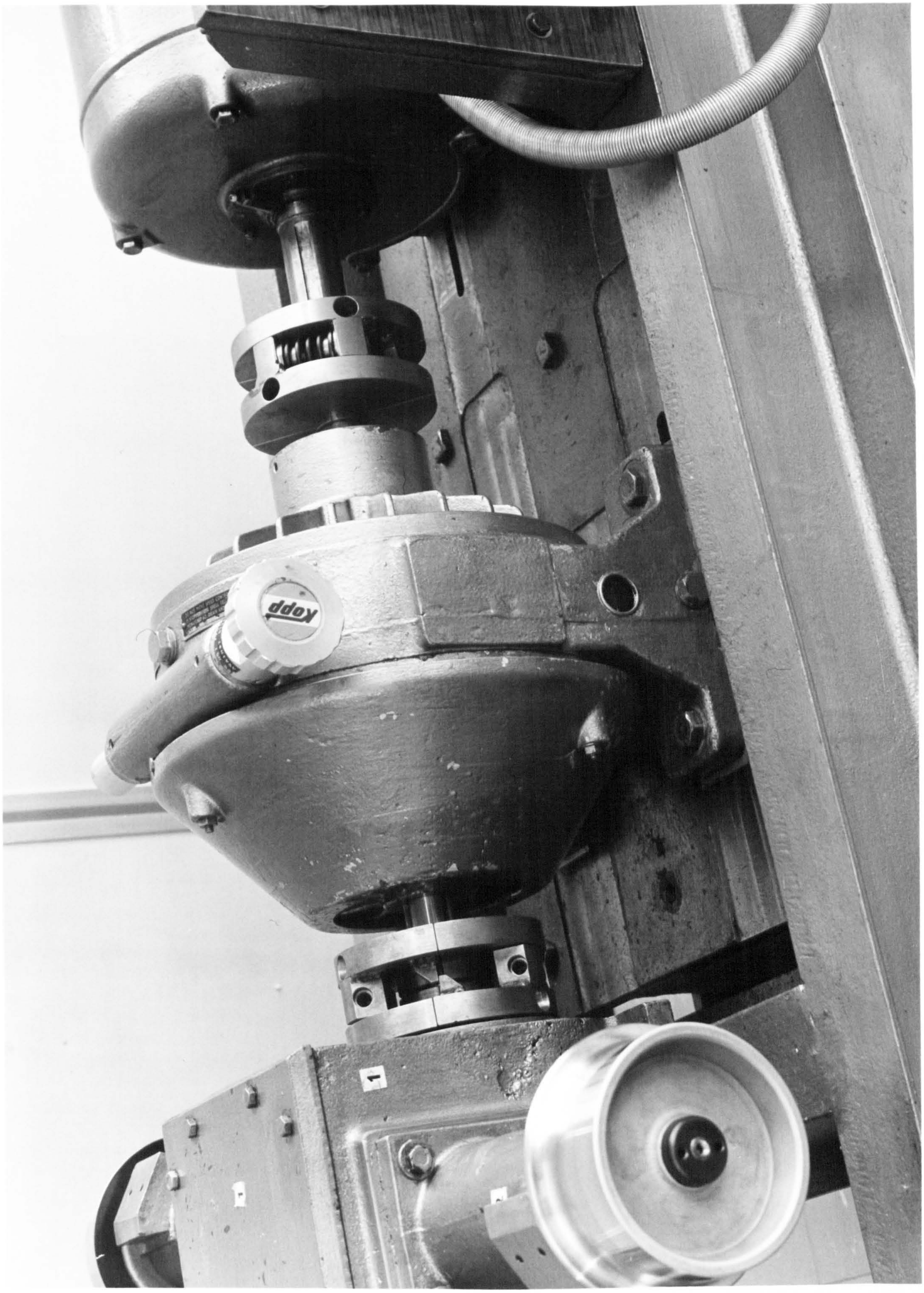

FIG. 7.2 Drive Arrangement for the Experimental Rig
(incorporating high flexibility couplings)

8. MEASUREMENT TECHNIQUES

8.1 Introduction

It has been seen (Section 4.2) that early experimental investigations into gearing dynamics concentrated on the measurement of individual tooth loads. More recently, the measurement of gear motions has assumed a greater importance as the problem has become recognised as one of vibration. Whilst both approaches would be appropriate to the current research, the latter is adopted in preference, since it is thought to provide a greater insight into gearing behaviour. It is also considered important to simultaneously monitor impact behaviour at several gear meshes within a particular drawbox.

At the outset of the research, it was proposed that direct measurements be made within the gearboxes of drawtwisters in normal production service. It would be necessary to make measurements on both solid and bushed-gear configurations and at any position within a total machine. Because access to drawboxes would be severely restricted, it was important that any necessary encoders or transducers should be carried on a small number of drawroll cartridges which could then be conveniently inserted anywhere in the drawbox system. At least two instrumental gear pairs would thus be required since both left and right handed bronze gears are employed within any gearbox.

The constraints outlined in the foregoing paragraph rendered established techniques, such as that of Munro, unsatisfactory for direct measurements in an oil lubricated gearbox environment.

It therefore became necessary to develop methods capable of application to this more practical class of problem.

8.2 Detection of Tooth Impact

8.2.1 General Remarks

Throughout the meshing cycle of a pair of mating gear teeth, it is normal for the teeth to be separated by a thin film of oil. The oil film thickness depends on a number of factors, among which is the contact pressure. If an electrical circuit were set up to pass a current through the tooth mesh, the potential drop across the mesh would depend on the film thickness and, hence, on the tooth contact pressure.

It has been seen (Section 4.2) that an early attempt to use mesh resistance in dynamic studies was not very successful, mainly owing to the unavailability of suitable electronic instrumentation at that time. More recently, the technique has been employed, with success, in the observation of lubrication behaviour and, in particular, the measurement of oil film thickness (57)(58). Because of its relative simplicity, (compared, for example, to the methods described in Sections 8.3 and 8.4) the resistance method has been resurrected for the detection of tooth impact behaviour.

8.2.2 Description of Method and Equipment

The wear pattern identified on drawtwister bronze gears (Section 3.1) requires that, in between heavy impacts, on normal and trailing tooth faces, there must be a period of no contact whilst the backlash is traversed. This behaviour may be investigated by employing

the circuit shown in Figure 8.1 and continuously monitoring the voltage drop across the gear mesh. The resistor R serves two purposes:-

1. It provides a comparator resistance without which the system would be insensitive.

2. It limits the maximum current flow, thereby reducing the possibility of spark erosion at the gear teeth.

Maximum mesh voltage will occur when tooth contact is lost and the mesh resistance is high compared to that of resistor R. The minimum voltage drop will be zero and occurs during metal to metal contact. Thus, for given values of battery voltage and resistor R, all measured potential drops will be within two definite limits.

To employ the foregoing in a practical circuit, it is necessary to electrically isolate the steel gear cartridge from the rest of the drawbox, so that the only electrical path is through the tooth contact. This was accomplished by means of three modifications, as follows:-

1. The cartridge diameter, locating the drawbox bore, was machine reduced and fitted with a nylon insulation sleeve, making up the original diameter.

2. A thin, non-conducting gasket was placed between the cartridge bolting flange and the drawbox.

3. The securing bolt clearances were increased to take nylon sleeves with an integral washer at the bolt head end.

The battery connection to the steel gear was attached to the pod casting so that the circuit was completed by flow through the ball bearings.

Three steel gear assemblies were thus modified so that the behaviour of three gear pairs could be observed simultaneously. By selecting two right and one left handed gears for the conversion, measurements could be made at all positions in a single drawbox, using ónly two set-ups.

Mesh voltage signals were displayed on a multi-channel cathode-ray oscilloscope with storage facility (Tektronix type 564B). Specimen records were obtained by means of a polaroid-type camera unit. In order to provide a continuous recording capability, an ultra-violet recorder (S.E. Laboratories type 2000) was employed, together with galvanometers (type A8000). Because the galvanometers had a resistance of only 40 ohms and a sensitivity of 1.0 ^{v}/cm., it was necessary to construct a suitable matching amplifier for each channel. It was important that the behaviour of all the amplifiers was identical within close limits and that D.C. drift was negligible over long periods of operation. Figure 8.2 shows the circuit developed to meet these requirements. The response characteristic of each amplifier was found to be flat up to a frequency of about 50 KHz.

8.3 Measurement of Gear Motions by Means of Magnetic Drums*

8.3.1 Description of Technique

Two small drums were fitted to a meshing pair of drawshaft gears and surface coated with a magnetic recording material. The gears were assembled in a double cartridge gearbox† (Figure 8.3) with a magnetic record/replay head tracking on the periphery of each drum.

The arrangement shown schematically in Figure 8.4 was used to calibrate the drums as follows. An optical radial grating fitted to the bronze gear shaft (replacing the drawroll) was employed to generate periodic voltage signals as the shaft was slowly rotated. These were recorded simultaneously on both magnetic drums whilst a brake load was applied to the steel gear shaft to maintain tooth contact throughout.

In this way the two drum signals were synchronised in time thereby eliminating the effects of transmission error and both drum and grating eccentricities.

Having thus calibrated the gear pair, the absent drawroll was replaced and relative gear motions studied under various

* Basic principles of magnetic recording are given in Appendix M.

† The 2-position box was driven by a Servomex .5 H.P., D.C. Motor (type D27H2) with a Servomex motor control unit (type MC 47).

running conditions by employing the drum heads in the "replay" mode (Figure 8.5). If the gears rotate without vibration, as during calibration, the replayed drum signals will appear in phase if displayed on a cathode-ray oscilloscope. Any loss of tooth contact or movement through the gear backlash will produce a varying phase shift between the two signals, proportional to the relative displacement.

Since the original calibration signals are written simultaneously at low speed, the method detects relative gear displacement with automatic compensation for static transmission error and eccentricity of the drums and the optical grating. /

Further details of the technique, together with practical considerations, now follow.

8.3.2 Gear - Drum Arrangement

The method described above would have to be applicable to flexibly mounted gears, as well as solid gears, and so this more difficult case was considered first. Perhaps the greatest problem was associated with the space restriction that the only access to a drawbox would be through the cartridge bore. The gear drum diameter, therefore, had to be small enough to afford room for the magnetic head arrangement and also to avoid fouling at the crossed helical mesh.

/ If it was desired to use the magnetic drum arrangement for the measurement of static or dynamic transmission error, then the compensation feature would not be required and uniform signals would be written independently onto each drum.

Figure 8.6 shows the solution adopted in practice. An interference fit located the drum on a reduced diameter shoulder on the gear. In order to provide a satisfactory clearance, it was necessary to reduce the outside diameter of the gear support bush and to cut a chamfer through the two rubber bushes. Drum eccentricity was minimised by finish machining the outer diameter with the unit rotating in the drawshaft bearings. It should be noted that low drum run-out was not required for the actual technique since it is automatically compensated for; however, it is important in respect of the magnetic head to drum clearance as will be seen later.

To minimise the possibility of magnetic signal noise, it is important to use a non-magnetic material for a recording drum. Non-metallic materials were found to be too flexible in thin sections and, therefore, phosphor-bronze was chosen. In retrospect, however, the author believes that aluminium would have been a better choice since the lower density would have provided a smaller modification to system inertia.

8.3.3 Mounting of Magnetic Head

Accuracy of head position is of paramount importance in magnetic drum recording. Signal strength is maximum when the head and drum touch lightly along a line coincident with the head gap. As the head profile is normally convex and the air gap is usually less than .0001 inch, a very precise setting-up capability is required for the mounting arrangement. It is usual, in drum applications, for the head to be separated from the recording material in order to avoid wear (60). Gaps are typically in the region of .0001 inch to .0005 inch and this tolerance dictates that drums and bearings should be manufactured to give an eccentricity of less than head-drum clearance,

unless floating heads are employed.

In this application, such precision could not be guaranteed, even by finish machining each drum in its own bearings and it was therefore decided to run with direct contact*. The mounting arrangement employed is shown in Figure 8.6. Two strips of .003 in. shimming steel supported the head between the sides of a forked bracket, the electrical connections being suitably insulated. The bracket was seated on rubber washers in compression against a flat surface machined on the draw pod casting. The washers were specially moulded to size using a neoprene-type rubber to minimise deterioration in the oil environment. Three 12 B.A. screws, forming an equilateral triangle in plan (Figure 8.9), permitted fine adjustment vertically and rotationally, in the vertical plane, about axes parallel to and perpendicular to the shaft axis.

Electrical connection wires were taken from the head via the inside of the pod casting to the drawroll side of the gearbox wall.

It was possible to insert the completely assembled unit, shown in Figure 8.7, into a drawbox via the standard location bore.

8.3.4 Magnetic Recording Medium

Initial experiments were carried out using magnetic tape of domestic quality; however, it was not possible to produce a satisfactory joint to give a continuous recording surface.

* In practice, an oil film would form a small clearance.

This problem can be overcome by means of continuous magnetic belts of the type used by the G.P.O. for pre-recorded telephone information. Unfortunately, these were not available in a convenient size but, in any case, those tested were found to be inferior to magnetic tape, particularly for frequencies above 10 KHz.

Stainless steel recording wire of the type used in "black box" flight recorders was considered but rejected in favour of coating compounds. Preliminary experiments showed that most of these had magnetic properties inferior to those of domestic recording tape. One exception was dispersion fluid B.255., manufactured by Minnesota Mining and Manufacturing Co. Ltd., which compared favourably with tape performance. The compound was therefore adopted for all further tests.

Before applying the compound, the bronze drums were washed in acetone to remove any grease and other extraneous dirt. The dispersion compound was diluted by the addition of 50% (by weight) of methyl-ethyl ketone. Each drum was dipped into the diluted compound and slowly withdrawn to produce an even deposition of about .001 in. which dried in air in about ten minutes.

8.3.5 Generation of Calibration Signal

The optical arrangement, shown schematically in Figure 8.4, was used to produce the calibration signal for the two gear drums. Light from the lamp passes through a collimating lens and produces light intensity changes when viewed from the photo cell, according to the rotary position of the scale grating with respect to the fixed index grating. The lamp, lens, index grating and photo cell arrangement is referred to as a 'normal incidence' reading head (61).

An electrical signal, proportional to light intensity, is output from the photocell. This is made compatible with the magnetic heads by a suitable amplifier and split to provide identical signals for simultaneous recording on the two gear drums.

The choice of grating lines per revolution depends on the measurement resolution required. Since it was desired to observe motions taking up the tooth clearance, a grating of 540 lines per revolution was selected. With 540 complete signals transferred to each drum, a phase shift of one complete cycle corresponds to a relative displacement equal to the maximum permitted backlash, i.e. .014 in. at the pitch radius.

8.3.6 Magnetic System and Recording Considerations

In order to evaluate the effectiveness and ease of application of the magnetic technique, it was decided to use a recording system no better in quality than that of an ordinary domestic tape recorder.

In this context, Marriott type X/RPS/36 quarter-track heads were used, having characteristics as follows:-

Air gap	0.0001 in.
Width	0.043 in.
Spacing	0.136 in.
Inductance at 1 kHz	70 mH
Bias at 50 kHz	11 V
Recording current for 2 dB below 2% distortion	110 μA
Output at 1 kHz using E.M.I. test tape	0.44 mV
Output at 2 kHz for 110 uA recording current	1.07 mV
Max. Frequency response at $7\frac{1}{2}$ in/sec.	20 kHz

A compatible recording amplifier was specially built for use with heads of this type. The circuit, shown in Figure 8.8 is based on a design published by Mullard Ltd. (62).

It is now appropriate to consider signal packing density in relation to head frequency response. The chief restriction to head response at high frequency is the air gap dimension. When the signal to be recorded would occupy a length of magnetic medium approaching the air gap size, then clear recording cannot take place. For the head characteristics quoted above, the limiting frequency of 20 kHz at $7\frac{1}{2}$ in/sec. corresponds to a packing density of 2670 signals/in. or a signal spacing of .0004 in. which is clearly of the same order as the air gap. Increasing the frequency beyond this limit would produce a correspondingly higher packing density and a lower spacing, thus causing a rapid fall off in recording quality.

The 540 signals recorded on the drum periphery correspond to a packing density of only 75 per inch or a spacing of .013 which is well within the handling capability of the poorest of heads. This low packing density also facilitates good high frequency replay performance. The replay frequency from the calibrated drums will depend on the drawroll running speed; for example, at a running speed of 2000 r.p.m. it will be 18 kHz.

8.3.7 Electronic Phase Comparator

In using the calibrated gear pair to study motions, it is clearly impracticable to simply display or even record the two output waveforms. Finding phase shifts of up to one cycle in every 540 cycles is an extremely laborious process and is best done

electronically. To this end, an electronic phase comparator was built, to the author's user specification, by the Cranfield Unit for Precision Engineering. The comparator receives two signals of nominally identical frequency and produces a continuous D.C. voltage proportional to the phase shift between them. This voltage may be used to produce permanent records, for example, by means of an ultra violet recorder.

Briefly, the principles used to translate phase shift to a proportional voltage are as follows. When one of the two input signals passes through zero to positive it switches on a D.C. output at a certain level. This persists until the second wave passes through zero to positive which switches the D.C. level off. The switching process continues so that a squared wave is produced whose "mark to space" ratio varies in time as the phase between the two input signals varies. A digital to analogue convertor is then employed to produce a smoothed D.C. output proportional to phase difference.

This type of apparatus is used together with optical gratings in single flank gear testers. More detailed accounts of its design and application appear elsewhere (63)(64).

8.3.8 Setting-up Procedure

After a satisfactory coating of magnetic dispersion compound had been applied to both steel and bronze gear drums, the units were assembled as shown in Figure 8.7. Magnetic head positions were set as accurately as possible by eye with the two cartridges still on the bench. Final adjustments were made with the cartridges inserted into the short gearbox as shown in Figure 8.9. This was accomplished by simply attempting to write the calibration signal onto each drum when set in motion and making fine head position

adjustments until replayed signals were of good quality from both drums. In order to check that the head gap was making a line contact on a drum, signals were written onto both recording tracks and adjustments made until replayed signals were of equal amplitude from each track.

At this point it was necessary to erase all signals and noise recorded on the drums during the testing and adjusting phase, ready for the actual calibration run. It was possible to completely erase drum records in situ using the record/replay heads in conjunction with the optical system. With the light source at normal recording intensity, the recording level, controlled by the recording amplifier, was reduced progressively to zero over several shaft revolutions. This gradual reduction of an oscillating signal produces a random orientation of particles comprising the magnetic material, that is, the surface is demagnetised.

In order to approach "static" conditions, the calibration run was completed at drawroll speeds not exceeding 60 r.p.m.* and a small brake load was applied to the outboard drawroll to maintain tooth contact. Signal recording was arranged to take place over several drum revolutions after which the recording quality was closely examined. Absence of any appreciable wave distortion confirmed that a reasonable static calibration had been achieved.

Gear motion studies were carried out using the calibrated pair in the multi-box rig previously described. In recreating the gear mesh, it was essential that the mating teeth were the same as previously, otherwise the static synchronisation would be invalid due to the change in gear transmission error.

* 60 r.p.m. corresponds to a (satisfactory) recording frequency of 540 Hz.

8.3.9 Performance of Magnetic System

Although the dynamic phase comparator, described in Section 8.3.7, was fitted with input channel amplifiers for waves of signal to noise ratio worse than 30 dB, their use was unnecessary in the testing range of 750 to 2000 r.p.m. Figures 8.10 and 8.11 show oscilloscope traces of the drum replay signals at 100 and 1800 r.p.m. respectively. Signal strength increased with speed up to the maximum test speed of 2000 r.p.m., corresponding to a frequency of 18 kHz. Typical signal strengths directly from the drum heads, that is, without amplification, were as follows:-

60 r.p.m. (recording speed)	-	10 mV (peak to peak)
750 r.p.m. (minimum speed of 4 box rig)	-	50 mV (peak to peak)
2000 r.p.m. (maximum test speed)	-	70 mV (peak to peak)

Figure 8.12 illustrates the effect of relative motions on the phasing of the two drum signals. The upper pair of waveforms, which are in phase, are typical of those produced when the gears were maintained in contact by means of an applied load. The lower pair were recorded under the same conditions except that the applied torque was removed, thus permitting motions through the backlash and, hence, a phase shift in the replayed signals.

Altogether a total of about 6 hours of measurements were performed, mainly at 1700 to 2000 r.p.m., before wear of the magnetic surface caused signal deterioration. It is felt that a much greater coating life could have been achieved by adopting a lower head to drum contact pressure.

8.4 Measurement of Gear Motions by means of Optical Gratings

8.4.1 Introduction

Optical gratings are used extensively in industry to measure relative displacement or position (61). This information may be important in itself as, for example, in the measurement of gear transmission error (65) or, it may be employed in a feed back loop to reduce manufacturing errors or to make positional adjustments in machinery(66).

It has been seen (Section 4.3.4) that application to gear vibration studies is hampered somewhat by the difficulty in separating motions, at once per revolution, from static transmission errors and, more particularly, mounting eccentricities. A method aimed at eliminating the problem is briefly described in this Section and, although a satisfactory technique has not been perfected in the time available, preliminary work is summarised.

8.4.2 Description of Technique

The technique proposed attempts to achieve an optical equivalent of the magnetic system described earlier. One way of doing this would be to generate reflective radial gratings on the two cartridge gears in such a way that transmission error and grating eccentricities were accounted for in the relative line spacings. To this end, a master grating could be employed on one drawshaft to simultaneously reproduce grating lines on the two meshed gears by a photographic process. It would be essential to perform the operation with tooth contact maintained throughout and in the absence of any vibration.

Having thus statically calibrated the gear pair, torsional motions could be continuously monitored by employing a light source and optical reading head in conjunction with each gear grating. The two wave forms thus produced would be input to a dynamic phase comparator in the same manner as described for the magnetic system. (Section 8.3.7). If, during operational measurements, the gears are free from vibration, as in the calibration, then no phase shift should be indicated. Relative gear motions, apart from that due to static transmission error, will result in a proportional phase variation which may be detected. Knowledge of the grating pitch allows a direct calibration of output signal in terms of motion amplitude.

Applying the principles of the foregoing to a reliable measurement technique first requires solution to two major practical problems:

1. the generation of reference gratings on the meshed gear pair.
2. the transmission of optical signals to and from instrumented gears assembled in a production drawbox.

Attention is now focussed on these problems, commencing with the latter.

8.4.3 Optical System Permitting Access to In-Situ Gearing*

One approach to the gearbox access problem is to employ fibre optics (67)(68). The basic principle of fibre optics is that a bundle of transparent fibres (termed a fibrescope) can transmit light

* ACKNOWLEDGEMENT - The experimental work described in this Section was carried out by Mr. R. W. Grundy (69) under the author's guidance. His cooperation is gratefully acknowledged.

from one end to the other even when its shape is distorted. This is accomplished by either internal reflection or refraction.

Preliminary experiments were performed with the arrangement shown in Figure 8.13 to examine the feasibility of fibre optics for this application. Two Y-branched fibrescopes (Dolan-Jener, type EEK 3036) were used to connect each sensing aperture to both light source and photocell (Ferranti, type MSI-B). Optical lasers (Spectra Physics, type 120) were used as light sources in order to provide a concentrated beam to allow for intensity losses. A reflective radial grating having 512 lines per revolution was attached by adhesive joint to each drawshaft gear as shown in Figure 8.14. The index grating and fibrescope were clamped to a perspex support bracket also shown in this illustration and both drawroll cartridges were inserted into the two-position gearbox rig as shown in Figure 8.15.

For a range of running speeds, signals taken directly from both photocells were displayed on a Tektronix storage oscilloscope (type 564 B) and permanent records obtained by means of a polaroid type camera unit. Typical waveforms produced by the twin optical system are shown in Figure 8.16, which illustrates good signal quality. Unlike the magnetic system, however, it was found that signal strength decreased with increasing speed. Typical measured amplitudes were as follows:-

100 r.p.m. - 20 mV (peak to peak)

450 r.p.m. - 16 mV (peak to peak)

2100 r.p.m. - 5 mV (peak to peak)

The conclusion to be drawn from these preliminary tests is that, whilst the application of fibre optics to remote gearing measurements looks promising, further development is required.

8.4.4 Generation of Gear Gratings in situ

It is suggested that the arrangement shown in Figure 8.17, which is based on standard grating duplication techniques (61), would be suitable for reproducing reflective gratings on meshed gears.

A master grating connected to one drawshaft would be used in conjunction with a reading head to produce a waveform on rotation. This would be converted to a train of pulses, by a trigger unit, each of which would simultaneously operate two flash tubes thereby projecting a single grating image onto photo sensitive coatings on each gear. (Object gratings and collimating lenses would be required, as shown, for this process). After exposure during a complete revolution, the photographic plate could be developed in situ (70).

The need to create each grating line separately, without exposing the remainder of the photographic plate, represents a difficulty in this approach. To overcome the problem, it might be necessary to employ an elaborate screening system in a specially constructed calibration rig.

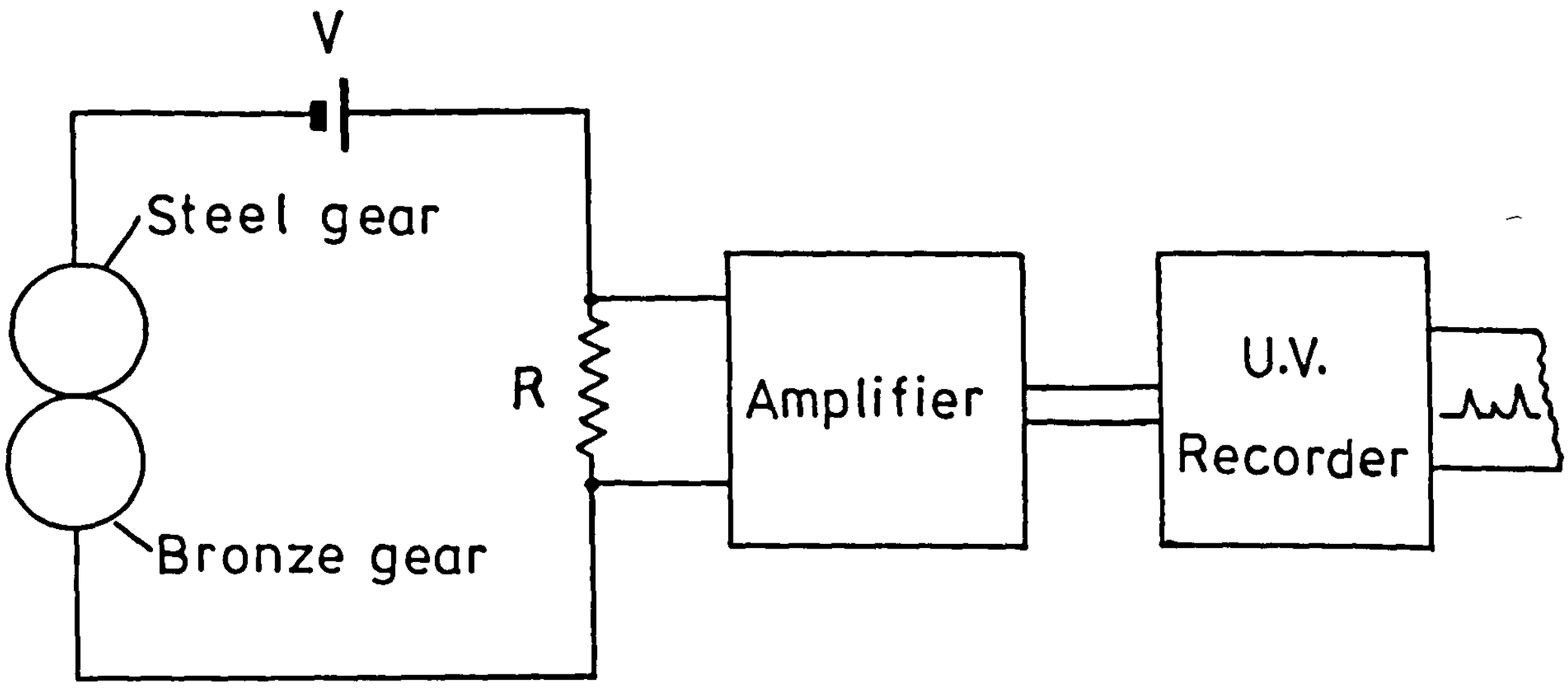

FIG. 8.1 Basic Electrical Circuit for the Detection of Tooth Impacts

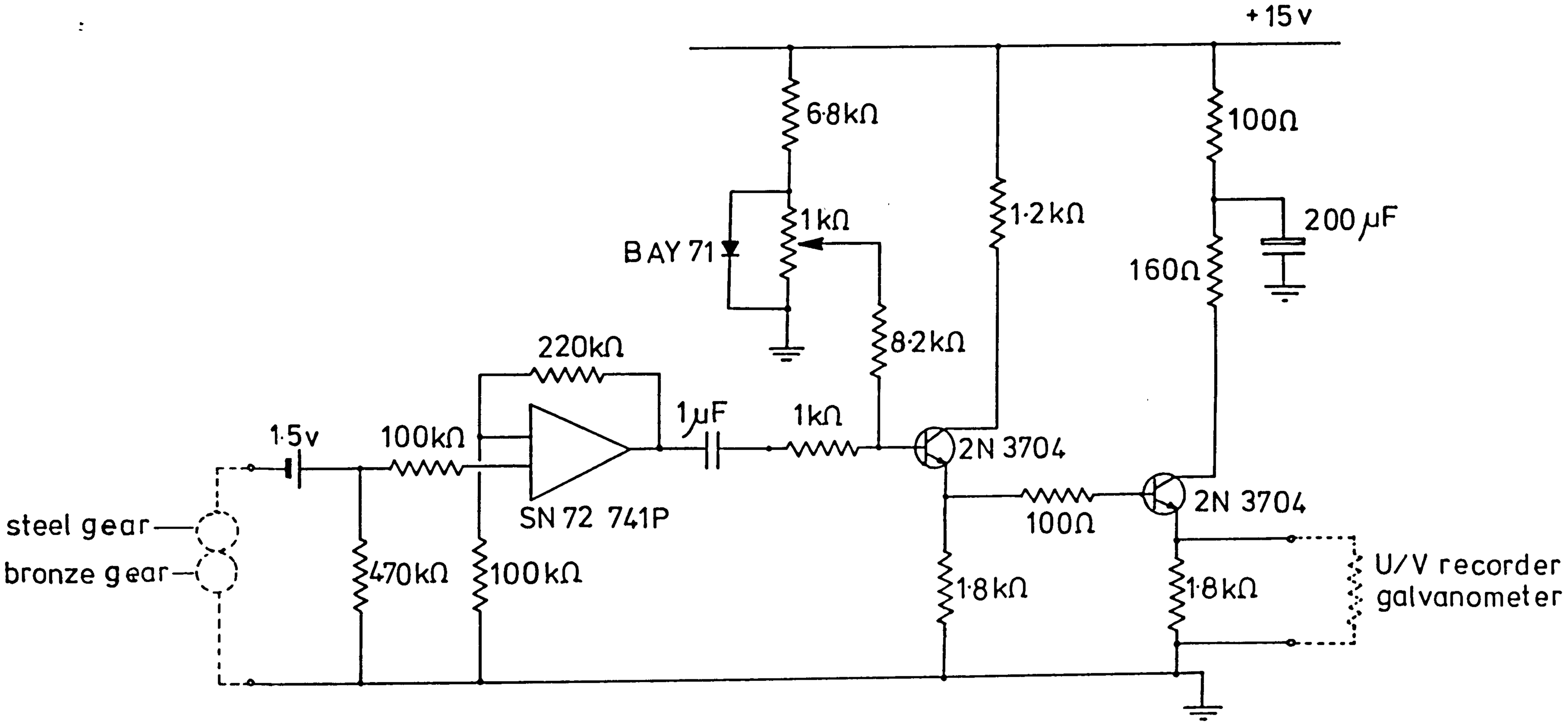

FIG. 8.2 Matching Amplifier Circuit for the Detection of Tooth Impacts

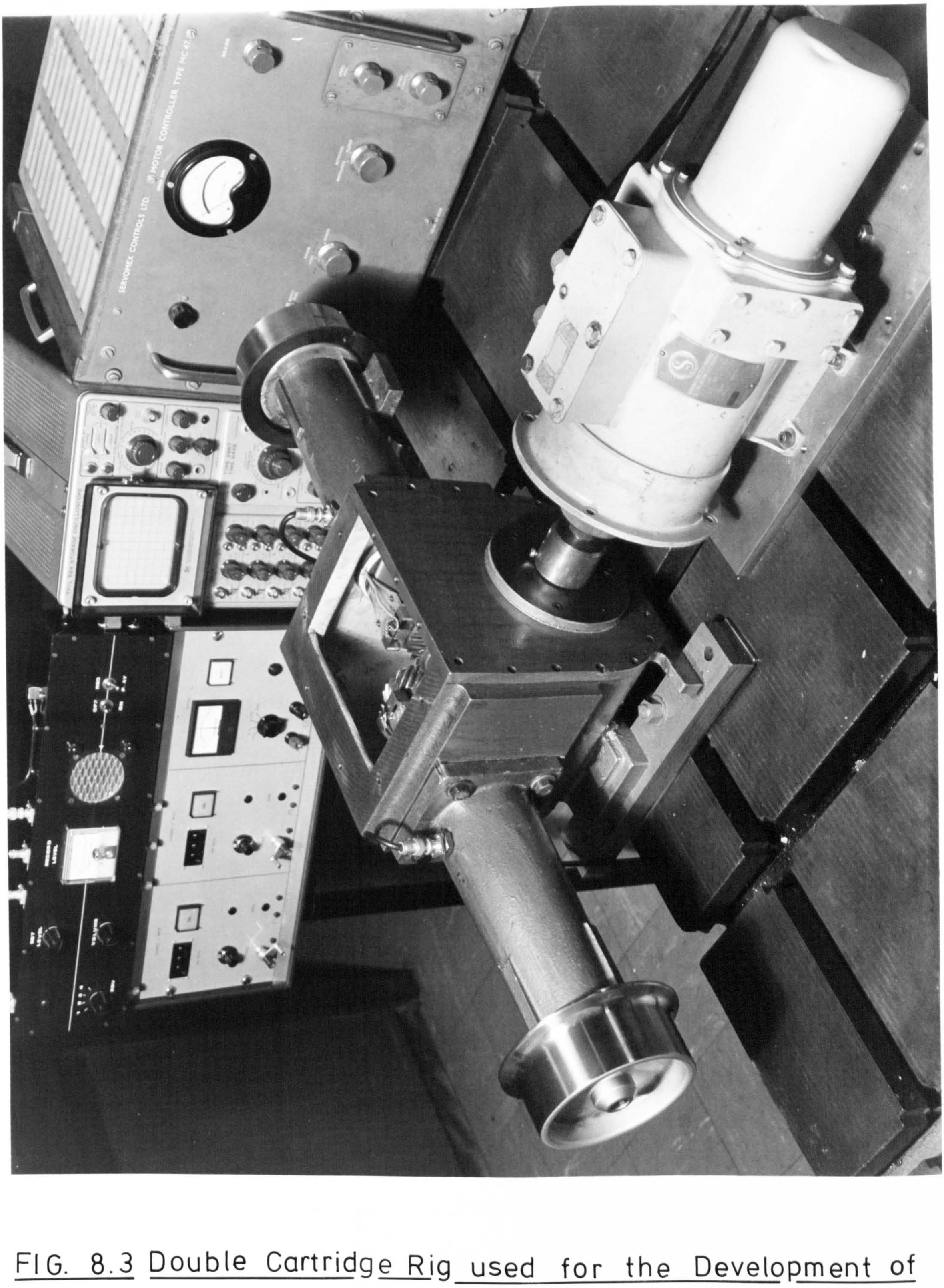

FIG. 8.3 Double Cartridge Rig used for the Development of Measurement Techniques

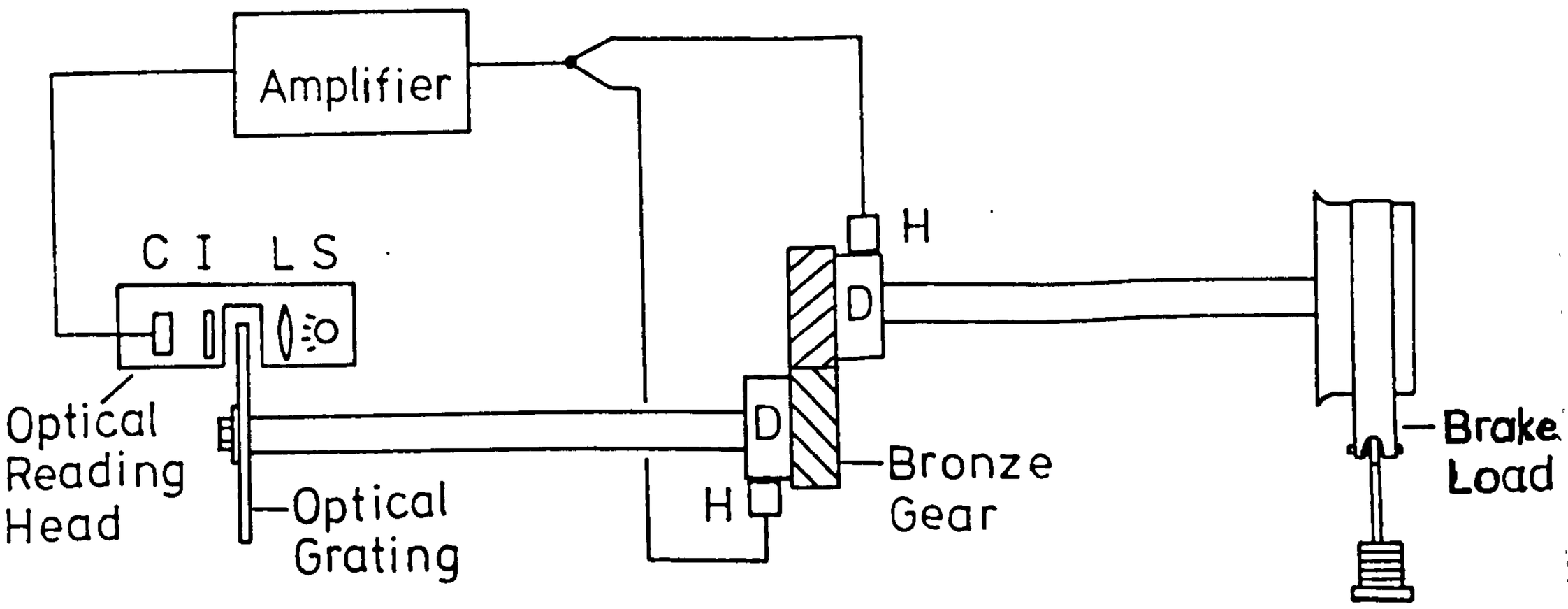

S - Light Source
L - Lens
I - Index Grating
C - Photocell
H - Magnetic Head
D - Magnetic Drum

FIG. 8.4 Calibration Arrangement for Magnetic Drum System

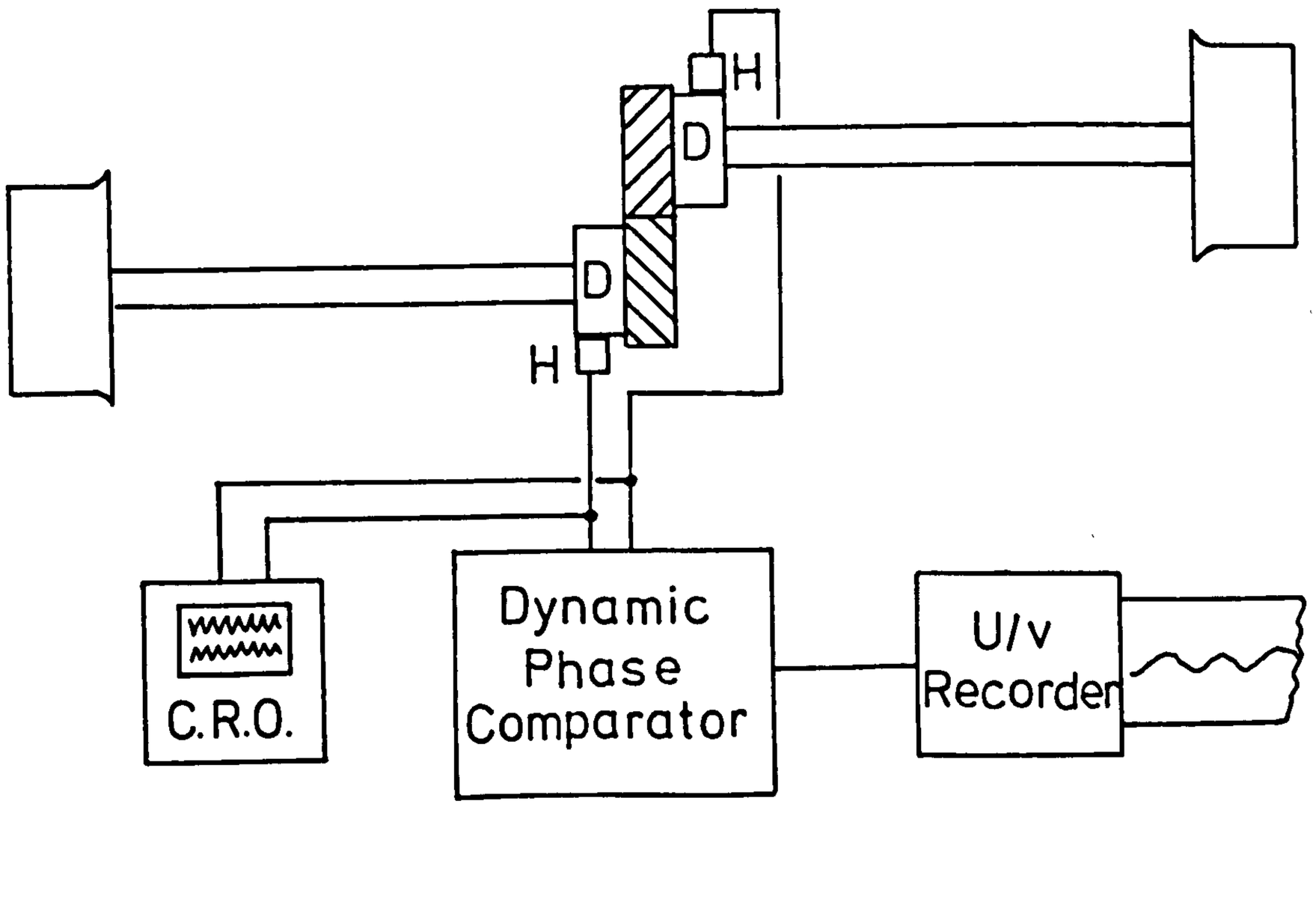

FIG. 8.5 Arrangement for the Measurement of Gear Dynamic Motions

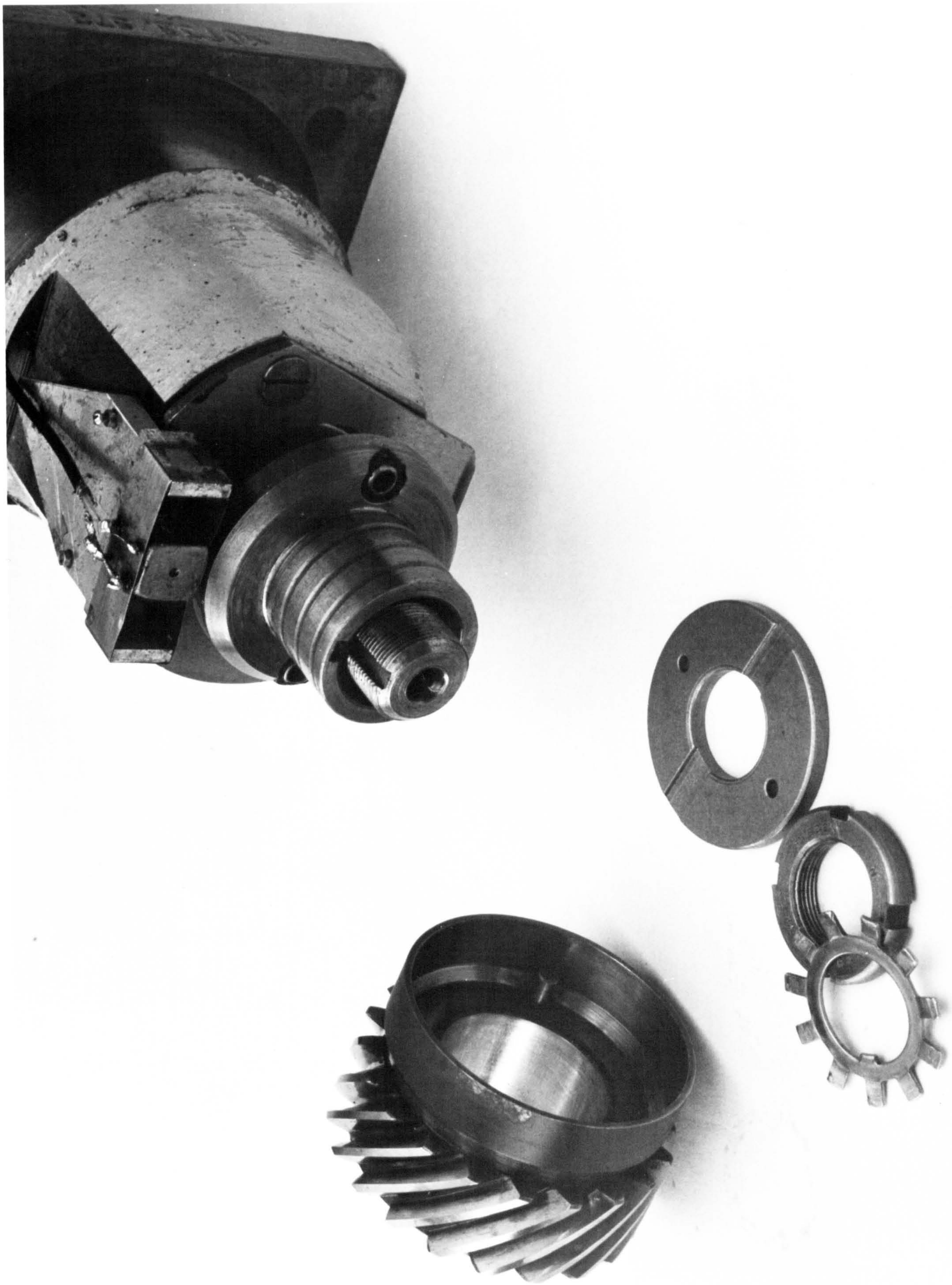

FIG. 8.6 Magnetic Recording Drum and Head Mounting Arrangement

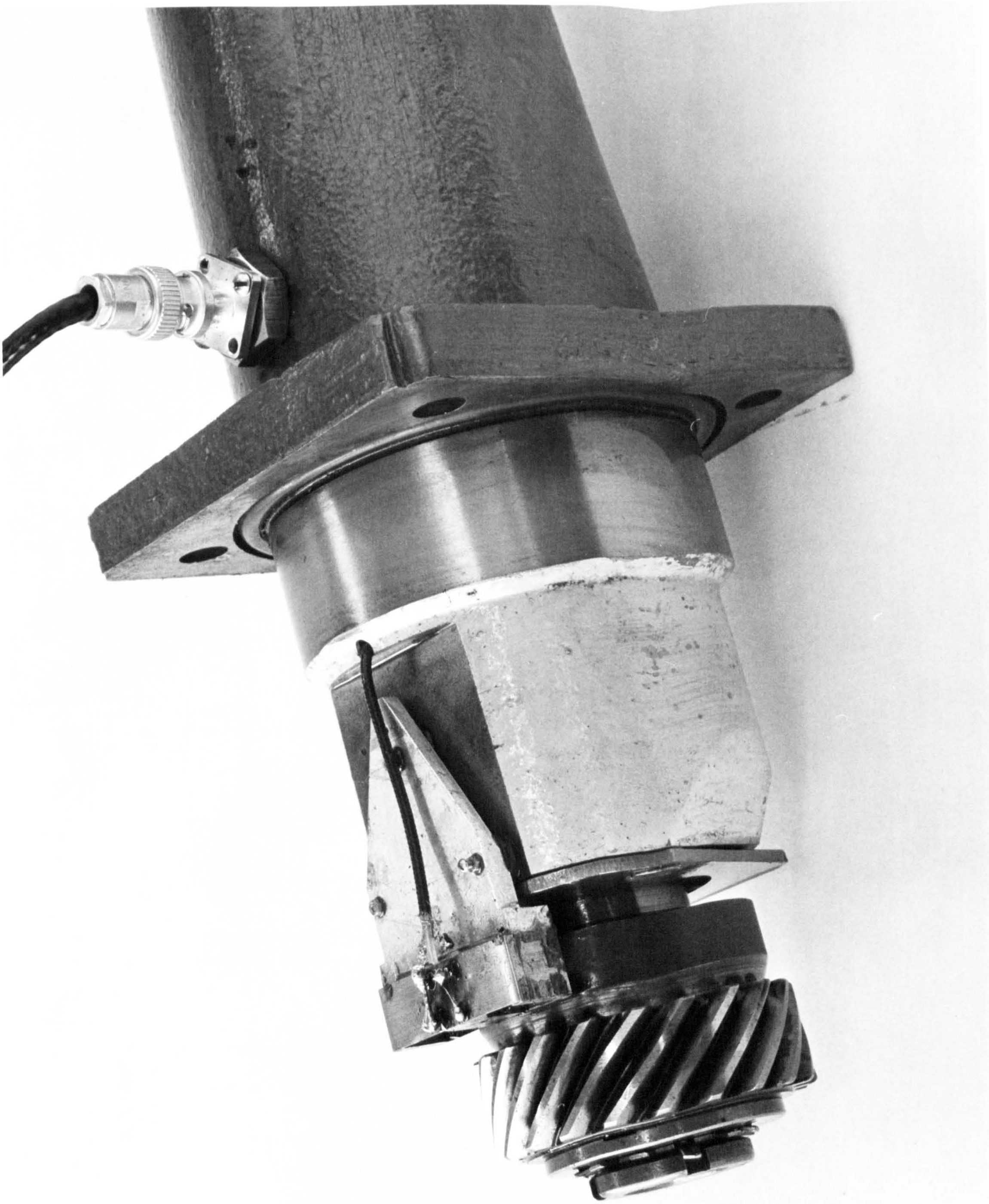

FIG. 8.7 Drawroll Cartridge Instrumented with Magnetic Encoding System

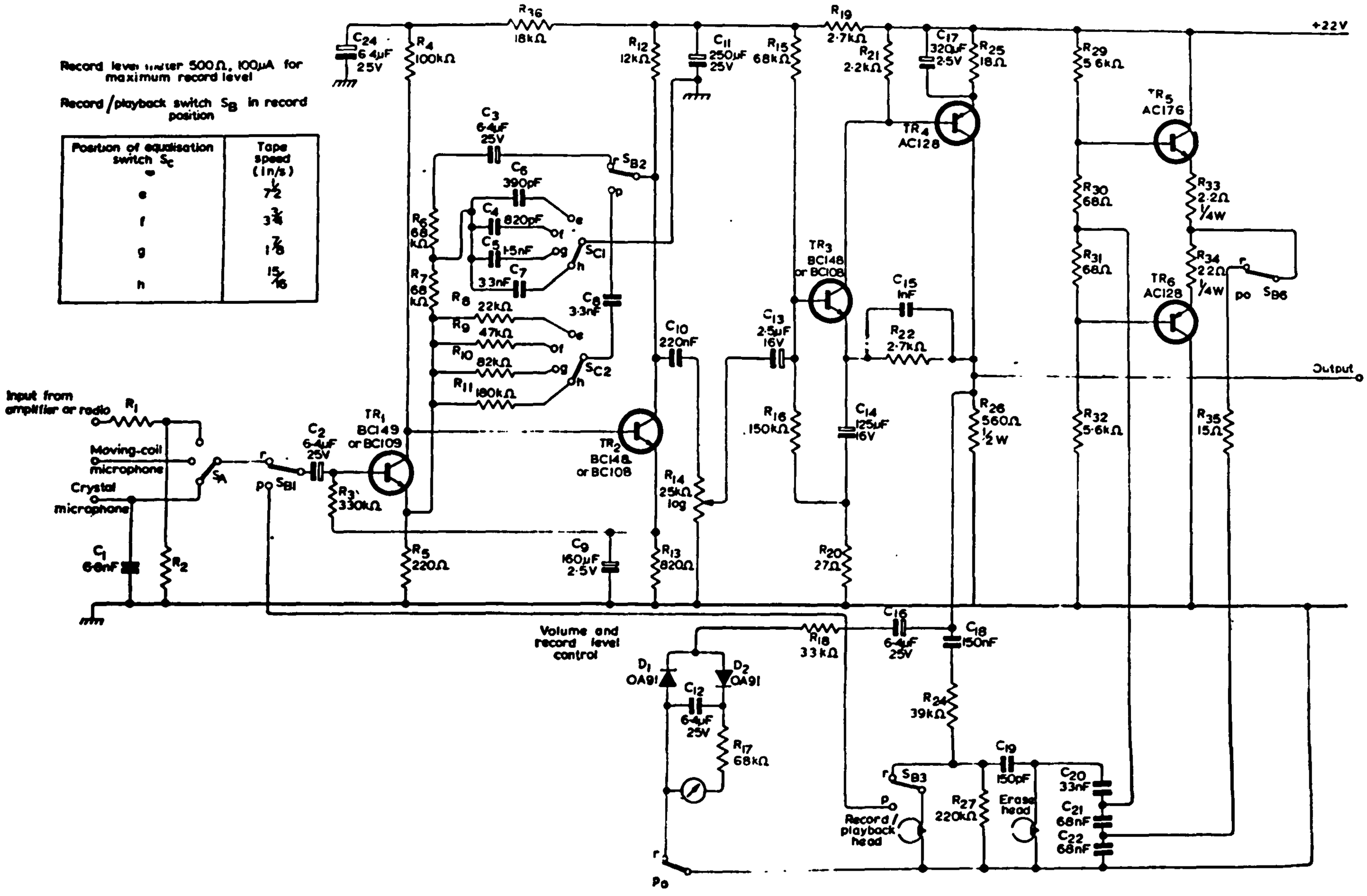

FIG. 8.8 Pre-amplifier Circuit for Magnetic Heads
(reproduced from reference (62))

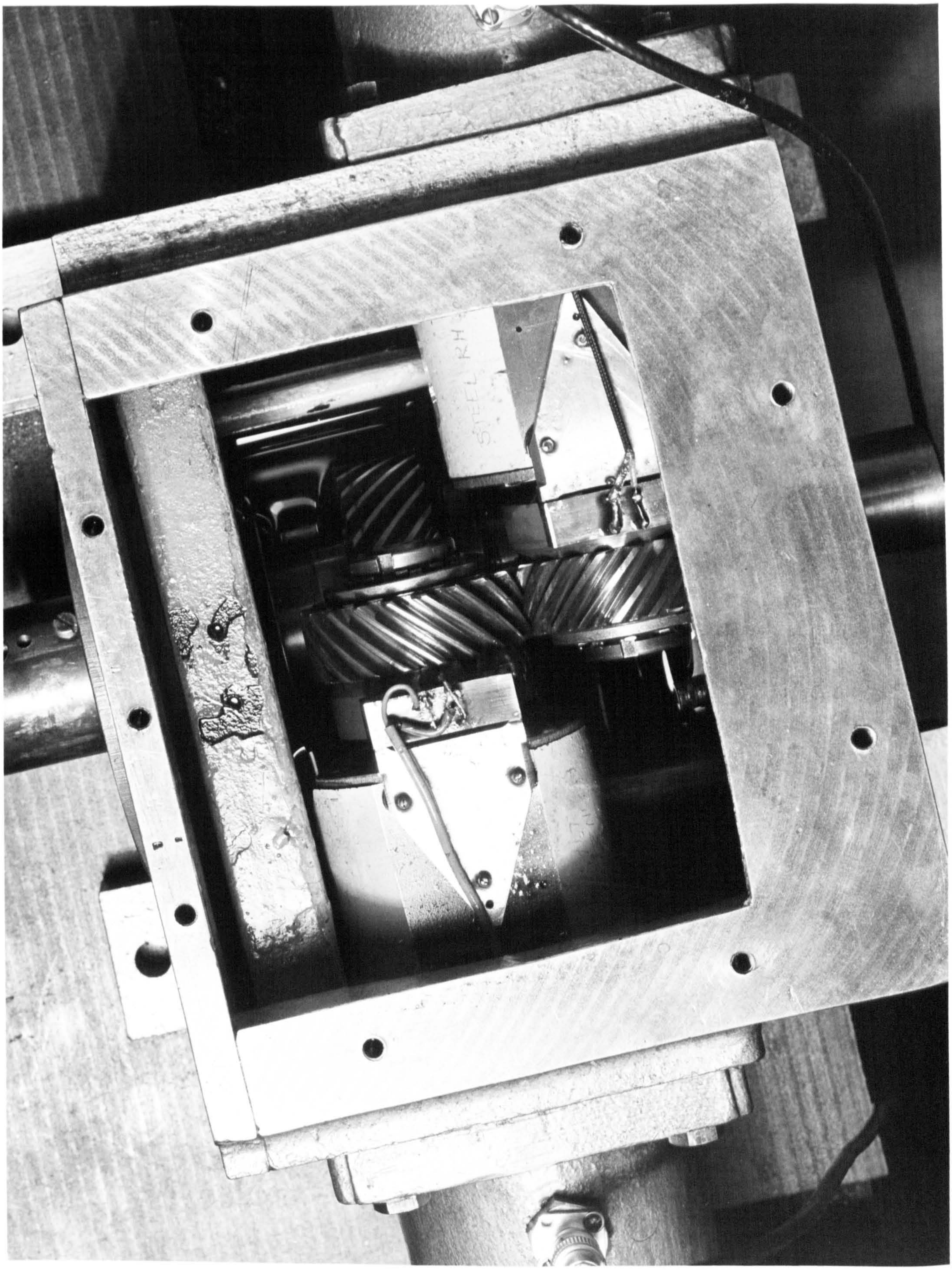

FIG. 8.9 Plan View of Test Gearbox showing Components of the Magnetic Recording System

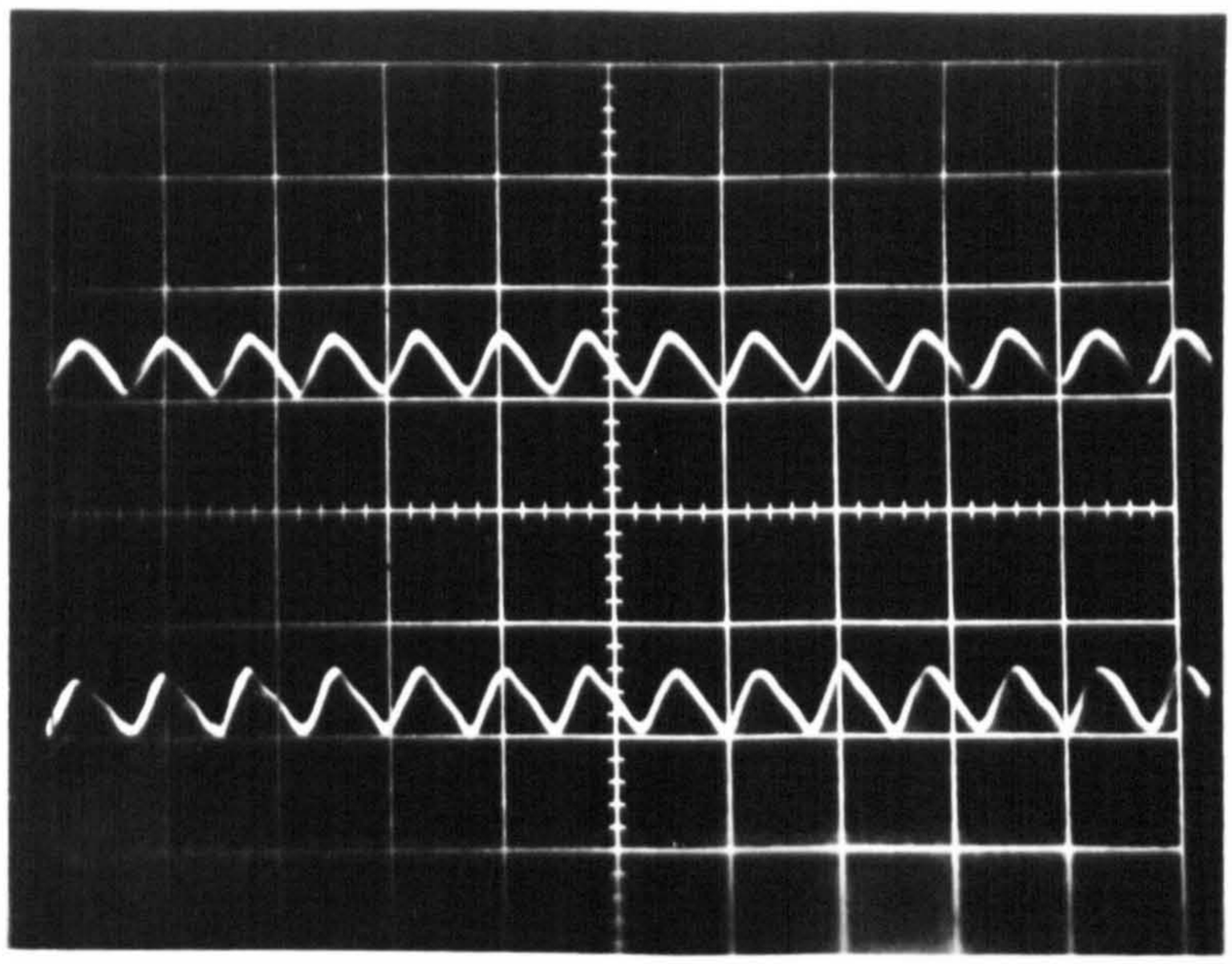

Fig. 8.10 Magnetic Drum Signals Replayed by Read/Write Heads at 100 r.p.m. (Scale - .02 v/cm). (Upper and Lower Traces are for Bronze and Steel Gears Respectively).

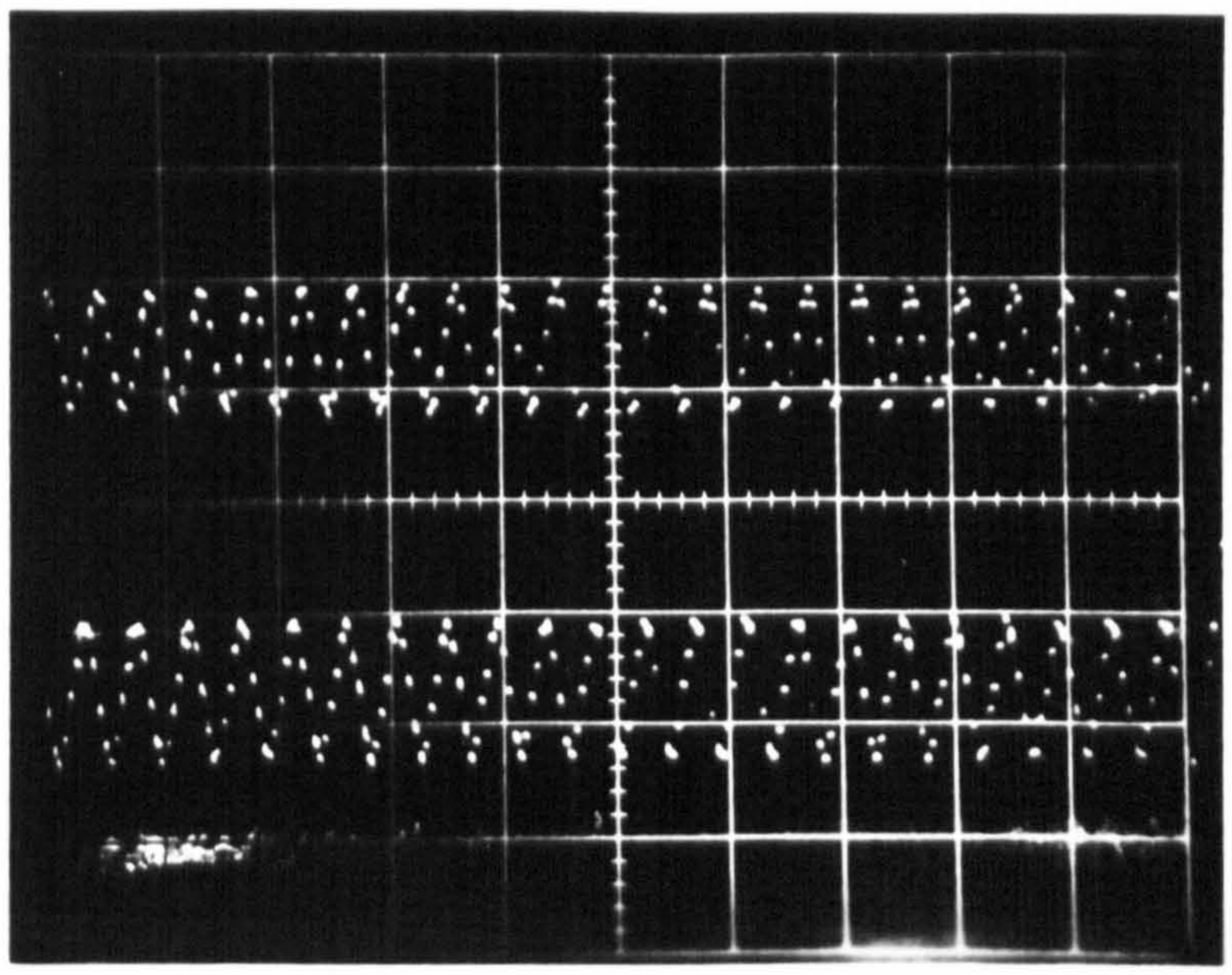

Fig. 8.11 Magnetic Drum Signals at 1800 r.p.m. (Scale .05 v/cm)

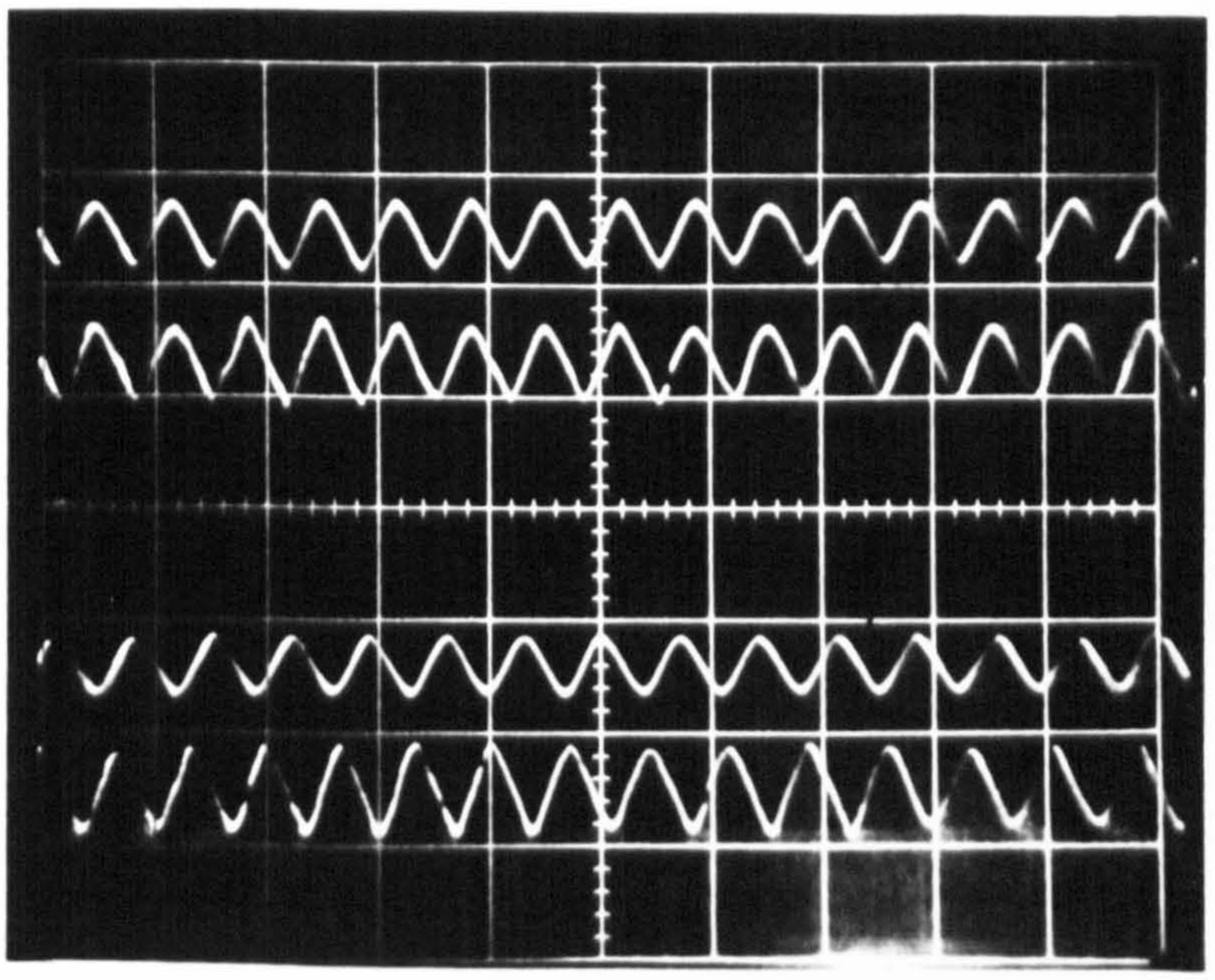

Fig. 8.12 Effect of Relative Motion on Phase Shift of Drum Signals: Upper Traces obtained at 150 r.p.m. with Loading applied to Mesh; Lower Traces obtained with Loading Removed.

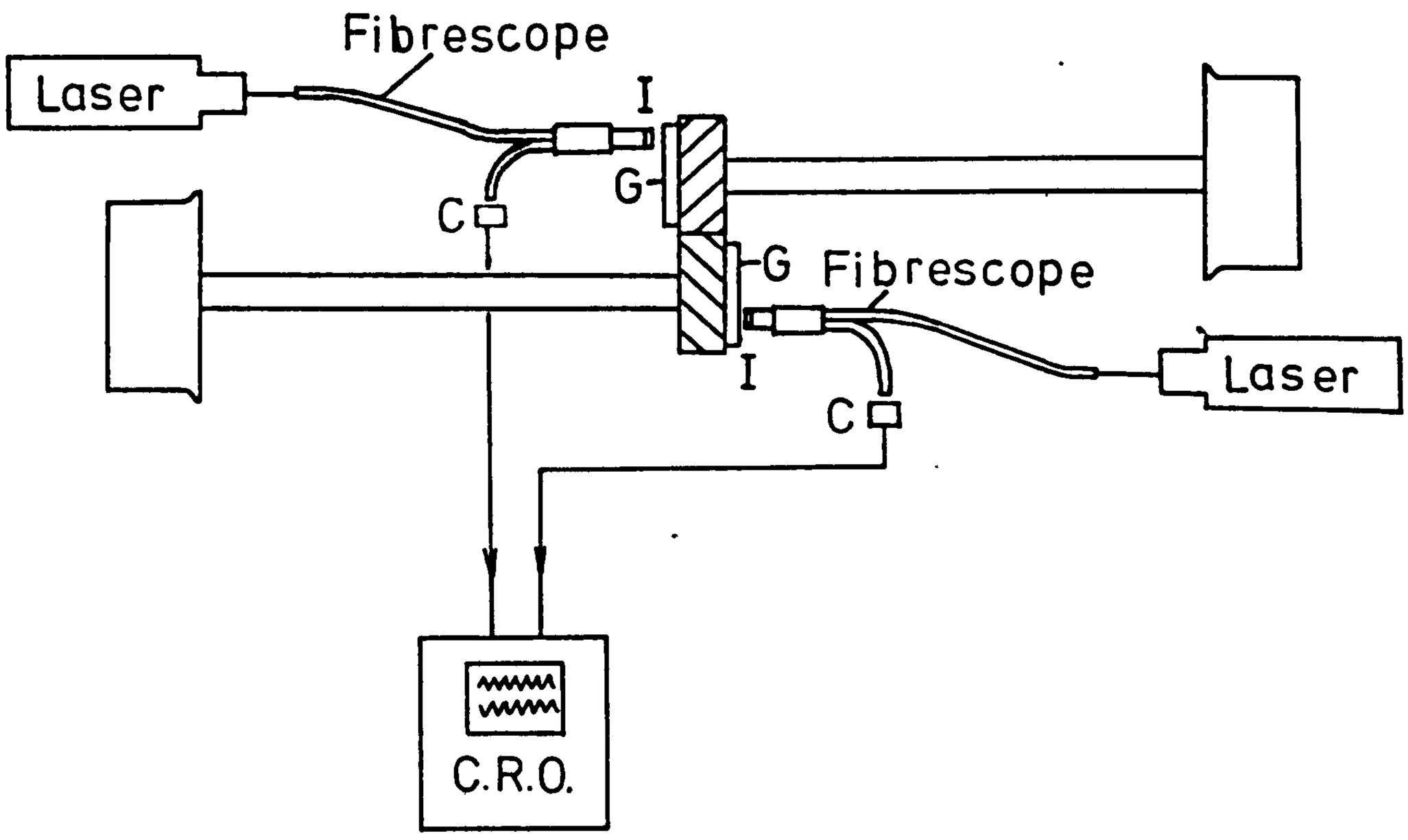

G - Reflective Grating I - Index Grating C - Photocell

FIG. 8.13 Optical Arrangement for Measuring Relative Gear Motions

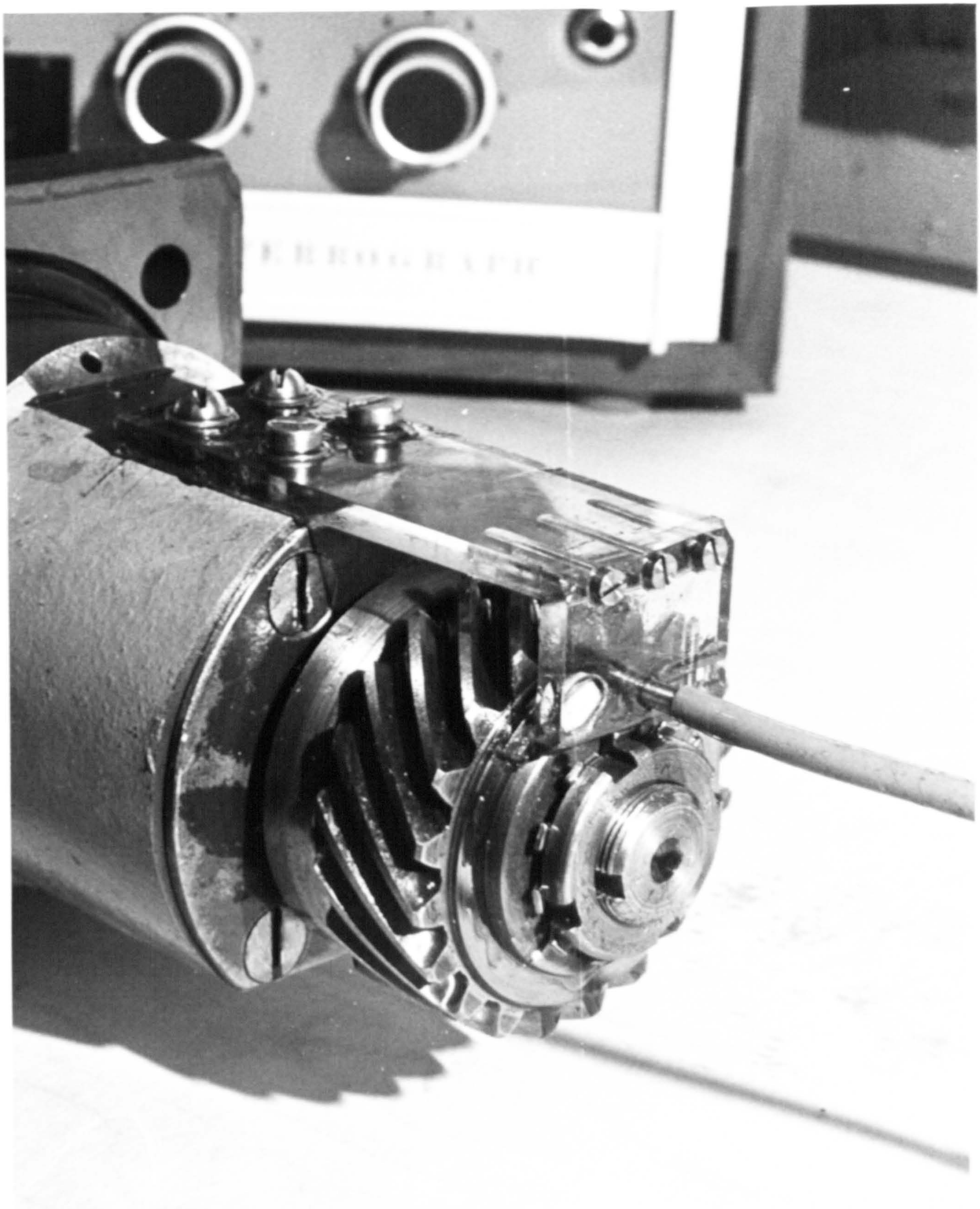

FIG. 8.14 View of a Cartridge Gear showing an attached Optical Grating and Fibrescope

(Reproduced from R.W. Grundy final year project report)

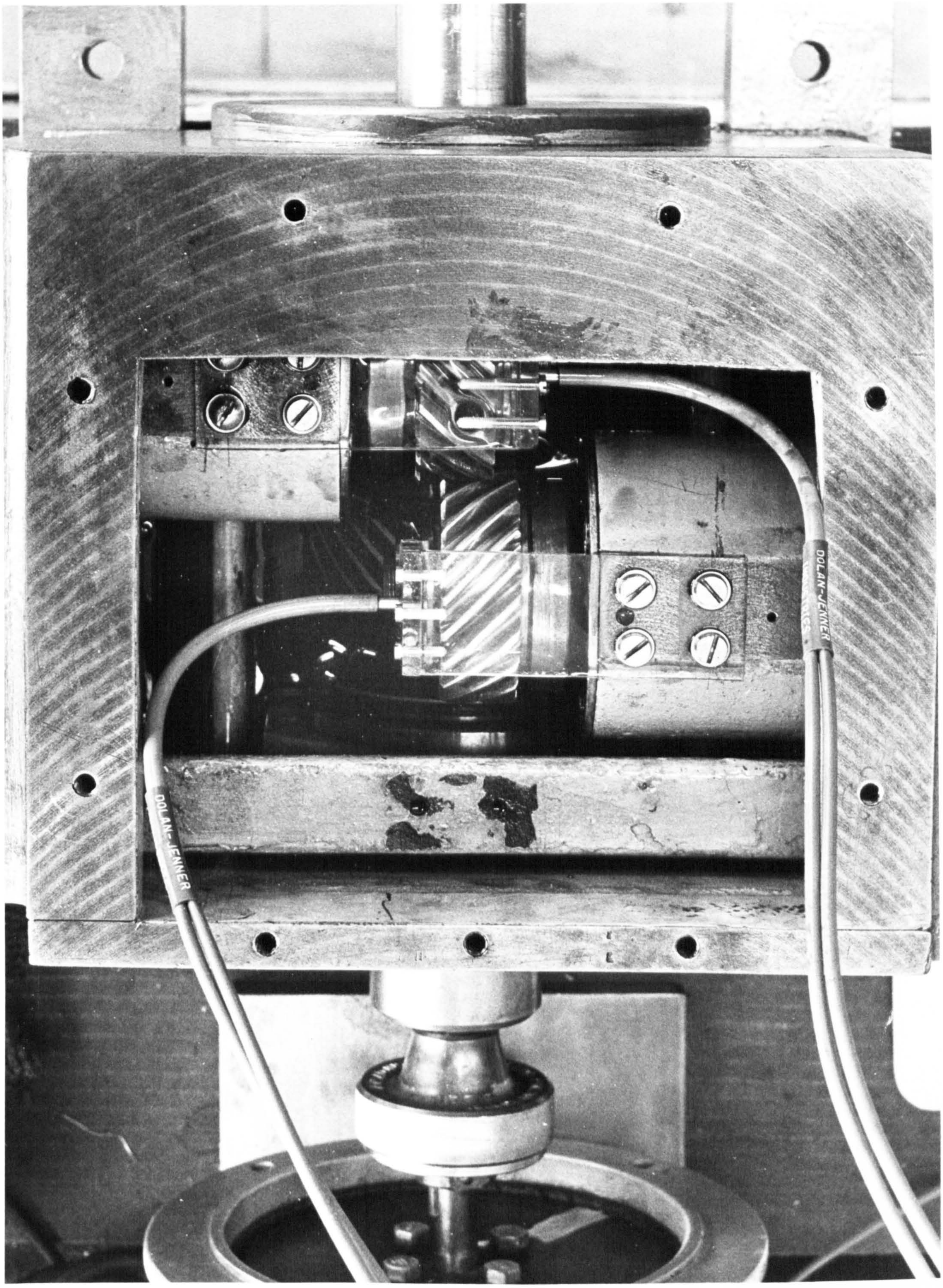

FIG. 8.15 Plan View of Test Gearbox Assembled for Measurements with the Optical System

(Reproduced from R.W. Grundy final year project report)

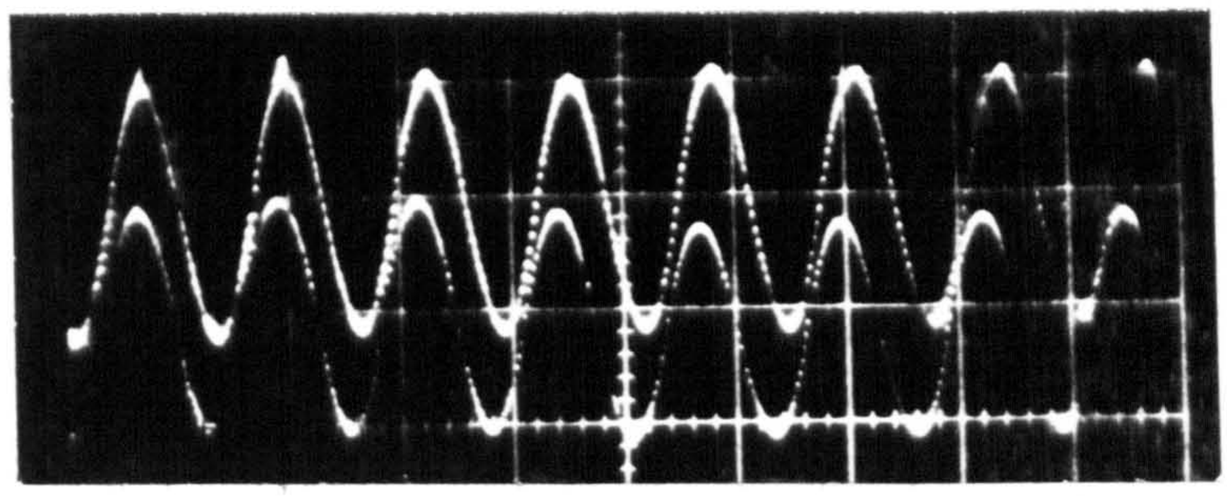

Figure 8.16 Typical Gear Signals derived from the Optical Measurement System at low speed.

(Reproduced from R.W. Grundy final year project report)

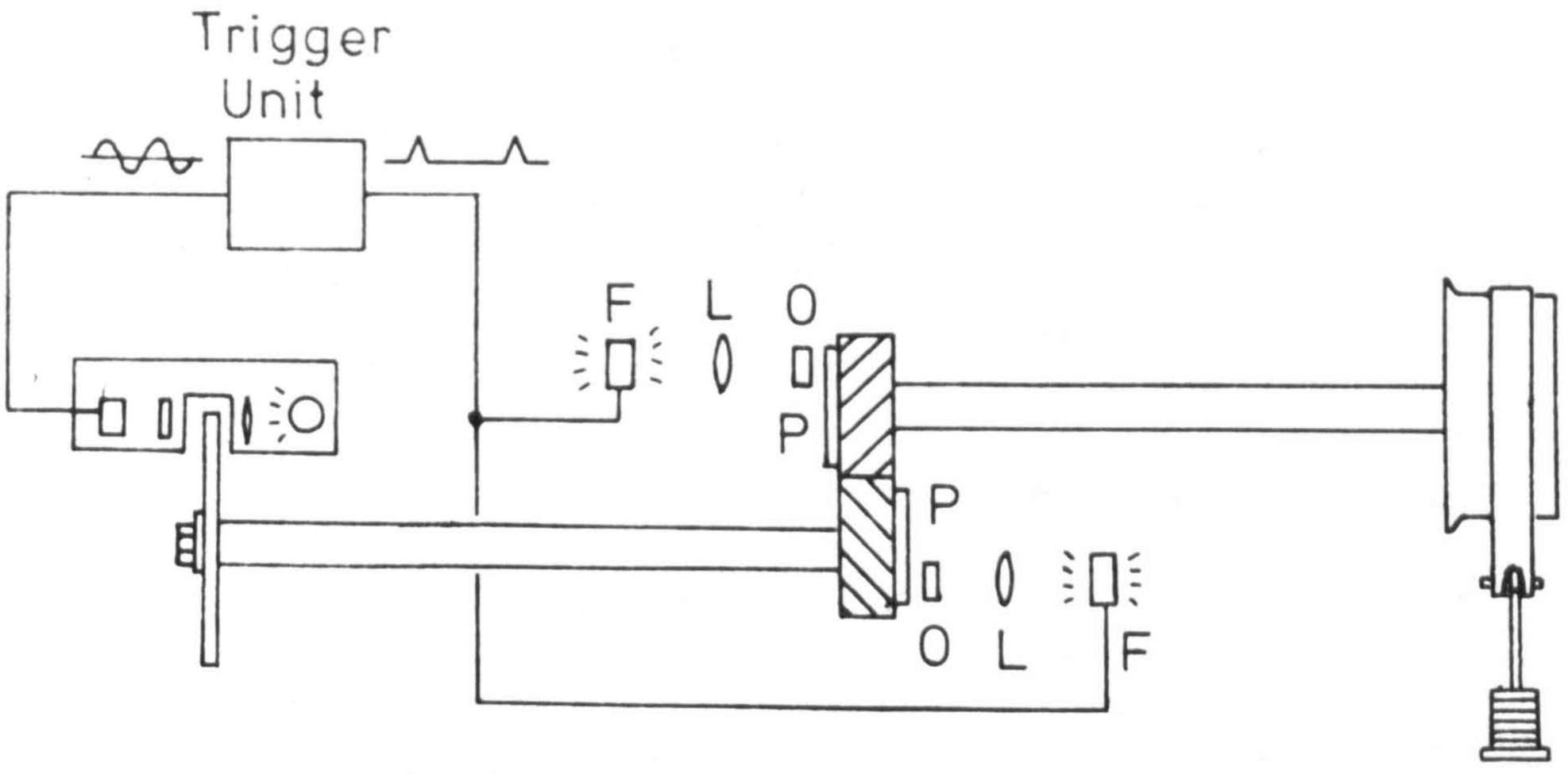

F - Flash Tube
L - Lens
O - Object Grating
P - Photographic Plate

FIG. 8.17 Generation of Gear Optical Gratings in situ

9. EXPERIMENTAL RESULTS

9.1 Introductory Remarks

The measurement techniques described in the preceding section have been applied to study gear impact behaviour and gear motions in the multibox experimental rig. A typical view of the rig and measuring instrumentation is given in Figure 9.1.

Preliminary experiments with the mesh resistance technique were aimed at establishing beyond doubt that a reversed impact cycle was associated with the gear damage patterns described in Section 3. Following this, it was of paramount importance to ascertain whether tooth dynamic loading was random or distributed in a characteristic fashion throughout the total geared system as predicted by theoretical results.

Although mesh voltage traces are very useful for detecting tooth impacts, they give only clues as to the motions described by a gear pair and, in this respect, the magnetic drum technique is clearly superior. Relative dynamic motions of a pair of bushed gears were monitored for a range of running speeds. Further tests investigated the effects of mesh applied loading and increased box coupling flexibility.

It is only possible in this Section to present a small representative sample from the very many records generated by the experimental investigation. In so far as the rig vibrational behaviour was highly non-linear in character, the results may be categorised as "typical" only.

9.2 Impact Behaviour derived from Mesh Voltage Measurements

9.2.1 Preliminary Experiments

In preliminary work mesh voltages were displayed directly on a cathode-ray oscilloscope with trace storage facility. Records were obtained by storing a single sweep and employing a polaroid type camera unit.

9.2.1.1 Nature of Typical Impact Traces

Figures 9.2 - 9.4 show typical mesh voltage traces for drawroll pair 2, box no. 2*, of the multi-box rig. The upper trace on each record is a reference signal at drawroll rotational frequency.

Figure 9.2 clearly shows evidence of contacts at once per revolution for a running speed of 725 r.p.m. As the speed is increased, the voltage amplitudes are increased (Figure 9.3) and the heavy contacts occur at twice per revolution. In view of the gear pitting pattern described earlier (Section 3.1), there is a distinct possibility that one of these occurs between the normal driving teeth and the other occurs between the trailing teeth after the backlash has been traversed. The contact resistance measurement does not, however, have the ability to prove that this is so.

One may observe from Figures 9.3 and 9.4 that, at times, heavy contacts are experienced by a succession of teeth.

* counting from the drive end.

9.2.1.2 Interpretation of Double Impact Cycle

A special experiment was undertaken to demonstrate that the twice per revolution pulses, illustrated in Figures 9.3 and 9.4, represent front and reverse face impacts. For slow speed running producing a single heavy contact each revolution, the mesh voltage and reference traces were physically synchronised by adjusting the position of the pulse generating wire on the drawroll periphery.* The rig was stopped, a thin coating of a black marking compound applied to both front and trailing faces of the bronze gear teeth, and the mesh recreated with the same teeth in contact. The machine was re-started and, after checking that reference and impact signals were still synchronised at low speed (Figure 9.5), the speed was increased to about 1500 r.p.m. giving a twice per revolution trace typified by Figure 9.6. The two displayed signals did not always remain in phase during the test, indeed, the phase relationship varied somewhat randomly (Figure 9.7). After running for about 40 minutes at this speed, the rig was stopped and the bronze gear cartridge removed. The teeth were visibly designated 1 to 20, no. 1 being the tooth in driving contact at synchronisation. Figure 9.8 presents photographs of front and reverse faces of the coated gear teeth after the test. One can readily identify the lighter areas where the black coating has been removed by contact with mating parallel and/or crossed helical gears. This wear distribution shows the same characteristic pattern as the pitting distribution observed on gears from the field (Figures 3.1 and 3.9). It also demonstrates quite clearly that the twice per revolution signals shown in Figures 9.3, 9.4, 9.6 and 9.7 represent a once per revolution total cycle of alternate driving and reverse face impacts.

* An electro-magnetic proximity pickup (Philips type PR 9262) was used to detect a onco per revolution pulse produced by a steel wire attached to a drawroll.

9.2.1.3 Simultaneous Impact Behaviour at Three Gear Meshes

Three pairs of drawshaft gears were modified for impact detection as described in Section 8.2.2. This not only allowed comparisons to be made between simultaneously recorded traces but it also reduced the number of different set-ups required to produce measurements at all gear stations in the test rig.

Since each drawbox has 4 left-hand and 2 right-hand layshaft helical gears, two of the three measuring pairs, referred to as pairs 'A' and 'B', had left-hand bronze gears whilst the third, pair 'C', had a right-hand bronze gear. To maintain uniformity, all measurements within a particular drawbox were completed in two stages. In the first stage pairs A, B and C were located at drawbox mesh stations 1, 2 and 4 respectively and in the second stage they were located at positions 3, 5 and 6.

Typical records obtained from box no. 1 are shown in Figures 9.9 - 9.11. In Fig. 9.9, the impacts appear at twice per revolution throughout and are of comparable intensity at each mesh. There is evidence of excitation at the second harmonic of gear rotational error and also at tooth meshing frequency.
In practice, it was found that mesh voltages measured for gear pair B were generally of significantly higher magnitude than for the other two (Figure 9.10) although this was not always the case (Figure 9.11).

The most likely explanation for this behaviour is associated with the backlash values for the 3 pairs. These have been measured as .0135 in., .009 in. and .014 in. at the pitch radius for A, B and C respectively. The higher backlash at meshes A and C will permit dissipative forces to act for a greater time during tooth separation than at mesh B. This will tend to reduce the relative

approach velocities of the gear pairs thus leading to less severe impacts. These results are in agreement with the findings of Oeppen (21) and illustrate the importance of high backlash in lightly loaded gear trains.

9.2.1.4 General Impact Behaviour

By far the most striking feature of the rig behaviour was a highly non-linear vibration with an absence of any clear sustained resonance condition. In view of the light applied loading, this was not unexpected.

In a previous section (6.9.1) it was noted that a resonance could be expected at about 2100 r.p.m. on the basis of linear theory and assuming a periodic disturbance at drawshaft rotational frequency. In the speed range 725 - 2600 r.p.m. no such resonance was observed, however, it was found that severest impact behaviour, in terms of magnitude and regularity, occurred at around 1700 - 1800 r.p.m.

At any particular mesh, impact patterns were broadly similar in that periods of high impact activity were interspersed with periods of relative calm in a somewhat random manner. The high impact periods lasted, in general, for up to about 20 revolutions but there were many examples where a greater persistence was observed. Typical records, obtained using slow trace sweeps on the oscilloscope, are given in Figures 9.12 - 9.14. The comparative inactivity at 1800 r.p.m., depicted in Figure 9.13, is contrary to the behaviour generally observed at this speed.

It is important to note that intervals of high impact activity were accompanied by noticeable increases in the acoustic noise level and fluctuations of 10 dB(A) were not uncommon*. Listening at about an inch or two from the face of particular drawrolls, one could easily sense a characteristic deep rattle often with a superimposed, higher pitched, "tinkling" quality.

The overall impression gained from the initial phase of the experimental work was that an unstable resonance existed at about 1700 - 1800 r.p.m. This was self-defeating for as soon as it built up, complex separation effects throughout the rig acted to detune the resonance. It is significant that the speed of maximum vibratory impact was lower than the predicted critical speed of 2100 r.p.m. for, in practice, separation effects cause the mean tooth flexibility to be higher than that used in theoretical computation. Thus calculated resonant speeds are an over-estimate of those occurring in the real system. Another effect of variable stiffness due to tooth separation is to allow an infinite number of combinations of system variables, including the forcing functions at each gear mesh. This, in turn, allows considerable randomness in the system behaviour, together with severe impact behaviour, over a wide range of speeds, rather than at particular speeds.

* The equipment used for noise measurements is described in Section 9.4 and illustrated in Figure 9.1.

9.2.2 Impact Behaviour throughout the Rig

The major part of the experimental measurement programme involved the recording of impact behaviour at each gear mesh for various running speeds. Using three modified gear pairs, as described in Section 9.2.1.3, required 8 different set-ups to cover the 24 positions in the 4 box rig. Permanent records were obtained by means of an ultra violet recorder which was found to be much more convenient than the oscilloscope camera arrangement previously used. Employing the 3 channel matching amplifiers, described in Section 8.2.2, raised the scale voltage drop from 1.5 v to 2.6 v.

Tests were generally carricd out at 725 r.p.m., 800 r.p.m. and at intervals of 100 r.p.m. up to 2600 r.p.m. After first switching on, the rig was run for 1 hour at 1600 r.p.m. and then for 30 minutes at each test speed before measurements were made. This procedure was designed to allow the gearbox oil to reach its operating temperature fairly quickly for a given speed. Since mesh voltage depends on the oil film thickness, which in turn is a function of oil viscosity, the preliminary running was essential. Ideally, it should have been prolonged further if time had permitted.

Typical traces from box no. 2 at 1000 r.p.m. are shown in Figure 9.15. Even at this low speed,double impact cycles are illustrated but the general mesh voltage levels are low compared to the maximum possible of 2.6 v.

Figures 9.16 - 9.19 present impact traces for box numbers 4, 3, 2 and 1 respectively, at 1800 r.p.m. Activity is clearly shown to increase towards the drive end of the rig and, indeed, in box number 1 there are substantial periods of uninterrupted double impact cycles. The explanation for this variation will be

discussed later (Section 9.2.3).

Although behaviour in box 4 was generally calm and uninteresting at all speeds, there were occasions of quite severe vibration, as illustrated in Figure 9.20.

Further evidence of high frequency contributions to the impact traces is presented in Figures 9.21 and 9.22, obtained using high paper speeds. In the former, components at $\frac{1}{2}$, 1 and 2 times tooth frequency are present whereas in the latter the high frequency components do not appear to be directly related to tooth frequency.

9.2.3 Distribution of Impact Densities throughout the Rig

The impact traces discussed in the foregoing paragraphs are useful for purposes of illustration but are insufficient to show, at a glance, the distribution of impact severity throughout the geared system. Since the mesh voltage levels are not calibrated to indicate dynamic load, it is necessary to introduce some arbitrary means of quantifying the voltage records. To this end, the number of impact pulses over a prescribed limit of 1 volt (equivalent to 1 cm.) were counted over a suitable trace length representing several hundred revolutions. In this way, an impact count per 100 revolutions could be made for each of the 24 different traces obtained at a particular test speed. The impact densities thus determined could be plotted in histogram form. First, however, it is necessary to introduce a weighting factor to eliminate the effect of different individual characteristics of the 3 measuring gear pairs (Section 9.2.1.3). The impact counts are related to the counts for gear pair A as follows. If, for a particular test speed, the impact counts from pairs A, B and C are N_A, N_B and N_C, then the weighted counts related to pair A are:-

$$N_{A/A} = N_A$$

$$N_{B/A} = N_B \times \frac{A_A}{A_B}$$

$$N_{C/A} = N_C \times \frac{A_A}{A_C}$$

where A_A is the average impact count for pair A in its 8 different locations $= \sum_{n=1}^{n=8} \frac{N_{A_n}}{n}$

A_B is the average impact count for pair B in its 8 different locations $= \sum_{n=1}^{n=8} \frac{N_{B_n}}{n}$

A_C is the average impact count for pair C in its 8 different locations. $= \sum_{n=1}^{n=8} \frac{N_{C_n}}{n}$

The arithmetic manipulation and graph plotting of impact densities has been programmed for computer and the statement listing is given in Appendix N.

Figures 9.23 to 9.35 show impact density histograms at various test speeds in the range 1000 to 2600 r.p.m. The weighting factors, discussed above, have been applied.

General levels are seen to be quite low at 1000 and 1250 r.p.m. rising substantially at 1500 r.p.m. and peaking at about 1700 or 1800 r.p.m. Further increase in speed initially produces a small decrease in impact levels which then remain fairly constant overall up to 2600 r.p.m., although local fluctuations occur throughout.

The most striking feature of the histograms is that the behaviour in boxes 1 and 2 is everywhere worse than in boxes 3 and 4 which confirms the observation made earlier (Section 9.2.2) in connection with mesh voltage records. This behaviour is almost

certainly the result of the physical differences between the two pairs of boxes and in particular their gears (Section 7.3). The brand new gears in boxes 3 and 4 clearly induce less dynamic activity than the worn gears in boxes 1 and 2.

In view of these findings, it is considered inappropriate to expect concrete conclusions to be drawn from a comparison between the impact distributions and theoretical distributions of dynamic loading, presented in Section 6.9. Nevertheless, the results are of some value for they demonstrate that the dynamic behaviour at a particular mesh is not independent of the errors in the surrounding gears, otherwise the striking variation in behaviour down the rig would not have been highlighted using the three instrumented cartridge pairs.

A comparison between experimental and theoretical results could be effected by a closer theoretical modelling of the actual system. This would involve the physical measurement of all gear transmission errors and relative error phasing throughout the rig for use as input data. In view of the time requirements of such a programme this was not pursued.

9.3 Measurements of Gear Dynamic Motions using Magnetic Drums

The magnetic recording technique, described in Section 8.3, was employed to investigate gear oscillatory motions under various operating conditions and a selection of the results derived is now discussed.

9.3.1 Calibration Check

Initial measurements were carried out with the calibrated bushed gear pair in the double cartridge gearbox.

It was appropriate, first of all, to check that a satisfactory "static" calibration had been accomplished. Accordingly, the relative motion was observed for low speed running under a brake load of 2.5 lbf.in. Unfortunately, the signals picked up from the magnetic drums were not strong enough for the dynamic phase comparator at 60 r.p.m. (calibration speed) and it was necessary to operate at 150 r.p.m. A typical trace, obtained under these conditions, is given in Figure 9.36. The base line, representing the zero phase shift calibration, is shown by an arrow at the left of the trace. Apart from a once per revolution pulse, which was subsequently traced to a mechanical. fault in the rig, the trace approaches the straight line expected for the static condition. Considering that the test speed was significantly above the signal generation speed, this result provides adequate confirmation of a satisfactory drum calibration. This point is further emphasised by comparing Figure 9.36 to Figure 9.37 which was obtained under the same conditions except that the brake load was removed. The motions are much greater in amplitude and at times traverse the full backlash.

9.3.2 Multi-Box Rig Tests at Various Speeds

The instrumented gear pair was carefully assembled at position 2 in box 4 and a series of records taken exemplified by Figures 9.38 - 9.45. These are now briefly discussed.

At 725 r.p.m. (Figure 9.38) it can be seen that intervals of motion at rotational frequency are interspersed with more random periods. There is also evidence of motions at twice rotational frequency, suggesting an excitation contribution by the second harmonic of gear error. No reverse face contacts are evidenced, although 80-90% of the tooth clearance is regularly traversed. (Excursions of the trace across the base line suggest either a D.C. drift of the displayed signal, or some tangential movement of one or both reading heads or tooth deformation including flexing).

Figure 9.39 shows vibration at a periodicity of layshaft gear rotation and also at half of this. Such behaviour was not common thus confirming the relative unimportance of transmission errors at the crossed helical gear mesh.

General amplitude levels are seen to increase at 1250 and 1500 r.p.m. (Figures 9.40 and 9.41) and there are several instances where impacts occur on reverse tooth faces as well as on normal contact faces. In general, the vibration occurs at drawshaft rotational frequency but some of the lower amplitude waves occur at half of this.

Figure 9.42 illustrates an interesting phenomenon, again recorded at 1500 r.p.m. The displacement amplitudes are seen to increase and decrease on alternate waves in a regular fashion this occurring at a periodicity of drawshaft gear rotation. The variations in phase and the smoothness and regularity of the

waveform together suggest that excitations at other gear meshes are here exerting considerable influence.

Further examples of this behaviour were detected at 1700 r.p.m. (Figure 9.43). It was noted that the tooth clearance was more often fully traversed at this speed than at any other for which records were obtained. This reinforces inferences drawn from impact measurements (Section 9.2.1.4) that a peak response occurred in the system at around 1700 r.p.m. but, more important, it further supports the view that the dynamic behaviour at a particular mesh is strongly influenced by excitations from more remote meshes.

Figures 9.44 and 9.45 show typical traces obtained at 1800 and 2000 r.p.m. respectively. A noticeable reduction in amplitude levels is apparent in the latter.

9.3.3 Effect of Applied Loads

A small scale test was carried out at 750 r.p.m. to examine the effect of mesh applied load on vibratory behaviour. Brake loads of 2.5 and 5.0 lbf. in. were applied to the steel gear shaft of the instrumented pair producing the records shown in Figures 9.46 and 9.47 respectively. Displacement amplitudes are considerably reduced, especially with the higher load, and motions at once per revolution are suppressed.

This result suggests that drawbox dynamic behaviour might be improved by increasing the normal loads transmitted by the drawshaft gears. It remains, however, to perform a more comprehensive programme of measurements before this could be suggested with confidence.

9.3.4 Influence of Highly Flexible Couplings

Theoretical results, reported in Sections 6.5.3 and 6.9.2 have predicted improved behaviour from the use of more flexible layshaft couplings for full machines and also for the multi box rig. Measurements were therefore performed on the experimental rig fitted with couplings having a torsional flexibility estimated to be 290 times that of the standard components*. Typical motion traces for a variety of test speeds are given in Figures 9.48 - 9.54.

At 750 r.p.m., general displacement levels are noticeably higher than those observed using standard couplings at the same speed and, as before, gear rotational frequency predominates. The regularity with which the backlash is fully traversed is comparable to that at the peak response speed of 1700 r.p.m. in the unmodified rig. This suggests the presence of a resonance at around 750 r p.m. or possibly at a slightly lower speed, since the drive arrangement precluded operation below this speed. Such a resonance coincides with the fourth torsional critical speed predicted by the linear theory on the basis of excitation at once per drawshaft revolution (Section 6.9.2).
In view of the considerable non-linearities in the system, it is not clear why such good agreement has been obtained especially when observed behaviour of the unmodified system was so different from the predicted linear response. It is possible that the value of modified coupling flexibility, used for computation, was an over-estimate. If the actual flexibilities were lower then the computed resonance speed would be higher than the actual peak response speed as was found for the system operating with standard couplings.

* The couplings each incorporated a pair of opposed helical compression springs and are shown, assembled on the rig drive shaft, in Fig. 7.2.

Amplitudes at 900 and 1250 r.p.m. (Figures 9.49 and 9.50) are generally slightly lower than at 750 r.p.m. and the dominance of rotational frequency is again apparent.

At 1500 r.p.m. a very interesting phenomena was observed as exemplified in Figure 9.51. Dramatic changes in the response frequency occurred producing some motions at half the rotational frequency, that is, motions where normal tooth contact occurred once in two complete revolutions of the gears. Such behaviour, referred to as $\frac{1}{2}$-order subharmonic vibration, only occurs in non-linear systems. It has been observed and reported elsewhere (19) in relation to gear tooth meshing frequency but is quite rare, in terms of publications, for excitation at rotational frequency. The subharmonic motion implies the presence of a resonant condition at half of this speed, i.e. at about 750 r.p.m., which is in line with the measured behaviour in this region.

9.4 Acoustic Noise Measurements

Although the subharmonic vibration in the modified rig (Section 9.3.4) produced displacement levels comparable with the peak levels in the unmodified rig (Section 9.3.2), the former occurred with only half the frequency. This suggested that dynamic behaviour in the system with flexible couplings should be less severe than that occurring with the standard units. Because a comprehensive test programme was impracticable in the available time, it was decided to record acoustic noise levels at various speeds for the two different systems. Such an approach is not ideal but is justified since gearing dynamic behaviour is, to a large extent, reflected in the generated

noise. Indeed, it has already been noted (Section 9.2.1.4) that severe impact behaviour was accompanied by considerable increases in acoustic noise level.

Overall levels were measured by means of a Brüel and Kjaer frequency analyser, type 2107, together with a B&K condenser microphone, type 4132. The microphone was permanently situated one metre from the drawroll faces in box number 3 and at an elevation equal to that of the drawshaft axes. It should be noted that the recorded noise was the mean value in each case, that is, the value midway between the maximum and minimum levels displayed during a test period of about two minutes.

The results of the tests are presented graphically in Figure 9.55. Except for the lowest speed, the modified system is shown to be quieter throughout the range, especially at the higher speeds where noise reductions of 7 dB were recorded. This tends to confirm that the rig dynamic behaviour was improved by the use of high flexibility couplings, as predicted by the theoretical analysis. (Measurements of gear behaviour reported earlier illustrate, however, that the system behaviour was much more complex than allowed for by linear analysis).

The noise records are also useful in demonstrating that drawbox noise is, to a large extent, a function of the dynamics of the total gearing system. In a class of machinery which has been found to be particularly noisy, this is an important finding. Previous investigations into drawtwister noise* (71)(72)(73) have concentrated on machine sub-assemblies in effecting creditable noise reductions but

* These studies were not related to machines manufactured by Platt International Ltd.

the above results give good reason to anticipate further substantial improvements by modification of the layshaft system characteristics, possibly by the adjustment of drawbox coupling flexibility.

9.5 Examination of Gears on Completion of Tests

In all, the experimental rig was run for a total of about 350 hours at drawroll speeds of 725 to 2600 r.p.m., including a period of about 200 hours at 1700 - 1800 r.p.m. Upon examination, most of the bronze gears in boxes 1 and 2 displayed shallow indentations on front and reverse tooth faces suggesting a repeated "hammering" action. In some cases, local indentations were significantly deeper than elsewhere and appeared to be an early stage of pitting.

The bronze gears in boxes 3 and 4 were generally less marked but still showed signs of hammering on both normal and reverse faces. All bronze gears displayed evidence of contact with the layshaft gear on both faces of each tooth.

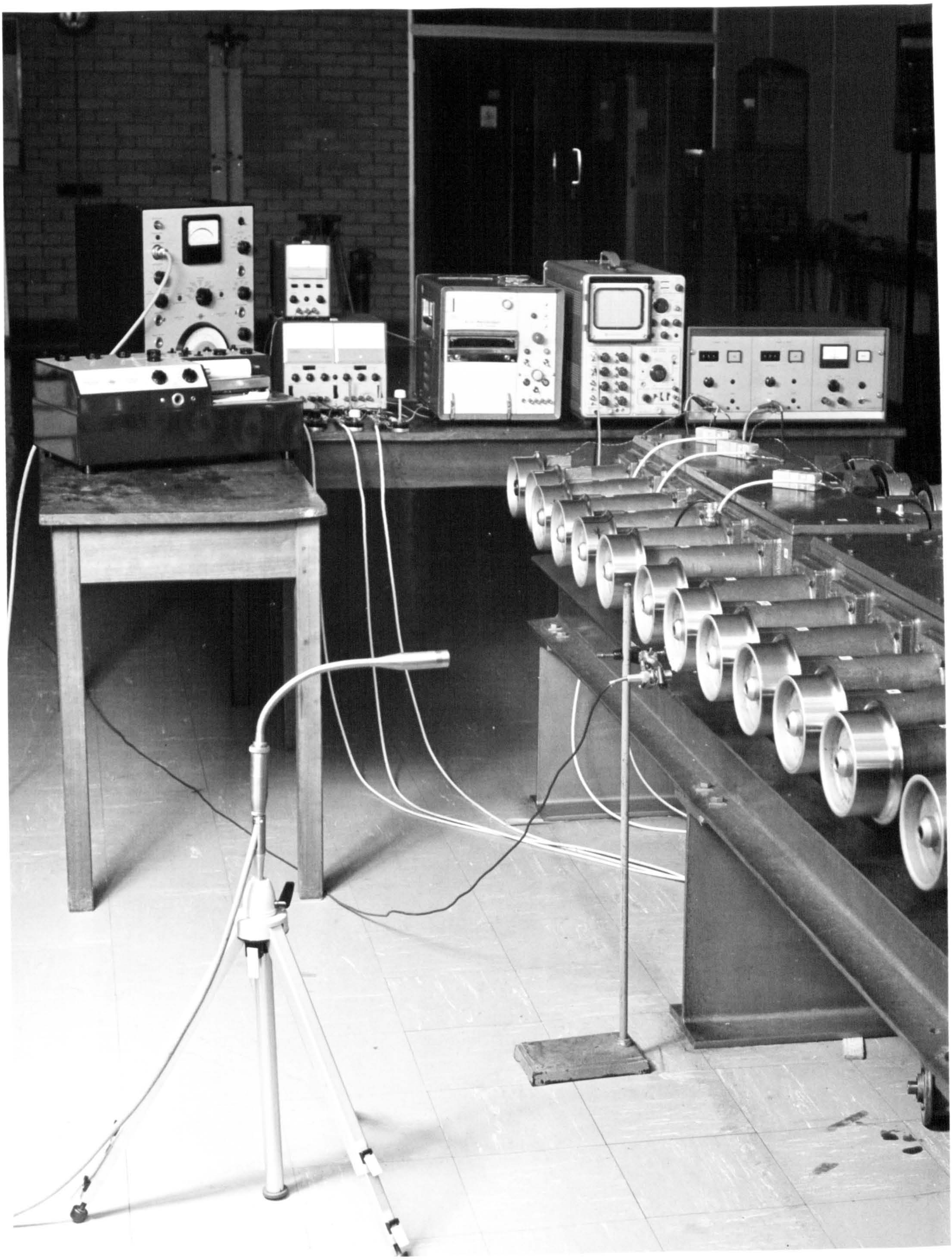

FIG. 9.1 General View of Multi-box Rig showing Instrumentation

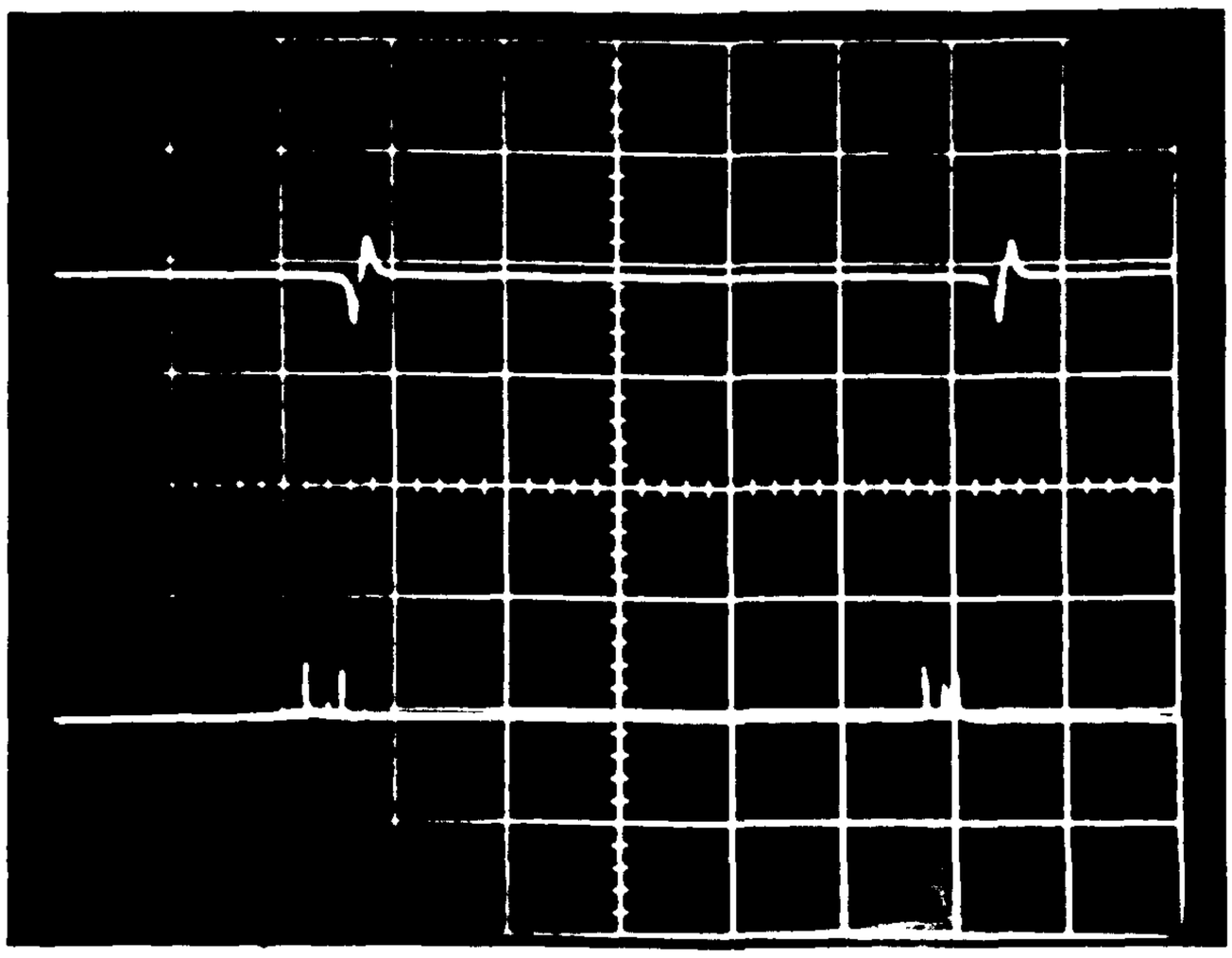

Fig. 9.2 Mesh Voltage of Gear Pair 2, Box 2, at a Drawroll Speed of 725 r.p.m. (Scale .5 v/cm); timing signal (upper trace) is at once per revolution.

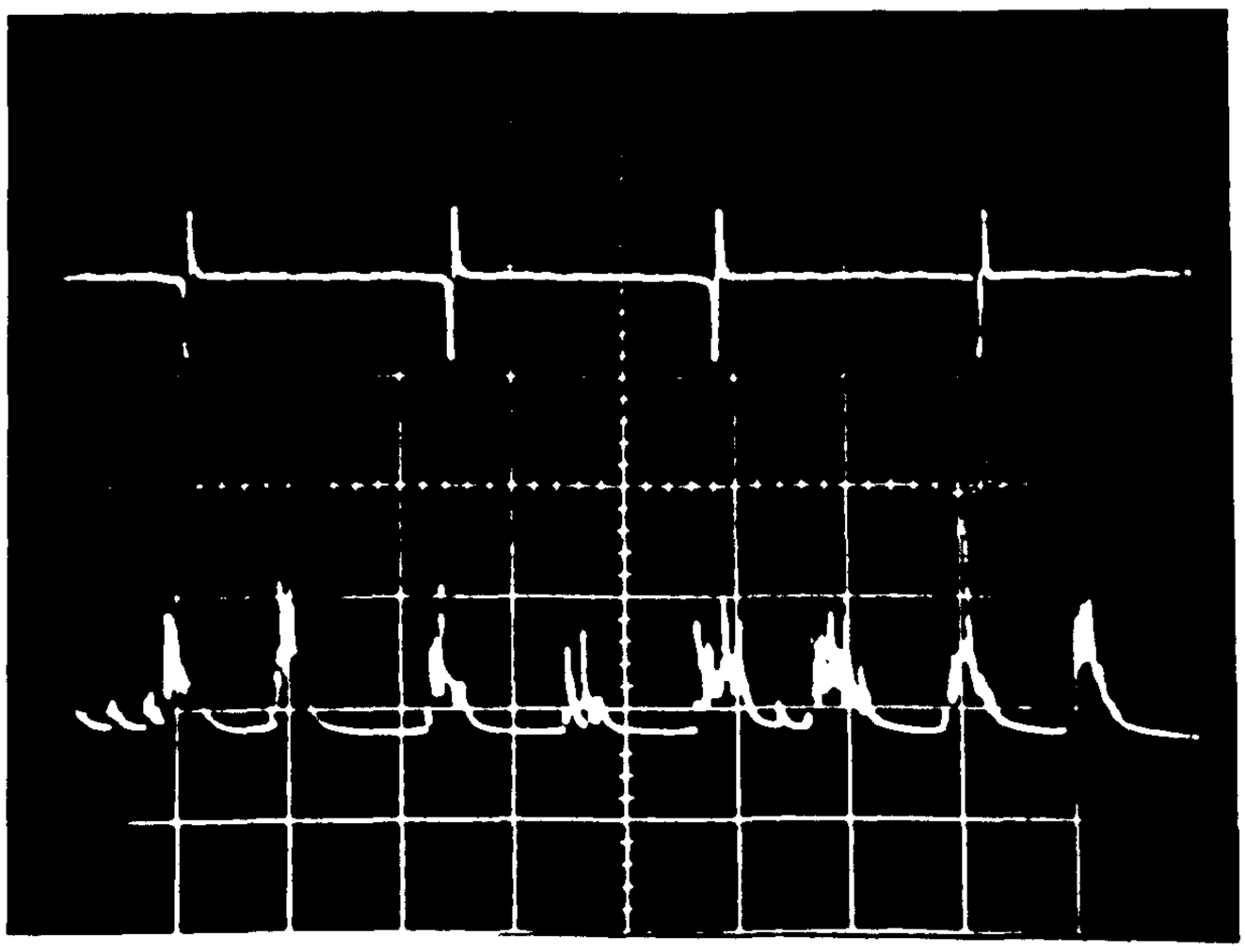

Fig. 9.3 Typical Mesh Voltage Trace at 1500 r.p.m.

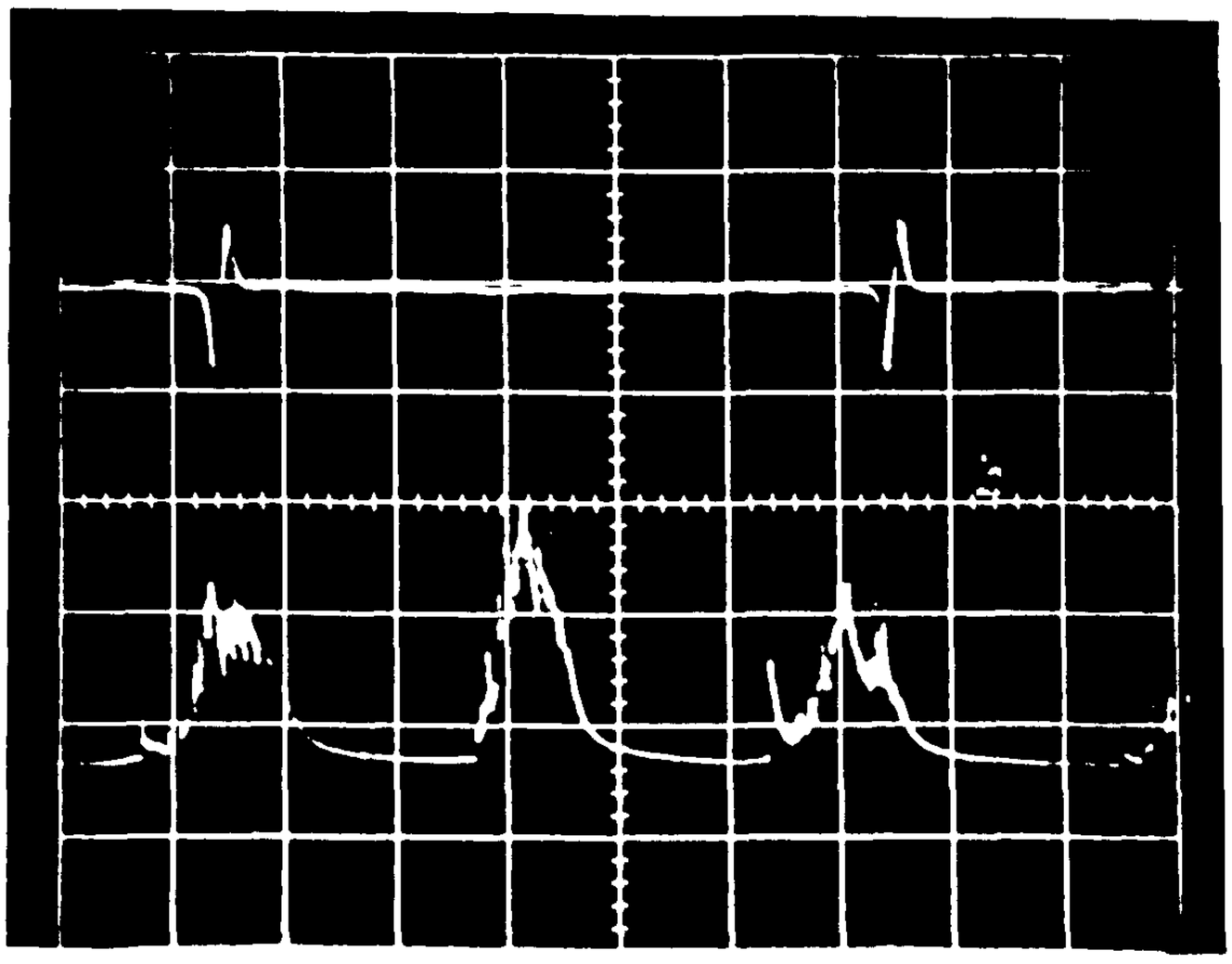

Fig. 9.4 Typical Mesh Voltage Trace at 1500 r.p.m.

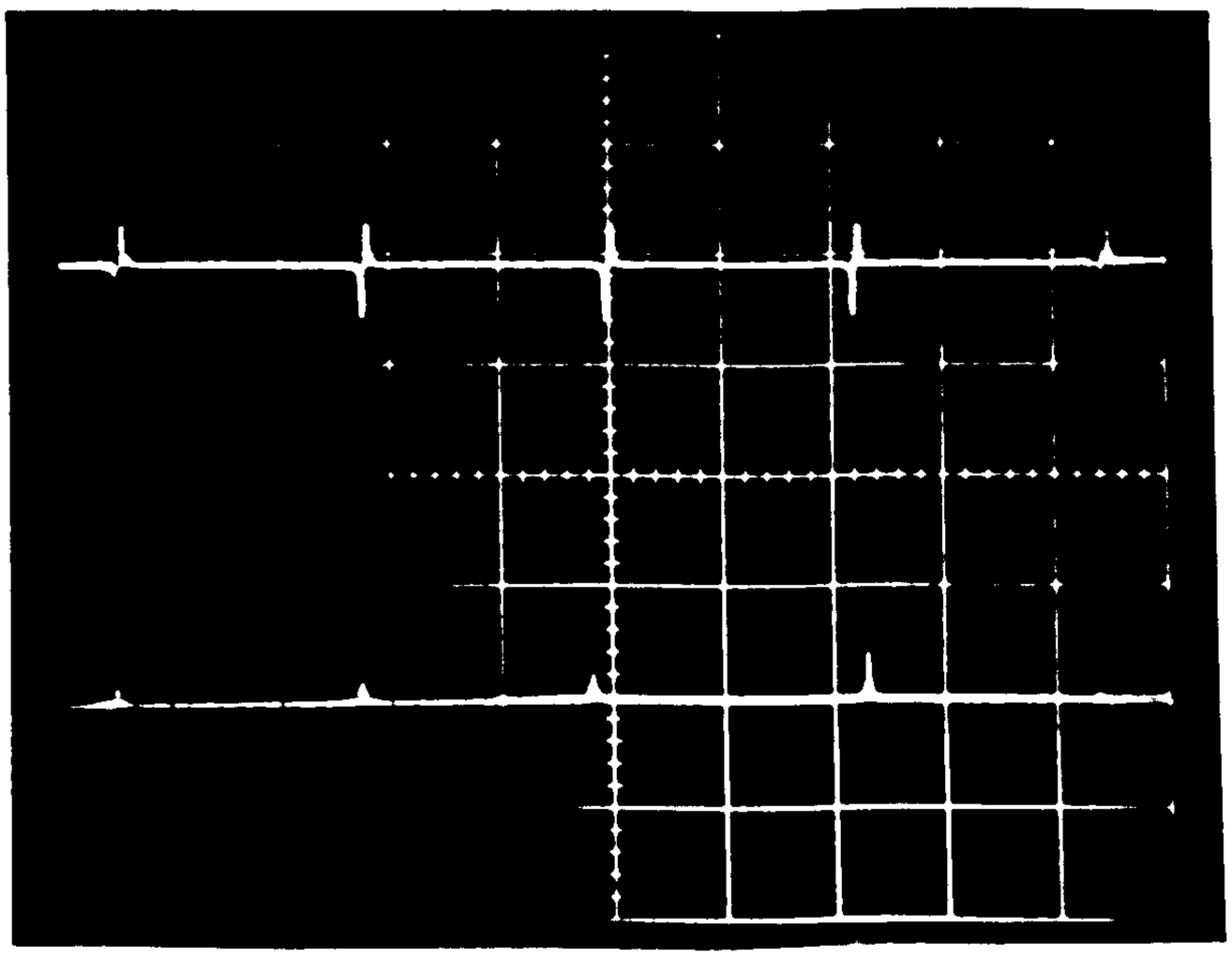

Fig. 9.5 Mesh Voltage at 725 r.p.m. after Bronze Gear Teeth coated with Marking Ink.

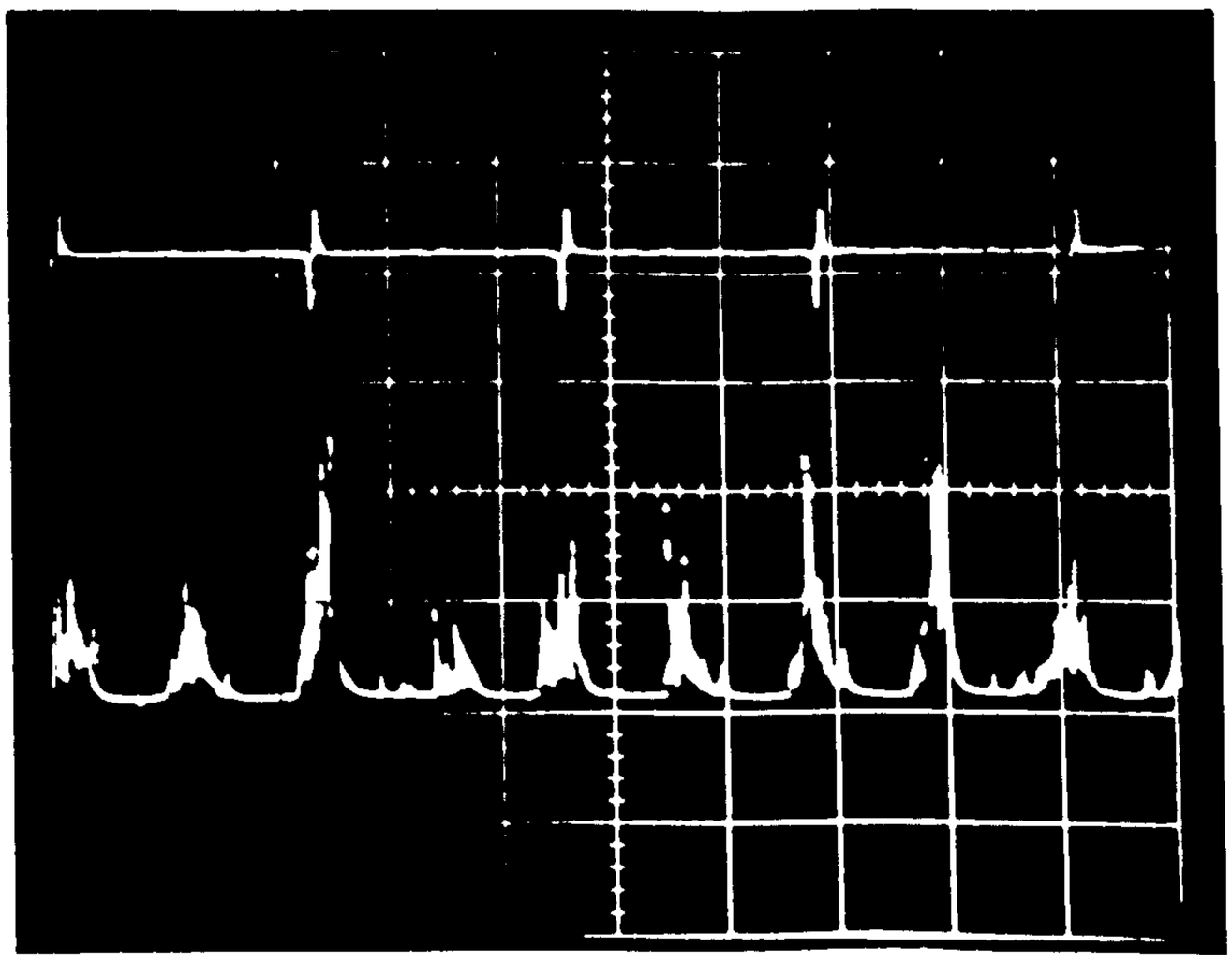

Fig. 9.6 Mesh Voltage at 1500 r.p.m. using coated Bronze Gear.

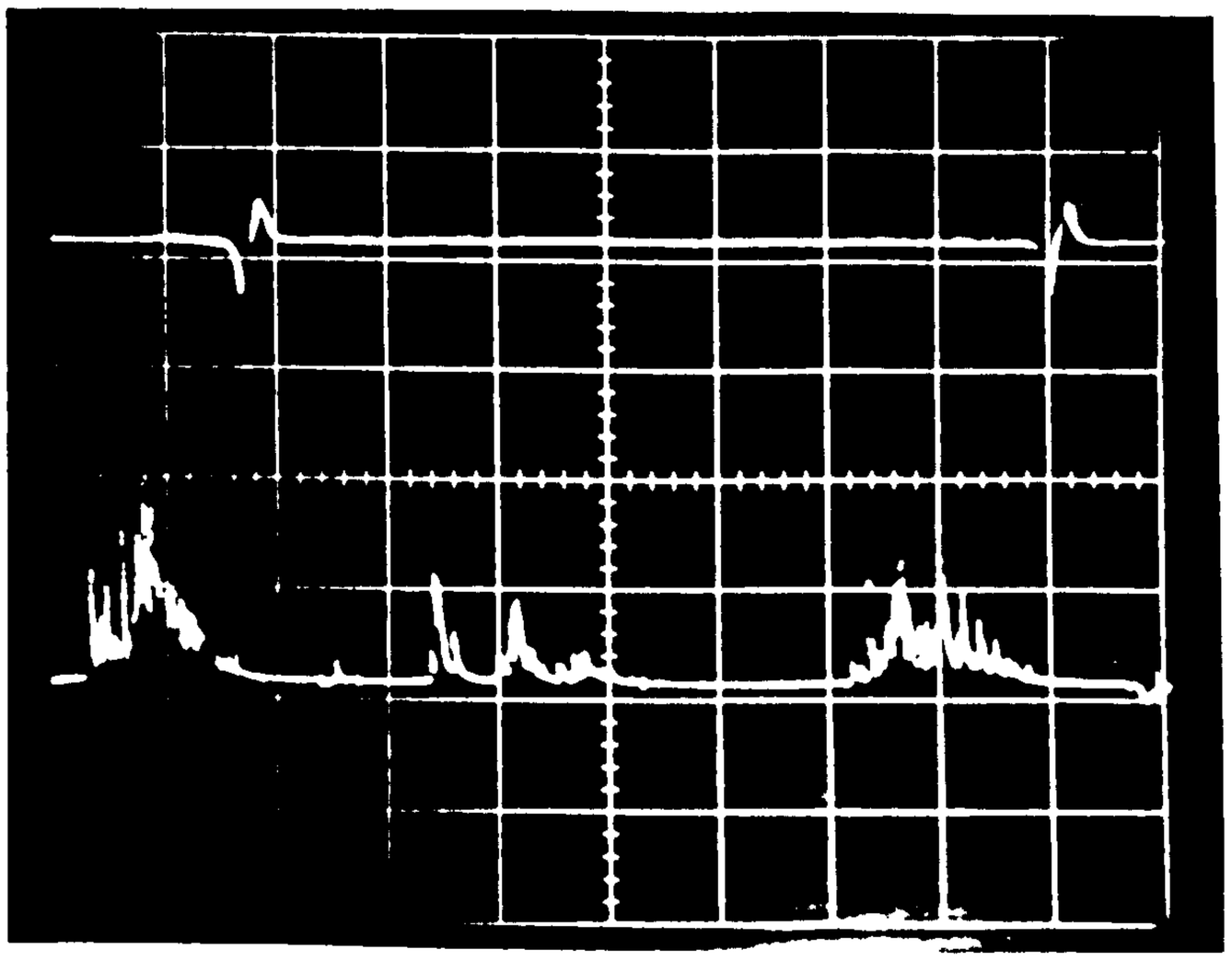

Fig. 9.7 Mesh Voltage at 1500 r.p.m. using coated Bronze Gear.

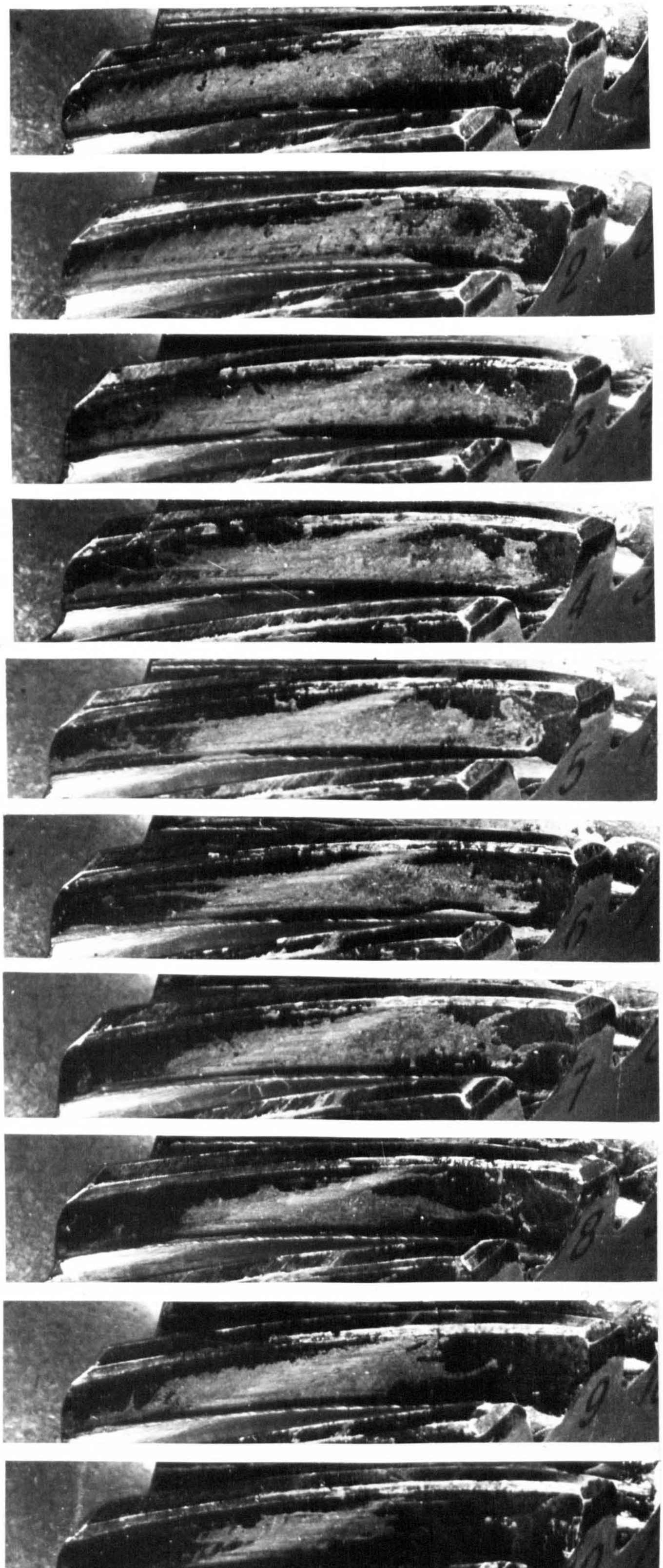

(a) Front Tooth Faces, numbers 1 - 10

Figure 9.8 Photographs of Surface Coating Wear on all Teeth of a Bronze Gear after running for 30 minutes at 1500 r.p.m.

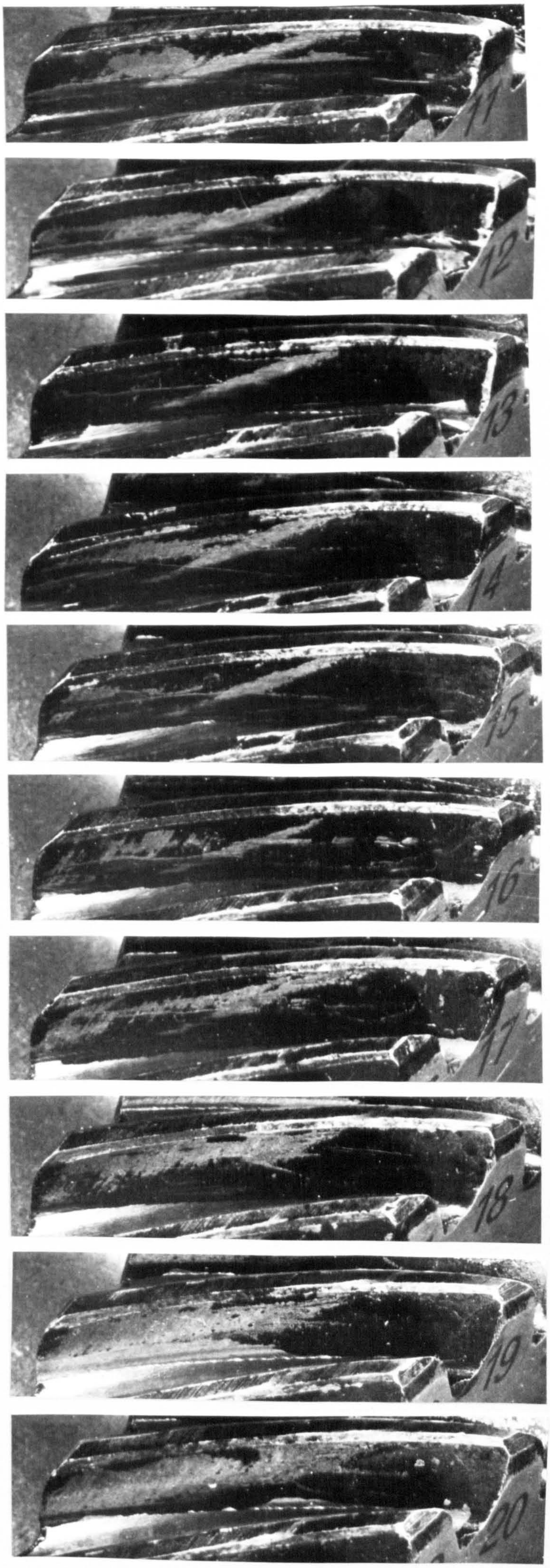

Fig. 9.8(b) Front Tooth Faces, numbers 11 - 20

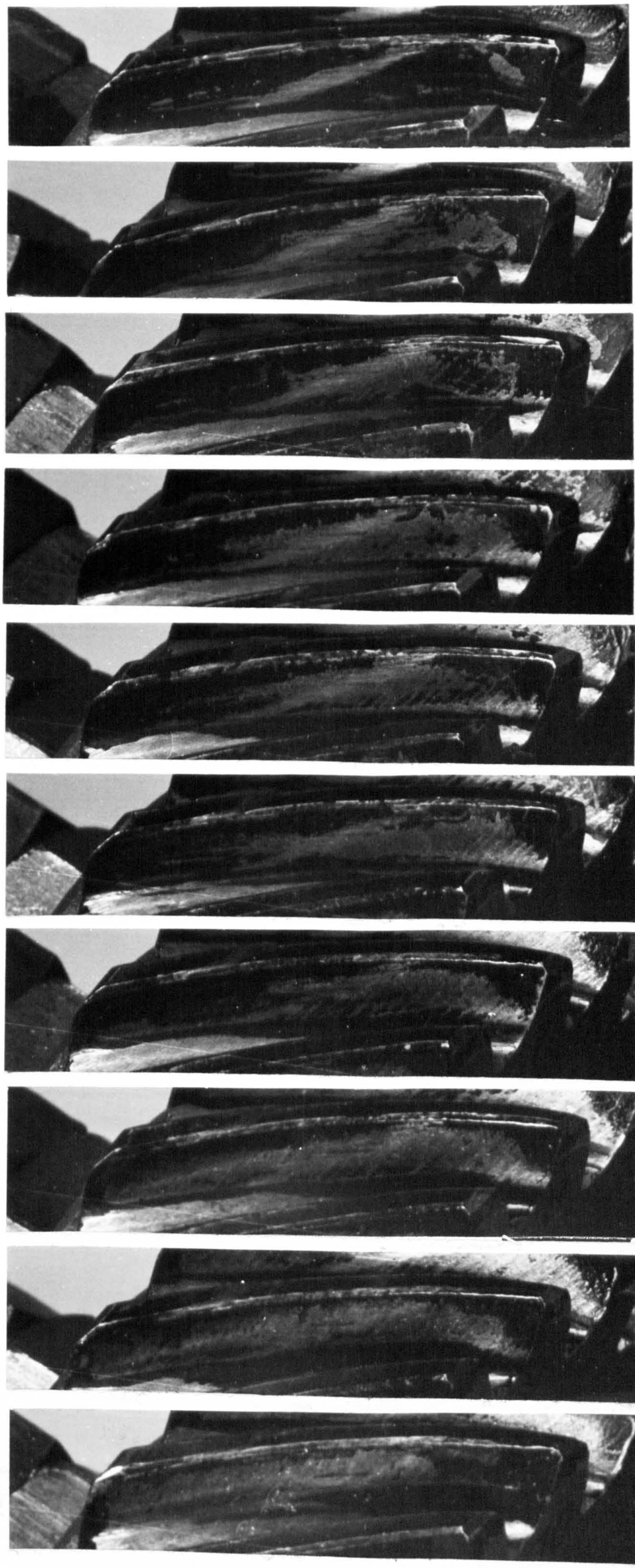

Fig. 9.8(c) Reverse Tooth Faces, numbers 1 - 10

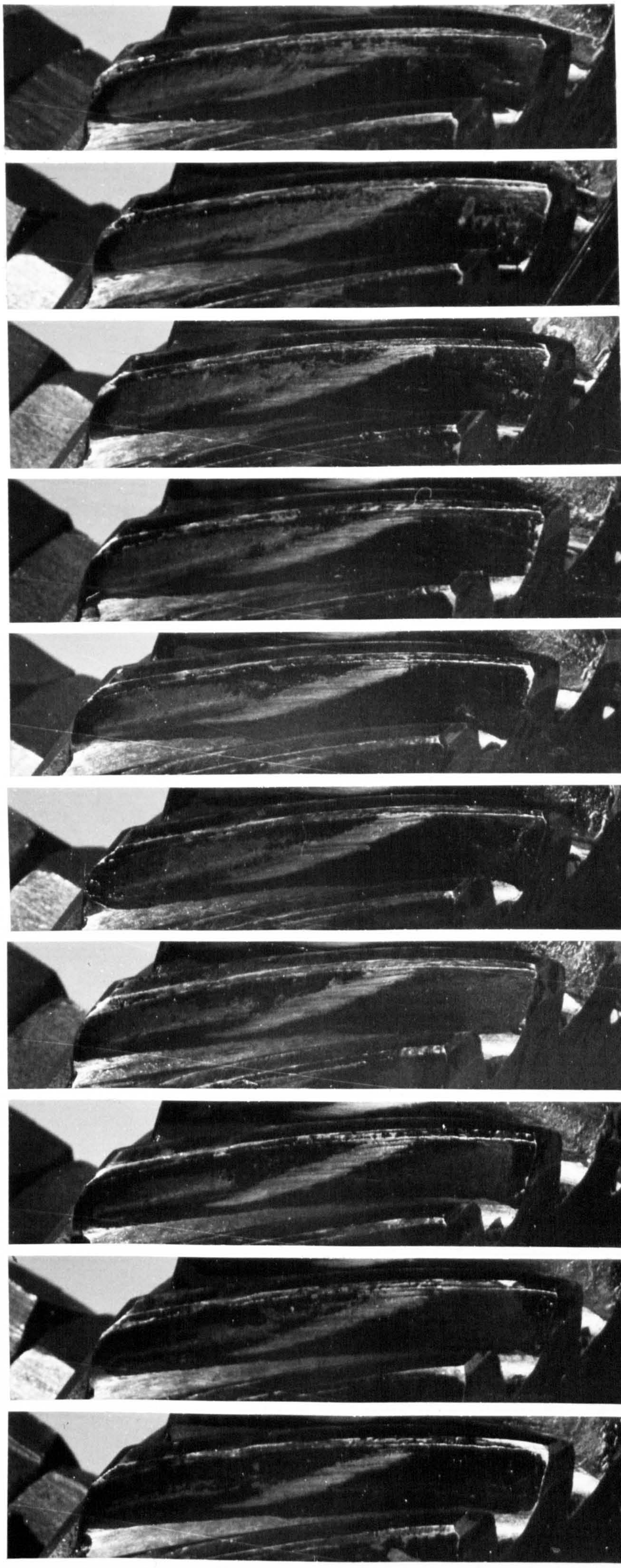

Fig. 9.8(d) Reverse Tooth Faces, numbers 11 - 20

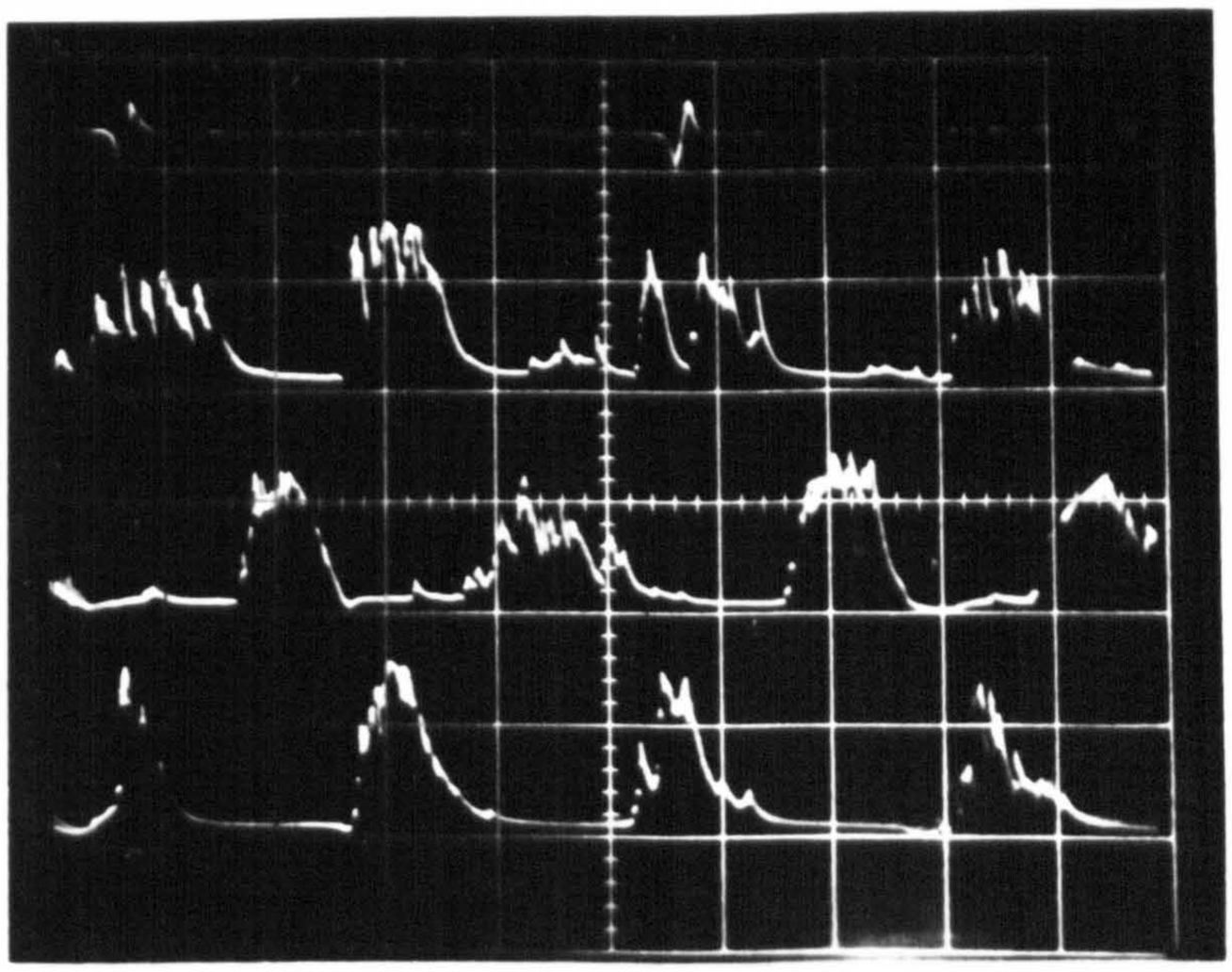

Fig. 9.9 Typical Mesh Voltage Records for Pairs 3, 5 and 6, Box No. 1, at 1800 r.p.m. (Scale 1 v/cm)

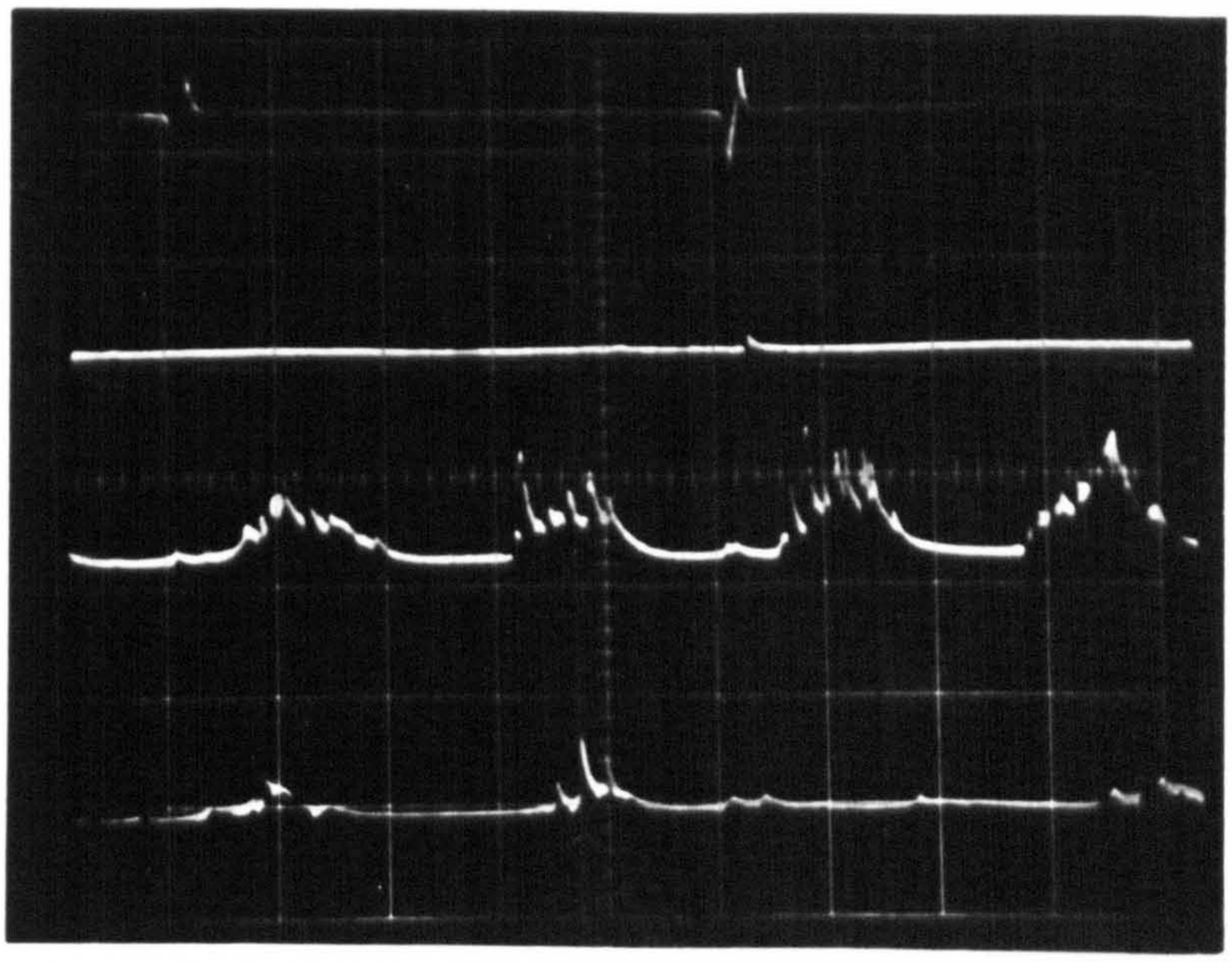

Fig. 9.10 Typical Mesh Voltage Records in Box 1 at 1800 r.p.m.

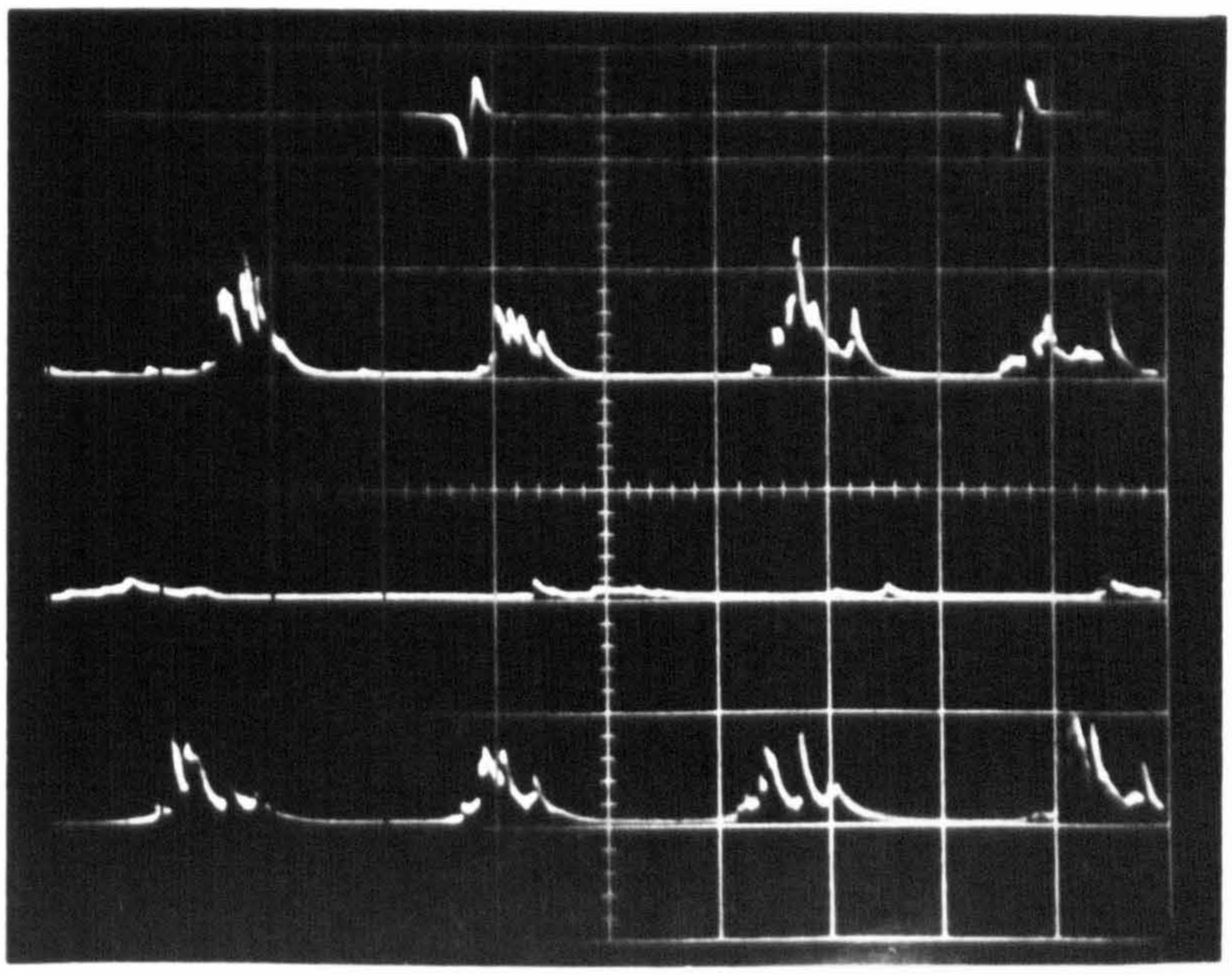

Fig. 9.11 Typical Mesh Voltage Records in Box 1 at 1700 r.p.m.

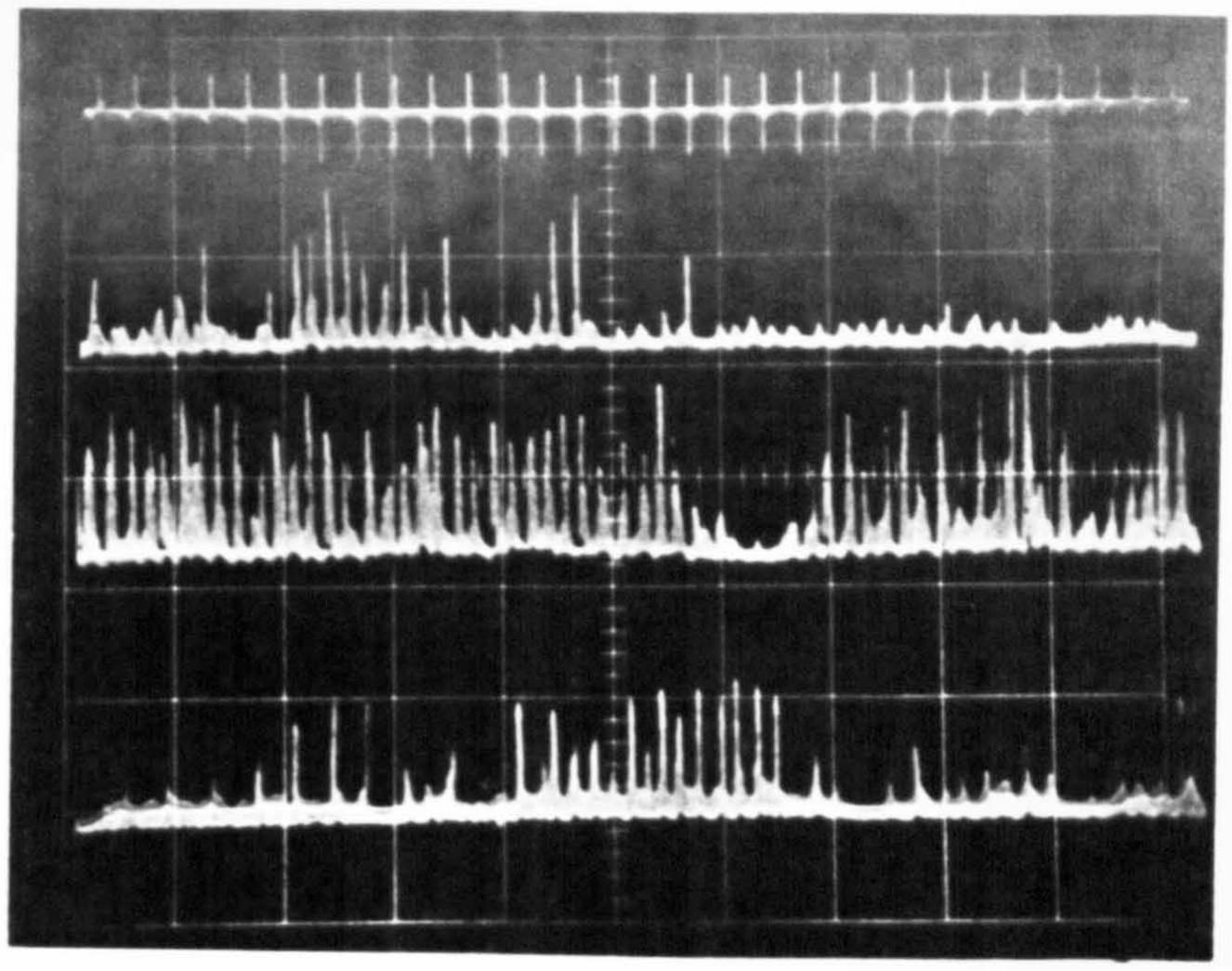

Fig. 9.12 Typical Mesh Voltage Traces at 1700 r.p.m. using a Low Scan Speed (Scale: .5 v/cm)

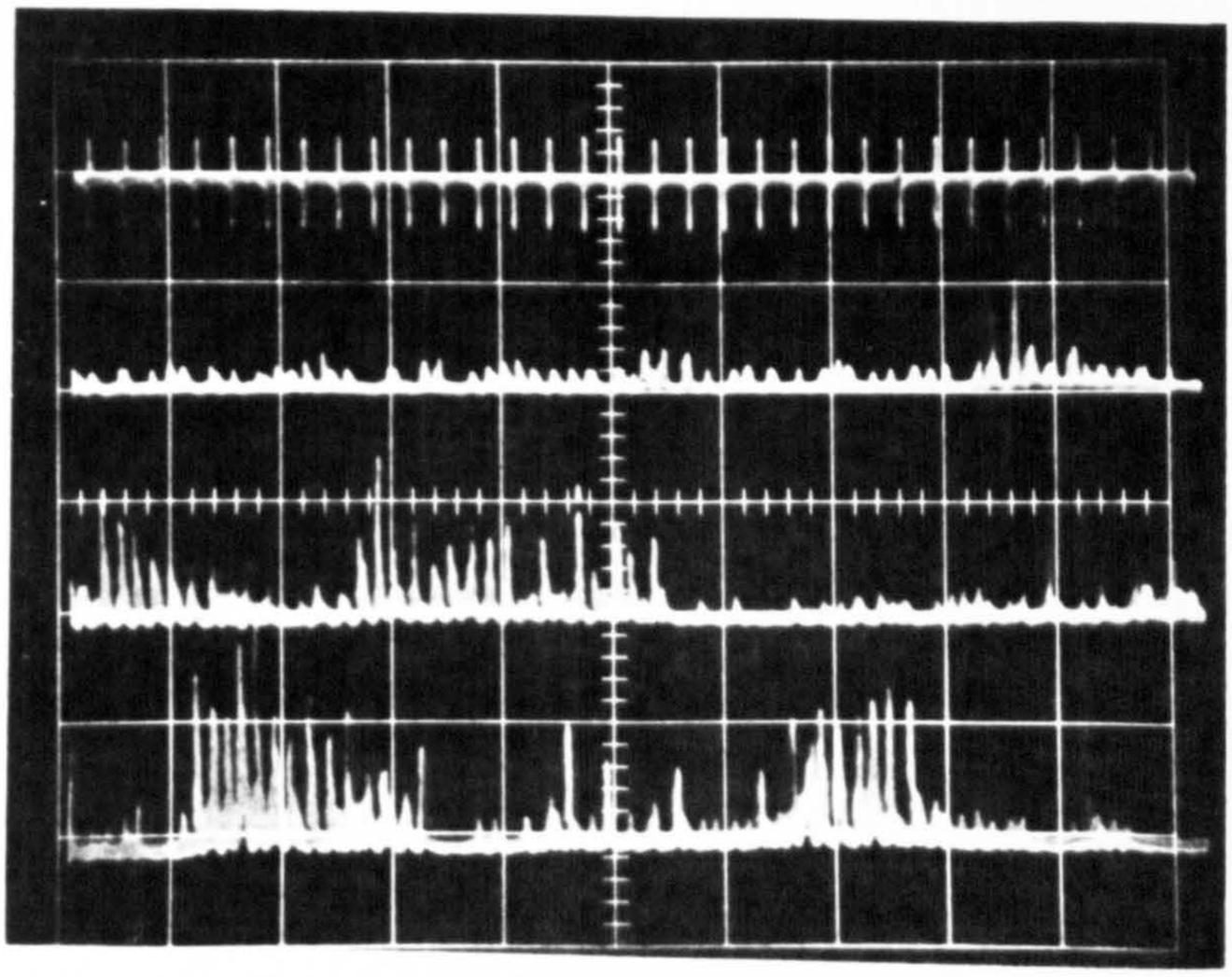

Fig. 9.13 Typical Mesh Voltage Traces at 1800 r.p.m.

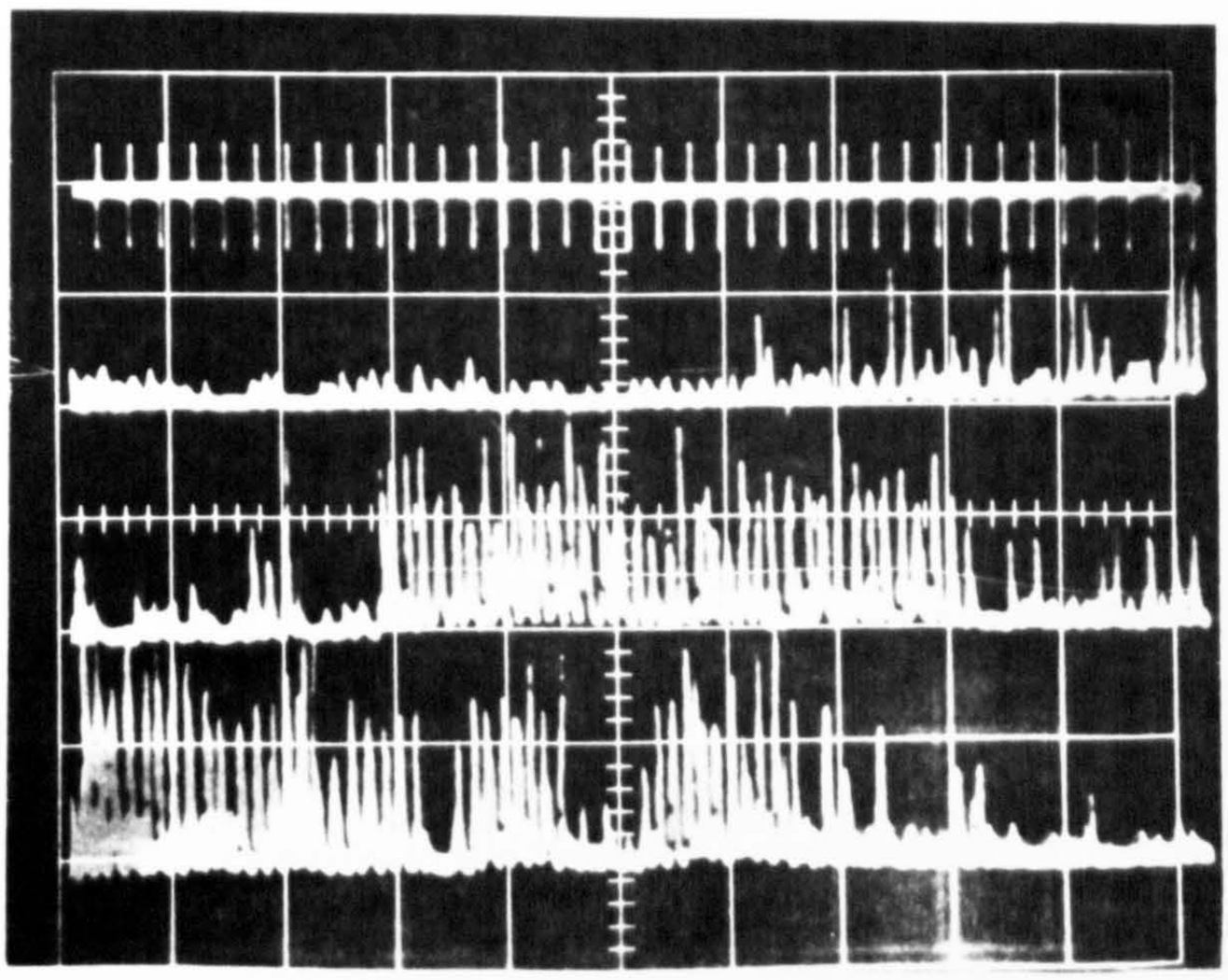

Fig. 9.14 Typical Mesh Voltage Traces at 2100 r.p.m.

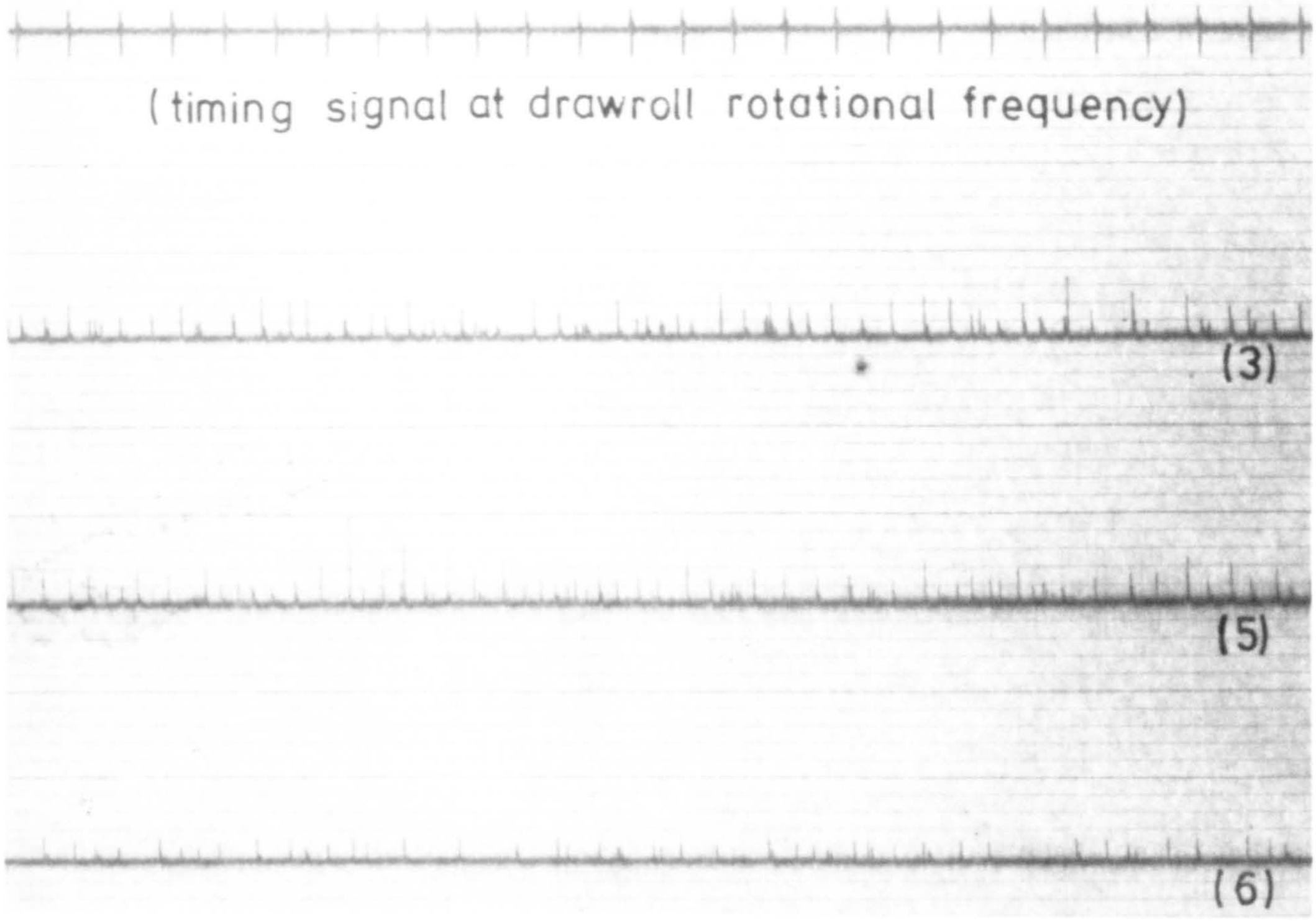

Fig. 9.15 Mesh Voltage Records from Box 2, Positions 3, 5 and 6, at 1000 r.p.m. (Scale 1 v/cm).

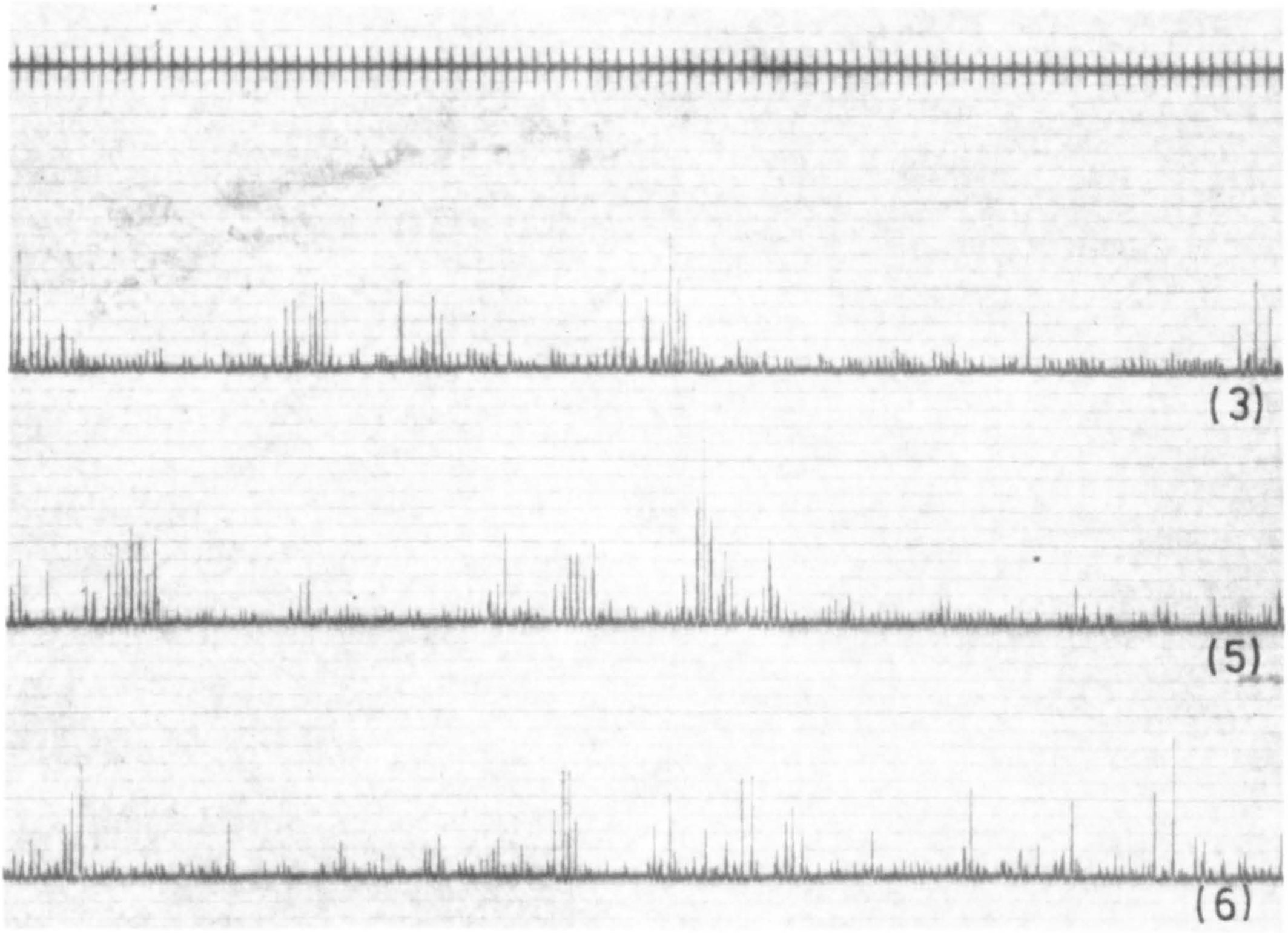

Fig. 9.16 Mesh Voltage Records from Box 4, Positions 3, 5 and 6, at 1800 r.p.m.

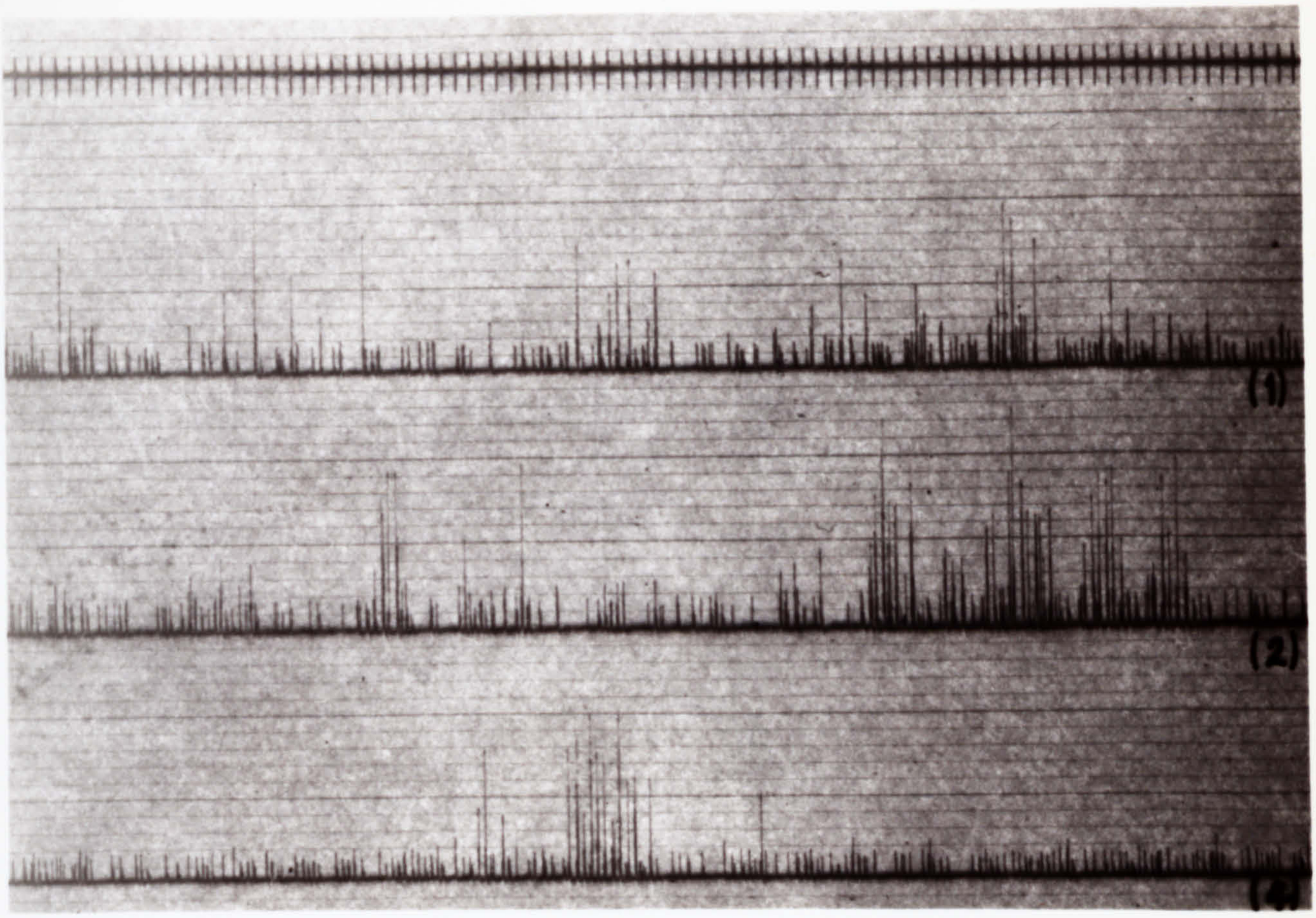

Fig. 9.17 Mesh Voltage Records from Box 3, Positions 1, 2 and 4, at 1800 r.p.m.

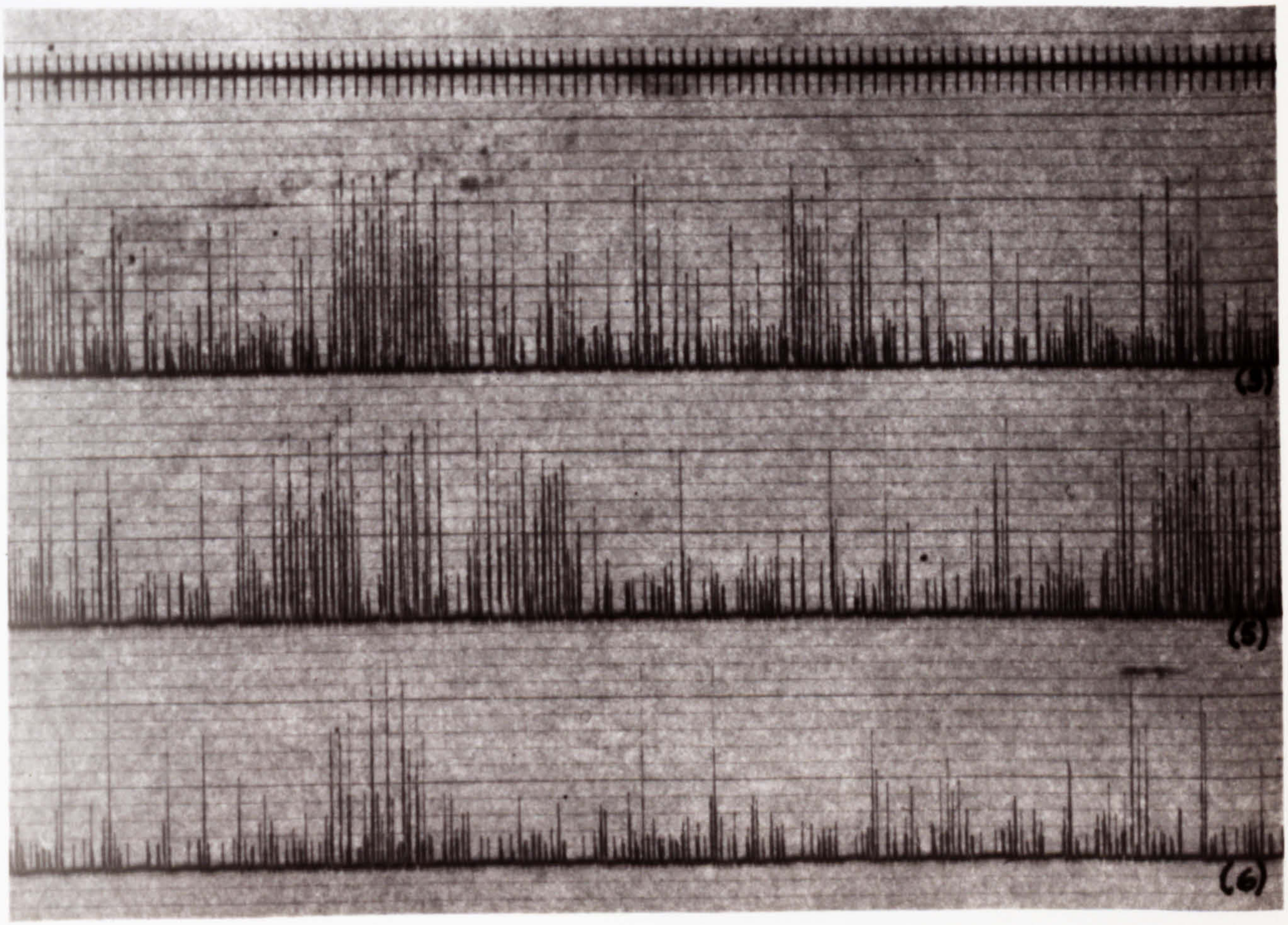

Fig. 9.18 Mesh Voltage Records from Box 2, Positions 3, 5 and 6, at 1800 r.p.m.

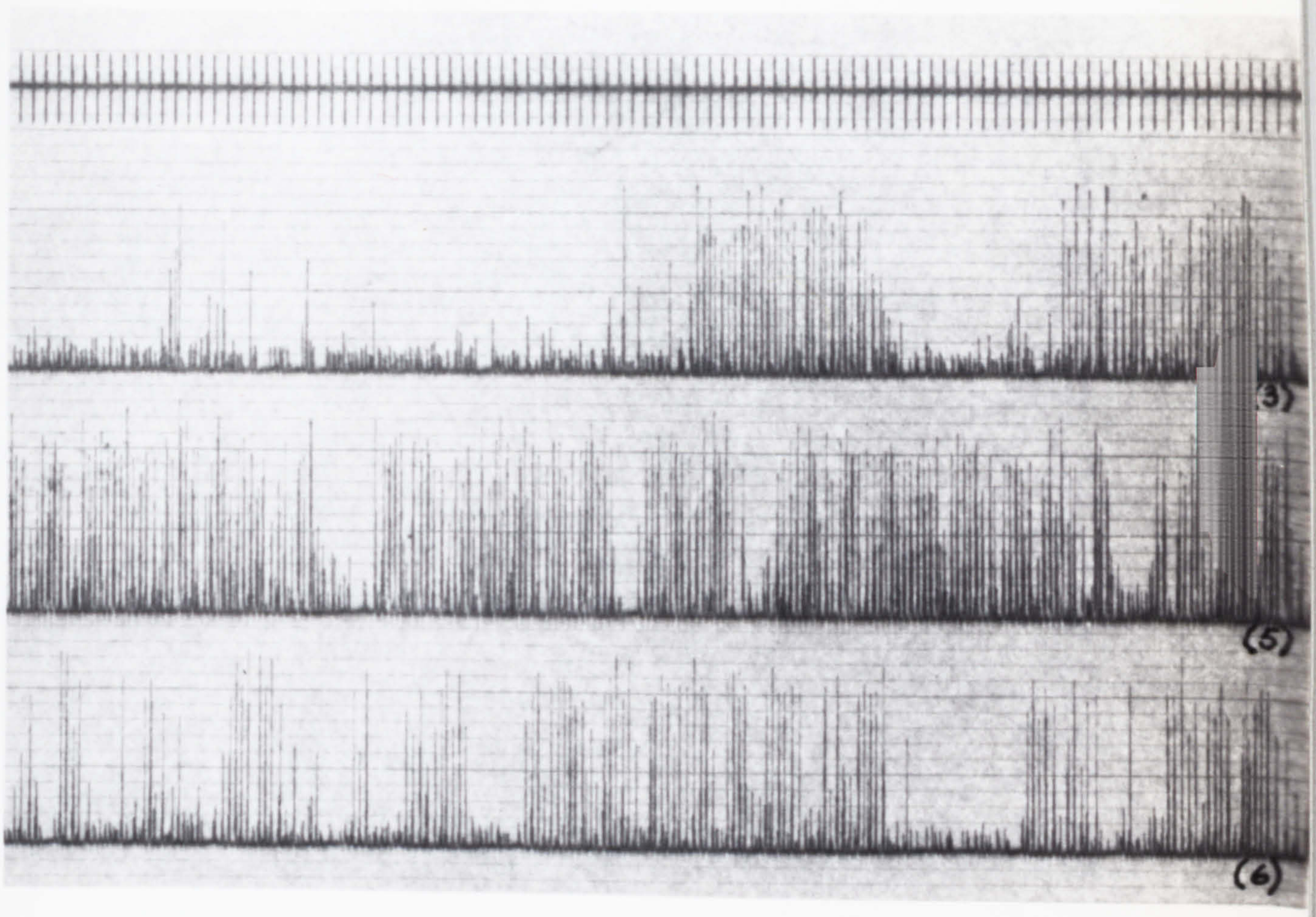

Fig. 9.19 Mesh Voltage Records from Box 1, Positions 3, 5 and 6, at 1800 r.p.m.

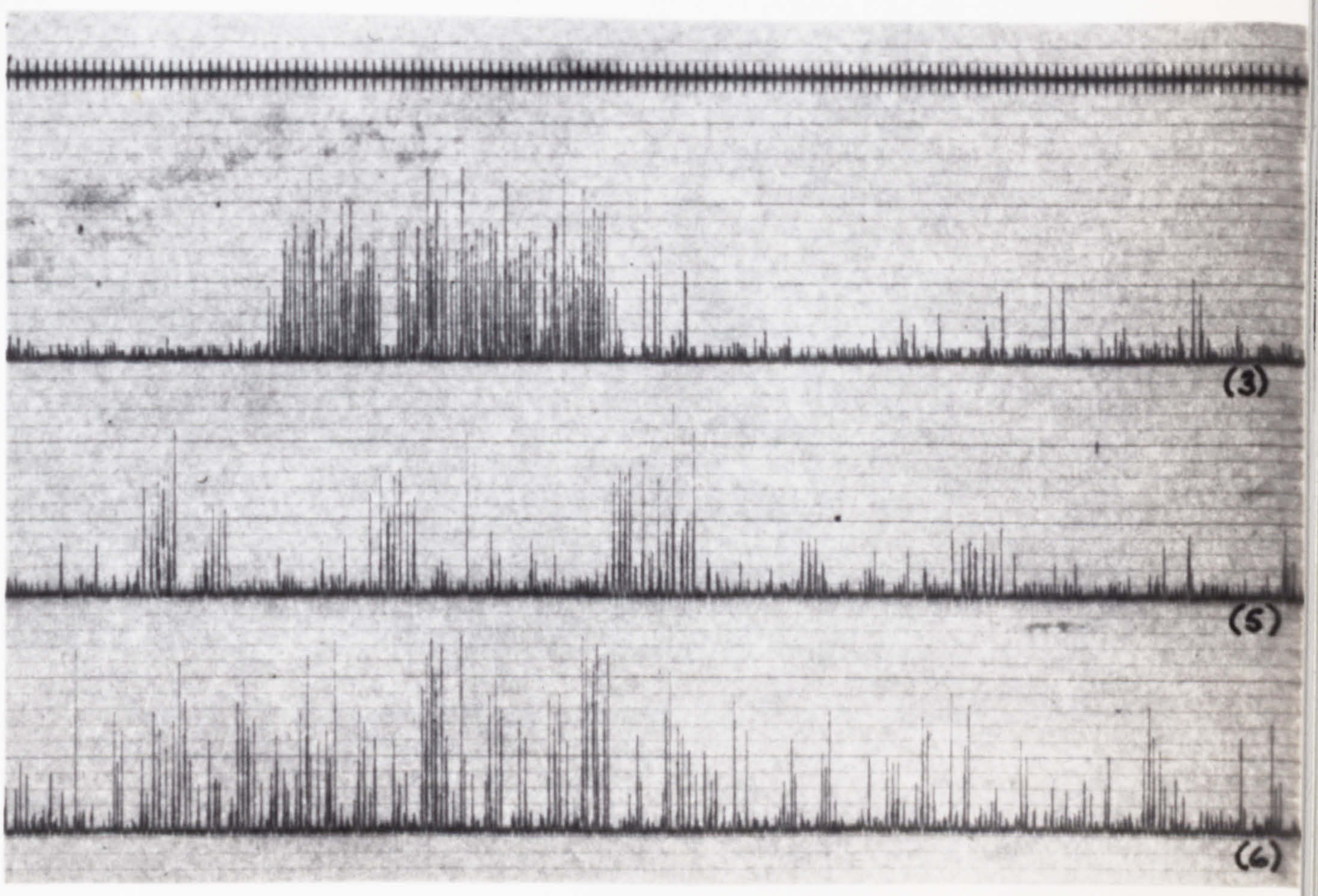

Fig. 9.20 Mesh Voltage Records from Box 4, Positions 3, 5 and 6, at 2400 r.p.m.

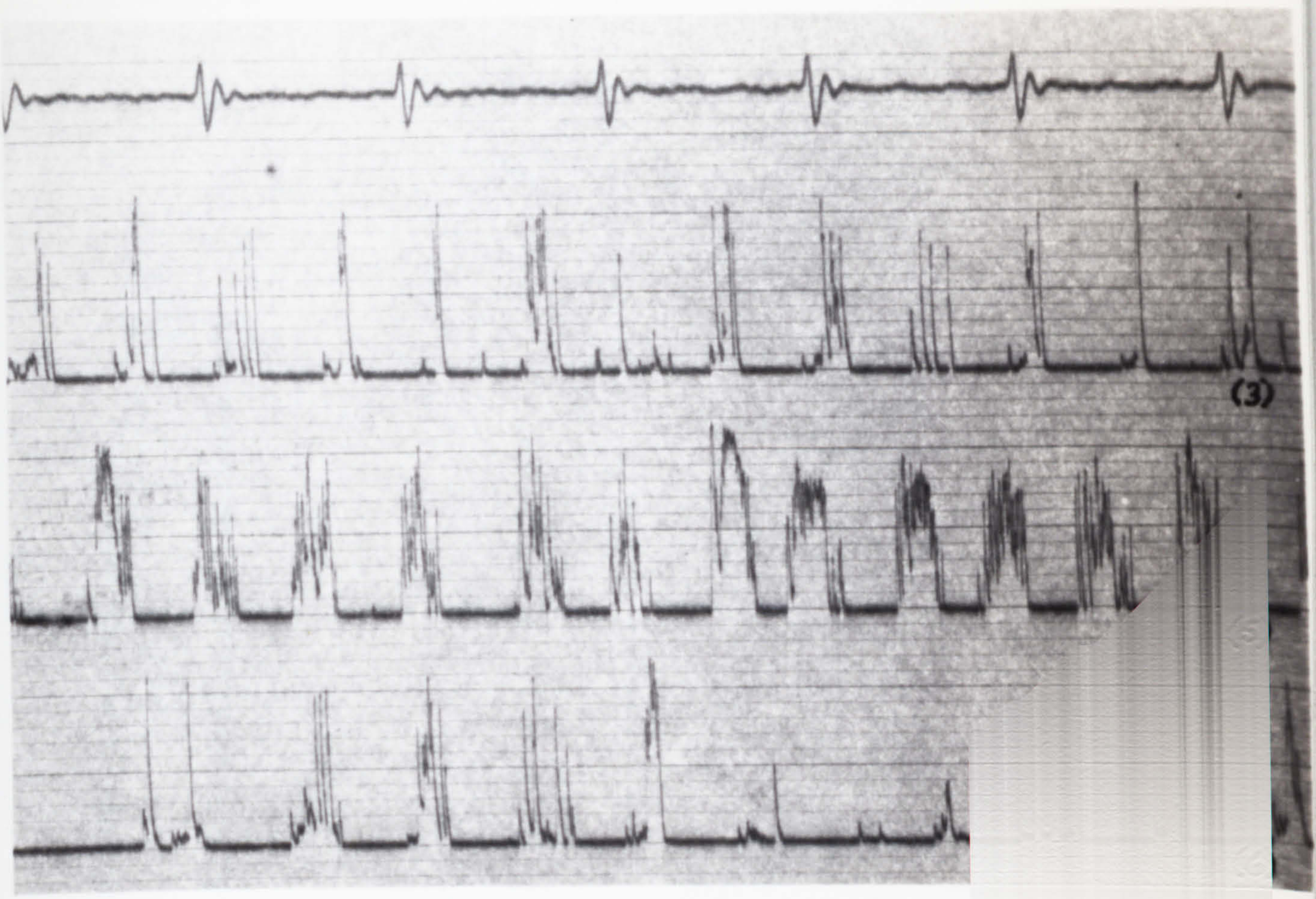

Fig. 9.21 Mesh Voltage Records from Box 1, Positions 3, 5 and 6, at 2300 r.p.m.

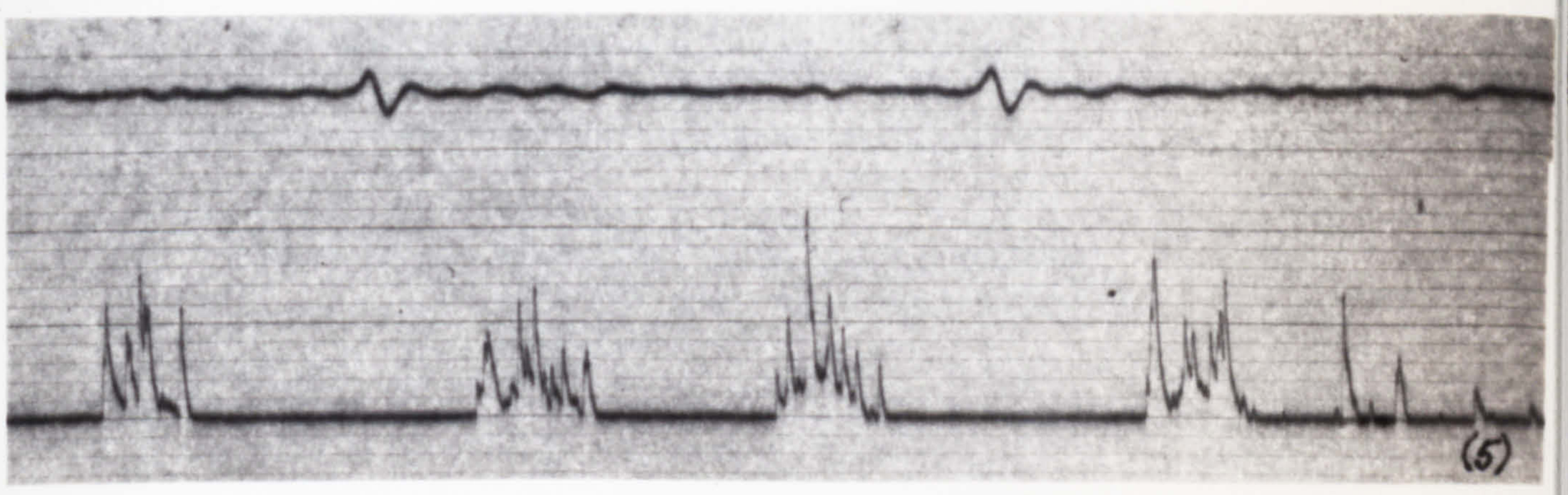

Fig. 9.22 Mesh Voltage Record from Box 3, Position 5, at 1800 r.p.m.

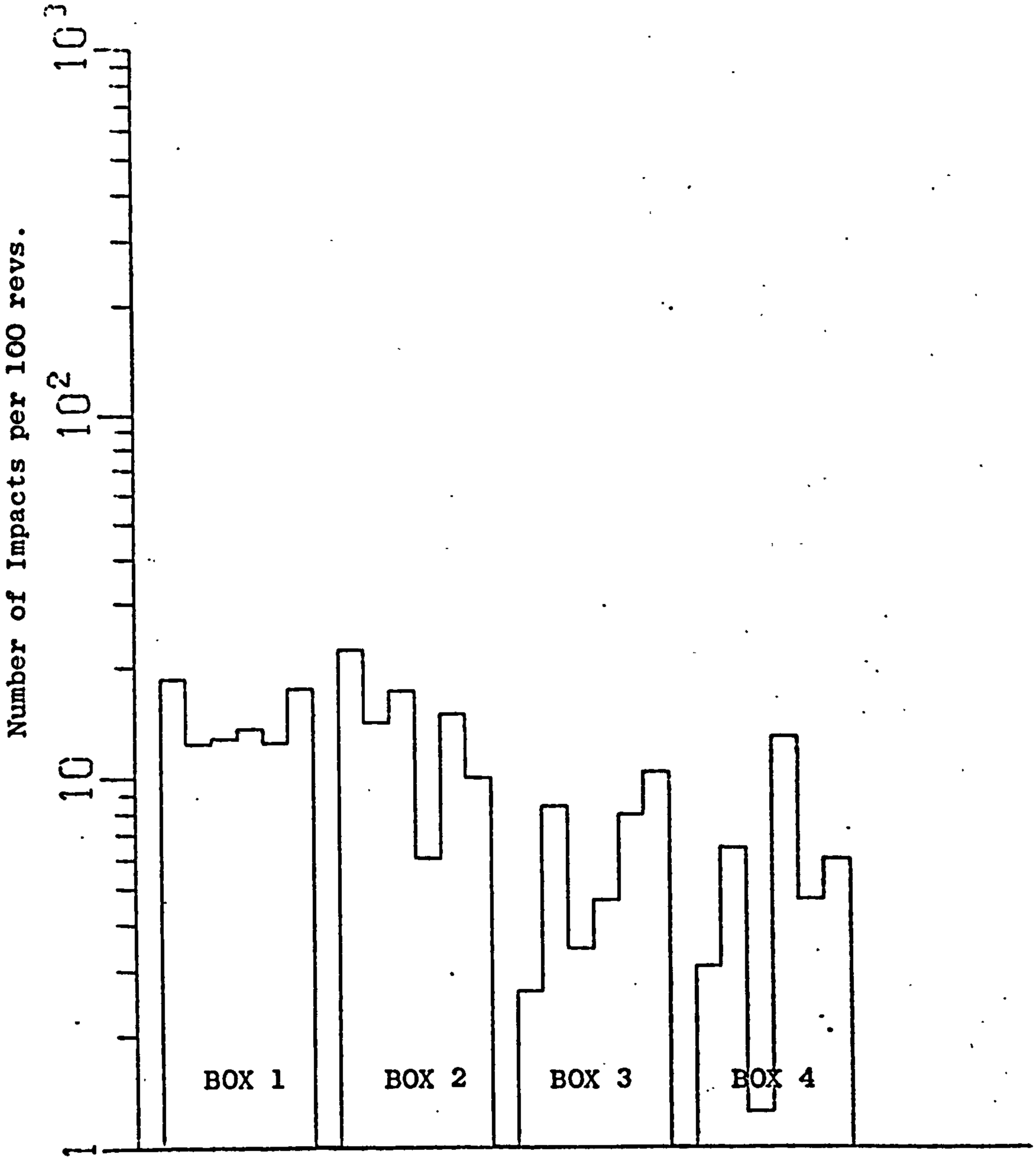

FIG. 9.23 Distribution of Impact Density, in 4 Box Rig, at a Test Speed of 1000 r.p.m.

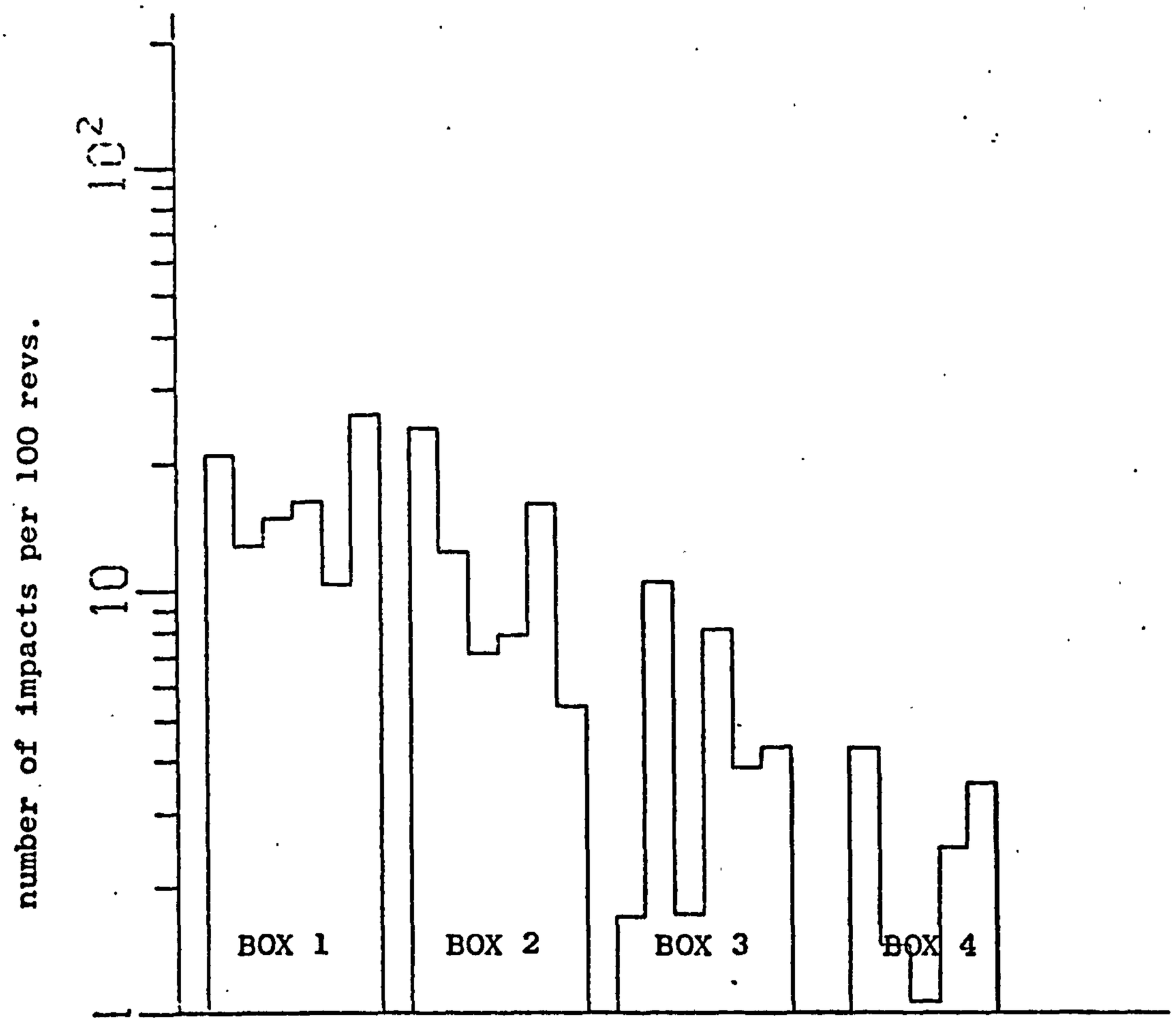

FIG. 9.24 Distribution of Impact Density at 1250 r.p.m.

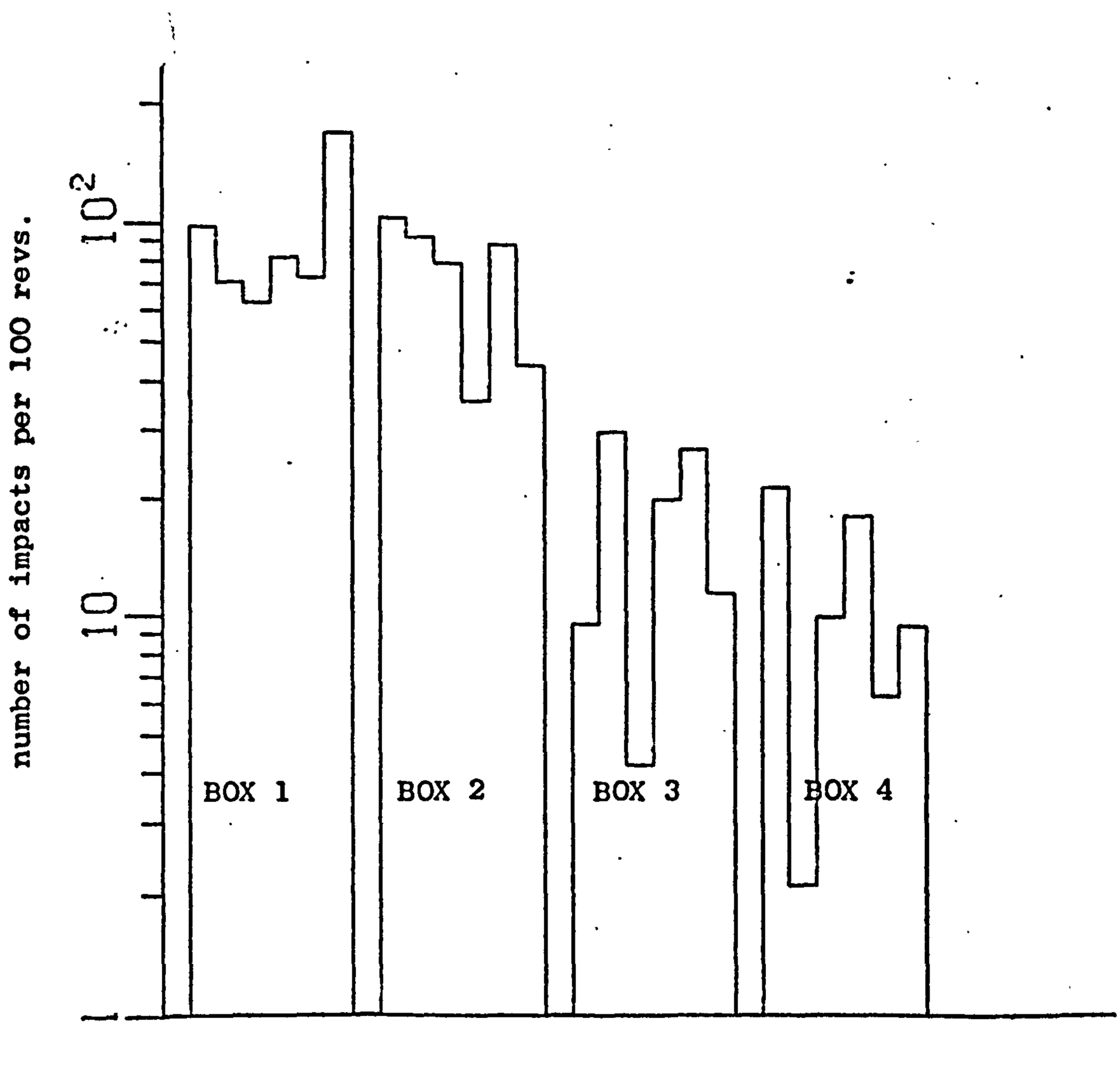

FIG.9.25 Distribution of impact density at 1500 r.p.m.

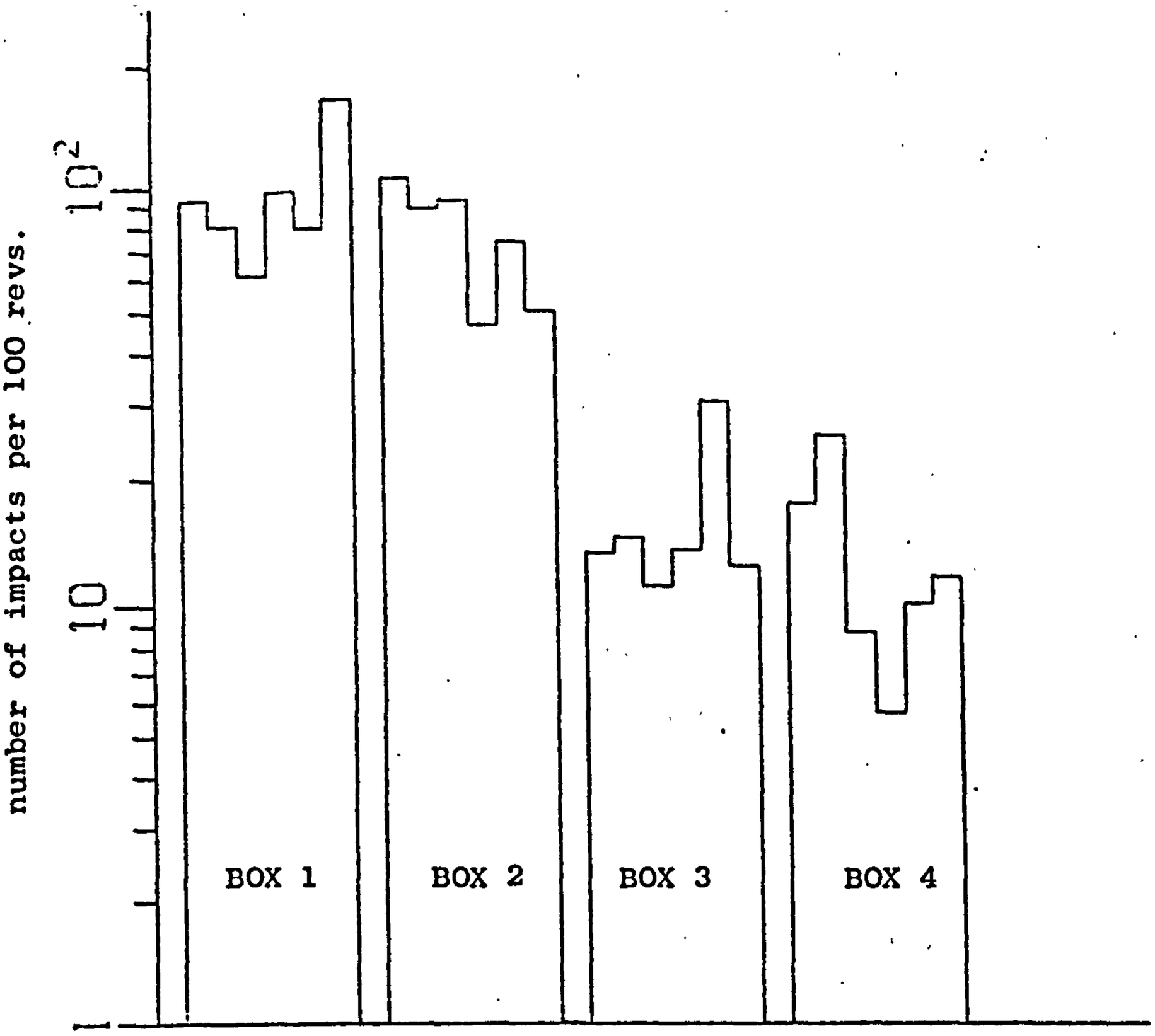

FIG. 9.26 Distribution of Impact Density at 1700 r.p.m.

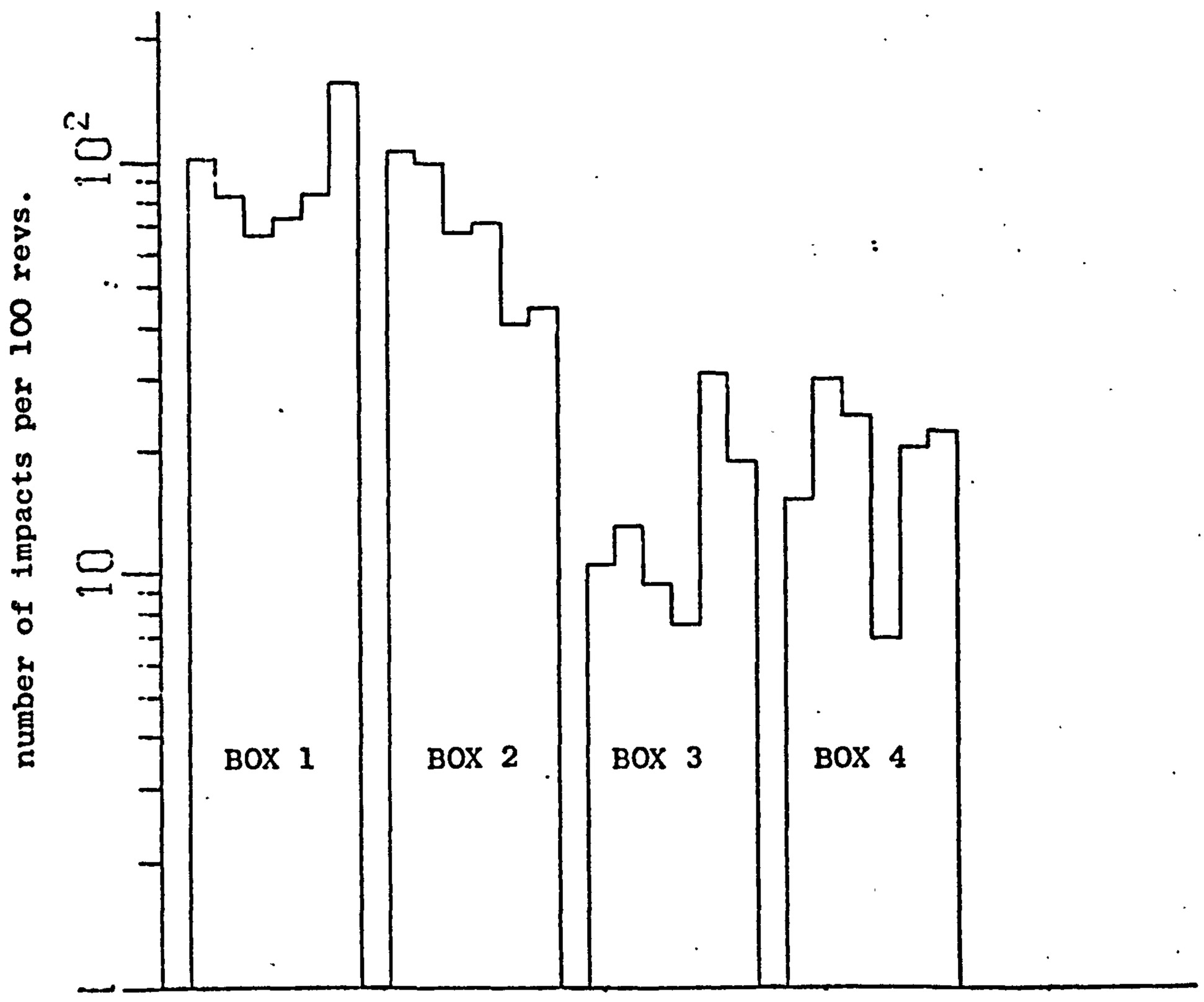

FIG. 9.27 Distribution of Impact Density at 1800 r.p.m.

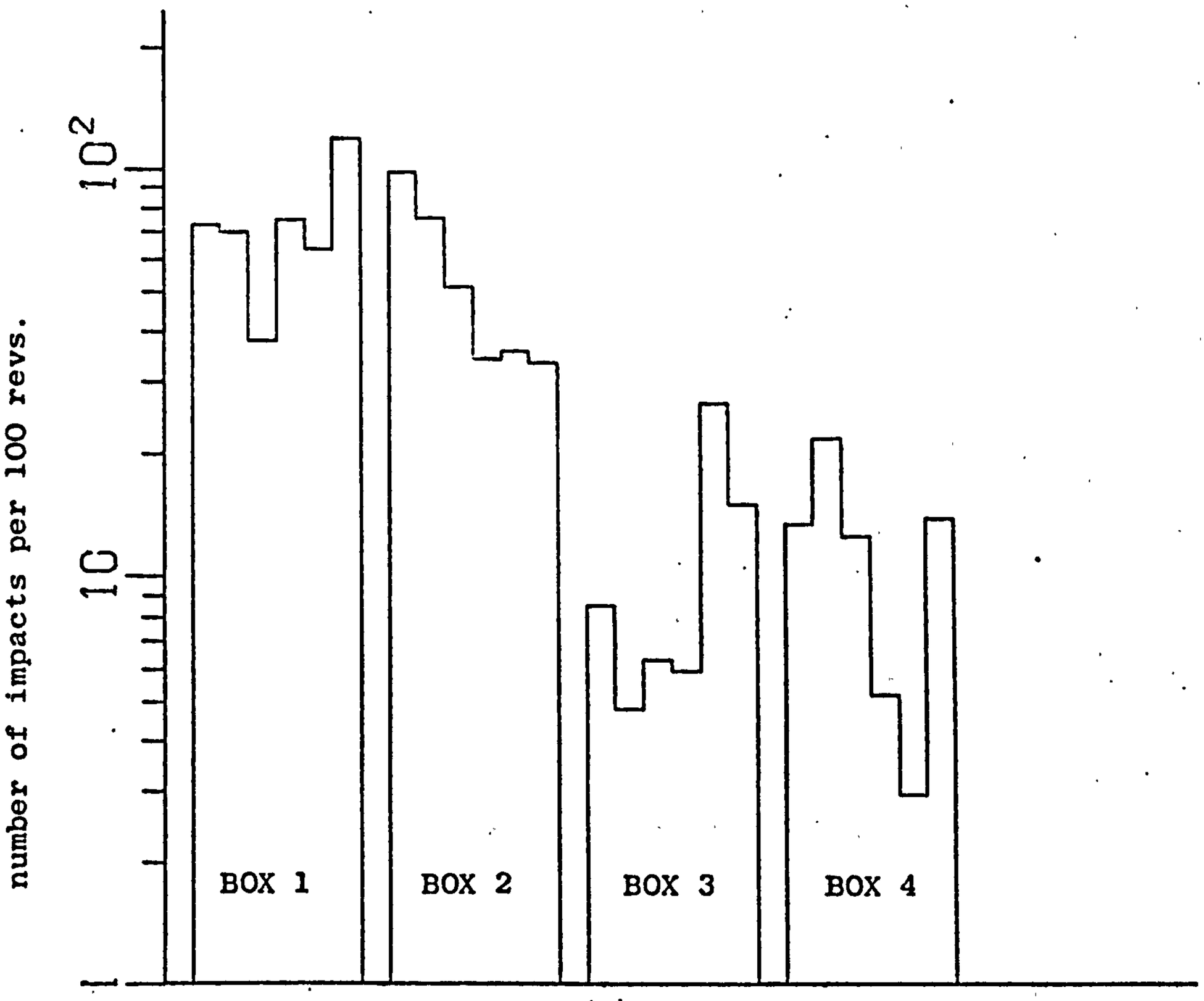

FIG. 9.28 Distribution of Impact Density at 1900 r.p.m.

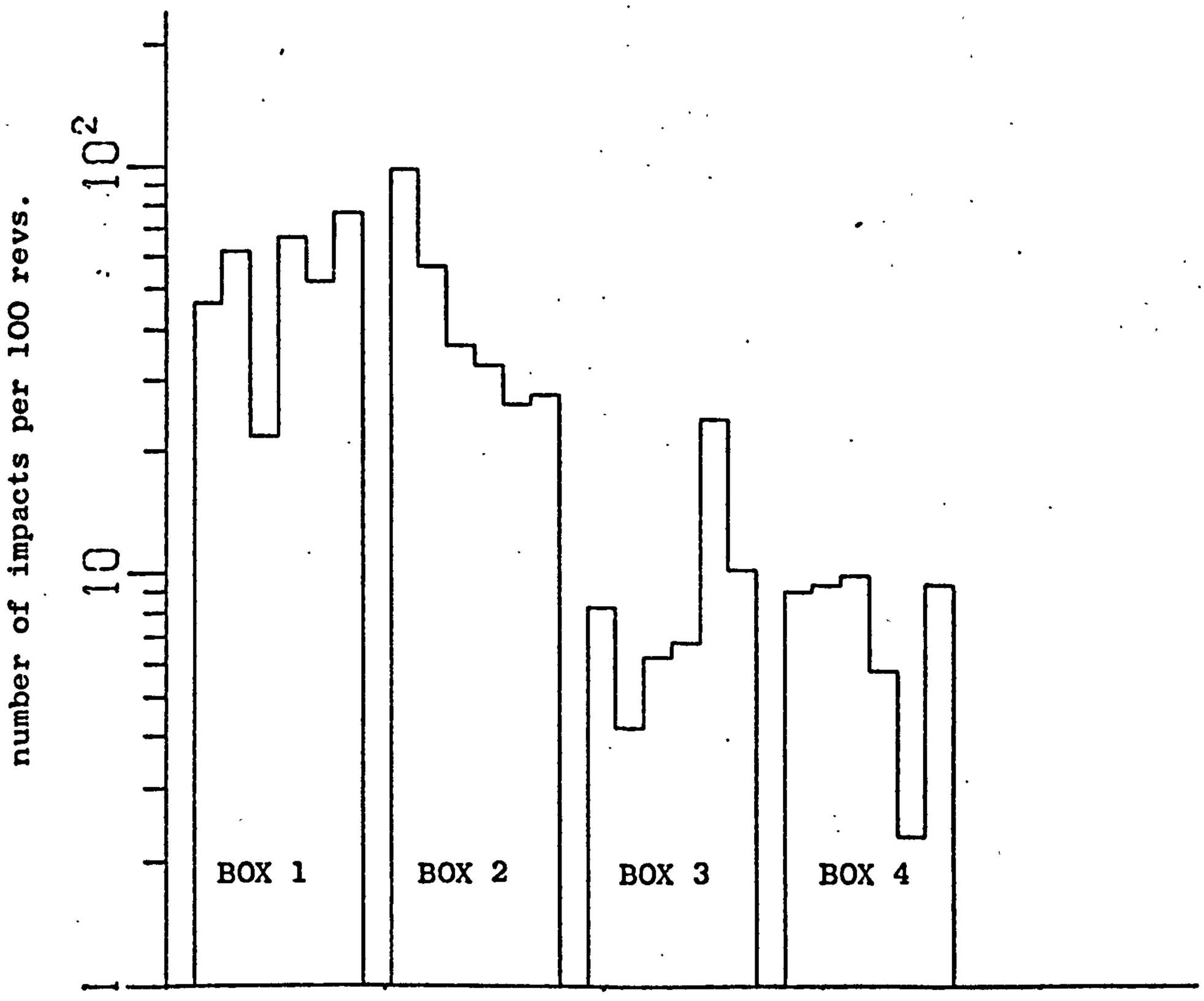

FIG. 9.29 Distribution of Impact Density at 2000 r.p.m.

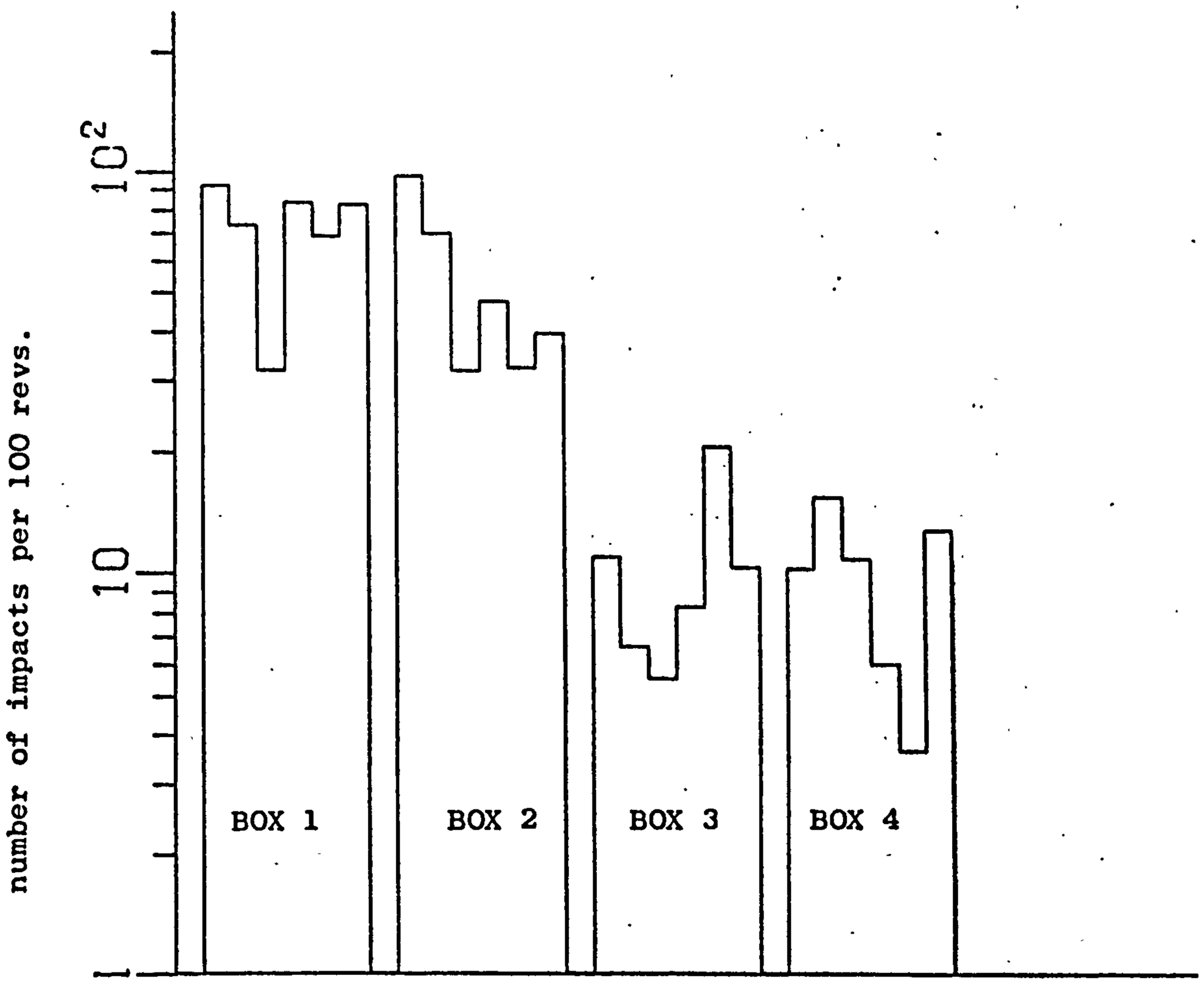

FIG. 9.30 Distribution of Impact Density at 2100 r.p.m.

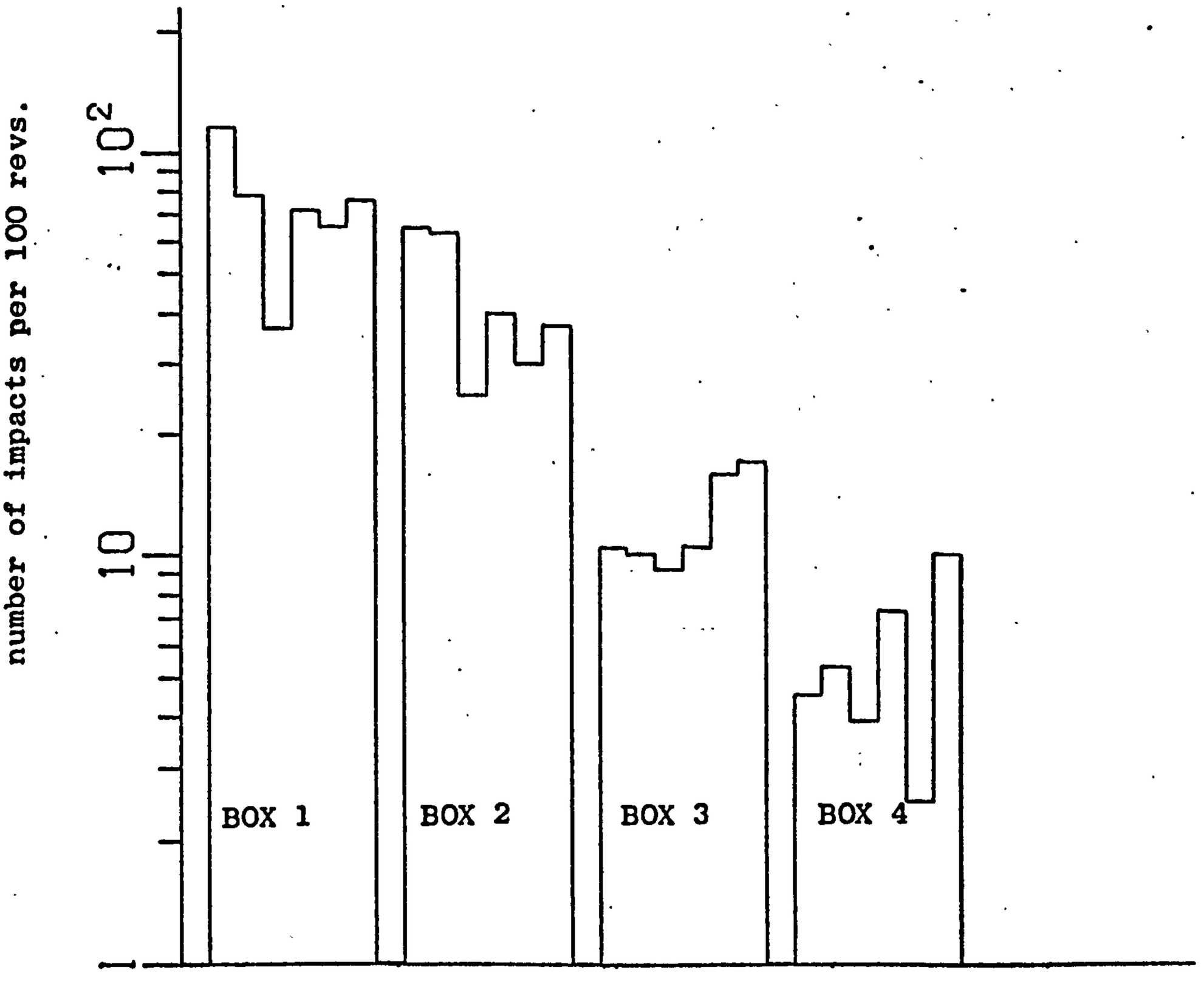

FIG. 9.31 Distribution of Impact Density at 2200 r.p.m.

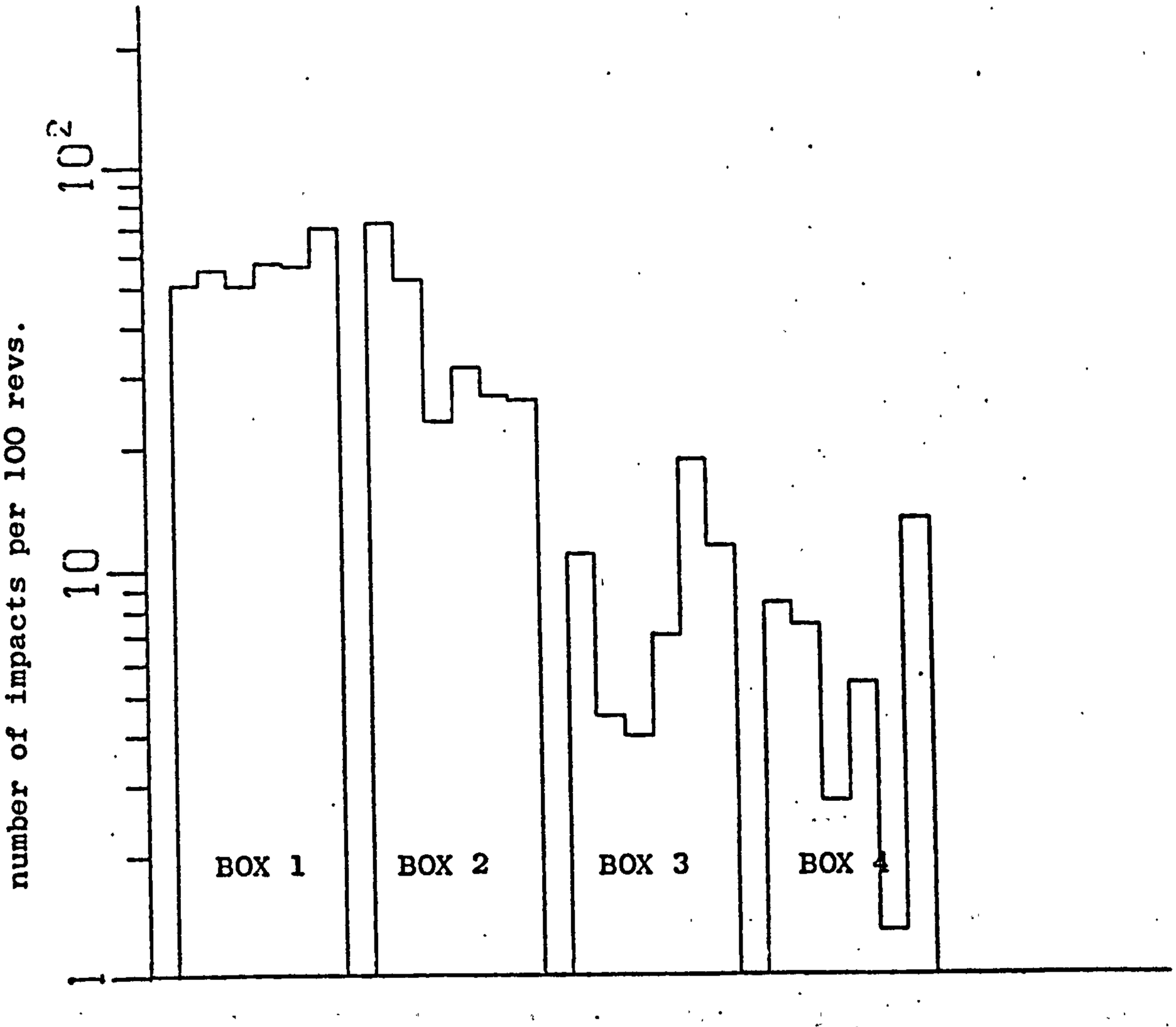

FIG. 9.32 Distribution of Impact Density at 2300 r.p.m.

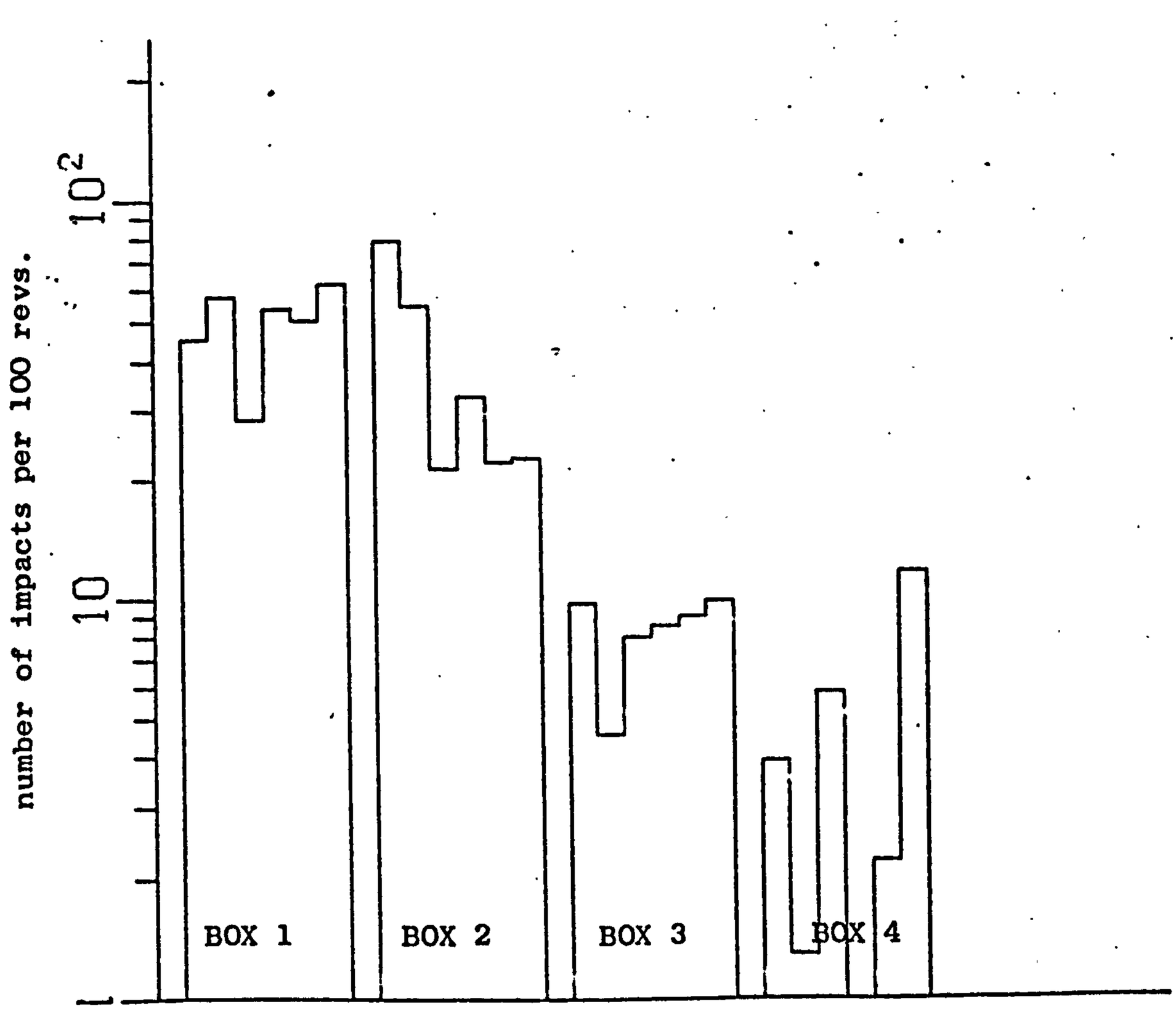

FIG. 9.33 Distribution of Impact Density at 2400 r.p.m.

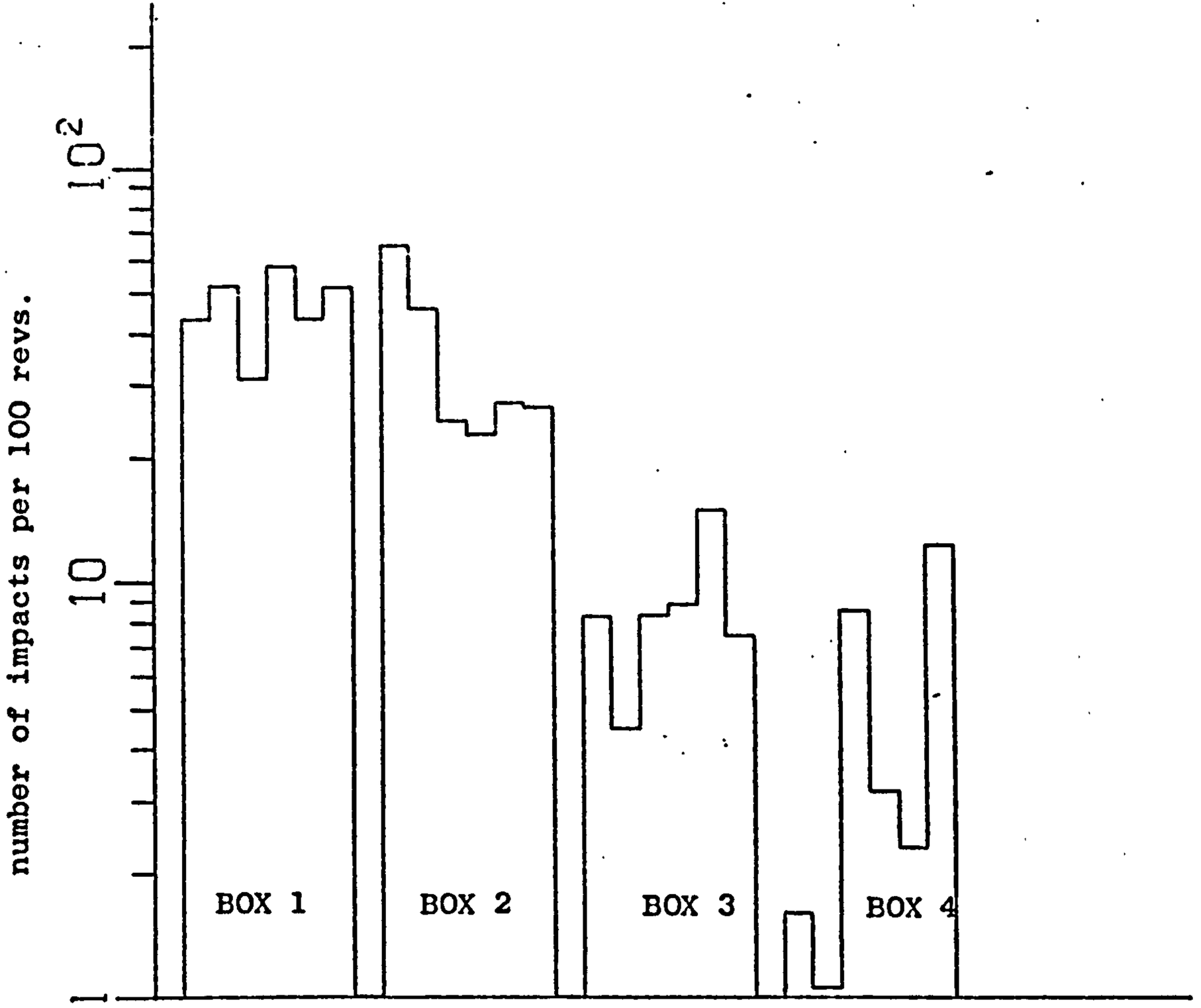

FIG. 9.34 Distribution of Impact Density at 2500 r.p.m.

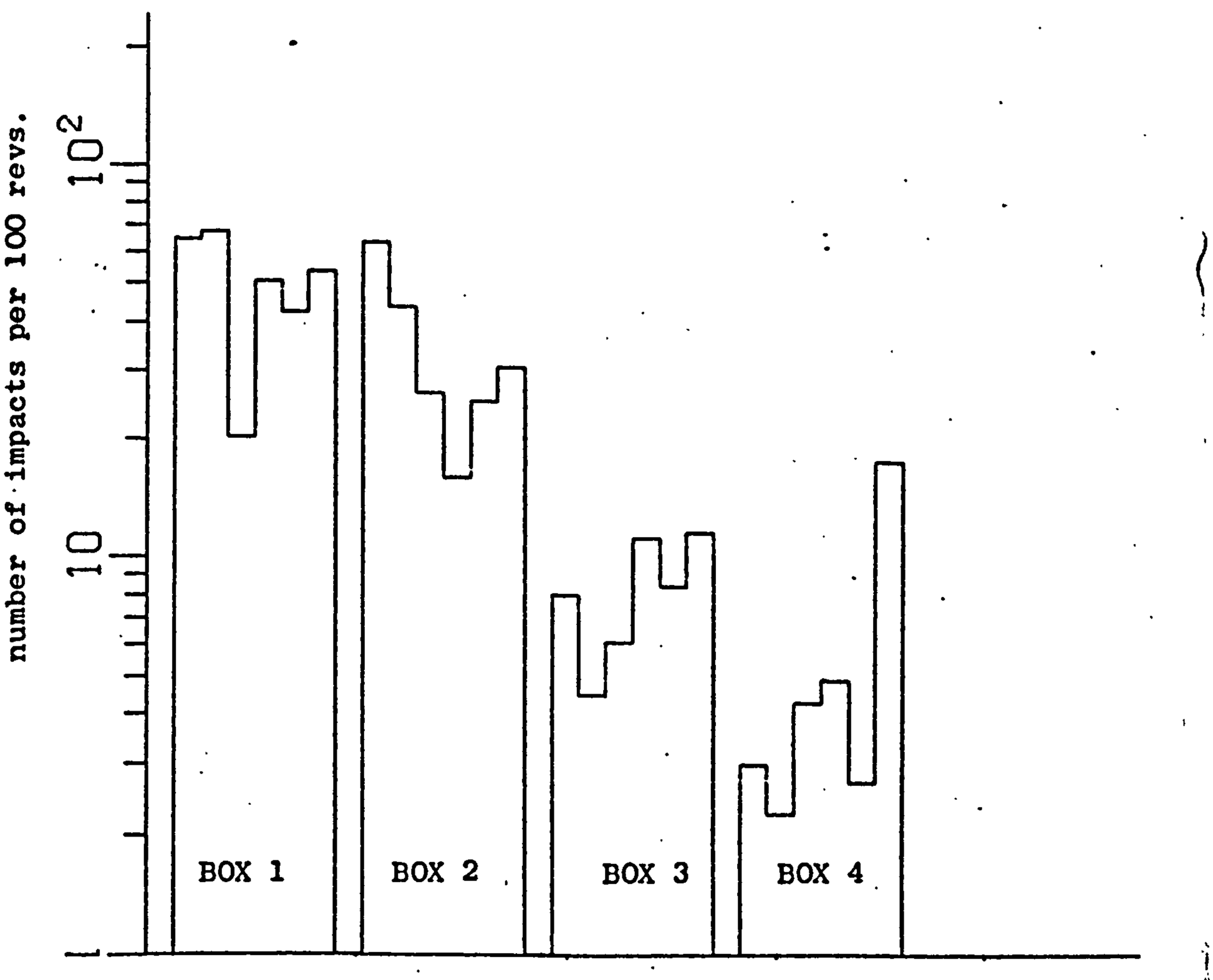

FIG. 9.35 Distribution of Impact Density at 2600 r.p.m.

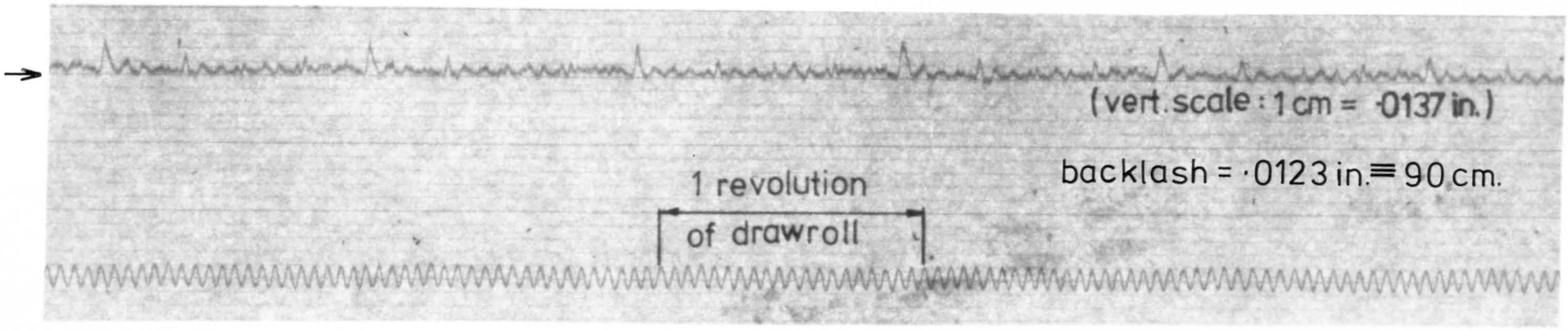

Fig. 9.36 Relative Dynamic Motion of Instrumented Gear Pair, at 150 r.p.m., with a Brake Load of 2.5 lbf.in. applied to the Steel Gear Shaft. (Test performed in short gearbox).

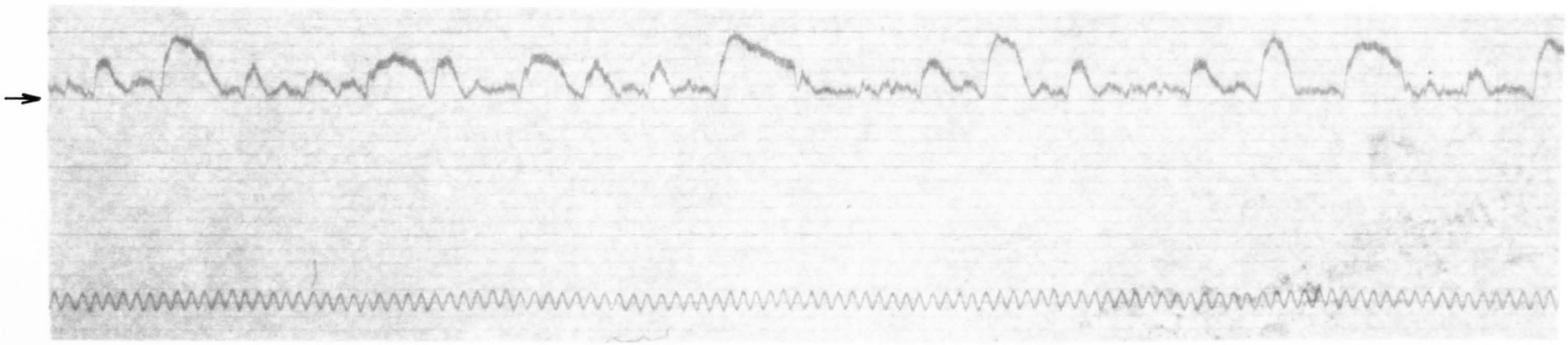

Fig. 9.37 Relative Dynamic Motion, at 150 r.p.m., with Load Removed.

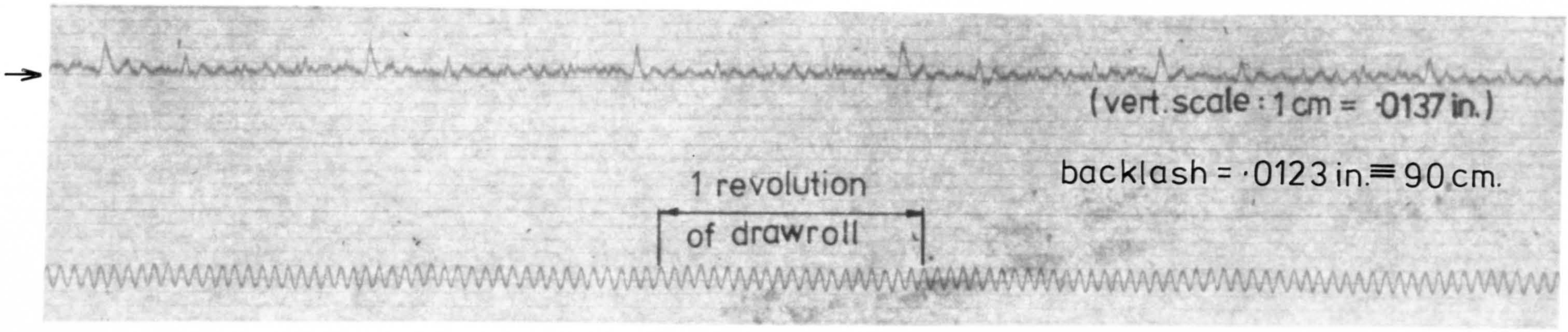

Fig. 9.36 Relative Dynamic Motion of Instrumented Gear Pair, at 150 r.p.m., with a Brake Load of 2.5 lbf.in. applied to the Steel Gear Shaft. (Test performed in short gearbox).

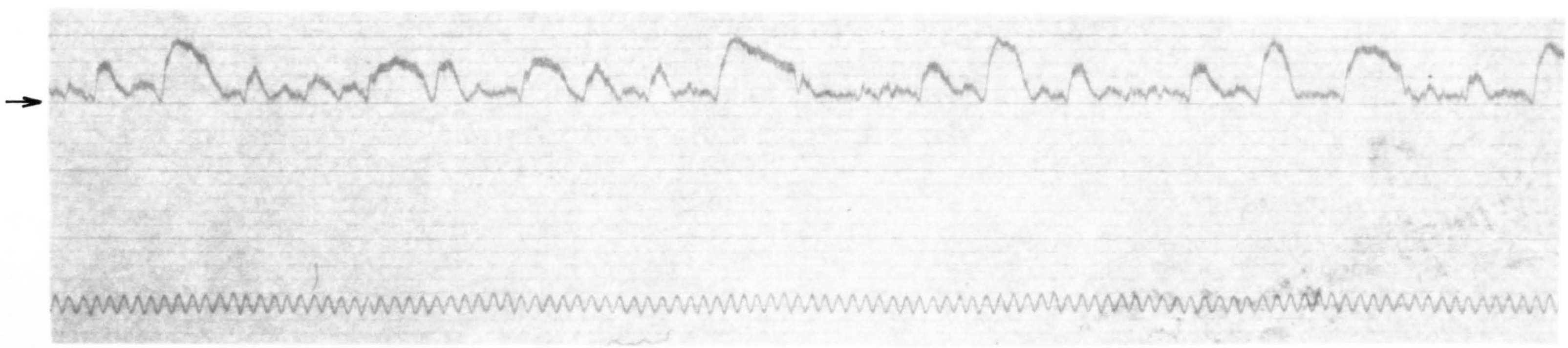

Fig. 9.37 Relative Dynamic Motion, at 150 r.p.m., with Load Removed.

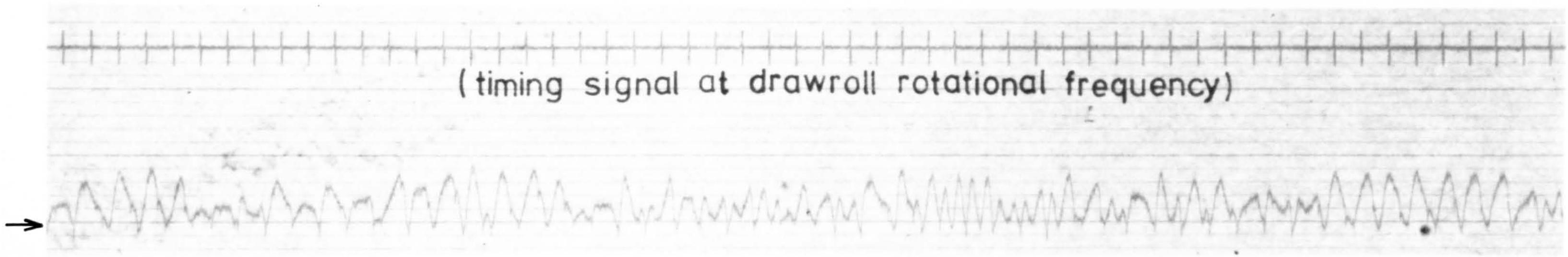

Fig. 9.38 Relative Dynamic Motion of Instrumented Pair, running at 725 r.p.m., in Multi-Box Rig (Box 4, Position 2).

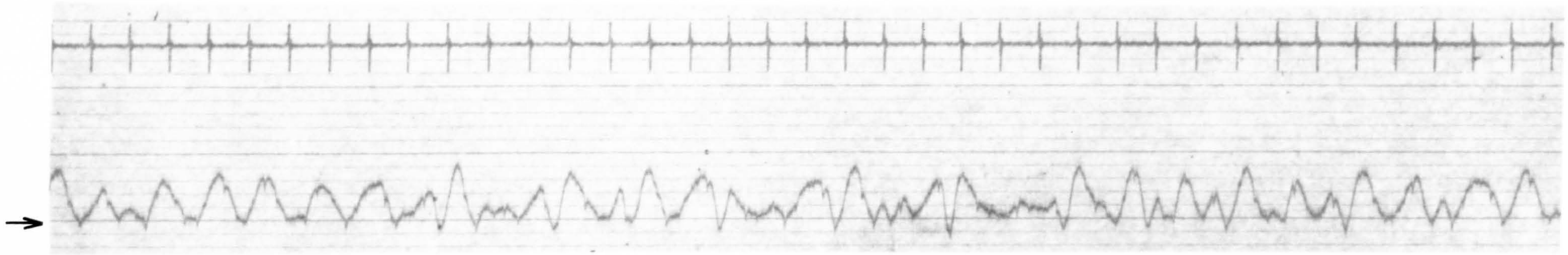

Fig. 9.39 Relative Dynamic Motion at 1000 r.p.m.

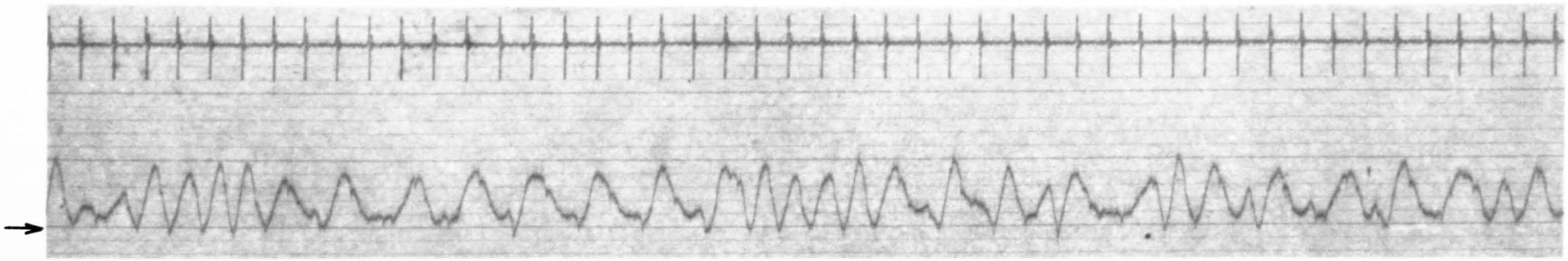

Fig. 9.40 Relative Dynamic Motion at 1250 r.p.m.

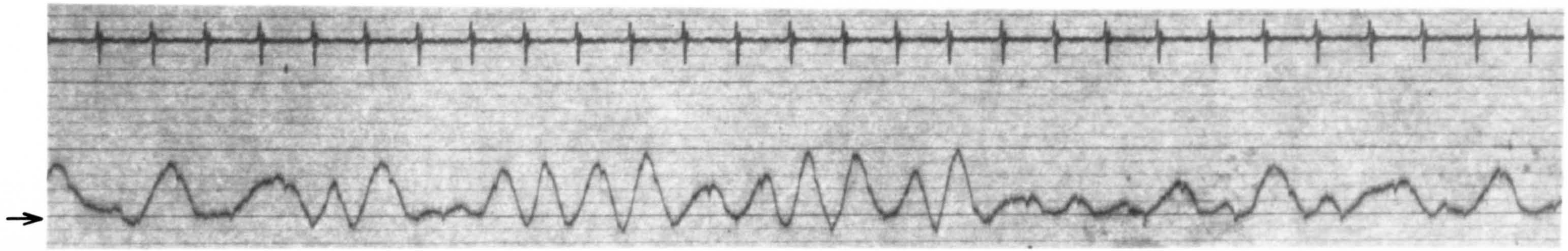

Fig. 9.41 Relative Dynamic Motion at 1500 r.p.m.

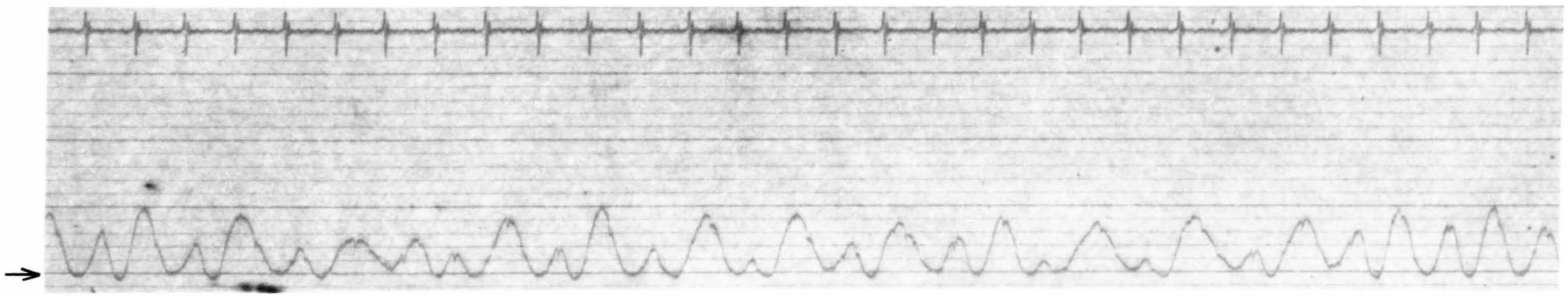

Fig. 9.42 Relative Dynamic Motion at 1500 r.p.m.

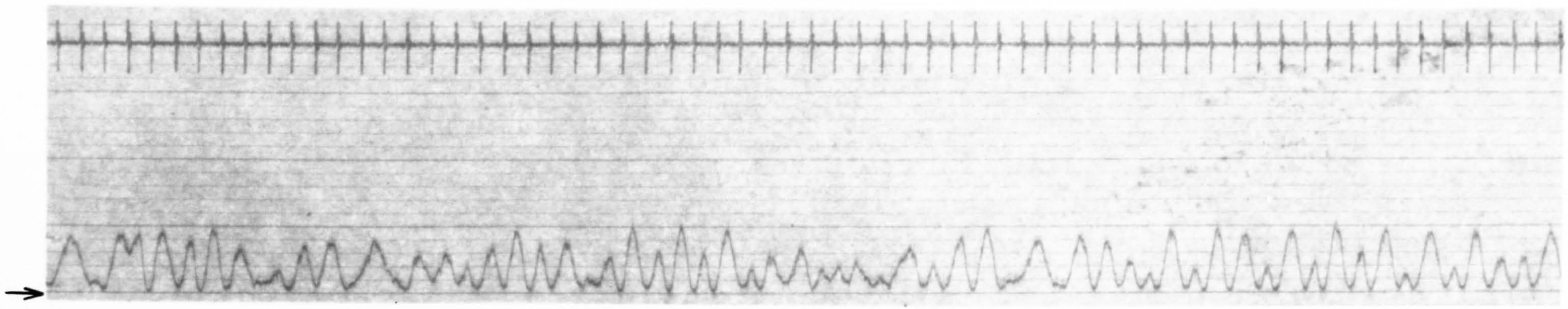

Fig. 9.43 Relative Dynamic Motion at 1700 r.p.m.

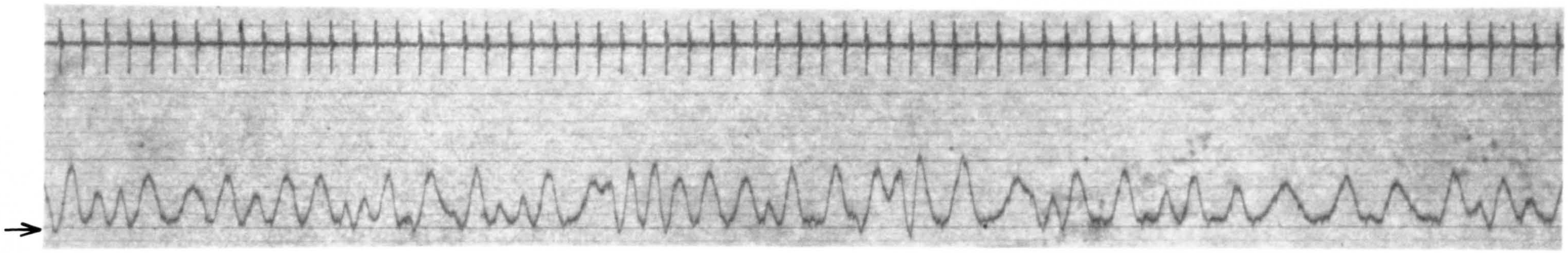

Fig. 9.44 Relative Dynamic Motion at 1800 r.p.m.

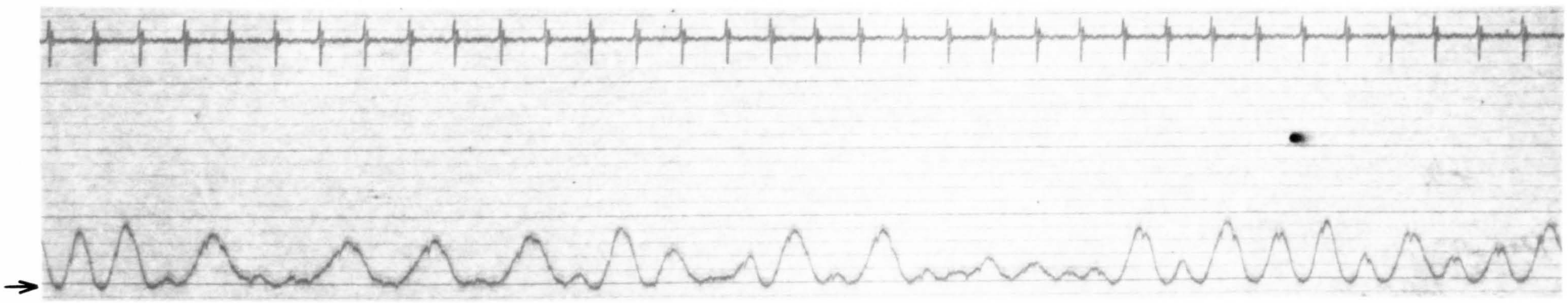

Fig. 9.45 Relative Dynamic Motion at 2000 r.p.m.

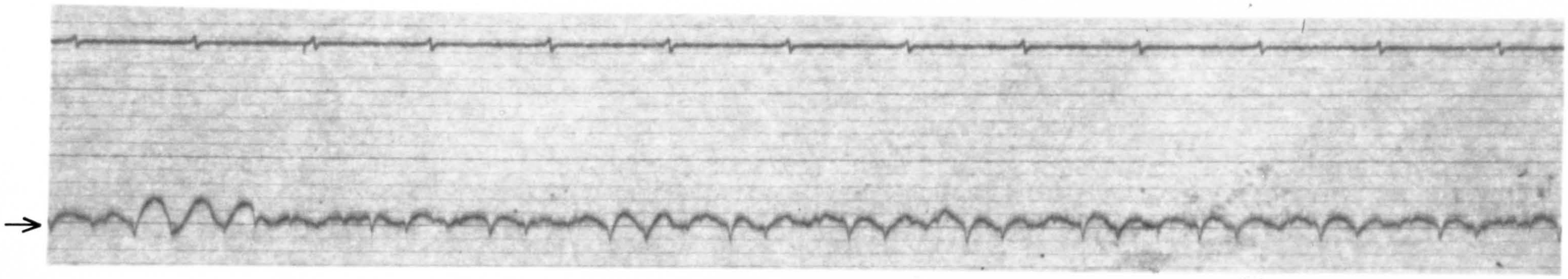

Fig. 9.46 Relative Dynamic Motion, at 750 r.p.m., with a Brake Load of 2.5 lbf.in. applied to Steel Gear Shaft.

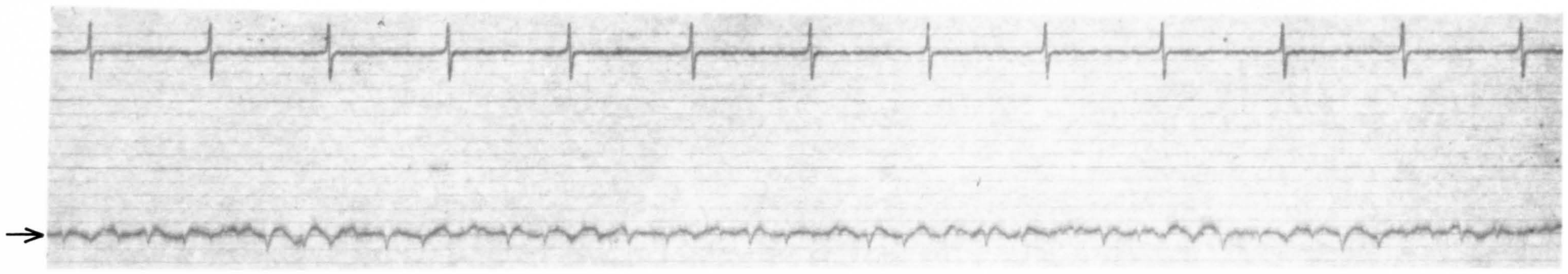

Fig. 9.47 Relative Dynamic Motion, at 750 r.p.m., with a Brake Load of 5 lbf.in. applied to Steel Gear Shaft.

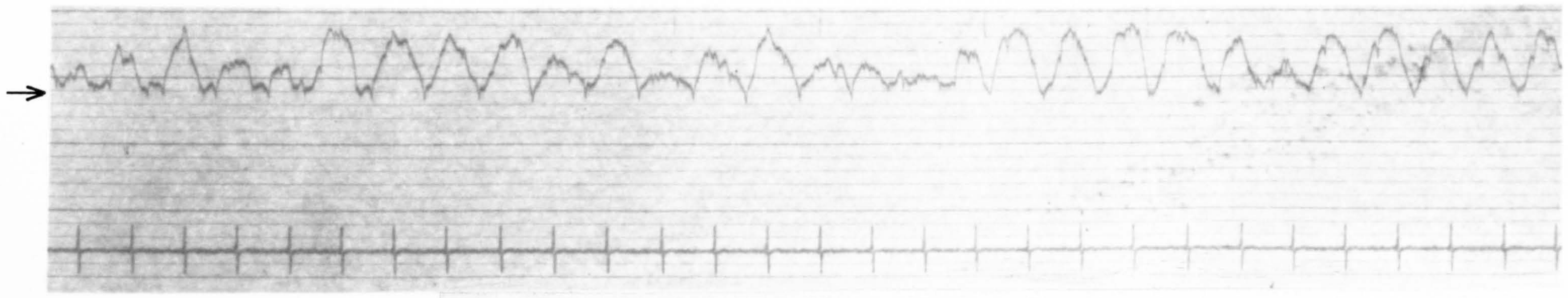

Fig. 9.48 Relative Dynamic Motion, at 750 r.p.m., with very Flexible Layshaft Couplings Replacing Standard Couplings in Multi-Box Rig.

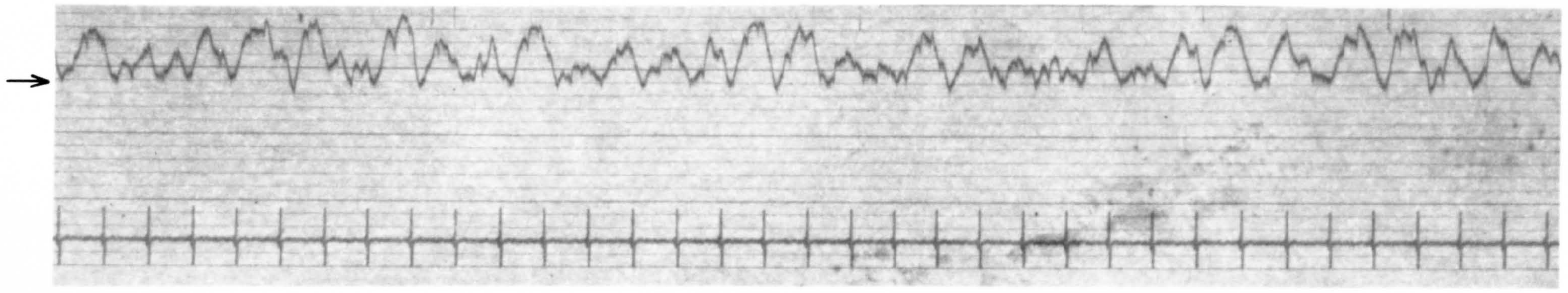

Fig. 9.49 Relative Dynamic Motion, with Modified Couplings, at 900 r.p.m.

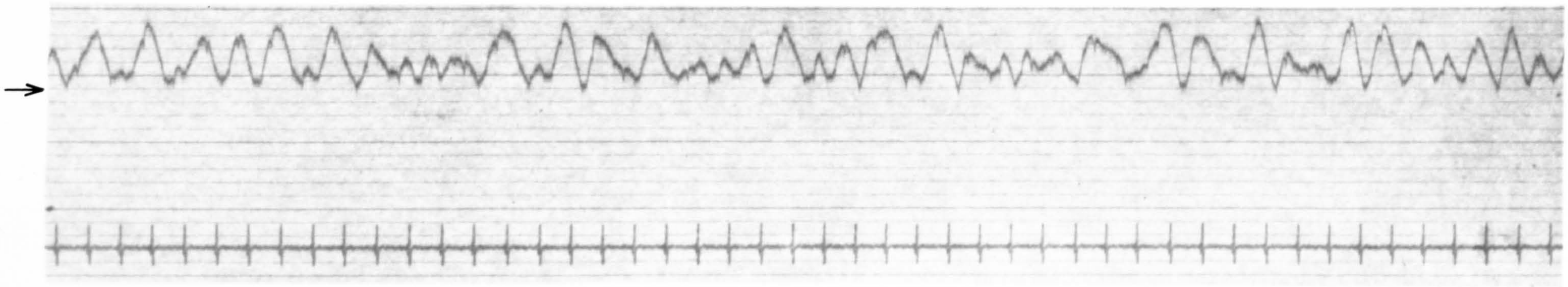

Fig. 9.50 Relative Dynamic Motion, with Modified Couplings, at 1250 r.p.m.

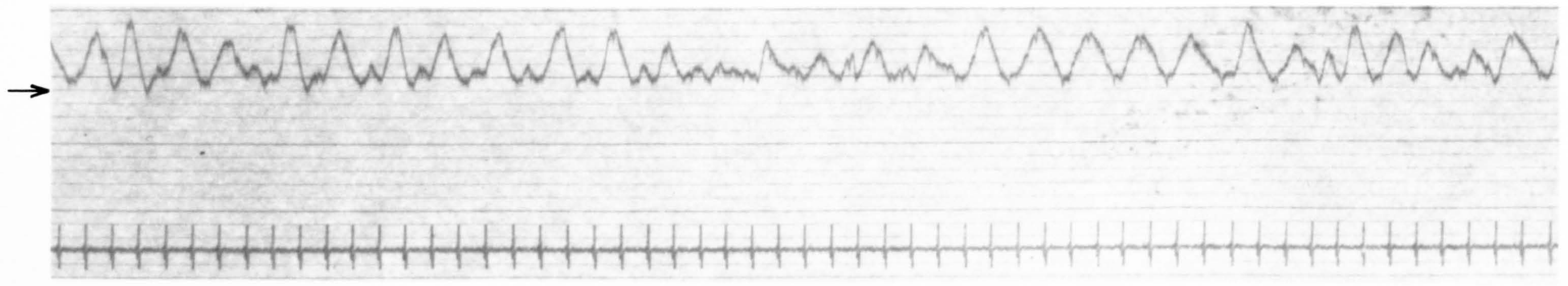

Fig. 9.51 Relative Dynamic Motion, with Modified Couplings at 1500 r.p.m.

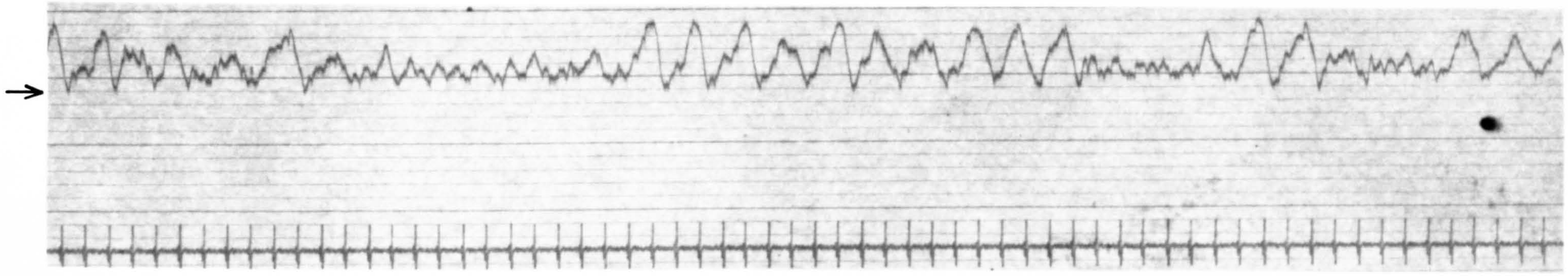

Fig. 9.52 Relative Dynamic Motion, with Modified Couplings, at 1700 r.p.m.

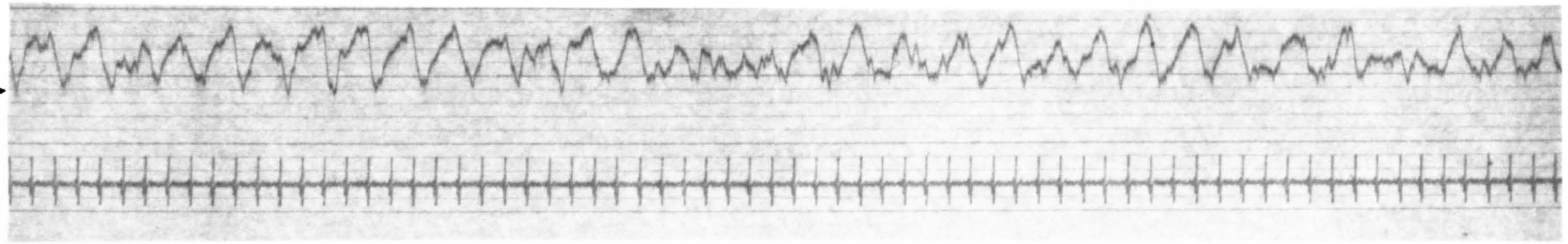

Fig. 9.53 Relative Dynamic Motion, with Modified Couplings, at 1800 r.p.m.

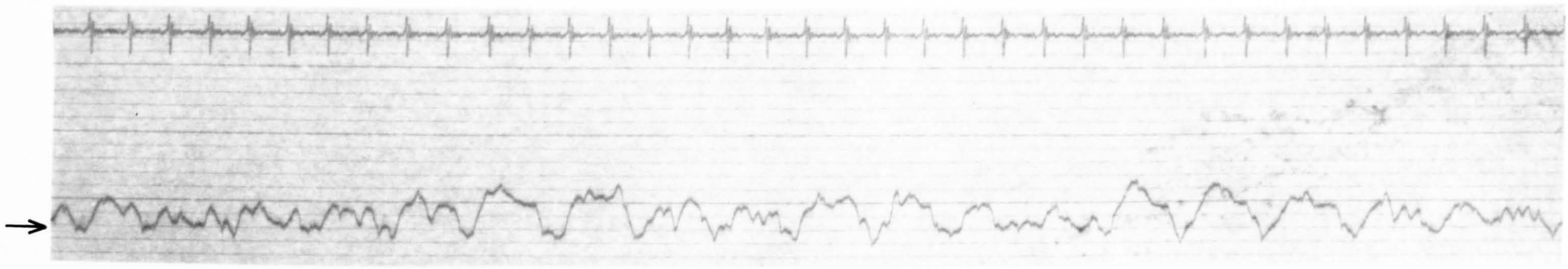

Fig. 9.54 Relative Dynamic Motion, with Modified Couplings, at 2000 r.p.m.

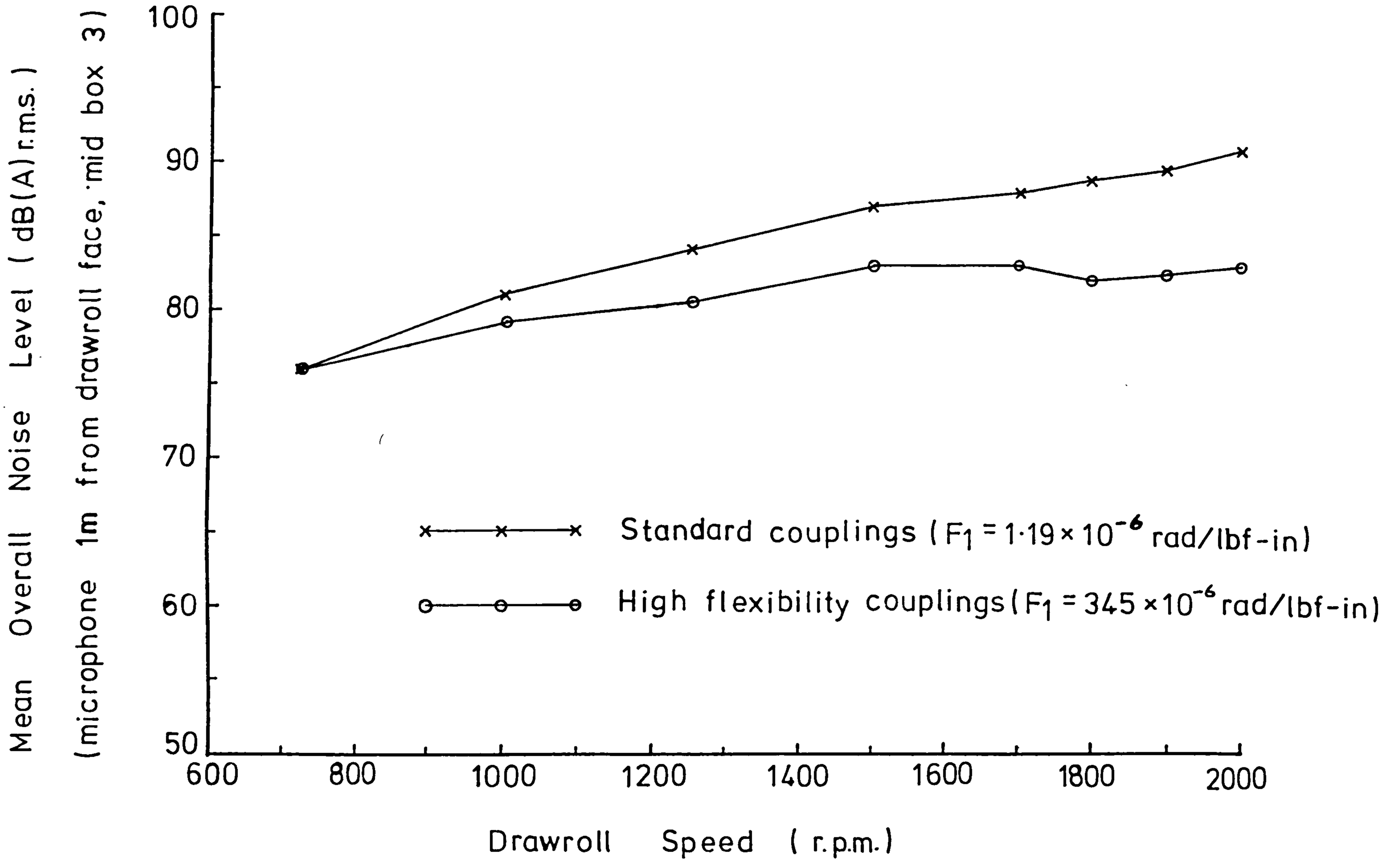

FIG. 9.55 Overall Noise Levels in 4-Box Rig

10. FURTHER CONSIDERATION OF MACHINE PERFORMANCE IN SERVICE

10.1 Introduction

Theoretical results presented in Section 6 have illustrated definite patterns of dynamic loading distribution within the drawbox systems of various drawtwisters operating at particular speeds. If such patterns existed in practice, one would expect a reflection in corresponding gear failure distributions to ensue, provided that each machine had run at one speed only. Even allowing for the masking effect of multiple speed operation, it is possible that damage characteristics for a particularly harmful speed would be evident. Of the various investigations reviewed in Section 3 only the N.E.L. study (R24) presented documentary evidence of failure distributions within machines.

In an attempt to locate further information on machine performance in service, especially failure distributions for recorded operating conditions, the author visited two synthetic fibre producers,

One, referred to as "Company A", had a polyester installation incorporating about 35 MDT. drawtwisters, of Type C and D. ; the other, referred to as "Company B", housed about 80 Type A machines in its polyamide installation.

NOTE: In all cases, the machines were standard, 10 drawbox units i.e. having 120 threadline positions.

10.2 Company A - Polyester Installation

The first seven MDT. machines installed at Company A were Mark I versions of Type C, so called because of the steel-bronze-bronze drawbox gear combination. A further 15 Type C Mark II machines (steel-bronze-steel combinations) were installed in the period September, 1965 - June, 1966, and twelve Type D machines were introduced soon afterwards. Before the last Mark II version of the Type C machine was installed, a gearing problem, involving cyclic pitting of the bronze gears, had already become apparent in machines which had operated for a few months. Accordingly gear failure/replacement records were introduced by the company on 18th June, 1966. Within 10 days, 20 replacements were recorded for machine number "N5", which had then been operating for 7 months. At this point, all drawbox gears were replaced by new stock and operation recommenced on 10th July. A gear failure was recorded after only 15 days of running and within 5½ weeks 18 failures had occurred. Unfortunately, the document recording the machine operating conditions could not be traced; however, it is known that part of the running was at a delivery speed of 3080 ft/min. (2355 r.p.m. of drawroll).

Because of the varying process requirements of different yarn batches, drawtwister operating speeds are varied in a somewhat random manner according to production demands. In this light, it can be appreciated that Company A had difficulty in establishing the most destructive running speeds when failures occurred after a complex operating history. Nevertheless, the view was expressed that failure levels reached quite serious proportions when delivery speeds were increased to 3080 ft/min.

The documents relating to the type D machines demonstrate this point quite clearly. Between 10th and 30th October, 1967, all (twelve) Type D machines were switched to drawspeeds of 3080 ft/min after previously operating at lower speeds. Before the end of November, gear failures of very significant proportions were observed; on average 19 gears per machine either completely failed or were so severely damaged as to necessitate replacement.

In the 15 weeks from 1st January to 16th April, 1967, a total of 268 bronze gear failures were recorded for 14* Type C Mark II machines, most of which had spent some time operating at 3080 ft/min. The number of failures per box for each machine was as shown in Table 10.1 which will be discussed in a later section (10.5).

In general, fewer gear failures occurred in Type C Mk I machines; however, this finding is inconclusive for these machines were generally operated at lower speeds than the Mk II version and the Type D machines.

Because of the risk of yarn package damage and costly down-time, all production was limited to drawspeeds below 2500 ft/min at which more tolerable performance was returned. Early in 1969, a machine fitted with rubber bushed gears was put on trial. No signs of distress were produced during several months of high speed running and, indeed, a noticeable reduction in drawbox noise was observed. As a direct result, all MDT. machines at the installation were modified by the fitting of bushed gears, the programme being completed in 1970.

To date, no pitting damage has occurred, even though some of the systems have now been in service for almost 5 years. Since the introduction of the modified gearing, maximum drawspeeds have increased to about 4500 ft/min.

* the 15th machine was used for experimental work at this time.

10.3 Company B - Polyamide Installation

Company B has about eighty Type B machines most of which were installed in 1963 and 1964.

In the first few years of operation, drawspeeds did not exceed 700 m/min, corresponding to a drawroll speed of about 1750 r.p.m. Machines operated at around this speed, however, developed pitting of the bronze gears and this was distributed in a cyclic pattern around the periphery, as described in Section 3. After the pitting was first observed, the gears could often be run for a further 2 months before the teeth disintegrated. It was estimated that a typical gear life at 700 m/min was about 6 months from new. Considering that machine utilisation was an average of about 75% of total time, this represents a life of about one third of the period between major services (10,000 hours).

As yarn processing technology improved, attempts were made to operate in the region of 1000 m/min. In June, 1968, four new machines, built to improved gearing standards ((R7), Section 3.2.7), were installed and, over the ensuing months, nine of the existing stock were refurbished to the same standards. The 13 machines were initially run in the region of 700 m/min until May, 1969, when production batches allowed them to be switched to 940 m/min (2355 r.p.m.). Within days, high noise levels and considerable overheating gave evidence of distress, resulting in the stopping of all machines and the charting of damaged gear positions. These have been used to compile the damage variations shown in Table 10.2.

As a result of these troubles, drawspeeds in the region of 1000 m/min were suspended whilst internal activity in search of a solution was increased. It was found that individual boxes could be

run at drawroll surface speeds of 1000 m/min and higher, without reproducing the severe behaviour induced in the total machine.

Tests were carried out with various lubricants and it was found that the use of a very high viscosity fluid grease* reduced gear damage. From early 1970, all drawtwister gearboxes having solid drawshaft gears were charged with this lubricant and dramatic increases in gear life were subsequently observed, resulting in the major service interval being extended from 10,000 to 14,000 hours.

Although gear pitting still occurs, complete failures are rare and damaged gears are replaced during the major service. Typical replacement numbers at 14,000 hours range from 15 to 30 (i.e. 25 - 50%) in the operating range 700 to 1000 m/min.

Company B has two Type A machines fitted throughout with rubber bushed gearing. At the time of writing, these have been in production service for over $4\frac{1}{2}$ years, during which no pitting failures have occurred.

10.4 A Note on Machine Trouble Zones

It is clear from Sections 10.2 and 10.3 that the greatest number of gear failures resulted from operation at 3080 ft/min (2355 r.p.m.) although there is evidence of failure occurring at other speeds, notably at about 1750 r.p.m. (Section 3). This behaviour is in good agreement with the computed graph of dynamic load against speed shown in Figure 6.1.

* "Sellarc 1150" manufactured by Sellarc Southern.

10.5 Discussion of Gear Damage Distributions

10.5.1 Records from Company A

From Table 10.1, it can be seen that a disproportionately large number of failures occurred in box number 7 of machine no. 100. The number of failures here is twice as high as the number occurring at any other position in any other machine. This unusual behaviour was predicted in Section 6.2, based on multiple excitation analysis.

It is very unlikely that a succession of "bad" gears were introduced to box 7 as replacements when failures occurred and therefore it is logical to conclude that the dominant error combinations inducing high dynamic loads in this box were external to it. Such behaviour is somewhat disturbing for it demonstrates the possibility of remotely induced damage by gear pairs which remain relatively unharmed themselves and which, therefore, remain undetected.

The results displayed in Table 10.1 were used to plot aggregate failure numbers per box shown in Figure 10.1. Curve (a) gives the overall distribution whilst curve (b) excludes contributions from machine 100. In view of the freak behaviour exhibited by this machine, the latter curve is thought to be more representative of typical Type C drawtwisters and, therefore, all subsequent discussion of Figure 10.1 relates to curve (b).

The existence of definite maxima in boxes 1,3,6 and 9 and minima in boxes 2,4,8 and 10 at once confirms that damage is not randomly distributed.

Since most of the gear damage was thought to be produced at 3080 ft/min (2355 r.p.m.), it is appropriate to make comparisons with the average theoretical distribution of dynamic loading at this speed, namely Figure 6.5. In general shape, the curves are quite similar, both showing peaks in boxes 3 and 6 and troughs in boxes 4 and 8, with generally higher relative levels in the second half of the system (boxes 6 to 10). There are, however, two significant differences, firstly, the trough at box 2 is not highlighted by the computed graph and, secondly, the number of failures occurring in box 10 was much lower than would be anticipated from the theoretical curve. The former is almost certainly due to the fairly crude modelling adopted for the headstock system. An absence of flexibility elements allows the high inertia of the headstock to exert influence over the total system but particularly over the first few boxes.

The reason for differences observed in box 10 is rather more complex. Generally the theoretical response follows the lines of a third torsional mode of vibration and thus it is reasonable to expect high amplitude levels in box 10 which is at the free end of the system. The damage distribution actually obtained, however, shows evidence of significantly lower activity at this location. Since the layshaft at the extreme tail end of MDT. drawtwisters is completely unrestrained, it is thought that the behaviour observed is related to the mechanism of excitation, as follows. The gear error induced disturbances at any mesh produce a secondary effect on all other meshes in the system by creating vibratory torques in the layshaft. In practice, attenuation factors would operate such that the reciprocal influence between a pair of meshes would decrease as the layshaft separation distance increased. Because boxes 1 and 10 are at the extremes of the system, external excitations are separated

by a greater average distance than, say, for boxes 5 and 6 which are centrally located. This mechanism would account for the low gear damage recorded for box 10*.

In the theoretical analysis, the attenuation factors, referred to above, are mainly provided by viscous damping elements across the inter-box couplings. The field results suggest that these are not sufficiently great in magnitude or they do not accurately model actual dissipative elements in a system which has been demonstrated to possess highly non-linear characteristics (Section 9).

Notwithstanding the differences discussed in the foregoing, the distribution of gear failures occurring in Type C drawtwisters shows reasonable agreement with the computed loading distribution at 2355 r.p.m.

10.5.2 Records from Company B

Overall gear damage numbers per drawbox are shown graphically in Figure 10.2 using the numerical results in Table 10.2. Although of the same general form, the graph is significantly different from curve (b) of Figure 10.1. In particular, the mid span peak occurs in box 5 where previously it was in box 6 and the graph shows no trough in box 8. A relative increase in the damage level for box 2 produces a more balanced overall distribution.

* Behaviour in box 1 would not of necessity be similar, for extra vibratory activity could be induced here by disturbances in the headstock system.

Whilst recalling that the severest behaviour resulted from operation at 2355 r.p.m., it must be remembered that the greater proportion of the running time producing the wear records was spent at about 1750 r.p.m. Accordingly, one must compare Figure 10.2 to both of Figures 6.5 and 6.9 in seeking correlation between theory and practice.

In general, the actual damage patterns are reasonably consistent with the combined characteristics of the theoretical curves. One exception, however, is that the combination of a damage peak in box 5 and a trough in box 6 would not be expected on the basis of the computed results. The comparative calm observed in box number 10 may be explained as in Section 10.5.1 and also Figure 6.9 illustrates lower relative loading for this location.

The wear distribution recorded for boxes 1 to 4 follows a similar pattern to the computed torque variation in these boxes at 2355 r.p.m. In contrast to the finding for the Type C results, this suggests that the headstock modelling is adequate for the Type A system.

10.5.3 Records Presented in the N.E.L. Report*

The origin of the records published by N.E.L. is not specified; however, it is thought that they may relate to drawtwisters on contract 'X'. The report does not specify the particular MDT. model(s) to which the results relate.

* (R24), Section 3.4.

Figure 10.3 illustrates distributions of the overall gear failure together with those occurring at a delivery speed of 3080 ft/min. The slight difference in numbers represented by the two curves confirms that most damage occurred at 3080 ft/min. Close resemblance between these graphs and Figure 10.2 strongly suggests that the drawtwisters in question were of Type A and therefore the comments made in Section 10.5.2 are also generally applicable to these results.

In general, the failure pattern at 3080 ft/min follows a similar shape to the theoretical plot in Figure 6.5 although local differences are apparent. For example, one would expect higher failure numbers in the middle peak (boxes 5 and 6) relative to those in box 3.

TABLE 10.1 BRONZE GEAR FAILURE DISTRIBUTIONS IN TYPE C MK.II MACHINES AT COMPANY A BETWEEN 1/1/67 AND 16/4/67.

Machine No.	Date Commissioned	Drawbox Position (from headstock end)										Totals per Machine
		1	2	3	4	5	6	7	8	9	10	
N1	2/3/66	1	2	1	0	2	6	1	0	0	0	13
N2	18/2/66	4	0	4	2	0	0	1	0	0	0	11
N3	15/9/65	0	4	0	1	2	3	16	6	4	0	36
N4	4/10/65	1	3	4	3	1	6	6	0	0	0	24
N5	19/11/65	5	2	0	1	0	1	1	0	4	5	19
N6	24/12/65	4	4	4	0	2	0	4	7	5	1	31
N7	16/12/65	0	0	0	0	0	0	0	0	2	0	2
N8	4/11/65	3	0	3	2	6	3	3	6	6	3	35
N9	28/10/65	5	1	4	4	3	0	1	3	4	3	28
N10	28/10/65	4	3	2	4	3	6	8	2	5	1	38
N11	1/4/66	0	0	3	1	0	0	0	0	2	0	6
N12	6/5/66	0	0	0	0	2	5	1	2	0	6	16
N13	19/5/66	0	0	0	0	0	2	1	0	0	0	3
N14	17/6/66	0	0	0	0	1	5	0	0	0	0	6
TOTALS PER BOX		27	19	25	18	22	37	43	26	32	19	268

TABLE 10.2 BRONZE GEAR DAMAGE DISTRIBUTIONS IN TYPE A MACHINES AT COMPANY B; 10TH MAY, 1969.

Machine No.	Date Refurbished (R) or Installed (I)	Drawbox Position (from headstock end)										Totals per Machine
		1	2	3	4	5	6	7	8	9	10	
M1	25/10/68 (R)	1	6	2	4	6	4	3	4	5	0	35
M2	1/11/68 (R)	6	5	6	5	6	6	6	6	5	6	57
M3	15/1/69 (R)	4	6	4	2	3	1	3	5	5	3	36
M4	24/1/69 (R)	6	6	6	5	5	2	3	5	5	0	43
M5	14/2/69 (R)	5	4	2	1	0	5	0	3	3	1	24
M6	4/3/69 (R)	3	2	2	1	4	0	4	4	4	2	26
M7	25/4/69 (R)	2	4	4	3	2	4	1	0	1	1	22
M8	2/5/69 (R)	0	2	1	1	4	0	2	0	1	0	11
M9	18/3/69 (R)	2	0	2	0	4	1	2	0	2	1	14
M10	8/6/68 (I)	6	4	4	5	5	4	1	3	0	0	32
M11	15/6/68 (I)	0	2	2	0	1	3	5	0	0	0	13
M12	15/6/68 (I)	2	5	2	0	5	0	0	1	4	0	19
M13	22/6/68 (I)	0	0	5	3	1	2	5	6	5	2	29
TOTALS PER BOX		37	46	42	30	46	32	35	37	40	16	361

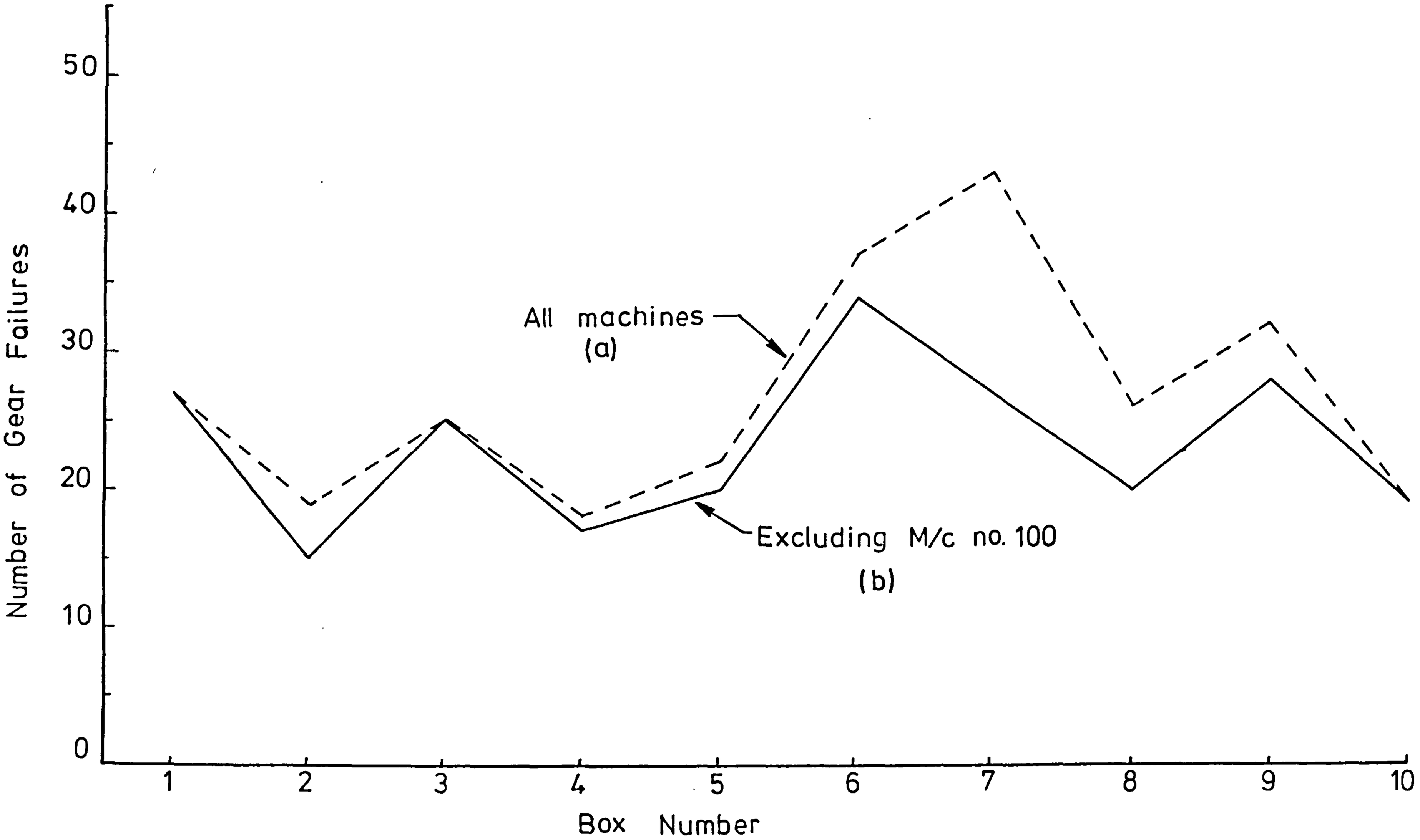

FIG. 10.1 Distribution of Gear Replacements in Type C Machines at Company A

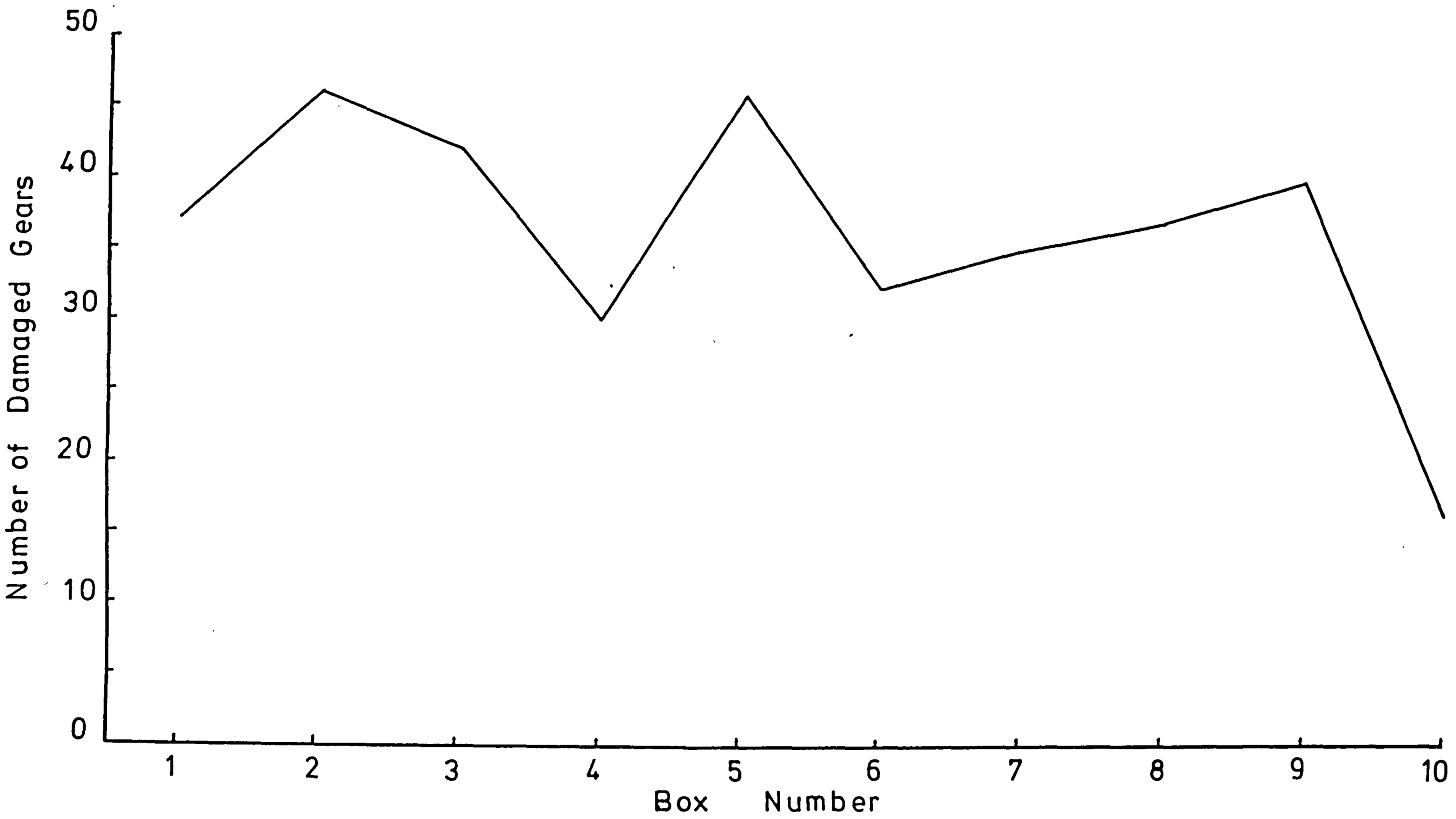

FIG. 10.2 Distribution of Gear Replacements in Type A Machines at Company B

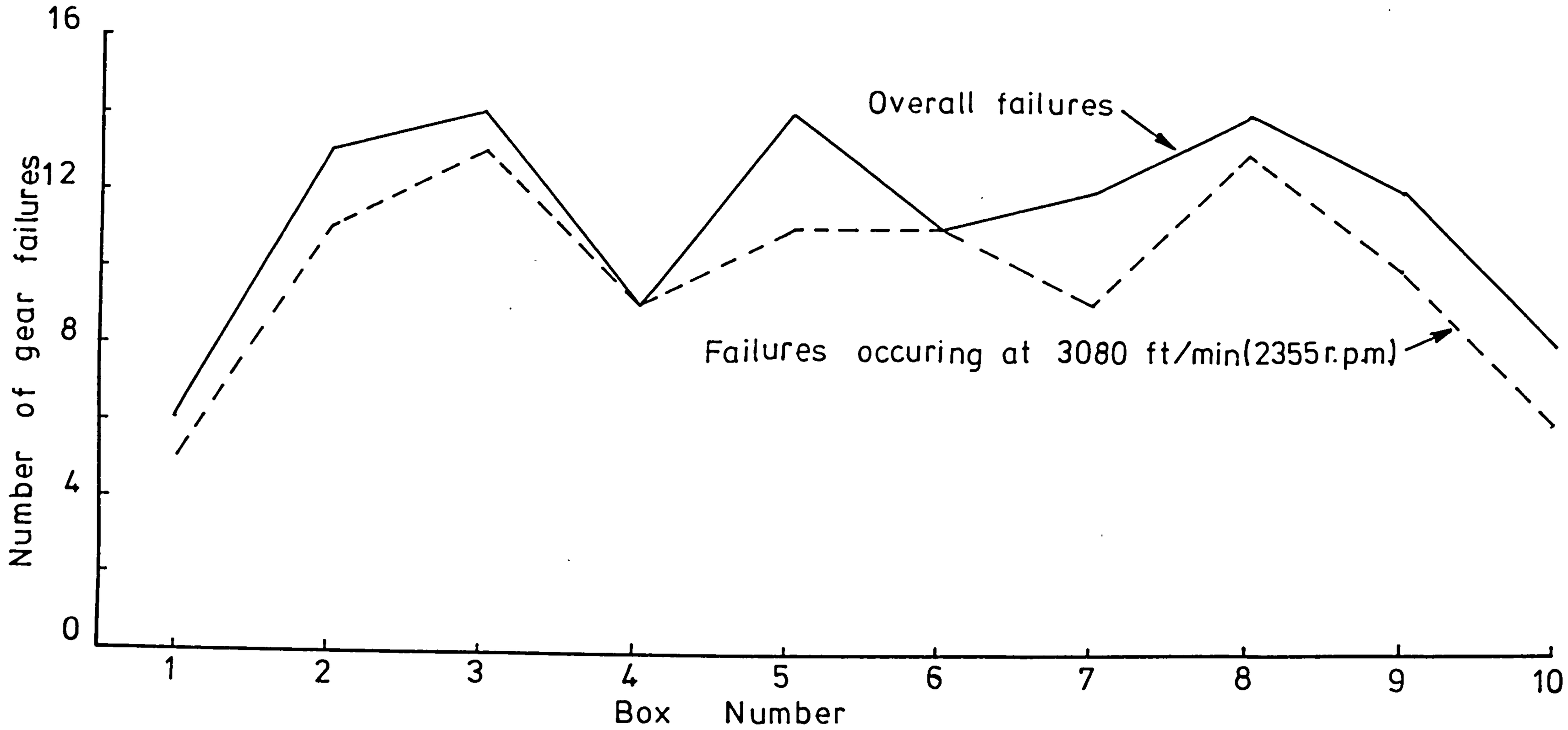

FIG. 10.3 Distribution of Gear Failures Reported by N.E.L.

11. DISCUSSION

11.1 Theoretical Analysis

In previous sections, results, computed on the basis of the theoretical model outlined in Section 5, have been compared with observed behaviour of machines in normal service and also with measurements made on the multi-box experimental rig.

Experimental results (Section 9) have shown that the distribution of impact severity in the test rig was strongly influenced by physical differences between the individual drawboxes (Section 7.3). Although these differences contributed towards the derivation of useful information, their existence limited the value of direct comparison with predicted behaviour.

In general, a reasonable agreement was obtained from comparisons between theoretical results and machine performance records discussed in Sections 3 and 10. For example, reported trouble zones are consistent with the computed dynamic load-speed curve, and gear failure distributions display a similar pattern to the theoretical plot of dynamic loading distribution. At first sight, such agreement may seem surprising since a steady-state, linear response has been computed for a system which experiments have clearly shown to exhibit strong non-linear behaviour. Consideration of the impact generating mechanism, however, provides a logical explanation for this correlation. If all of the gears remain in contact, allowing a steady-state vibration to develop, then the theory used is valid (although not exact). As soon as high vibratory forces produce separation at any mesh, the theory fails to account for

the ensuing non-linear motions. The important point, however, is that the severity of impact on the trailing faces is a function of the separation velocities which, in turn, depend on the initial vibratory load. Thus, gear pairs for which a high dynamic loading is predicted using linear theory are likely to experience high impact loads during the ensuing non-linear motions.

An important effect of tooth separation is to modify system mesh flexibilities in a complex manner, not predicted by theory, and this accounts for the deviation between computed and observed peak response speed in the experimental machine. That predicted high loading speeds coincided with recorded failure speeds is perhaps fortuitous in this light and suggests some compensating factor in the theoretical modelling; possibly introduced in the headstock representation. It must be remembered, however, that the rig tests were performed without applied loading whereas the failure records relate to machines in actual service and thus subject to yarn tension on each drawroll. The effect of increased applied loading would be to reduce the tendancy for gears to separate and thus to provide dynamic behaviour slightly more compatible with linear analysis.

Subharmonic vibration, reported in Section 9, is a non-linear phenomenon and is therefore not predicted by linear forced analysis. Knowing the system critical speeds one could estimate the possible speeds for subharmonic resonance using the relationship $\frac{\omega_f}{\omega_n} = 2, 3, 4 \ldots$ where ω_f is the forcing radiancy and ω_n is the natural radiancy. This procedure, however, would provide no indication of amplitude levels.

Notwithstanding the crudeness of assumptions underlying the theoretical model, a reasonable agreement between theory and practice has been achieved. Further improvement should be possible, by the adoption of minor modification; for example, a separation based

estimate of mean tooth flexibility could be employed to improve frequency predictions and headstock models could be improved by the consideration of flexibility elements.

Such modifications are still in accordance with the assumptions set out in Section 5 and it is appropriate to briefly consider whether non-linear elements could be included in the analysis. In essence, the problem is one of scale and complexity. Previous investigators (19)(21) have remarked on the difficulties in obtaining forced solutions for a single degree of freedom system (representing a gear pair) with non-linear tooth stiffness. The most satisfactory solutions were obtained, in the end, using analogue modelling techniques. The system of 10 drawboxes considered in Section 5 has over 300 degrees of freedom together with 60 separate excitation sources and, clearly, the non-linear response of such a large scale problem could not be obtained by theoretical analysis at the present time. Even simulation techniques would require a much larger analogue computer than is normally available for research purposes unless a subsystem only were selected for investigation. This approach would only be profitable if, in practical conditions, the subsystem behaviour was independent of surrounding systems; for example, if individual drawboxes were dynamically decoupled from each other in a drawtwister by means of increased flexibility couplings, then it would be informative to perform an analogue study of the behaviour in a single drawbox.

11.2 Measurement Techniques

11.2.1 Impact Detection through Variation in Mesh Resistance

The electrical circuit technique described in Section 8 has been satisfactorily employed to investigate impact behaviour in the experimental rig. It was possible to compare simultaneous impact patterns at different gear meshes by carrying out the simple insulation modification to three separate steel gear cartridges.

Although the method was found to be straightforward in operation, it suffers from an inherent limitation, namely that no information is given on the gear motions except that which can be deduced from the impacts and it requires a further measurement technique to identify the motions producing the impacts. Thus a twice per revolution impact pattern could indicate contacts on front and reverse tooth faces or contact on the normal face only due to a second harmonic of gear error.

The technique would be more useful in gearing studies if a calibration were achieved such that dynamic loads could be deduced from mesh voltages. This might involve the fitting of resistance strain gauges to provide a dynamic calibration of mesh voltages (following static calibration of the strain gauges). It is doubtful whether a satisfactory calibration could be achieved in this manner due to the nature of the oil film thickness which varies, for example, with running speed. Thus a calibration carried out under one set of conditions would only be valid for those conditions and no others. Before measurements could be made over a speed range and perhaps with different applied loads, it would be necessary to carry out extensive preliminary calibration.

11.2.2 Measurement of Gear Motions using Magnetic Drum Encoders

The results discussed in Section 9 illustrate the effectiveness of the magnetic drum technique in studying motions of a gear pair of 1 : 1 ratio. The directness of the technique is particularly suited to measurements of resiliently mounted gears where, for example, shaft measurements would be of very limited use. Generation of the drum signals, in situ, from a grating mounted on one of the gear shafts provides an automatic compensation for transmission error and drum eccentricity and thus overcomes the limitation of a previously used technique (19).

Some care is required in setting head positions with respect to the drums, especially if a long magnetic coating life is required. This may be performed on a "trial and error" basis by attempting to write the drum signals (simultaneously) and then "playing back". Providing that mutli-track heads are used, the setting up procedure can be assisted by writing twin tracks on each drum and adjusting to give equal replay amplitude from each. Unsatisfactory attempts may be terminated by using the magnetic heads to completely erase the drum recordings in situ.

The magnetic heads and recording amplifier used to demonstrate the method (Section 8) were of cheap domestic quality yet the replay signal strength continued to increase at the upper test frequency of 18 kHz. At low frequencies, however, the signal amplitudes were much lower and suggest a need for better quality heads and instrumentation in applications involving low frequency measurements.

In future applications of the technique, a greater flexibility could be obtained by employing multi-track heads to produce different signal densities on the various drum tracks.

This would simply involve repeating the calibration process for a variety of different optical gratings and switching to the appropriate track. For example, four discrete tracks could be written by means of gratings having, say, 500, 2000, 5000 and 20,000 lines per revolution. The higher density tracks could be used both to increase the resolution of measurement and also to provide an improved head response at very low rotational speeds whilst the low density tracks would be employed for high speed measurements.

Although measurements have only been carried out with a 1 : 1 gearing ratio, the method should apply equally to all integral ratios, that is 2 : 1, 3 : 1 etc., providing that the reference optical grating is attached to the shaft of the smaller gear.

11.2.3 Optical Method for Gear Motion Studies

Achieving an optical equivalent to the magnetic technique discussed above requires that optical gratings be generated on the two gears simultaneously by a single reference grating attached to one of them. Further work will be required to establish the practicality of this approach.

11.3 The Drawtwister Gear Failure Problem

Having examined the validity of the theoretical model and the effectiveness of the experimental techniques, it is now appropriate to summarise the understanding of the failure problem gained from all aspects of this research.

The effect of pitch errors, eccentricities and other small manufacturing errors at the 1 : 1 helical mesh is to provide a static transmission error having a substantial component at the fundamental periodicity of gear rotation. The amplitudes and relative phasing of all such components throughout the drawbox system will vary according to production distributions and, thus, in a 10 box machine, 60 independent sources of relative displacement excitation exist. For a particular operating speed, these are able to induce a torsional vibration response in the layshaft system, which interacts with drawshaft gearing to produce vibratory loads depending on the mesh position in the total system.

For a particular mesh, continuous contact is maintained so long as the vibratory forces are not sufficient to overcome the combined effects of the applied load and system inertia loads. Beyond this point, loss of contact occurs and, when sufficiently high vibratory forces act, the full backlash is traversed giving a front and reverse face impact cycle, generally at rotational frequency. It is clear that this type of motion, involving very high impact loads, was the cause of MDT. drawbox gear failures and of the characteristic pitting pattern observed on gears which had not completely failed (Section 3).

In relation to system excitation and response behaviour, the following additional comments should be made. From a situation where the vibratory motion at running speed is nil or random, many forcing

cycles are required to build up the vibratory energy to the point at which loss of contact first occurs. Energy may still be feeding in when a few of the meshes are involved in loss of contact behaviour and this may become severe enough to generate heavy impacts. By this time an increased number of lost contacts may have detuned the system producing an interval of smoother running during which vibratory energy is again fed into the system through transmission error effects *.

Measurements, reported in Section 9, have shown that motions involving double impact cycles can be sustained over several revolutions before collapse and that periods of high impact activity are interspersed with periods of relative calm in a random manner. The dynamic load at a particular mesh depends on contributions from excitations throughout the system. These may be considered to add together in a vector sense to produce the resultant load. Since the individual transmission errors vary in phasing as well as in amplitude, the actual behaviour in a machine is strongly influenced by the particular error combination. This accounts for some machines being more prone to gear failure than others and for the presence of a "rogue" box (Table 10.1). Furthermore, the presence of so many sources of periodic disturbance allows the possibility of very high dynamic loads, possibly of the order of 100 times greater than applied loads. Such magnification contrasts sharply with measured loads in single gear pairs where previous investigations (Section 4) have found that maximum dynamic loads are about three times the applied load.

* It should be noted that the dynamic stiffness analysis, presented in Section 5, determines only the steady state vibrational behaviour.

Mesh voltage records, discussed in Section 9, illustrate many examples where dynamic loads were sufficient to cause breakdown of the oil film between meshing teeth. The presence of wear (Section 9.5) after only a relatively short period of running demonstrates the results of such behaviour.

Evidence from the field (Sections 3 and 10) has established that most failures occurred at speeds of about 1750 r.p.m. and 2355 r.p.m. with the latter being by far the more troublesome region. Measurements in the experimental rig have indicated that clear and sustained resonance conditions would not exist at a particular speed but rather that zones of high impact activity would prevail due to system non-linearity. These zones could span several hundred r.p.m. of running speed. Machine performance records (Section 10) also show that gear failures displayed a definite distributional pattern throughout the machine thus demonstrating the influence of layshaft torsional vibration modes.

It has been remarked earlier (Section 9) that some of the impact traces showed evidence of high frequency contributions. These were also observed in a previous investigation (R24) and suggest that, during loss of contact, the drawshaft assemblies vibrate naturally due to impact or tooth frequency excitation preceding separation. A "chatter" effect would be produced on the return of contact and this would be highlighted on the impact records. Such behaviour explains the high pitched ringing tones radiated from some of the drawroll faces (Section 9.2.1.4). It is possible that high frequency vibration could contribute to the damage caused at gear rotational frequency but such contributions would probably be of secondary importance.

11.4 Existing Solutions to the Gear Problem

11.4.1 Rubber Bushed Gearing

The effectiveness of bushed gearing has been conclusively demonstrated by several years of normal running during which time no gear failures have been reported. Furthermore, the solution of the gear impact problem has automatically provided a significant reduction in drawbox radiated noise levels (Sections 3.3.15 and 10.2).

In the theoretical modelling, rubber bushes were represented as a series combination of linear flexibility and viscous damping elements situated at each gear-shaft connection. The resulting dynamic loading plots showed considerable reductions in overall levels when compared to the corresponding results for the "solid" gear system. Nevertheless, the absence of gear failures in the field suggests that the computed loads overestimate the loads occurring in practice. This could be due to a lack of accuracy in the bush modelling since in practice the bush characteristics are highly non-linear (R24), the flexibility being dependent on both load and time. The bushes also serve to cushion impacts resulting from non-linear motions and this would tend to produce considerably lower tooth loads in practice.

Computed results (Section 6.7) indicate that high bush damping may be less satisfactory than low damping or even none at all. This suggests that further benefits may derive from the careful examination of bush properties before selection.

The only significant disadvantage with this design is that, being more elaborate than conventional gearing, it increases manufacturing costs. Viewed against a background of high failure rates and lost production, however, the bushed gears represent a good engineering solution.

11.4.2 High Viscosity Lubricant

It has been seen (Section 10.3) that one Company has effected a partial solution to the gear damage problem by employing a high viscosity, fluid grease lubricant.

The effect of high viscosity is to create a more substantial lubricant film thickness at each mesh, thus providing greater damping during in-contact running and a greater cushioning effect during non-linear motions. In contrast to rubber bushed gears, more viscous lubrication would not provide a large change in mesh flexibility and this is born out by the continuation of gear wear, by pitting, at an operating speed of 2355 r.p.m. That the wear is greatly reduced is due to energy dissipation effects rather than to any shift in system response characteristics.

This solution, although less successful in the field than bushed gearing, nevertheless allows the continued use of standard, keyed gears.

12. SOME DESIGN CONSIDERATIONS

This section discusses various design features in relation to improved dynamic behaviour. Two known solutions to the gearing problem have been discussed in the previous section and these are, therefore, excluded from further consideration.

12.1 Variation of Selected Machine Parameters

12.1.1 Box Coupling Flexibility

Computed results (Section 6.5.3) have suggested that a considerable reduction in dynamic loading might be effected by the use of gearbox couplings having a torsional flexibility of about 100 times that of standard couplings. Preliminary tests with more flexible units (Sections 9.3.4 and 9.4) have tended to support this idea.

In essence, this approach attempts to modify the total system response by dynamically decoupling individual boxes from each other within the operating range. Thus, to a certain extent, each box behaves as if completely isolated from the rest of the system and is, therefore, much less sensitive to low frequency excitation. The inability to induce gear failures in single gearbox tests (Sections 3 and 10) confirms this deduction.

It would be relatively straightforward to manufacture the required couplings and replacing existing units on a 10 box machine should take less than one hour to complete. Subject to further investigation, therefore, it appears that a less costly alternative solution to the gear problem is available, requiring straightforward selection, or design, of a suitable coupling.

12.1.2 Drawroll Damping

The theoretical analysis has shown that damping at the drawroll location exerts a strong controlling influence over the system response levels (Section 6.4.2). Although it would be relatively straightforward to design a suitable damper, the need to provide these at 120 locations in a 10 box machine would, almost certainly, add significantly to the costs of manufacture.

A second disadvantage is that grounded dampers of sufficient dissipative capacity would cause prohibitive increases in machine power consumption. In this particular case, therefore, increased damping is not a satisfactory means of reducing tooth loads.

12.1.3 Parallel Helical Mesh Gear Ratio

The knowledge that damage behaviour was induced by the fundamental component of transmission error suggests that the problem may have been avoided by employing a 20 : 19 helical mesh ratio in the first instance. Since the original design was based on a 20 : 20 ratio, however, it would be impractical to change this because existing drawboxes would then be incompatible, in terms of gear centre distance, and also it would be necessary to introduce two sizes of drawroll, in the same ratio as the gears, to maintain equal draw speeds.

12.1.4 Drawshaft Diameter

An alteration to drawshaft diameter has two distinct effects on gear behaviour; firstly, it modifies the total system vibration characteristics and, secondly, it modifies the effective inertia of the drawshaft gear. Regarding the latter, it is generally desirable to reduce the effective gear inertia in order to reduce the severity of impact between meshing gears. Computed results (Section 6.5.1) showed that system dynamic behaviour could be substantially improved by reducing drawshaft diameters to $\frac{1}{2}$ in.; however, dynamic loads would still remain at damaging levels in some zones within the operating range. Further reduction in diameter would not be recommended owing to the increasing possibility of lateral oscillations due to component imbalance.

12.1.5 Drawroll Inertia

Further to the preceding paragraph, a second way of reducing effective gear inertia is to directly reduce the drawroll inertia. (This is only worthwhile, of course, if it does not worsen the system vibration response). The analysis shows (Section 6.5.2) that, although significant improvements are possible, this approach is not sufficient on its own to produce acceptable behaviour. Combined with other modifications, for example non-metallic gears (see below), it may offer a satisfactory solution.

12.1.6 Non-Metallic Gears

Considering that drawshaft mesh applied loads are very low, it seems wasteful, from a design point of view, to employ good quality steel and bronze gears of about 1 in. face width. Non-metallic gears would be much cheaper and might effect a satisfactory cure through their inherent resilience.

Following the successful work of Crawford (71) in reducing drawbox noise using polyurethane gears, a programme of tests was carried out at Platt Research Centre (R20). Non-metallic gears were found to be unreliable in contrast to Crawford's finding that they had outlasted the duration of his tests (1000 hours). Most (Platt) failures occurred during start-up conditions and this gives a clue to the reason for the lack of success. The 5 in. diameter drawrolls would produce a considerably higher inertia loading at start-up than the much smaller units (approximately 4 in. diameter) employed in Crawford's rig. A reduction in drawroll inertia would, therefore, be suggested as the starting point for any further development work on non-metallic gearing. Any selected gear material would have to be capable of withstanding significant overloads, applied by operatives, during the removal of yarn wraps, from a drawroll, following thread breakage.

12.1.7 Gear Backlash

Backlash is largely unimportant in dynamic considerations provided that tooth contact is maintained at all times*. It assumes a greater significance in relation to non-linear motions occasioned by tooth separation. During separation the primary excitation source is

* Here the chief concern is that there is sufficient clearance to accommodate thermal expansion effects and to permit adequate lubrication.

disconnected and the severity with which contact is made between the reverse faces is influenced by dissipative elements. Increasing the backlash would provide a greater time for such elements to act, thus reducing relative approach velocities and hence impact severity. With a sufficiently large backlash, the periods of sustained double impact cycles could be greatly curtailed in comparison to the periods of low activity. Measurements made with gear pairs of different backlash values (Section 9.2.1.3) reinforce the argument for increased tooth clearance.

12.2 Drawroll Drive Arrangements used by Other Manufacturers

The 6th International Exhibition of Textile Machinery, held in Paris in 1971, provided an excellent opportunity to compare drawtwister designs of the major European manufacturers. A brief summary of some of these design features is now given.

12.2.1 Bevel Gear Drive

Most of the designs employed a separate layshaft for each side of the machine, thus requiring two sets of small drawboxes. Power take-off to the individual drawrolls was by means of bevel gear drives having perpendicular axes. This arrangement permits a steel-steel combination, thus increasing the capacity for withstanding dynamic loads. It was noted during demonstration runs that these machines were considerably noisier than the Platt exhibit fitted with rubber bushed gearing. This was particularly so at the higher drawspeeds.

12.2.2 Crossed Helical Drive

One Company's exhibit incorporated a steel-bronze crossed-helical mesh to drive each drawroll from a central layshaft, thus requiring 120 layshaft gears in a 120-spindle drawtwistor. It is known from a previous research (71) that this company originally used a steel-bronze-steel "two-over-one" arrangement similar to that employed by Platt International Ltd., having a 1 : 1 drawshaft helical gear ratio. The effect of this modification is to eliminate a potential trouble source due to multiplication of a 1 : 1 ratio. However, the reason for the changeover is unknown to the author.

12.2.3 Independent Drive System

A West German manufacturer demonstrated the most radical of all designs observed. This featured individual D.C. motor drives for each drawroll and each spindle; for example, a 120-position machine would employ 240 small D.C. motors. A central console allowed each thread line position to be operated independently of any other by automatic programming.

The company had previously employed a conventional bevel gear arrangement for drawroll drives but had found that high speed operation was restricted by premature gear failure and intolerable noise levels. Although costing considerably more to manufacture, the new model could operate reliably and reasonably quietly at 2000 m/min. The maximum rated delivery speed of all other machines exhibited was 1200 m/min.

12.3 Application of Dynamics Principles to the Design Function.

It is hoped that the general principles highlighted by this research will serve as a useful feedback to machine designers, particularly those concerned with lightly loaded transmission systems having multiple take-offs. By way of illustration, it is now proposed to examine how these principles might be applied to the design of a drawroll drive system.

The main factors contributing to high dynamic loading have been found to be:-

1. a large number of gear meshes, each acting as an excitation source due to transmission error effects.

2. 1 : 1 gearing ratios, allowing high disturbance amplitudes at gear rotational periodicity.

3. light applied loading of gears, facilitating separation and non-linear motions.

4. high effective inertias of each drawshaft gear, due to the directly attached drawroll inertias.

Bearing these in mind, together with normal design considerations such as simplicity and cost, one might consider the preliminary designs shown in Figures 12.1 and 12.2 to be worthy of further consideration. Both employ gearing to effect the transfer of rotary motion to an axis perpendicular to the input shaft. In design A, a further mesh of non-integral ratio is used to provide the necessary change of direction for drawroll rotations on one side of the machine. Laterally flexible belting is then employed to drive a number of (parallel) drawshafts.

The provision of fewer gear meshes would serve to reduce the number of system excitation sources and simultaneously increase the applied loading on each mesh, thus increasing resistance to separation effects. Common factors between the gear tooth numbers should be avoided, in order to minimise the excitation factor; for example, in design A, a tooth combination of 29 : 20 : 19 might be employed with speed equalisation provided by adjusting the drive pulley diameters in the ratio 20 : 19. This parallel axis gear ratio would serve to lower the fundamental excitation frequency by a factor of about 20 times (compared to the 1 : 1 ratio) and thus lower the excitation factor by about 400 times. To reduce inertia loading during start-up and the magnitude of gear tooth dynamic loads would require a significant reduction in drawroll inertia compared to that of the standard unit. This might involve an inertia-based redesign exercise, possibly introducing 4 in. diameter units as standard.

Although essentially similar, these designs have their own particular advantages and disadvantages; for example, the twin belting arrangement in design A would allow a reduction in drawroll pitch (spacing) from 7 in. to 5 in.; whereas design B eliminates the need for a parallel axis gear mesh and requires no inter-pulley tensioner wheels. Both designs show 12 drawrolls being driven by a single power take off from the layshaft. It may be more convenient, especially in relation to design B, to reduce this number to 10 or even 8. It would require much further consideration and test work to arrive at a satisfactory final arrangement incorporating minor design details.

It should be noted that the foregoing does not constitute a recommendation for drawtwister system redesign; it is intended solely to exemplify how the knowledge gained from this research might be interpreted by designers in approaching such an exercise.

Belting Arrangement

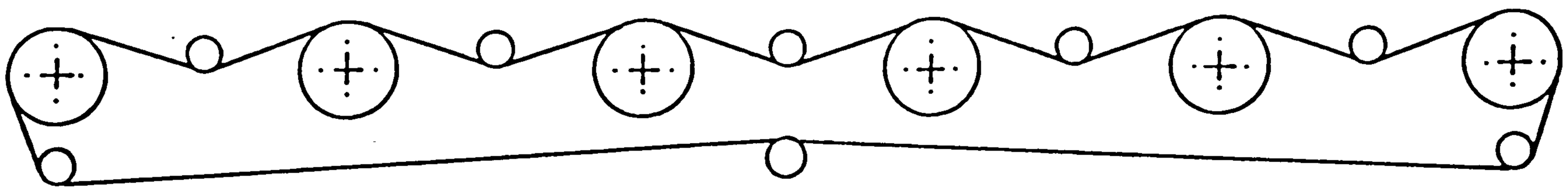

FIG. 12.1 Design A for Drawroll Drive Arrangement

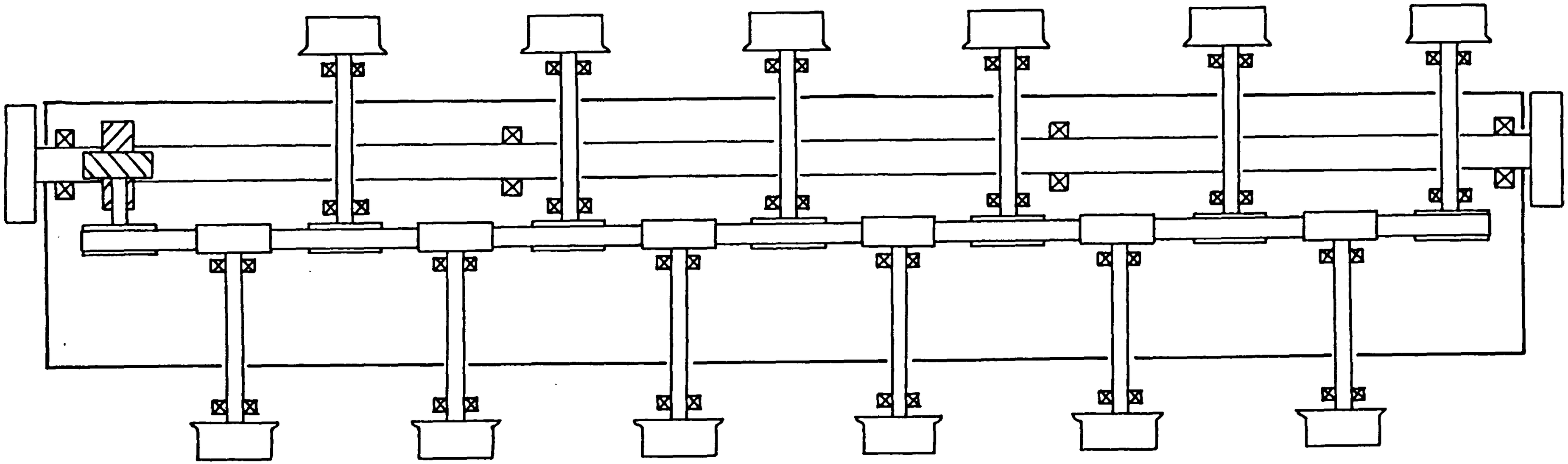

Belting Arrangement

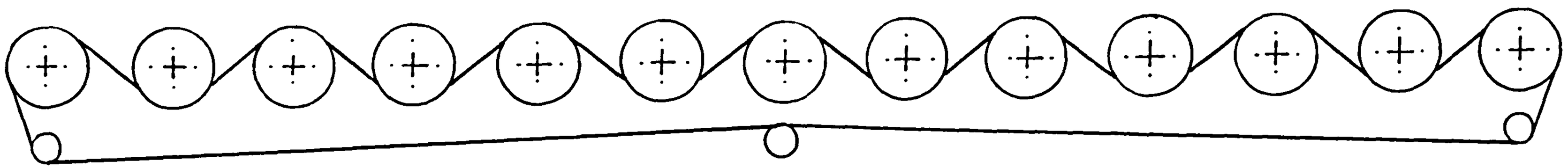

FIG.12.2 Design B for Drawroll Drive Arrangement

13. TERMINATION

13.1 Conclusions

The dynamic stiffness theoretical method has been developed to consider, steady state, forced vibration response due to relative displacement excitation and applied to a complicated drawtwister system in which many such disturbance sources exist. In this way, it has been possible to gain a reasonable insight into the dynamic behaviour of the lightly loaded gear trains. However, the analysis does not allow for system non-linearities which have been shown to exist.

Computed results of tooth dynamic loading are compatible with records of gear failures occurring in production service. The influence of transmission error combinations in determining machine behaviour has been demonstrated by the prediction and subsequent confirmation that "good" and "bad" machines and "rogue" drawboxes can exist. These results also support the contention that dynamic loads at a particular mesh are the result of excitation inputs throughout the total geared system.

Two experimental techniques have been developed and satisfactorily applied to the direct measurement of gear dynamic behaviour. One of these studied tooth impacts through the effect on mesh electrical resistance. A more novel technique employing magnetic drum encoders was used to make a direct study of gear motions. By generating magnetic "gratings" in situ, from a master grating on one of the gear shafts, transmission error and all eccentricities were automatically compensated for.

Experimental measurements confirm beyond doubt that the source of gear trouble was the fundamental component of transmission error at each parallel helical mesh. These induced non-linear oscillations during which the tooth clearances were completely traversed producing heavy impacts alternately on normal and reverse tooth faces. This behaviour was clearly part of a complex total system response involving interaction between the various meshes. It will require further work to provide a clearer understanding of this behaviour.

The bushed gear solution introduced by Platt International is clearly successful. Experimental measurements have shown that the rubber bushes do not prevent tooth separation and oscillations through the backlash. However, they deflect readily to accommodate any impressed forces.

Computed results and preliminary experiments suggest that a much simpler solution exists requiring only the substitution of more flexible box couplings. For a ten box machine, the flexibility would need to be increased by a factor of about 100 times. Before adopting such a measure in practice, it is important that further studies of non-linear system behaviour be made, for pronounced subharmonic motions were observed during the testing of highly flexible couplings.

In a more general context, it is concluded that high backlash serves to reduce the possibility of reverse face contacts in lightly loaded gears and in such applications, it would therefore be recommended.

Perhaps the most important conclusion, so far as the machine designer is concerned, is that there is no simple rule or method for predicting the dynamic loads in complicated geared systems operating under light applied loading.

13.2 Recommendations

13.2.1 Design of Lightly Loaded Gear Systems

It is important that any proposed machine be dynamically analysed at the design stage. Systems having only a few degrees of freedom can be accurately modelled using electrical analogue techniques but more complicated systems require a greater degree of approximation for solution. A forced, linear analysis of the type developed in this research, could be applied in such cases to give a reasonable indication of system dynamic behaviour.

When a prototype machine is erected, it should be subjected to careful measurement of dynamic performance, apart from functional tests. This should include a practical study of gear motions for selected gears.

In complex systems integral gear ratios should be avoided, as far as possible, since these contribute regular and pronounced components of transmission error. This is particularly important in systems, like a drawtwister, which employ the same gearing unit at many stations throughout the machine, since a low frequency total system vibration is potentially excitable.

High backlash should be used to reduce the severity of impact loading resulting from tooth separation.

13.2.2 Further Work

Any further work on MDT. drawtwister dynamics should first check the validity of increased coupling flexibility as an alternative solution to the gear failure problem. This would involve the testing of a full size machine incorporating the original solid

drawshaft gears. The testing of such couplings would also be recommended in relation to work on the reduction of acoustic noise levels.

In a more general context, it is suggested that a more penetrating study of multiple excitation systems be undertaken to examine non-linear behaviour. This should involve experimental and theoretical/analogue aspects and would probably necessitate the consideration of a much simpler system than a drawtwister machine. Of particular importance would be the dynamic interaction between the various gear meshes.

Despite recent advances, the process of allocating torsional damping quantities in forced vibration analyses is still a somewhat intuitive process and further work on damping is, therefore, recommended.

REFERENCES

1. BUCKINGHAM, E: Analytical Mechanics of Gears, McGraw-Hill Book Co., Inc., New York, 1949.

2. TUPLIN, W.A.: Gear Tooth Stresses at High Speed, Proc.Instn.Mech.Engrs., London, Vol. 163, 1950, p.162.

3. McINTYRE, J.E.: Man-made Fibres, Manufacture, Encyclopaedia of Polymer Science, Vol. 8, J. Wiley & Sons, Inc., New York, 1970, p.374.

4. HEINEMANN, A.: Strechzwirnmaschinen und ihre Bedeutung für Chemiefaser-Endlosgarne, (Drawtwisters and their Importance for Man-made Continuous Filament Yarns), Chemiefasern, Vol. 14, 1964, p.780.

5. BRITISH STANDARDS INSTITUTION: British Standard Specification for Machine Cut Gears, B.S. 436, B.S.I., London, 1940.

6. BISHOP, R.E.D. and JOHNSON, D.C.: The Mechanics of Vibration, Cambridge University Press, 1960.

7. A.S.M.E.: Dynamic Loads on Gear Teeth, Amer.Soc.Mech.Engrs., New York, 1931.

8. TUPLIN, W.A.: Dynamic Loads on Gear Teeth, Machine Design, Oct. 1953, p.203.

9. TUPLIN, W.A.: Dynamic Loads on Gear Teeth, Proc.Int.Conf.Gearing, 1958, p.24. (Instn.Mech.Engrs., London).

10. RESWICK, J.B.: Dynamic Loads on Spur and Helical Gear Teeth, Trans.Amer.Soc.Mech.Engrs., Vol.77, 1954, p.635.

11. STRAUCH, H.: Zahnradschwingungen, Z.Ver.Dtsch.Ing., Vol. 95, 1953, p.159.

12. HARRIS, S.L.: Dynamic Loads on the Teeth of Spur Gears, Proc.Instn.Mech.Engrs., London, Vol. 172, 1958, p.87.

13. NAKADA, T. and UTAGAWA, M.: The Dynamic Loads on Gears Caused by the Varying Elasticity of the Mating Teeth, Proc. 6th Jap.Nat.Cong.App.Mech., 1956, IV-15, p.493.

14. UTAGAWA, M.: Dynamic Loads on Spur Gear Teeth, Bull.Jap.Soc.Mech.Engrs., Vol. 1, 1958, p.397.

15. ZEMAN, J.: Dynamische Zusatzkräfter in Zahnradgetrieben, Z.Ver.Dtsch.Ing., Vol. 99, 1957, p.244 (Abstract in Engrs. Digest, Vol.18, 1957, p.161)

16. WALKER, H.: Gear Tooth Deflection and Profile Modification, The Engineer, Oct. 1938, pp.410 and 435, Aug.1940, p.102.

17. JOHNSON, D.C.: Excitation of Resonant Vibrations by Gear Tooth Meshing Effects, Proc.Int.Conf.Gearing 1958, p.18, (Instn.Mech.Engrs., London)

18. KOHLER, H.K.: The Mechanisms and Measurement of Dynamic Loading in Spur Gears, Ph.D. thesis, University of Sheffield, 1959.

19. MUNRO, R.G.: The Dynamic Behaviour of Spur Gears, Ph.D. thesis, University of Cambridge, 1962.

20. GREGORY, R.W., HARRIS, S.L. and MUNRO, R.G.: Torsional Motions of a Pair of Spur Gears, Applied Mechanics Convention, Proc.Instn. Mech.Engrs., London, 1963-64, Vol. 178, Pt. 3J, paper 8.

21. OEPPEN, B.: Torsional Vibrations of Spur Gears, Ph.D. thesis, University of Cambridge, 1964.

22. BOLLINGER, J.G. and HARKER, R.J.: Instability Potential of High Speed Gearing, J.Indus.Math.Soc., Vol. 17, pt.2, 1967, p.39.

23. BÖHM, F.: Drehschwingungen von Zahnradgetrieben, Öst.Ing.-Arch., Vol. 13, 1959, p.82.

24. OPITZ, H.: Dynamic Behaviour of Spur and Helical Gears, Semi-Int. Symposium (Gears), Tokyo 1967, (Jap.Soc.Mech.Engrs.)

25. KER WILSON, W.: Practical Solution of Torsional Vibration Problems, Vol. 1 - Frequency Calculations, Chapman-Hall, London, 1956.

26. B.I.C.E.R.A. (Ed. NESTORIDES, E.J.) A Handbook on Torsional Vibration, Cambridge University Press, 1958.

27. YATES, H.G.: Prediction and Measurement of Vibration in Marine Geared-Shaft Systems, Proc.Instn.Mech.Engrs., London, Vol. 169, 1955, p.611.

28. TORDION, G.V.: The Mechanical Impedance Approach to the Dynamics of Geared Systems, 47th Annual Meeting of Amer. Gear Mfrs. Assoc., 1963.

29. ATTIA, A.Y.: Dynamic Loading of Spur Gear Teeth, Ph.D. thesis, University of Sheffield, 1956.

30. ATTIA, A.Y.: Dynamic Loading of Spur Gear Teeth, Trans.Amer.Soc.Mech.Engrs., Vol. 81, (Series B), 1959, p.1.

31. UTAGAWA, M.: Measurements of Dynamic Loads on Gear Teeth, Proc. 6th.Jap.Nat.Cong.App.Mech., 1956, IV-14, p.489.

32. RICHARDSON, M. H.: Static and Dynamic Load, Stress and Deflection Cycles in Spur-Gear Systems, Sc.D. thesis, Massachusetts Institute of Technology, 1958.

33. HARRIS, S.L.: Dynamic Stresses in Gear Teeth, M.E.R.L. Report P.M. 196, 1956.

34. HEYMANS, P. and KIMBALL, A.L.: Stress Distribution in Rotating Gear Pinions as Determined by the Photoelastic Method, Mech.Engng., Vol.46, 1924, p.129

35. NIEMANN, G. and RETTIG, H.: Dynamische Zahnkräfte, Z.Ver.Dtsch.Ing., Part I, Vol. 99, No.3, pp. 89-96, Part II, Vol 99, No. 4, pp 131-137, 1957.

36. NIEMANN, G. and RETTIG, H.: Error-induced Dynamic Gear Tooth Loads, Proc.Int.Conf.Gearing 1958, p.31, (Instn.Mech.Engrs., London)

37. KOHLER, H.: Measuring Dynamic Loads on Gear Teeth, Engineering, 5th Feb. .1960.

38. GREGORY, R.W., HARRIS, S.L. and MUNRO, R.G.: A Method of Measuring Transmission Error in Spur Gears of 1/1 Ratio. J.Sci.Instr., Vol. 40, 1963, p.5.

39. GREGORY, R.W., HARRIS, S.L. and MUNRO, R.G.: Dynamic Behaviour of Spur Gears, Proc.Inst.Mech.Engrs., London, Vol. 178 (Pt.1, No. 8), 1963-64, p.207.

40. WOOD, B.: Sources of Vibration Excitation in Spur Gears. Ph.D. thesis, University of Leeds, 1960.

41. WOOD, B. and HUNT, T.M.: Excitation of Resonant Vibrations in Spur and Helical Gear Systems, Proc.Inst.Mech.Engrs., London, Vol. 178, Part 3J, 1963-64, p.189.

42. TORDION, G.V. and GERARDIN, H.: Dynamic Measurement of the Transmission Error in Gears, Semi-Int. Symposium (Gears), Tokyo 1967, (Jap.Soc.Mech.Engrs.)

43. PRATT, A.: Dynamic Characteristics of Helical Gears, Ph.D. thesis, University of Sheffield, 1971.

44. DOWNS, B.: Vibration Analysis Methods Utilising the Concept of "Dynamic Stiffness" or "Dynamic Flexibility" Parts I, II and III, Bulletin of Mech.Engng. Education, nos. 9, 10, 11, 1956-57.

45. HANSEN, H.M. and CHENEA, P.F.: Mechanics of Vibration, J. Wiley & Sons, Inc., New York, 1952.

46. CHENEA, P.F.: On the Application of the Impedance Method to Continuous Systems, J.App.Mech., June 1953, pp.233-236.

47. MICHALEC, G.W.: Precision Gearing: Theory and Practice, J.Wiley & Sons, Inc., New York, 1966.

48. WELBOURN, D.B.: Forcing Frequencies due to Gears, Conf.Vibrns. Rotating Systems, Instn. Mech. Engrs., London, 1972.

49. MERRITT, H.E.: Gears, Pitman & Sons Ltd., London, 1942.

50. WEBER, C.: The Deformation of Loaded Gears and the Effect on their Load-Carrying Capacity, D.S.I.R., London, Sponsored Research (Germany), Report No. 3 (Part 1), 1949.

51. WEBER, C. and BANASCHEK, K.: The Deformation of Loaded Gears and the Effect on their Load-Carrying Capacity, D.S.I.R., London, Sponsored Research (Germany), Report No. 6 (Part 5), 1950.

52. SEAGER, D.L.: Some Elastic Effects in Helical Gear Teeth, Ph.D. thesis, University of Cambridge, 1967.

53. LAZAN, B.J.: Damping of Materials and Members in Structural Mechanics, Pergamon Press, Oxford, 1968.

54. KIMBALL, A.L.: Vibration Problems - Part V: Friction Damping in Vibrations, Problems in Applied Mechanics, Amer.Soc. Mech.Engrs., 1943, p.159.

55. ASHFIELD, P.E.A.: Vibratory Energy Dissipation in Vibrating Gears and Gear-Shaft Bearings, Ph.D. thesis, University of Sheffield, 1969.

56. Private Communication with Dr. W. Bergwerk of Platt International Ltd., 4th May, 1971.

57. CROOK, A.W.: Simulated Gear Tooth Contacts, Proc.Instn.Mech.Engrs., London, Vol. 171, 1957, p.187.

58. MacCONOCHIE, I.O. and CAMERON, A.: The Measurement of Oil-Film Thickness in Gear Teeth, Trans.Amer.Soc.Mech.Engrs., (series D), Vol. 82, 1960, p.29.

59. SPRATT, H.G.M.: Magnetic Tape Recording, Temple Press Books Ltd., London, 2nd Ed. 1964.

60. PEAR, C.B. (Ed): Magnetic Recording - in Science and Industry, Reinhold Publ. Co., New York, 1967.

61. SAYCE, L.A.: Automatic Measuring, Penguin Technology Survey 1967, Ed. A. Garratt, Penguin Books, London, p.109.

62. MULLARD LTD.: Transistor Audio and Radio Circuits, Mullard Ltd., London, 1969.

63. DINSDALE, J.: Electro-Optical Gearbox using Moire Fringe Technique, Wireless World, Aug. 1971.

64. GRANEEK, M.: Measurement of Mechanical Transmission Errors in Printing Machines, Pira Printing Journal, Vol. 1, No. 3, 1969, pp. 8-11.

65. TIMMS, C., SHARP, R, HUNTER, O.R. and EWING, D.K.: Performance of the N.E.L. Single-flank Gear Tester, N.E.L. Report No. 227, 1966.

66. TIMMS, C.: Recent Developments in Spur and Helical Gears, (the 1959 Nuffield Paper) The Prod. Engr., London, Vol. 39, No. 6, 1960, p.321 (Instn.Prod.Engrs.)

67. DERICK, B.N.: Fibre Optics, Machine Design, Vol. 42, 15th Oct., 1970, pp. 142-147.

68. BALLANTINE, J.M. and ALLEN, W.B.: Fibre Optics, Science Journal, Sept. 1965, pp.77-79.

69. GRUNDY, R.W.: A Technique for Examining the Torsional Vibrations in Gears, Undergraduate Project, Department of Mech.Eng., Loughborough University of Technology, 1973.

70. COOK, R.W.E.: Recording Distortion in Irregularly Shaped Objects, Optics & Laser Technology, Vol. 3, Feb. 1971, pp. 71-73.

71. CRAWFORD, R.: Textile Machinery Noise, Ph.D. thesis, I.S.V.R., University of Southampton, 1968.

72. SATTER, M.A.: Studies of the Dynamic Behaviour of Two Machine Assemblies with Particular Respect to Noise Reduction at the Design Stage, Ph.D. thesis, Loughborough University of Technology, 1970.

73. SATTER, M.A., DOWNS, B. and WRAY, G.R.: Reduction of Noise at the Design Stage: A Case Study of a Lightly Loaded Assembly. Proc.Instn.Mech.Engrs. 1969-70, Vol. 184, Pt. 1.

74. NIEMANN, G. and BAETHGE, J.: Drehwegfehler, Zahnfeder-härte und Geräusch be Stirnrädern (Transmission Error, Tooth Stiffness, and Noise of Spur and Helical Gears), Z.Ver.Dtsch.Ing., Vol. 112, 1970, p.205 (Pt. 1), p.495 (Pt. 2).

Platt International Ltd., Reports on the Drawbox Gear Problem

R1. MORRIS, R.: High Speed Draw Winder-Drawbox Gear Failures, Jan., 1962.

R2. PRIEST, A.V.N.: Report on Gear Failures on Dobson & Barlow Draw Winders, Jan., 1962.

R3. NEEDHAM, E.: Laboratory Report on Failed Gear, Feb., 1962.

R4. TUPLIN, W.A.: Accuracy of Helical Gears Produced by Dobson & Barlow Ltd., Nov., 1963.

R5. TUPLIN, W.A.: Letter concerning the surface deterioration of a gear, Jan., 1964.

R6. ASHTON, D.J.: Type 962 Light/Medium Drawtwister, Tech.Memo. No. TM 2024, July, 1964.

R7. SCOWCROFT, H.: Report on MDT. Drawboxes, May, 1967.

R9. TUPLIN, W.A.: Crossed Helical Gears in MDT. Drawtwister, Jan., 1968.

R10. HALL, W. (P.E.R.A.): Investigation into Gear Failures in MDT. 4 Drawboxes, Jan., 1968.

R11. TUPLIN, W.A.: Inspection of MDT. Drawtwister Gears, Jan., 1968.

R12. Anonymous: Examination of phosphor bronze gears from Contract 'X' Laboratory Report, Feb., 1968.

R13. SCOWCROFT, H.: Failure of gears on contract 'X' Feb., 1968.

R14. WHITELEY, J.: An Investigation of the Possible Causes of MDT.3 Drawbox Gear Failures, Tech.Memo. No. TM/2459, Apr. 1968.

R15. LEE, G.: Calculations on Drawbox Gear Drives, May, 1968.

R16. WHITELEY, J.: MDT. Bronze Drawroll Gear Failures, Tech.Memo. No. TM/2520, Oct., 1968.

R17. SCOWCROFT, H.: Drawroller Gearboxes, Oct., 1968.

R18. SCOWCROFT, H.: Progress Report on MDT. Cushioned Drive, Dec., 1968.

R19. MAKEHAM, P.: Surface Texture of Drawbox Gears, Feb., 1969.

R20. WAUGH, B.: Type C Drawbox Gear Failures (2nd Progress Report) Tech.Memo. No. TM/2550, Mar., 1969.

R21. MAKEHAM, P.: Measurement of Angular Displacement at the Drawroller of an MDT. Drawbox, May, 1969.

R22. MAKEHAM, P.: Calculation of the Principal Natural Frequencies in the "two-over-one" MDT. Drawbox, June, 1969.

R23. MAKEHAM, P.: Various Noise Tests for Different MDT. Drawbox Configurations, 1969.

R24. N.E.L.: Investigation into the Cause of Gear Failures on Drawtwister Machines, National Engineering Laboratory, Report X2/13/6810/1 SP/58, Nov., 1970.

R25. DOWNS, B.: Preliminary Study of Gear Failure Problems of Dobson and Barlow Drawtwisters. June 1970

APPENDIX A - THE DYNAMIC STIFFNESS METHOD

When a mechanical system is subjected to static loading conditions, its response behaviour is determined solely by its elastic (or spring) elements which exert forces at each end. The stiffness of a spring element is defined as the quotient of force/extension and the inverse is termed flexibility. In torsional systems, the same relationships hold except that torque and angular twist replace force and extension respectively. It is important to differentiate between series and parallel arrangements when several springs are combined together. A parallel combination exists when an applied force or torque follows a multiple path as in Figure A.1(a). In this case, the equivalent stiffness is equal to the sum of the individual stiffnesses. In a series arrangement, there is only a single force or torque path (Figure A.1(b)) and here the equivalent flexibility is equal to the sum of the individual flexibilities.

When a mechanical system is disturbed by a harmonic force, the problem becomes one in vibration where inertia, damping and spring elements determine the response behaviour. The Dynamic Stiffness Method (44)(25)(45) allows these to be treated by the same basic rules relating to static problems by introducing the following definitions:

DYNAMIC STIFFNESS (between ends of an element), $\bar{K} = \dfrac{\text{FORCE VECTOR}}{\text{EXTENSION VECTOR}}$

DYNAMIC FLEXIBILITY (between ends of an element), $\bar{F} = \dfrac{\text{EXTENSION VECTOR}}{\text{FORCE VECTOR}}$

Since it is convenient in vector analysis to work in complex variables, the usual representation of harmonic force, $P\cos\omega t$, may be replaced by complex notation, $Pe^{j\omega t}$ $(= P\cos\omega t + j\,P\sin\omega t)$ provided that the imaginary part is suppressed at the end of analysis. Dynamic stiffnesses and dynamic flexibilities may now be determined for each of the three idealised elements of a vibrating system by considering the response to an applied harmonic force.

Spring Element (Figure A.2(a))

Relative displacement between ends is in phase with force.

i.e. Relative displacement $= \dfrac{Pe^{j\omega t}}{K}$

Therefore dynamic stiffness between ends, $\bar{K} = K$

and dynamic flexibility between ends, $\bar{F} = F$.

Viscous Damping Element (Figure A.2(b))

Relative velocity between ends is in phase with force.

Relative velocity $= \dfrac{Pe^{j\omega t}}{D}$

Relative displacement $= \dfrac{Pe^{j\omega t}}{j\omega d}$

Therefore dynamic stiffness between ends $\bar{K} = j\omega D$

and dynamic flexibility between ends $\bar{F} = \dfrac{1}{j\omega D}$

Mass Element (Figure A.2(c))

Acceleration is in phase with force.

Acceleration $= \dfrac{Pe^{j\omega t}}{M}$

Velocity $= \dfrac{Pe^{j\omega t}}{j\,M}$

$$\text{Displacement} = \frac{Pe^{j\omega t}}{-\omega^2 M}$$

Therefore dynamic stiffness $\bar{K} = -\omega^2 M$

and dynamic flexibility $\bar{F} = -\frac{1}{\omega^2 M}$

The significance of these derivations is as follows:

The vector displacement between the ends of a spring element is independent of frequency and is in phase with the harmonic disturbance force.

The vector displacement between the ends of a damping element is inversely proportional to the forcing frequency and lags the force vector by 90 degrees.

The vector displacement of a mass element is inversely proportional to the square of forcing frequency and lags the force vector by 180 degrees.

These relationships, together with the rules associated with series and parallel combinations, may be applied to determine the dynamic stiffness at any point in a mechanical system. The response of the total system to a harmonic excitation may be computed from the simple relationships:-

$$\bar{x}_{ip} = \bar{P}_i / \bar{K}_i \qquad \text{(A.1)}$$

and

$$\bar{P}_{jx} = \bar{K}_j \bar{x}_j \qquad \text{(A.2)}$$

In equation (A.1) $\bar{x}_{ip}$ is the displacement of a point i in the system where a harmonic force $\bar{P}_i$ is impressed and the dynamic stiffness is $\bar{K}_i$. In equation (A.2) $\bar{P}_{jx}$ is the force transmitted through point j in the system where the displacement is $\bar{x}_j$ and the dynamic stiffness is $\bar{K}_j$. The same relationships hold for torsional motions and torques provided that compatible torsional stiffnesses are used.

Apart from yielding the response to a periodic force excitation, the dynamic stiffness method may also be used to provide natural frequencies. The frequency equation is obtained by determining the total system dynamic stiffness expression which must equate to zero at natural frequencies. Examples of both types of analysis are given in the literature (44)(45).

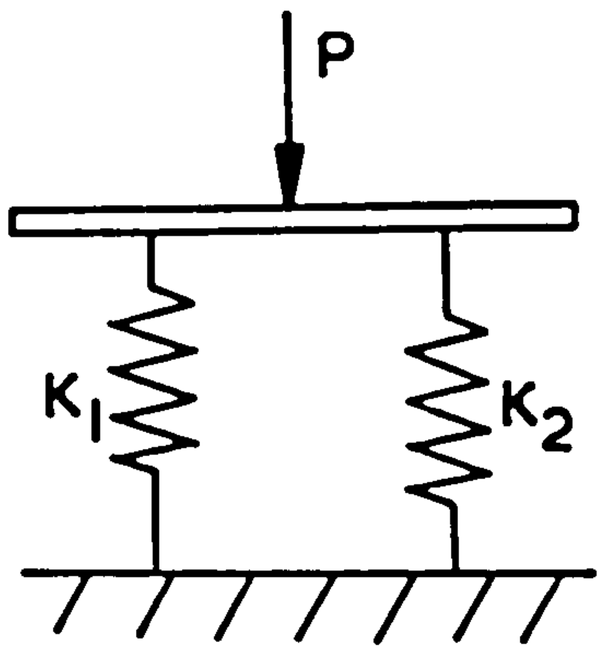

$$K = K_1 + K_2$$

(a) PARALLEL SYSTEM

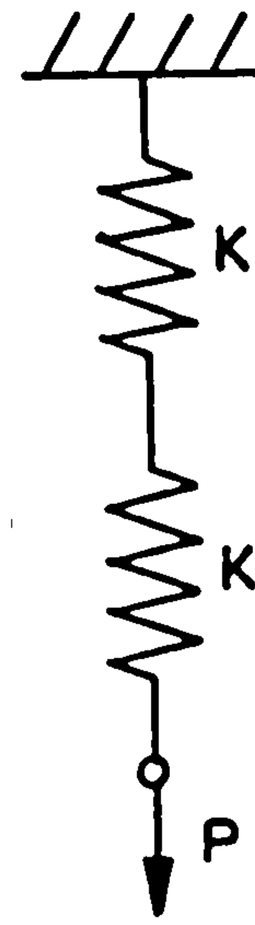

$$\frac{1}{K} = \frac{1}{K_1} + \frac{1}{K_2}$$

(b) SERIES SYSTEM

FIGURE A.1 SPRING COMBINATIONS

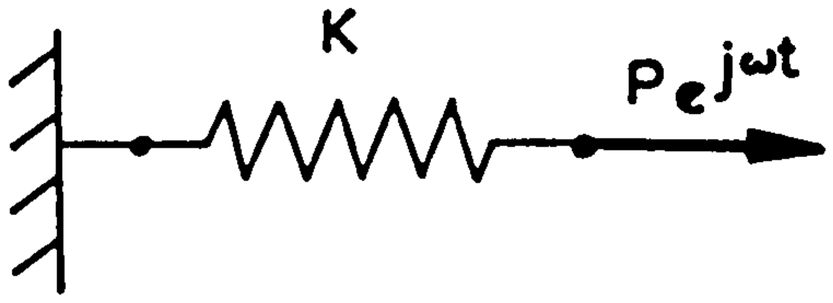

$$\bar{K} = K \; ; \quad \bar{F} = \frac{1}{\bar{K}} = F$$

(a) SPRING ELEMENT

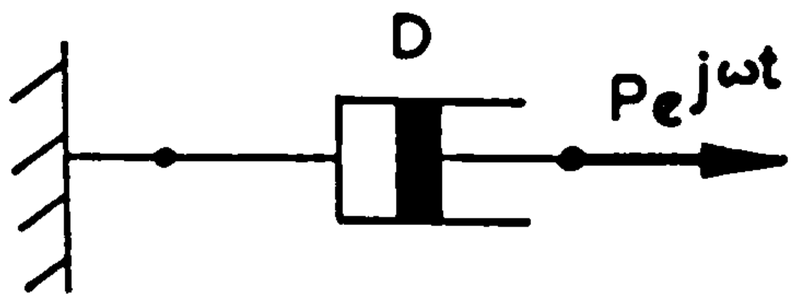

$$\bar{K} = j\omega D \; ; \quad \bar{F} = \frac{1}{j\omega D}$$

(b) DAMPING ELEMENT

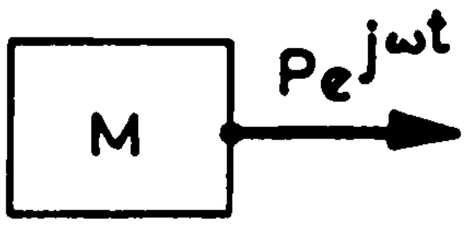

$$\bar{K} = -\omega^2 M \; , \quad \bar{F} = -\frac{1}{\omega^2 M}$$

or $$\bar{K} = -\omega^2 J \; ; \quad \bar{F} = -\frac{1}{\omega^2 J}$$

for INERTIA elements

(c) MASS ELEMENT

FIGURE A.2 ELEMENTS OF A VIBRATING SYSTEM

APPENDIX B

Numerical Data used in Computation

B.1 List of Input Variables

Basic Quantities

PI	π
R	mass density of shaft material.
G	modulus of rigidity of shaft material.

Drawshaft Dimensions

SL(1)	length of drawshaft adjacent to drawroll.
SD(1)	diameter of this section of drawshaft.
SL(2)	length of mid-section of drawshaft.
SD(2)	diameter of this section of drawshaft.
SL(3)	length of drawshaft adjacent to gear.
SD(3)	diameter of this section of drawshaft.

System Inertias (shown as $J_1 - J_{11}$ in Figure 5.4)

AJ(1), AJ(8)	polar moment of inertia at half coupling station.
AJ(2)	polar moment of inertia at layshaft gear 1.
AJ(3)	polar moment of inertia at layshaft gear 2.
AJ(4)	polar moment of inertia at layshaft gear 3.
AJ(5)	polar moment of inertia at layshaft gear 4.
AJ(6)	polar moment of inertia at layshaft gear 5.
AJ(7)	polar moment of inertia at layshaft gear 6.
AJ(9)	polar moment of inertia of bronze drawshaft gear.
AJ(10)	polar moment of inertia of steel drawshaft gear.
AJ(11)	polar moment of inertia of drawroll.

System Stiffnesses (shown as flexibility elements $F_1 - F_{11}$ in Figure 5.4)

AK(1), AK(9)	torsional stiffness of box coupling.
AK(2)	torsional stiffness of layshaft section between coupling and mesh no. 1.
AK(3)	torsional stiffness of layshaft section between mesh no. 1 and mesh no. 2.

AK(4) -- torsional stiffness of layshaft section between mesh no. 2 and mesh no. 3.

AK(5) torsional stiffness of layshaft section between mesh no. 3 and mesh no. 4.

AK(6) torsional stiffness of layshaft section between mesh no. 4 and mesh no. 5.

AK(7) torsional stiffness of layshaft section between mesh no. 5 and mesh no. 6.

AK(8) torsional stiffness of layshaft section between *mesh no. 6 and coupling.*

AK(10) torsional stiffness of crossed helical mesh.

AK(11) torsional stiffness of parallel helical mesh.

System Dampers (shown as D_1 - D_{11}, FD_1, FD_{10} and FD_{11} in Figure 5.4)

AJD(1),AJD(8) torsional damping associated with box half coupling.

AJD(2) torsional damping associated with layshaft gear no. 1.

AJD(3) torsional damping associated with layshaft gear no. 2.

AJD(4) torsional damping associated with layshaft gear no. 3.

AJD(5) torsional damping associated with layshaft gear no. 4.

AJD(6) torsional damping associated with layshaft gear no. 5.

AJD(7) torsional damping associated with layshaft gear no. 6.

AJD(9) torsional damping associated with bronze drawshaft gear.

AJD(10) torsional damping associated with steel drawshaft gear.

AJD(11) torsional damping associated with drawroll.

DCPLG torsional damping in the box coupling.

FFD(10) torsional damping at the crossed helical mesh.

FFD(11) torsional damping at the parallel helical mesh.

Other Quantities

SRAT speed ratio (drawshaft speed/layshaft speed, = dia. layshaft gear/dia. drawshaft gear).

ERR	amplitude of fundamental component of transmission error at parallel helical mesh.
FXBSH	torsional flexibility due to rubber bushes in bushed drawshaft gears.
DXBSH	torsional damping due to rubber bushes in bushed drawshaft gears.
NBM	number of drawboxes in machine.
SS	machine spindle speed.
DR	draw ratio (polyamide machines).
CDR	cold draw ratio (polyester machines).
HDR	hot draw ratio (polyester machines).

B.2 Numerical Values

PI	3.141593	
R	0.00072	$lbf.sec^2/in^4$
G	11.8×10^6	lbf/in^2

Variable	Machine Types A & C	Machine Types B & E	Units
SL(1)	1.187	1.187	in.
SD(1)	0.985	0.985	in.
SL(2)	11.0	11.0	in.
SD(2)	1.225	1.225	in.
SL(3)	2.375	2.375	in.
SD(3)	0.985	0.985	in.
AJ(1),AJ(8)	0.0561	0.0567	$lbf.in.sec^2$
AJ(2)	0.0147	0.0101	$lbf.in.sec^2$
AJ(3)	0.0145	0.0102	$lbf.in.sec^2$
AJ(4)	0.0136	0.00939	$lbf.in.sec^2$
AJ(5)	0.0146	0.0103	$lbf.in.sec^2$
AJ(6)	0.0145	0.0103	$lbf.in.sec^2$
AJ(7)	0.0137	0.00931	$lbf.in.sec^2$
AJ(9)	0.00201	0.00201	$lbf.in.sec^2$
AJ(10)	0.00175	0.00175	$lbf.in.sec^2$
AJ(11)	0.0610	0.0410	$lbf.in.sec^2$

Machine.

Variable	Types A & C	Types B & E	Units
AK(1),AK(9)	0.840×10^6	0.840×10^6	lbf.in/rad
AK(2)	0.174×10^7	0.170×10^7	lbf.in/rad
AK(3)	0.153×10^7	0.167×10^7	lbf.in/rad
AK(4)	0.153×10^7	0.161×10^7	lbf.in/rad
AK(5)	0.272×10^7	0.250×10^7	lbf.in/rad
AK(6)	0.106×10^7	0.118×10^7	lbf.in/rad
AK(7)	0.274×10^7	0.250×10^7	lbf.in/rad
AK(8)	0.174×10^7	0.170×10^7	lbf.in/rad
AK(10)	0.154×10^7	0.154×10^7	lbf.in/rad
AK(11)	0.154×10^7	0.154×10^7	lbf.in/rad
AJD(1),AJD(8)	0.03	0.03	lbf.in.sec/rad
AJD(2)	0.03	0.03	lbf.in.sec/rad
AJD(3)	0.03	0.03	lbf.in.sec/rad
AJD(4)	0.03	0.03	lbf.in.sec/rad
AJD(5)	0.03	0.03	lbf.in.sec/rad
AJD(6)	0.03	0.03	lbf.in.sec/rad
AJD(7)	0.03	0.03	lbf.in.sec/rad
AJD(9)	0.03	0.03	lbf.in.sec/rad
AJD(10)	0.03	0.03	lbf.in.sec/rad
AJD(11)	1.45	1.45	lbf.in.sec/rad
DCPLG	31.2	31.2	lbf.in.sec/rad
FFD(10)	0.625	0.625	lbf.in.sec/rad
FFD(11)	0.625	0.625	lbf.in.sec/rad
SRAT	1.45	1.25	-
ERR	0.0021	0.0021	radians
FXBSH	-	0.0005	rad/lbf.in
DXBSH	-	25.0	lbf.in.sec/rad

NBM	variable, but normally 10
SS	variable up to 12 000 r.p.m.
DR	variable 1.0 - 6.0 (Polyamide Machines)
CDR	variable 1.0 - 3.0 (Polyester Machines)
HDR	variable 1.0 - 6.0 (Polyester Machines)

Appendix C

Main Computer Program DT Total Analysis

```
      MASTER DT TOTAL ANALYSIS
C *****  DT TOTAL ANALYSIS COMPUTES DYNAMIC TORQUES AT EVERY PARALLEL HELICAL
C        GEAR MESH IN A DRAWTWISTER DRAWBOX SYSTEM FOR ANY RUNNING SPEED. THE
C        DYNAMIC LOAD AT ANY PARTICULAR MESH IS FORCED BY RELATIVE DISPLACEMENT
C        EXCITATION, DUE TO STATIC TRANSMISSION ERRORS , AT EVERY PARALLEL AXIS
C        MESH IN THE TOTAL GEARBOX SYSTEM. ALTERNATIVE HEADSTOCK CONFIGURATIONS
C        ARE MODELLED BY 3 SUBROUTINES , AS FOLLOWS .
C
C        SUBROUTINE MDT.2 DRIVE  -  FOR POLYAMIDE MACHINES
C
C        SUBROUTINE MDT.3 DRIVE  -  FOR POLYESTER MACHINES
C
C        SUBROUTINE V.S. DRIVE  -  FOR A VARIABLE SPEED DRIVE AS EMPLOYED IN
C                                  EXPERIMENTAL INVESTIGATIONS
C
C        SYSTEM REFERENCE POSITIONS ARE COMPATIBLE WITH DYNAMIC STIFFNESS
C        ANALYSIS DIAGRAMS
C *** THE FOLLOWING DATA IS INPUT ON PUNCHED CARDS .
C
C      NMK  -  MACHINE TYPE = 2 FOR POLYAMIDE MACHINES
C                           = 3 FOR POLYESTER MACHINES
C
C      MOD  -  MACHINE MODEL  = 200 , FOR MDT. 2
C                             = 300 , FOR MDT. 3
C                             = 600 , FOR MDT. 6
C                             = 111 , FOR MULTI-BOX RIG
C
C     FOR POLYAMIDE MACHINE (PLATT DRG. NO. MDT. 22/34) :
C      SS  -  SPINDLE SPEED (R.P.M.)
C      DR  -  DRAW RATIO
C      SR4  -  DIAMETER RATIO OF PULLEY 'A' TO PULLEY 'B'
C      NG21  -  NO OF TEETH ON GEAR 'N'
C      NG2  -  NO OF TEETH ON GEAR 'M'
C
C     FOR POLYESTER MACHINE (PLATT DRG. NO. MDT. 32/114) :
C      SS  -  SPINDLE SPEED (R.P.M.)
C      HDR  -  HOT DRAW RATIO
C      CDR  -  COLD DRAW RATIO
C      NG4  -  NO OF TEETH ON GEAR'K'
C      NG5  -  NO OF TEETH ON GEAR'G'
C      NG28  -  NO. OF TEETH ON GEAR 'S'
C      NG20  -  NO. OF TEETH ON GEAR 'T'
C
C      SD(1)-(3)  -  DIAMETERS OF DRAWSHAFT SECTIONS (IN)
C
C      SL(1)-(3)  -  LENGTHS OF DRAWSHAFT SECTIONS (IN)
C
C      AJ(1)-(11)  -  GEARBOX SYSTEM INERTIAS (LBF-IN-SEC2)
C
C      AK(1)-(11)  -  GEARBOX SYSTEM STIFFNESSES (LBF-IN/RAD)
C
C      NRM  -  NUMBER OF DRAWBOXES IN SYSTEM (LOWER BOXES ONLY FOR POLYESTER
C                 MACHINES)
C
C      SRAT  -  SPEED RATIO OF CROSSED HELICAL MESH ( = 1.45 FOR MDT. 2/3 AND
C                  = 1.25 FOR MDT. 6N/P)
C
C      FDDIA  -  FACTOR FOR MODIFYING DRAWROLL SHAFT DIAMETER
C
C      FRGLY  -  FACTOR FOR MODIFYING LAYSHAFT GEAR INERTIA
C
```

```
C       FRGDR  -  FACTOR FOR MODIFYING DRAWSHAFT GEAR INERTIA
C
C       FXBSH  -  RUBBER BUSH FLEXIBILITY (BUSHED GEARS ONLY)
C
C       FRGTX  -  FACTOR FOR MODIFYING GEAR MESH FLEXIBILITY
C
C       FCTRR  -  FACTOR FOR MODIFYING BOX COUPLING STIFFNESS
C
C       NDAY  -  NO. OF SETS OF CALCULATIONS REQUIRED
C
C       REV  -  DRAWROLL SPEED (R.P.M.)
C
C
C ***** REAL AND COMPLEX VARIABLES ARE SPECIFIED AND APPROPRIATE ARRAY SPACE
C         ALLOCATED
      COMPLEX JAY.K(250).F(250),RHK(15),RHF(15),LHK(15),LHF(15),FD10,
     1 FD11,JW.CDUM.Q(250),T(250),GE,TDYN,TCPX(10,6),BDUM
      REAL JJ(12).JJD(12).K161A,NG4.NG5.NG28.NG29.NG21.NG2
      DIMENSION AJ(11),AJD(11),AK(12),FF(12),FFD(12),SL(3),SD(3)
      DIMENSION TD(10,6).PHI(10.6)
C *** IDENTIFY VARIABLES COMMON TO MAIN PROGRAM AND THE VARIOUS SUB-PROGRAMS
      COMMON/CROSSTOP/JAY.JW,W2.F,RHK.RHF,LHK.LHF,SRAT2,NBM
     1/STIFFNESS/K/DEFLN/Q/POLAR/TCPX/TMATJ/AJG,DIAP
C  ***** FIXED DATA INSERTED
      DATA PI,R,G/3.141593.0.00072,11.8E6/
C ***** DAMPING DATA INSERTED
      DATA FFD(10).FFD(11).AJD(11),AJD(1),AJD(2),AJD(3),AJD(4),AJD(5),
     1      AJD(6) AJD(7).AJD(8).AJD(9),AJD(10)/2*.675,1.45,10*.01/
      DATA DXBSH.DCPLG /0.00.31.2/
      EXTERNAL TAN.SQRT
C ***** FORMATS ARE SPECIFIED FOR PUNCHED CARD INPUT AND PRINTED OUTPUT
 1020 FORMAT(F0.0)
 1025 FORMAT(I2)
 1030 FORMAT(1H .F7.1.2X.5HR.P.M.2X.E10.4,2X,6HLBF-IN)
 1035 FORMAT(17H BUSH FLEXIBILITY.2X.E12.5,6X,11HNO OF BOXES.2X,I2)
 1040 FORMAT (8H FRGTX  .F6.3,10H   FRGLY  .F6.3,10H   FRGDR  ,F6.3,
     1 10H   FCTRR  .F6.3,10H   SRAT  .F6.3,10H   FDDIA  ,F6.3)
 1045 FORMAT(11F0 0)
 1050 FORMAT(1H .11(E9.3.2X)//)
 1055 FORMAT(I1.2X.I3)
 1060 FORMAT(////15H MACHINE   MDT .I1,2X,4HMOD .I3//)
 1065 FORMAT(1H .17H SPINDLE SPEED = ,F7.2,6H RPM. .14H DRAW RATIO = ,
     1 F7 4,2X,8HSR(4) = .F7.4,2X,9HNG(21) = ,F6.2,2X,8HNG(2) = ,F6.2)
 1070 FORMAT(1H .//.18H DELIVERY SPEED = ,F7.1,8H FT/MIN ,15H NG(4),NG(5
     1) = .F7.2.5H AND .F7.2.19H TEETH RESPECTIVELY)
 1075 FORMAT(1H ./.17H SPINDLE SPEED = .F7.1,6H RPM. ,18H HOT DRAW RATIO
     1 = .F8.4)
 1080 FORMAT(1H ./.19H COLD DRAW RATIO = ,F8.4,2X,17H NG(28).NG(29) = ,
     1 F7 2.5H AND .F7.2.19H TEETH RESPECTIVELY)
 1085 FORMAT(1H ./.18H DELIVERY SPEED = .F7.1,8H FT/MIN ,9H SR(4) = ,
     1 F7 4)
 1090 FORMAT(E9.3.12)
 1095 FORMAT(25H RELATIVE DISPT. ERROR = ,E9.3,5H RAD.,6H TYPE ,I2//)
 1100 FORMAT(//8H REVL = ,F6.0.2X,8H REVH = .F6.0,2X,8H REVI = ,F4.0/)
 1105 FORMAT(119H    AJ(1)       AJ(2)       AJ(3)       AJ(4)       AJ(5)
     1    AJ(6)       AJ(7)       AJ(8)       AJ(9)       AJ(10)      AJ(11))
 1110 FORMAT(119H    AK(1)       AK(2)       AK(3)       AK(4)       AK(5)
     1     AK(6)       AK(7)       AK(8)       AK(9)       AK(10)      AK(11))
 1115 FORMAT(9F0.0)
 1120 FORMAT(6F0.0)
 1125 FORMAT(1H .6(F9.3.2X))
 1130 FORMAT(1H .F12.0,4X.F12.6.6X.F12.6.2X.E12.6)
```

```
 1135 FORMAT(1H ,///,22H *** DRAWROLL SPEED = ,F9.3)
 1140 FORMAT(1H ,/,25H TORQUE AMPLITUDE(LBF-IN),4X,17H PHASE ANGLE(DEG))
 1145 FORMAT(1H ,//)
 1150 FORMAT(1H ,8X,E10.4,10X,F7.2,5X,E10.4,2X,E10.4)
      ERR = .0021
C *****  (MAXIMUM GEAR ERROR AMPLITUDE)
      READ(1,1055) NMK,MOD
C *****  MACHINE PARAMETERS READ ACCORDING TO TYPE OF MACHINE,IE., POLYAMIDE
C        (NMK = 2),POLYESTER (NMK = 3) OR EXPERIMENTAL RIG (MOD = 111)
      IF (MOD .EQ. 111) GO TO 1220
      IF (NMK .EQ. 3 .AND. MOD .NE. 111) GO TO 1210
      READ(1,1045) SS,DR,SR4,NG21,NG2
      WRITE(2,1065) SS,DR,SR4,NG21,NG2
      GO TO 1220
 1210 CONTINUE
      READ(1,1045) SS,HDR,CDR,NG4,NG5,NG28,NG29
      WRITE(2,1075) SS,HDR
      WRITE(2,1080) CDR,NG28,NG29
 1220 CONTINUE
      WRITE(2,1060) NMK,MOD
      WRITE(4)NMK,MOD
      READ(1,1120) SD(1),SD(2),SD(3),SL(1),SL(2),SL(3)
      WRITE(2,1125)SD(1),SD(2),SD(3),SL(1),SL(2),SL(3)
      READ(1,1045) (AJ(J),J=1,11)
      WRITE(2,1105)
      WRITE(2,1050) (AJ(J),J=1,11)
      READ(1,1115) (AK(J),J=1,11)
      WRITE(2,1110)
      WRITE(2,1050) (AK(J),J=1,11)
      STOR1=AK(1)
      STOR2=AK(10)
      READ(1,1025) NBM
      WRITE(4)NBM
      READ(1,1020) SRAT
      READ(1,1020) FDDIA
C     *****  REDUCE DRAWROLL SHAFT DIAMETER
      SD(2)=SD(2)*FDDIA
      READ(1,1020) FRGLY
C*****REDUCE LAYSHAFT GEAR INERTIAS **********************
      DO 1230 JLY=2,7
 1230 AJ(JLY)=AJ(JLY)-(4.36*(1.-FRGLY))/(32.2*12.)
      READ(1,1020) FRGDR
C *****  REDUCE DRAUROLL GEAR INERTIAS BY *FRGDR
      AJ(9)=AJ(9)*FRGDR
      AJ(10)=AJ(10)*FRGDR
      READ(1,1020) FXBSH
      READ(1,1020) FRGTX
C *****  INCREASE FLEXIBILITY OF GEAR TOOTH CONTACT
      AK(10),AK(11)=STOR2/FRGTX
      READ(1,1020) FCTRR
C *****  REDUCE COUPLING STIFFNESS BY FACTOR FCTRR
      AK(1),AK(9)=STOR1/FCTRR
      WRITE(2,1040) FRGTX,FRGLY,FRGDR,FCTRR,SRAT,FDDIA
      WRITE(2,1035) FXBSH,NBM
      SRAT2=SRAT*SRAT
C *****  INERTIAS AND FLEXIBILITIES ON LAYSHAFT ARE RELATED TO DRAWROLL SPEED
      DO 1240 N=1,8
      JJ(N)=AJ(N)/SRAT2
      JJD(N)=AJD(N)
 1240 FF(N) = SRAT2/AK(N)
      FF(9)=SRAT2/AK(9)
      JJ(9)=AJ(9)
```

```
      JJD(9)=AJD(9)
      DO 1250 N=10,11
      JJ(N)=AJ(N)
      JJD(N)=AJD(N)
 1250 FF(N) = 1. /AK(N)
      READ(1,1025) NDAT
C ****** (NUMBER OF RUNNING SPEEDS FOR WHICH COMPLETE ANALYSIS REQUIRED )
      WRITE(4) NDAT
C ******  CONTROL PARAMETERS SET FOR 2 INDEPENDENT SERIES OF RANDOM NUMBERS .
C        WITH UNIFORM PROBABILITY .  -  TO BE GENERATED BY THE COMPUTER
      IAA = 1
      JAA = 0
      IBB = 3
      JBB = 0
      KAA = 0
      KBB = 0
      DO 1660 I=1,NDAT
 1260 READ(1,1020) REV
      WRITE(4)REV
      WRITE(2,1135) REV
      DO 1270 IB=1,NBM
      DO 1270 IDR = 1,6
C ****** DYNAMIC LOADS AT EVERY GEAR STATION ARE INITIALLY SET TO ZERO
 1270 TCPX(IB,IDR) = (0.0,0.0)
  ****** EXCITATION PROVIDED AT DRAWROLL ROTATIONAL FREQUENCY (W RADIANS/SEC)
 1280 W = (RFV/60 )*2.*PI
      W2=W*W
C ****** COMPLEX  NOTATION INTRODUCED
      JAY = (0.,1 )
      JW=JAY*W
      K(126)=-(AJ(11)*W2)+JW*AJD(11)
      K(160) = K(126)
C ****** DYNAMIC STIFFNESS OF DRAWSHAFT COMPUTED BY CONSIDERATION OF DISTRIBUTED
C        INERTIA AND FLEXIBILITY PLUS DIAMETER CHANGES
      DO 1290 L=1,3
      K(118)=K(126)-SQRT(G*R)*W*PI*SD(L)**4/32.*TAN(W*SL(L)/SQRT(G/R))  DUMMY V
      CDUM=1.+K(126)/(SQRT(G*R)*W*PI*SD(L)**4/32.)*TAN(W*SL(L)/SQRT(G/R)
     1 )
 1290 K(126) = K(118)/CDUM
C ****** DYNAMIC STIFFNESSES COMPUTED FOR DRAWSHAFT PAIR ASSEMBLIES
      CDUM = 1./K(126) + 1./(1./FXBSH + JW*DXBSH)
      K(115),K(122),K(200),K(204),K(218),K(224)=1./CDUM
      K(157),K(226)=CMPLX(W2*(-AJ(10)),0.)
      K(156),K(225)=AJD(10)*JW
      F(121)=1./(K(157)+K(156)+K(122))
      K(121) = 1./F(121)
      F(114)=F(121)+1./(1./FF(11)+JW*FFD(11))
      K(114),K(208)=1./F(114)
      K(117),K(210),K(214)=CMPLX(W2*(-AJ(9)),0.)
      K(116),K(209),K(213)=AJD(9)*JW
      F(113)=1./(K(117)+K(116)+K(114)+K(115))
      K(113) = 1./F(113)
      F(108)=F(113)+1./(1./FF(10)+JW*FFD(10))
      K(108)=1./F(108)
      K(100) = (0.0,0.0)
C        DYNAMIC STIFFNESS OF HEADSTOCK/DRIVE SYSTEM CALCULATED BY APPROPRIATE
C        SUBROUTINE , ACCORDING TO MACHINE TYPE , AND ATTACHED TO BOX NO. 1
      IF (MOD .EQ. 111 ) GO TO 1300
      IF (NMK .EQ. 2 .AND. MOD .NE. 111) GO TO 1310
      IF (NMK .EQ. 3 .AND. MOD .NE. 111) GO TO 1320
      GO TO 1330
 1300 CONTINUE
```

```
      CALL VS DRIVE(REV,SRAT,AJ(1))
      GO TO 1330
 1310 CONTINUE
      DS = REV*PI*5.00/12.0
      WRITE(2,1085) DS,SR4
      CALL HDT2 DRIVE(DS,SR4,SS,DR,NG21,NG2,AJ(1))
      GO TO 1330
 1320 CONTINUE
      DS = REV*PI*5.00/12.0
      WRITE(2,1070) DS,NB4,NG5
      CALL HDT3 DRIVE(DS,NG4,NG5,SS,HDR,CDR,NG28,NG29,AJ(1))
 1330 CONTINUE
      NDIR=1
      IP = 1
      DO 1340 L=1,NBM
C *****  DYNAMIC STIFFNESSES CONNECTED AT THE HEADSTOCK END OF EACH DRAWBOX ARE
C        COMPUTED BY SUBROUTINE 'CROSSBOX'
 1340 CALL CROSSBOX (JJ(1),JJ(2),JJ(3),JJ(4),JJ(5),JJ(6),JJ(7),JJ(8),
     1 JJD(1),JJD(2),JJD(3),JJD(4),JJD(5),JJD(6),JJD(7),JJD(8),FF(1),
     2 FF(2),FF(3),FF(4),FF(5),FF(6),FF(7),FF(8),FF(9),NDIR,L,DCPLG,IP)
      NDIR=2
      DO 1350 L=1,(NBM-1)
C *****  DYNAMIC STIFFNESSES CONNECTED AT THE TAIL END OF EACH DRAWBOX ARE
C        COMPUTED BY SUBROUTINE 'CROSSBOX'
C ***  FLOW DIRECTION IS REVERSED BY SUPPLYING LAYSHAFT DATA IN REVERSE ORDER
 1350 CALL CROSSBOX (JJ(8),JJ(7),JJ(6),JJ(5),JJ(4),JJ(3),JJ(2),JJ(1),
     1 JJD(8),JJD(7),JJD(6),JJD(5),JJD(4),JJD(3),JJD(2),JJD(1),FF(9),
     2 FF(8),FF(7),FF(6),FF(5),FF(4),FF(3),FF(2),FF(1),NDIR,L,DCPLG,IP)
      LOOPA=1
      LOOPT=NBM
 1360 DO 1610 NB=LOOPA,LOOPT
      K(187)=LHK(NB)
      K(161)=RHK(NB)
      IF (RHK(NB) .NE.0.) GO TO 1370
      K(162)=(0.0,0.0)
      GO TO 1380
 1370 F(162) = 1./K(161) + 1./(1./FF(9) + JW*DCPLG)
      K(162) = 1./F(162)
C *****  DYNAMIC STIFFNESSES ARE COMPUTED FOR VARIOUS DRAWBOX POSITIONS.
C        MASTER STATIONS ARE IDENTIFIED FOR ECONOMY OF COMPUTATION. (SEE DYNAMIC
C        STIFFNESS ANALYSIS DIAGRAMS)
 1380 K(165)=K(162)*JW*JJD(8)-W2*JJ(8)
      K(166)=1./(1./K(165)+FF(8))
      K(169)=K(166)*K(108)*JW*JJD(7)-W2*JJ(7)
      K(170)=1./(1./K(169)+FF(7))                                    MASTER
      K(173)=K(170)*K(108)*JW*JJD(6)-W2*JJ(6)
      K(174)=1./(1./K(173)+FF(6))                                    MASTER
      K(177)=K(174)*K(108)*JW*JJD(5)-W2*JJ(5)
      K(178)=1./(1./K(177)+FF(5))                                    MASTER
      K(181)=K(178)*K(108)*JW*JJD(4)-W2*JJ(4)
      K(182)=1./(1./K(181)+FF(4))                                    MASTER
      K(185)=K(182)*K(108)*JW*JJD(3)-W2*JJ(3)
      K(186)=1./(1./K(185)+FF(3))                                    MASTER
      AK250 = CABS(K(250))
      IF ( AK250 .NE. 0.0 ) GO TO 1390
      K(188) = (0.0,0.0)
      GO TO 1400
 1390 F(188) = 1./K(187) + 1./(1./FF(1) + JW*DCPLG)
      K(188) = 1./F(188)
 1400 K(191)=K(188)*JW*JJD(1)-W2*JJ(1)
      K(192)=1./(1./K(191)+FF(2))                                    MASTER
      K(208)=K(192)*K(108)*JW*JJD(2)-W2*JJ(2)
```

```
      K(229)=1./(1./K(228)+FF(3))                                        MASTER
      K(230)=K(229)+K(108)+JW+JJD(3)-W2+JJ(3)
      K(231)=1./(1./K(230)+FF(4))                                        MASTER
      K(232)=K(231)+K(108)+JW+JJD(4)-W2+JJ(4)
      K(233)=1./(1./K(232)+FF(5))                                        MASTER
      K(234)=K(233)+K(108)+JW+JJD(5)-W2+JJ(5)
      K(235)=1./(1./K(234)+FF(6))                                        MASTER
      K(236)=K(235)+K(108)+JW+JJD(6)-W2+JJ(6)
      K(237)=1./(1./K(236)+FF(7))                                        MASTER
      LEEPA=1
      LEEPT=6
C *****  SYSTEM CONNECTION IS MADE AT STATION 195 (SEE ANALYSIS DIAGRAM)
C          ACCORDING TO WHICH DRAWROLL PAIR IS UNDER CONSIDERATION
 1410 DO 1600 NDR=LEEPA,LEEPT
      GO TO (1421,1422,1423,1424,1425,1426),NDR
 1421 K(195)=K(192)+K(186)
      GO TO 1430
 1422 K(195)=K(229)+K(182)
      GO TO 1430
 1423 K(195)=K(231)+K(178)
      GO TO 1430
 1424 K(195)=K(233)+K(174)
      GO TO 1430
 1425 K(195)=K(235)+K(170)
      GO TO 1430
 1426 K(195)=K(237)+K(166)
 1430 K(195)=K(195)+JW+JJD(NDR+1)-W2+JJ(NDR+1)
      F(196)=1./K(195)+1./(1./FF(10)+JW+FFD(10))
      K(196) = 1./F(196)
      K(211)=1./F(196)+K(200)+K(208)+K(209)+K(210)                       MASTER
      K(219)=1./F(196)+K(213)+K(214)+K(218)
      F(220)=1./K(219)+1./(1./FF(11)+JW+FFD(11))
      K(220) = 1./F(220)
      K(227)=1./F(220)+K(224)+K(225)+K(226)
C *****  RANDOM NUMBERS 'A' AND 'B' ARE GENERATED FOR THE ALLOCATION OF
C          TRANSMISSION ERROR AND ERROR PHASE ANGLE AT EACH GEAR MESH
      A = UTR1(IAA,JAA,KAA)
      B = UTR1(IBB,JBB,KBB)
 1440 FORMAT(1H ,5H A = ,F9.3,4X,5H B = ,F9.3,4X,6H **** )
      WRITE(2,1440) A,B
      ERAA = ERR+A
      FI = 2.+PI+B
C *****  TRANSMISSION ERROR VECTOR REPRESENTED IN COMPLEX FORM
      XGE = ERAA+COS(FI)
      YGE = ERAA+SIN(FI)
      GE = CMPLX(XGE,YGE)
C *****  TOOTH DYNAMIC TORQUES COMPUTED
      TDYN = GE/(1./K(208)+F(220)-1./(1./FF(11)+JW+FFD(11)))
C *****  TRANSFER OF DYNAMIC TORQUE TO BOTH ENDS OF THE SAME BOX IS COMMENCED
      IB = NB
      Q(211) = TDYN/K(208)
      T(196) = K(196)+Q(211)
      Q(195) = T(196)/K(195)
      GO TO (1451,1452,1453,1454,1455,1456),NDR
 1451 T(136) = K(186)+Q(195)
      T(192) = K(192)+Q(195)
      TCPX(IB,1) = TDYN + TCPX(IB,1)
       GO TO 1461
 1452 T(182) = K(182)+Q(195)
      T(229) = K(229)+Q(195)
      TCPX(IB,2) = TDYN + TCPX(IB,2)
       GO TO 1462
```

```
1453 T(178) = K(178)*Q(195)
     T(231) = K(231)*Q(195)
     TCPX(IB.3) = TDYN + TCPX(IB,3)
      GO TO 1463
1454 T(174) = K(174)*Q(195)
     T(233) = K(233)*Q(195)
     TCPX(IB,4) = TDYN + TCPX(IB,4)
      GO TO 1464
1455 T(170) = K(170)*Q(195)
     T(235) = K(235)*Q(195)
     TCPX(IB,5) = TDYN + TCPX(IB,5)
      GO TO 1465
1456 T(166) = K(166)*Q(195)
     T(237) = K(237)*Q(195)
     TCPX(IB.6) = TDYN + TCPX(IB,6)
      GO TO 1466
C ***** RESPONSE AT OTHER GEAR STATIONS TOWARDS TAIL END OF BOX ARE COMPUTED
C       BY TRACING TORQUE FLOW THROUGH BOX. RUNNING TOTALS OF DYNAMIC LOAD ARE
C       KEPT FOR EACH POSITION
1461 Q(185) = T(186)/K(185)
     T(108) = K(108)*Q(185)
     Q(113) = T(108)/K(113)
     T(114) = K(114)*Q(113)
     TCPX(IB,2) = T(114) + TCPX(IB,2)
     T(182) = K(182)*Q(185)
1462 Q(181) = T(182)/K(181)
     T(108) = K(108)*Q(181)
     Q(113) = T(108)/K(113)
     T(114) = K(114)*Q(113)
     TCPX(IB.3) = T(114) + TCPX(IB,3)
     T(178) = K(178)*Q(181)
1463 Q(177) = T(178)/K(177)
     T(108) = K(108)*Q(177)
     Q(113) = T(108)/K(113)
     T(114) = K(114)*Q(113)
     TCPX(IB.4) = T(114) + TCPX(IB,4)
     T(174) = K(174)*Q(177)
1464 Q(173) = T(174)/K(173)
     T(108) = K(108)*Q(173)
     Q(113) = T(108)/K(113)
     T(114) = K(114)*Q(113)
     TCPX(IB,5) = T(114) + TCPX(IB,5)
     T(170) = K(170)*Q(173)
1465 Q(169) = T(170)/K(169)
     T(108) = K(108)*Q(169)
     Q(113) = T(108)/K(113)
     T(114) = K(114)*Q(113)
     TCPX(IB,6) = T(114) + TCPX(IB,6)
     T(166) = K(166)*Q(169)
C ***** DISPLACEMENT AT EXTREME TAIL-END OF DRAWBOX IS CALCULATED
1466 Q(165) = T(166)/K(165)
     T(162) = K(162)*Q(165)
     K161A = CABS(K(161))
     IF (K161A .EQ. 0.) GO TO 1470
     Q(161) = T(162)/K(161)
1470 CONTINUE
C ***** RESPONSE AT OTHER GEAR STATIONS ,TOWARDS HEADSTOCK END OF BOX , IS
C       CALCULATED BY TRACING TORQUE FLOW THROUGH BOX. RUNNING TOTALS OF DYNAMIC
C       LOAD ARE KEPT FOR EACH POSITION
     GO TO (1481,1482,1483,1484,1485,1486),NDR
1486 Q(236) = T(237)/K(236)
     T(108) = K(108)*Q(236)
```

```
Q(113) = T(108)/K(113)
T(114) = K(114)*Q(113)
TCPX(IB,5) = T(114) + TCPX(IB,5)
T(235) = K(235)*Q(236)
Q(234) = T(235)/K(234)
T(108) = K(108)*Q(234)
Q(113) = T(108)/K(113)
T(114) = K(114)*Q(113)
TCPX(IB,4) = T(114) + TCPX(IB,4)
T(233) = K(233)*Q(234)
Q(232) = T(233)/K(232)
T(108) = K(108)*Q(232)
Q(113) = T(108)/K(113)
T(114) = K(114)*Q(113)
TCPX(IB,3) = T(114) + TCPX(IB,3)
T(231) = K(231)*Q(232)
Q(230) = T(231)/K(230)
T(108) = K(108)*Q(230)
Q(113) = T(108)/K(113)
T(114) = K(114)*Q(113)
TCPX(IB,2) = T(114) + TCPX(IB,2)
T(229) = K(229)*Q(230)
Q(228) = T(229)/K(228)
T(108) = K(108)*Q(228)
Q(113) = T(108)/K(113)
T(114) = K(114)*Q(113)
TCPX(IB,1) = T(114) + TCPX(IB,1)
T(192) = K(192)*Q(228)
** DISPLACEMENT AT EXTREME HEADSTOCK END OF DRAWBOX IS CALCULATED
Q(191) = T(192)/K(191)
A187K = CABS(K(187))
IF ( A187K .NE. 0.0) GO TO 1490
GO TO 1500
CONTINUE
T(188) = K(188)*Q(191)
Q(187) = T(188)/K(187)
CONTINUE
NDIR=1
IP = 2
NL1 = NB-1
** ATTENTION IS NOW FOCUSSED ON BOX NO. IB = NB - 1
IB=NB-1
IF (IB .EQ. 0) GO TO 1530
K(250) = LHK(IB)
L = 1
** DYNAMIC STIFFNESSES FOR FLOW TOWARDS HEADSTOCK END OF BOX IB ARE
   COMPUTED BY MEANS OF SUBROUTINE 'CROSSBOX'
CALL CROSSBOX(JJ(1),JJ(2),JJ(3),JJ(4),JJ(5),JJ(6),JJ(7),JJ(8),
 JJD(1) JJD(2),JJD(3),JJD(4),JJD(5),JJD(6),JJD(7),JJD(8),FF(1),
 FF(2),FF(3),FF(4),FF(5),FF(6),FF(7),FF(8),FF(9),NDIR,L,DCPLG,IP)
** SUBROUTINE 'BOXTORK' CALCULATES DYNAMIC TORQUES AT ALL GEAR MESHES IN
   BOX NO. IB DUE TO A DYNAMIC LOAD IN BOX NO. NB .
   A RUNNING TOTAL IS KEPT OF  LOADS FOR EACH POSITION
CALL BOXTORK(NDIR,IB)
NL1 = NL1-1
IB=IB-1
GO TO 1510
NDIR = 2
IP = 2
NL2 = NBM-NB
** WHEN DYNAMIC TORQUE FLOW HAS BEEN TRACED TO THE BEGINING  OF BOX NO. 1
   ATTENTION IS SWITCHED TO BOX NO. IB = NB + 1 FOR FLOW TOWARDS THE TAIL
```

```
      IB = NB+1
 1540 IF (IB .GT. NBM) GO TO 1560
      K(100) = RHK(IB)
      L = 1
C ***** DYNAMIC STIFFNESSES FOR FLOW TOWARDS THE TAIL END OF BOX IB ARE
C       COMPUTED BY MEANS OF SUBROUTINE 'CROSSBOX'. TORQUE FLOW IS TRACED TO
C       THE EXTREME OF BOX NO. NBM
C *** FLOW DIRECTION IS REVERSED BY SUPPLYING LAYSHAFT DATA IN REVERSE ORDER
 1550 CALL CROSSBOX(JJ(8),JJ(7),JJ(6),JJ(5),JJ(4),JJ(3),JJ(2),JJ(1),
     1 JJD(8),JJD(7),JJD(6),JJD(5),JJD(4),JJD(3),JJD(2),JJD(1),FF(9),
     2 FF(8),FF(7),FF(6),FF(5),FF(4),FF(3),FF(2),FF(1),NDIR,L,DCPLG,IP)
      CALL BOXTORK(NDIR,IB)
      NL2 = NL2-1
      IB = IB+1
      GO TO 1540
 1560 CONTINUE
 1600 CONTINUE
 1610 CONTINUE
 1620 CONTINUE
      WRITE(2,1140)
      DO 1650 IB=1,NBM
      WRITE(2,1145)
      DO 1640 IDR=1,6
C ***** THE MODULUS OF EACH DYNAMIC LOAD VECTOR IS DETERMINED FROM THE COMPLEX
C       FORM
      TD(IB,IDR) = CABS(TCPX(IB,IDR))
C *** PHASE ANGLE OF EACH DYNAMIC LOAD VECTOR IS DETERMINED FROM COMPLEX FORM
      PHI(IB,IDR) = ACOS(REAL(TCPX(IB,IDR))/TD(IB,IDR))*180./PI
      TIM = AIMAG(TCPX(IB,IDR))
      IF (TIM .GE. 0.) GO TO 1630
      PHI(IB,IDR) = -PHI(IB,IDR)
 1630 CONTINUE
C ***** ALL RESULTS ARE WRITTEN ONTO MAGNETIC TAPE FOR SUBSEQUENT USE BY GRAPH
C       PLOTTING COMPUTER PROGRAMS
      WRITE(4)TD(IB,IDR)
C ***** DYNAMIC LOAD VECTORS ARE OUTPUT IN PRINT
      WRITE(2,1150) TD(IB,IDR),PHI(IB,IDR)
 1640 CONTINUE
 1650 CONTINUE
 1660 CONTINUE
      STOP
      END
```

Appendix D

Computer Subroutine Crossbox

```
      SUBROUTINE CROSSBOX (B1,B2,B3,B4,B5,B6,B7,B8,D1,D2,D3,D4,D5,D6,D7,
     1 D8,H1,H2,H3,H4,H5,H6,H7,H8,H9,NDIR,L,DCPLG,IP)
C *****  SUBROUTINE 'CROSSBOX' IS USED FOR DYNAMIC STIFFNESS TRANSFERS IN EITHER
C        DIRECTION ACROSS A COMPLETE DRAWBOX. IT CALCULATES THE TOTAL DYNAMIC
C        STIFFNESS ATTACHED TO  EITHER THE HEADSTOCK END OR THE TAIL END OF ALL
C        DRAWBOXES. SYSTEM REFERENCE POSITIONS ARE COMPATIBLE WITH
C        THE APPROPRIATE DYNAMIC STIFFNESS ANALYSIS DIAGRAM.
C *** THE FOLLOWING MUST BE SUPPLIED IN THE SUBROUTINE CALL STATEMENT :
C
C       B1-B8  -  LAYSHAFT STATION INERTIAS RELATED TO DRAWROLL SPEED
C
C       D1-D8  -  LAYSHAFT STATION DAMPING COEFFICIENTS
C
C       H1-H9  -  LAYSHAFT SECTION FLEXIBILITIES RELATED TO DRAWROLL SPEED
C
C       NDIR  -  DIRECTION CONTROL. FACTOR. IF NDIR = 1 , THE SUBROUTINE WORKS
C                FROM HEADSTOCK END TO TAIL END THEREBY COMPUTING, IN EACH CASE,
C                DYNAMIC STIFFNESS (LHK) ATTACHED TO HEADSTOCK END OF THE NEXT
C                BOX  IF NDIR = 2 , THE DIRECTION OF OPERATION IS REVERSED AND
C                THE DYNAMIC STIFFNESS AT THE TAIL END OF EACH BOX IS COMPUTED
C                (RHK)
C
C       L  -  LOOP CONTROL FACTOR
C
C       DCPLG  -  DAMPING COEFFICIENT OF BOX COUPLING
C
C       IP  -   CONTROL FACTOR. IP = 1 FOR NORMAL USE BUT IP = 2 WHEN DYNAMIC
C               STIFFNESSES ARE REQUIRED FOR ONLY A SINGLE DRAWBOX WITHIN A MULTI-
C               BOX MACHINE (EG. FOR USE WITH SUBROUTINE 'BOXTORK')
C
C *** SPECIFY COMPLEX VARIABLES AND RESERVE SPACE FOR COMPLEX ARRAYS
      COMPLEX JAY,JW,K(250),F(250),RHK(15),RHF(15),LHK(15),LHF(15)
C *** IDENTIFY VARIABLES COMMON TO SUBROUTINE AND CALLING SEGMENT
      COMMON/CROSSTOP/JAY,JW,W2,F,RHK,RHF,LHK,LHF,SRAT2,NBM
     1/STIFFNESS/K
      AK250 = CABS(K(250))
      IF (NDIR .EQ. 2) GO TO 9010
      IF    (L.NE.1) GO TO 9020
      IF (IP .EQ. 2) GO TO 9005
C *** ATTACH HEADSTOCK/DRIVE SYSTEM DYNAMIC STIFFNESS TO BOX NO. 1
      LHK(1),K(155) = K(250)
      IF ( AK250 .EQ. 0.0 ) GO TO 9035
      GO TO 9030
 9005 K(155) = K(250)
      IF ( AK250 .EQ. 0.0 ) GO TO 9035
      GO TO 9030
 9010 IF (L.NE.1) GO TO 9020
      IF (IP  EQ  2) GO TO 9015
C *** SET DYNAMIC STIFFNESS OF EXTREME TAIL END OF LAYSHAFT IN BOX NO. NBM EQUAL
C     TO ZERO
      K(153),RHK(NBM) = (0.0,0.0)
      GO TO 9040
 9015 K(153) = K(100)
      GO TO 9040
 9020 K(155)=K(101)
 9030 F(154)=1./K(155)
      K(154) = 1./F(154)
      F(153) = F(154) + 1./(1./H1 + JW*DCPLG)
      K(153) = 1./F(153)
      GO TO 9040
 9035 K(153) = (0.0,0.0)
```

```
9040 K(150)=K(153)+JW*D1-W2*B1
     K(149)=1./(1./K(150)+H2)
     K(146)=K(140)+K(108)*JW*D2-W2*B2
     K(145)=1./(1./K(146)+H3)
     K(142)=K(145)+K(108)*JW*D3-W2*B3
     K(141)=1./(1./K(142)+H4)
     K(138)=K(141)+K(108)+JW*D4-W2*B4
     K(137)=1./(1./K(138)+H5)
     K(134)=K(137)+K(108)*JW*D5-W2*B5
     K(133)=1./(1./K(134)+H6)
     K(130)=K(133)+K(108)*JW*D6-W2*B6
     K(129)=1./(1./ K(130)+H7)
     K(105)=K(129)+K(108)*JW*D7-W2*B7
     K(104)=1./(1./ K(105)+H8)
     K(101)=K(104)+JW*D8-W2*B8
     IF (IP .EQ. 2) GO TO 9060
     IF (NDIR .EQ. 2) GO TO 9050
     LHK(L+1)=K(101)
     GO TO 9060
9050 RHK(NBM-L)=K(101)
9060 CONTINUE
C *** RETURN TO MAIN PROGRAM OR CALLING SUBROUTINE
     RETURN
     END
```

Computer Subroutine Boxtork

```
      SUBROUTINE BOXTORK(NDIR,IB)
C ***** SUBROUTINE 'BOXTORK' COMPUTES DYNAMIC TORQUES AT EVERY PARALLEL AXIS
C       GEAR MESH DUE TO PERIODIC LAYSHAFT DISPLACEMENT INDUCED BY TORQUE FLOW
C       THROUGH AN ADJOINING DRAWBOX. SYSTEM REFERENCE POSITIONS ARE COMPATIBLE
C       WITH THE APPROPRIATE DYNAMIC STIFFNESS ANALYSIS DIAGRAM
C *** THE FOLLOWING MUST BE SUPPLIED IN THE SUBROUTINE CALL STATEMENT :
C
C      NDIR  -  DIRECTION CONTROL FACTOR  NDIR = 1 FOR TORQUE FLOW TOWARDS
C               HEADSTOCK AND NDIR = 2 FOR TORQUE FLOW TOWARDS TAIL END
C
C      IB  -  NUMBER OF DRAWBOX IN WHICH INDUCED TORQUE RESPONSE (TO EXCITATION
C             IN BOX NO. NB) IS REQUIRED
C
C *** SPECIFY COMPLEX VARIABLES AND RESERVE SPACE FOR COMPLEX ARRAYS
      COMPLEX X(250),Q(250),T(250),TCPX(10,6)
C *** RESERVE SPACE FOR ARRAYS
      DIMENSION TD(10,6),PHI(10,6)
C *** IDENTIFY VARIABLES COMMON TO SUBROUTINE AND CALLING SEGMENT
      COMMON /STIFFNESS/K/DFFLN/Q/POLAR/TCPX
      PI = 3.141593
      IF (NDIR .EQ. 2) GO TO 8010
      Q(101) = Q(187)
      GO TO 8020
 8010 Q(101) = Q(161)
 8020 T(104) = K(104)*Q(101)
      Q(105) = T(104)/K(105)
      T(108) = K(108)*Q(105)
      Q(113) = T(108)/K(113)
      T(114) = K(114)*Q(113)
      IF (NDIR .EQ. 2) GO TO 8030
      TCPX(IB,6) = T(114) + TCPX(IB,6)
      GO TO 8032
 8030 TCPX(IB,1) = T(114) + TCPX(IB,1)
 8032 T(129) = K(129)*Q(105)
      Q(130) = T(129)/K(130)
      T(108) = K(108)*Q(130)
      Q(113) = T(108)/K(113)
      T(114) = K(114)*Q(113)
      IF (NDIR .EQ. 2) GO TO 8034
      TCPX(IB,5) = T(114) + TCPX(IB,5)
      GO TO 8036
 8034 TCPX(IB,2) = T(114) + TCPX(IB,2)
 8036 T(133) = K(133)*Q(130)
      Q(134) = T(133)/K(134)
      T(108) = K(108)*Q(134)
      Q(113) = T(108)/K(113)
      T(114) = K(114)*Q(113)
      IF (NDIR .EQ. 2) GO TO 8038
      TCPX(IB,4) = T(114) + TCPX(IB,4)
      GO TO 8040
 8038 TCPX(IB,3) = T(114) + TCPX(IB,3)
 8040 T(137) = K(137)*Q(134)
      Q(138) = T(137)/K(138)
      T(108) = K(108)*Q(138)
      Q(113) = T(108)/K(113)
      T(114) = K(114)*Q(113)
      IF (NDIR .EQ. 2) GO TO 8042
      TCPX(IB,3) = T(114) + TCPX(IB,3)
      GO TO 8044
 8042 TCPX(IB,4) = T(114) + TCPX(IB,4)
 8044 T(141) = K(141)*Q(138)
```

```
      Q(142) = T(141)/K(142)
      T(108) = K(108)*Q(142)
      Q(113) = T(108)/K(113)
      T(114) = K(114)*Q(113)
      IF (NDIR .EQ. 2) GO TO 8046
      TCPX(IB,2) = T(114) + TCPX(IB,2)
      GO TO 8048
 8046 TCPX(IB,5) = T(114) + TCPX(IB,5)
 8048 T(145) = K(145)*Q(142)
      Q(146) = T(145)/K(146)
      T(108) = K(108)*Q(146)
      Q(113) = T(108)/K(113)
      T(114) = K(114)*Q(113)
      IF (NDIR .EQ. 2) GO TO 8050
      TCPX(IB,1) = T(114) + TCPX(IB,1)
      GO TO 8052
 8050 TCPX(IB,6) = T(114) + TCPX(IB,6)
 8052 T(149) = K(149)*Q(146)
      Q(150) = T(149)/K(150)
      T(153) = K(153)*Q(150)
      Q(154) = T(153)/K(154)
      IF (NDIR .EQ. 2) GO TO 8080
      Q(187) = Q(154)
      GO TO 8082
 8080 Q(161) = Q(154)
 8082 CONTINUE
C *** RETURN TO MAIN PROGRAM
      RETURN
      END
```

Appendix F

Computer Subroutine MDT2 Drive

```
      SUBROUTINE MDT2 DRIVE(DS,SR4,SS,DR,NG21,NG2,AJ1)
C *****  SUBROUTINE 'MDT 2 DRIVE' COMPUTES THE TOTAL DYNAMIC STIFFNESS  OF
C        A POLYAMIDE DRAWTWISTER HEADSTOCK SYSTEM. THIS IS CONSIDERED AS A PURE
C        INERTIA SYSTEM ACCORDING TO  PLATT DRG. NO. MDT.22/34
C *** THF FOLLOWING MUST BE SUPPLIED IN THE SUBROUTINE CALL STATEMENT :-
C
C       DS  -  DRAWSPEED (FT./MIN.)
C
C       SR4  -  SPEED RATIO BETWEEN PULLEYS 'A' AND 'B' ( DRG. MDT.22/34 )
C
C       SS  -  SPINDLE SPEED (R.P.M.)
C
C       DR  -  DRAWRATIO
C
C       NG21  -  NO. OF TEETH ON GEAR 'N' ( DRG. MDT 22/34 )
C
C       NG2  -  NO OF TEETH ON GEAR 'H'  (   ''   ''   ''  )
C
C       AJ1  -  INERTIA OF HALF COUPLING
C
C *** IDENTIFY COMPLEX VARIABLES AND RESERVE SPACE FOR COMPLEX ARRAYS
      COMPLEX JAY,K(250),F(250),RHK(15),RHF(15),LHK(15),LHF(15),FD10,
     1 FD11,JW,CDUM
C *** IDENTIFY REAL VARIABLES AND RESERVE SPACE FOR REAL (AND ASSUMED REAL)
C     VARIABLES
      REAL JJ(12),JJD(12),NG(50),NG21,NG2,NT
      DIMENSION SR(25),SR2(25),HJ(50),HJS(50),MT(50)
C *** IDENTIFY VARIABLES COMMON TO SUBROUTINE AND CALLING SEGMENT
      COMMON/CROSSTOP/JAY,JW,W2,F,RHK,RHF,LHK,LHF,SRAT2,NBM
     1/STIFFNESS/K/TMATJ/AJG,DIAP
C *** SPECIFY FIXED GEAR TOOTH NUMBERS
      DATA NG(6),NG(5),NG(24),NG(23),NG(22),NG(10),NG(11)/ 67.,82.,82.,
     1 81. ,83. ,86. ,55. /
C *** SPECIFY FIXED INERTIA VALUES
      DATA HJMOT,HJ(9),HJ(7),HJ(14),HJ(16) / 6.5,2*.4840,2*.0451 /
      DATA HJ(8),HJ(15) / 2*0.0 /
C *** SPECIFY SHAFT AND ASSOCIATED INERTIAS
      DATA HJS(26),HJS(30),HJS(1),HJS(6),HJS(13),HJS(23)/2*.0872,.1269,
     1 .0294,.1238,.0047 /
      DATA HJS(4),HJS(12),HJS(21),HJS(24),HJS(28) / 5*.0141 /
      DATA HJS(2),HJS(3),HJS(5),HJS(10),HJS(11),HJS(22),HJS(25),HJS(29)
     1 / 8*0.0 /
      PI = 3.14159
      SRAT = 1.48
      NG(28) = NG(24)
C *** COMPUTE INERTIA VALUES FOR TAPESHAFT, SPINDLE AND FEEDROLL SYSTEMS
      HJ(17) = 0.7792*NBM
      HJ(18) = 0.0939*NBM
      HJ(27),HJ(31) = 0.2696*NBM
C *** ESTABLISH ALL REMAINING GEAR TOOTH NUMBERS AND SHAFT SPEED RATIOS FROM
C     OPERATING CONDITIONS AND RELATIONSHIPS GIVEN IN PLATT DRG.NO.MDT.22/34
      SR(13) = NG(28)/NG(22)
      SR(4) = SR4
      NG(21) = NG21
      NG(2) = NG2
      SR(9) = NG(21)/NG(2)
      SR(3) = NG(6)/NG(5)
      SR(11) = NG(24)/NG(23)
      SR(10) = NG(23)/NG(22)
      SR(5) = NG(11)/NG(10)
      SR(2),SR(7) = 1.0
```

```
      NG(4) = NG(5)
      SR(8) = 2.125/9.0
      SR(14),SR(12) = (DR*(3.25/5.0))/(SRAT*SR(11)*SR(10)*SR(9))
      NG(25),NG(29) = 167.0/(1. + SR(12))
      NG(26),NG(30) = 167.0 - NG(25)
      SR(1) = 12.*DS/(1450.*5.0*PI*SRAT*SR(3)*SR(4))
      NG(1) = 150.0/(1.0 + SR(1))
      NG(3) = 150.0 - NG(1)
      SR(6) = 1450.*SR(8)*SR(4)/(SS*SR(5)*SR(7))
      NG(12) = 109.0/(1. + SR(6))
      NG(13) = 109.0 - NG(12)
C *** COMPUTE THE SQUARE OF ALL SPEED RATIOS
      DO 4100 N=1,14
      SR2(N) = SR(N)*SR(N)
 4100 CONTINUE
C *** IDENTIFY THE MATERIAL TYPE FOR HEADSTOCK FIXED GEARS.(IF MT = 1 , THE
C     MATERIAL IS CAST IRON ! IF MT = 2 , THE MATERIAL IS TUFNOL)
      MT(11),MT(5),MT(22),MT(24),MT(2) = 1
      MT(10),MT(6),MT(4),MT(23),MT(28) = 2
C *** ESTABLISH THE MATERIAL TYPE FOR CHANGE GEARS ACCORDING TO GEAR SIZE
C     RELATIONSHIPS GIVEN IN PLATT DRG. NO. MDT. 22/38
      IF(NG(12) .GE. 55.) GO TO 4110
      MT(12) = 1
      MT(13) = 2
      GO TO 4120
 4110 MT(12) = 2
      MT(13) = 1
 4120 CONTINUE
      IF(NG(3) .GE. 76.) GO TO 4130
      MT(3) = 1
      MT(1) = 2
      GO TO 4140
 4130 MT(3) = 2
      MT(1) = 1
 4140 CONTINUE
      IF(NG(25) .GE. 84.) GO TO 4150
      MT(25),MT(29) = 1
      MT(26),MT(30) = 2
      GO TO 4160
 4150 MT(25),MT(29) = 2
      MT(26),MT(30) = 1
 4160 CONTINUE
C *** COMPUTE ALL GEAR INERTIAS BY MEANS OF SUBROUTINE 'GEARDATA'
      DO 4170 N=1,6
      NT = NG(N)
      MAT = MT(N)
      CALL GEARDATA(NT,MAT)
      HJ(N) = AJG + HJS(N)
 4170 CONTINUE
      DO 4180 N=10,13
      NT = NG(N)
      MAT = MT(N)
      CALL GEARDATA(NT,MAT)
      HJ(N) = AJG + HJS(N)
 4180 CONTINUE
      DO 4190 N=21,26
      NT = NG(N)
      MAT = MT(N)
      CALL GEARDATA(NT,MAT)
      HJ(N) = AJG + HJS(N)
 4190 CONTINUE
      HJ(28) = HJ(24)
```

```
      HJ(29) = HJ(25)
      HJ(30) = HJ(26)
C *** COMPUTE EQUIVALENT INERTIA OF HEADSTOCK SYSTEM WITH RESPECT TO DRAWROLL
C     SPEED
      HAJL = HJ(18)/SR2(8) + HJ(17) + HJ(16)
      HAJ1 = HAJL/SR2(7) + HJ(15) + HJ(13) + HJ(14)
      AJL1 = HAJL/SR2(6) + HJ(12) + HJ(11)
      AJL2 = (HJMOT + HJ(9))/SR2(4)
      HAJL = AJL1/SR2(5) + HJ(10) + HJ(6) + HJ(7) + HJ(8) + AJL2
      HAJL = (HAJL/SR2(3) + HJ(5))/SR2(2) + HJ(4) + HJ(3)
      AJL3 = HAJL/SR2(1) + HJ(1) + HJ(2)
      HAJL = 2.*((HJ(27) + HJ(26))/SR2(12) + HJ(25) + HJ(24))
      HAJL = (HAJL + HJ(23)/SR2(11))/SR2(10) + HJ(22) + HJ(21)
      HAJL = HAJL/SR2(9) + AJL3 + AJ1
C *** COMPUTE HEADSTOCK DYNAMIC STIFFNESS BASED ON AN EQIVALENT INERTIA
      K(250) = CMPLX(-W2*HAJL/SRAT2,0.0)
C *** RETURN TO MAIN PROGRAM
      RETURN
      END
```

Appendix G

Computer Subroutine MDT3 Drive

```
      SUBROUTINE MDT3 DRIVE(DS,NG4,NG5,SS,HDR,CDR,NG28,NG29,AJ1)
C *****  SUBROUTINE 'MDT 3 DRIVE' COMPUTES THE TOTAL DYNAMIC STIFFNESS OF  A
C        POLYESTER DRAWTWISTER HEADSTOCK SYSTEM. THIS IS CONSIDERED AS A PURE
C        INERTIA SYSTEM ACCORDING TO PLATT DRG. NO. MDT.32/114
C        UPPER DRAWBOXES ARE MODELLED IN THE SAME WAY AS LOWER DRAWBOXES
C *** THE FOLLOWING MUST BE SUPPLIED IN THE SUBROUTINE CALL STATEMENT :-
C
C       DS  -  DRAWSPEED (FT./MIN.)
C
C       NG4  -  NO. OF TEETH ON GEAR 'H' ( DRG. NO. MDT. 32/114 )
C
C       NG5  -  NO OF TEETH ON GEAR 'G'
C
C       SS  -  SPINDLE SPEED (R.P.M.)
C
C       HDR  -  HOT DRAW RATIO
C
C       CDR  -  COLD DRAW RATIO
C
C       NG28  -  NO. OF TEETH ON GEAR 'S'
C
C       NG29  -  NO. OF TEETH ON GEAR 'T'
C
C       AJ1  -  INERTIA OF HALF COUPLING
C
C *** IDENTIFY COMPLEX VARIABLES AND RESERVE SPACE FOR COMPLEX ARRAYS
      COMPLEX JAY,K(250),F(250),RHK(15),RHF(15),LHK(15),LHF(15),FD10,
     1 FD11,JW,CDUH,KHL
C *** IDENTIFY REAL VARIABLES AND RESERVE SPACE FOR REAL (AND ASSUMED REAL)
C     VARIABLES
      REAL JJ(12),JJD(12),NG(50),NT,NG4,NG5,NG28,NG29
      DIMENSION SR(25),SR2(25),HJ(50),HJS(50),MT(50),FF(12)
C *** IDENTIFY VARIABLES COMMON TO SUBROUTINE AND CALLING SEGMENT
      COMMON/CROSSTOP/JAY,JW,W2,F,RHK,RHF,LHK,LHF,SRAT2,NBM
     1 /STIFFNESS/K/TMATJ/AJG,DIAP
C *** SPECIFY FIXED GEAR TOOTH NUMBERS
      DATA NG(6),NG(10),NG(1),NG(21),NG(22),NG(26),NG(27),NG(30),NG(31)/
     1  87.0,70.0,49.0,107.0,96.0,58.0,111.0,2*74.0/
C *** SPECIFY FIXED INERTIA VALUES
      DATA HJMOT,HJ(7),HJ(9),HJ(13),HJ(15)/8.0,2*.4840,2*.0451/
      DATA HJ(8),HJ(14),HJ(23) / 3*0.0 /
C *** SPECIFY SHAFT AND ASSOCIATED INERTIAS
      DATA HJS(1),HJS(5),HJS(12),HJS(21),HJS(22),HJS(28),HJS(33),HJS(36)
     1 /.1270,.0294,.1238,.0047,.0294,.1237,.0872,.0872/
      DATA HJS(3),HJS(10),HJS(26),HJS(30),HJS(31),HJS(34) / 6*.0141/
      DATA HJS(2),HJS(4),HJS(6),HJS(11),HJS(24),HJS(25),HJS(27),HJS(29),
     1 HJS(32),HJS(35) / 10*0.0 /
      DATA DXBSH,DCPLG / 0.0,5.0 /
      PI = 3.14159
      SRAT = 1.45
      SRTDR = 1.45
C *** COMPUTE INERTIA VALUES FOR TAPESHAFT, SPINDLE AND FEEDROLL SYSTEMS
      HJ(16) = 0.7792*NBM
      HJ(17) = 0.0939*NBM
      HJ(37) = 0.2696*NBM
      HJ(38) = HJ(37)
      NG(4) = NG4
      NG(5) = NG5
      NG(28) = NG28
      NG(29) = NG29
C *** ESTABLISH ALL REMAINING GEAR TOOTH NUMBERS AND SHAFT SPEED RATIOS FROM
```

```
C       OPERATING CONDITIONS AND RELATIONSHIPS GIVEN IN PLATT DRG.NO.MDT.32/114
        SR(4) = NG(10)/NG(6)
        SR(8) = NG(21)/NG(1)
        SR(9) = NG(22)/NG(21)
        SR(17) = NG(27)/NG(26)
        SR(16) = NG(31)/NG(30)
        SR(3),SR(6) = 1.0
        SR(7) = 2.125/9.0
        SR(2) = NG(5)/NG(4)
        NG(34) = NG(29)
        SR(1) = 12.*DS/(1450.*5.001*PI*SR(2)*SR(3)*SRAT)
        NG(2) = 138./(1. + SR(1))
        NG(3) = 138. - NG(2)
        SR(5) = 1450./(SS*SR(7)*SR(4))
        NG(11) = 145./(1. + SR(5))
        NG(12) = 145. - NG(11)
        SR(11) = HDR*(4.9905/5.001)/(SR(12)*SR(8)*SR(9))
        NG(24) = 169./(1. + SR(11))
        NG(25) = 169. - NG(24)
        SR(18),SR(15) = NG(29)/NG(28)
        SR(14),SR(17) = CDR*(3.25/4.9905)/(SRAT*SR(13))
        NG(32),NG(35) = 122./(1. + SR(14))
        NG(33),NG(36) = 122. - NG(32)
C ***   COMPUTE THE SQUARE OF ALL SPEED RATIOS
        DO 5100 N=1,17
        SR2(N) = SR(N)*SR(N)
 5100   CONTINUE
C ***   IDENTIFY THE MATERIAL TYPE FOR HEADSTOCK FIXED GEARS.(IF MT = 1 , THE
C       MATERIAL IS CAST IRON ; IF MT = 2 , THE MATERIAL IS TUFNOL)
        MT(1),MT(5),MT(10),MT(22),MT(26),MT(29),MT(30),MT(33),MT(34),MT(3
       16) = 1
        MT(4),MT(6),MT(21),MT(27),MT(28),MT(31),MT(32),MT(35) = 2
C ***   ESTABLISH THE MATERIAL TYPE FOR CHANGE GEARS ACCORDING TO GEAR SIZE
C       RELATIONSHIPS GIVEN IN PLATT DRG. NO. MDT. 32/109
        IF (NG(11) .GE. 73.0) GO TO 5110
        MT(11) = 1
        MT(12) = 2
        GO TO 5120
 5110   MT(11) = 2
        MT(12) = 1
 5120   CONTINUE
        IF (NG(3) .GE. 70.0) GO TO 5130
        MT(3) = 1
        MT(2) = 2
        GO TO 5140
 5130   MT(3) = 2
        MT(2) = 1
 5140   CONTINUE
        IF (NG(24) .GE. 86.0) GO TO 5150
        MT(24) = 1
        MT(25) = 2
        GO TO 5160
 5150   MT(24) = 2
        MT(25) = 1
 5160   CONTINUE
C ***   COMPUTE ALL GEAR INERTIAS BY MEANS OF SUBROUTINE 'GEARDATA'
        DO 5170 N=1.6
        NT = NG(N)
        MAT = MT(N)
        CALL GEARDATA(NT,MAT)
        HJ(N) = AJG + HJS(N)
 5170   CONTINUE
```

```
      DO 5180 N = 10,12
      NT = NG(N)
      MAT = MT(N)
      CALL GEARDATA(NT,MAT)
      HJ(N) = AJG + HJS(N)
5180  CONTINUE
      DO 5190 N = 21,22
      NT = NG(N)
      MAT = MT(N)
      CALL GEARDATA(NT,MAT)
      HJ(N) = AJG + HJS(N)
5190  CONTINUE
      DO 5200 N = 24,36
      NT = NG(N)
      MAT = MT(N)
      CALL GEARDATA(NT,MAT)
      HJ(N) = AJG + HJS(N)
5200  CONTINUE
C ***  COMPUTE EQUIVALENT INERTIA OF BRANCHED SYSTEMS
      HAJL = HJ(17)/SR2(7) + HJ(16) + HJ(15)                          DUMMY V
      HAJL = HAJL/SR2(6) + HJ(14) + HJ(13) + HJ(12)
      AJL1 = HAJL/SR2(5) + HJ(11) + HJ(10)
      AJL2 = (HJMOT + HJ(9))/SR2(3)
      HAJL = AJL1/SR2(4) + AJL2 + HJ(8) + HJ(7) + HJ(6) + HJ(5)
      HAJL = HAJL/SR2(2) + HJ(4) + HJ(3)
      AJL3 = HAJL/SR2(1) + HJ(2) + HJ(1)
      HAJL = (HJ(38) + HJ(33))/SR2(17) + HJ(32) + HJ(31)
      HAJL = (HAJL/SR2(16) + HJ(30) + HJ(29))/SR2(15) + HJ(28) + HJ(27)
      HAJL = HAJL + ((HJ(37) + HJ(36))/SR2(14) + HJ(35)+HJ(34))/SR2(13)
      K(250) = (0.0000000001,0.0)
      NDIR = 1
      IP = 1
C ***  USE SUBROUTINE 'CROSSBOX' TO COMPUTE THE DYNAMIC STIFFNESS OF UPPER
C      DRAWBOXES (MODELLED IN THE SAME WAY AS LOWER BOXES)
      DO 5210 L = 1,NBM
5210  CALL CROSSBOX (JJ(1),JJ(2),JJ(3),JJ(4),JJ(5),JJ(6),JJ(7),JJ(8),
     1 JJD(1),JJD(2),JJD(3),JJD(4),JJD(5),JJD(6),JJD(7),JJD(8),FF(1),
     2 FF(2),FF(3),FF(4),FF(5),FF(6),FF(7),FF(8),FF(9),NDIR,L,DCPLG,IP)
C ***  PROCEED TO SHAFT COUPLING WITH LOWER DRAWBOXES TO CALCULATE TOTAL DYNAMIC
C      STIFFNESS OF HEADSTOCK WITH RESPECT TO DRAWROLL SPEED
      KHL = LHK(NBM+1) + CMPLX(-W2*HAJL,0.0)
      KHL = KHL/SR2(12) + CMPLX(-W2*(HJ(26) + HJ(25)),0.0)
      KHL = KHL/SR2(11) + CMPLX(-W2*(HJ(24) + HJ(23) + HJ(22)),0.0)
      KHL = (KHL/SR2(9) + CMPLX(-W2*HJ(21),0.0))/SR2(8)
      KHL = KHL + CMPLX(-W2*(AJL3 + AJ1),0.0)
      K(250) = KHL/SRAT2
C ***  RETURN TO MAIN PROGRAM
      RETURN
      END
```

Appendix H

Computer Subroutine VS Drive

```
      SUBROUTINE VS DRIVE(REV,SRAT,AJ1)
C***** SUBROUTINE 'V S DRIVE' COMPUTES THE DYNAMIC STIFFNESS OF THE VARIABLE
        SPEED DRIVE ARRANGEMENT EMPLOYED IN THE MULTI-BOX EXPERIMENTAL RIG
        DESCRIBED IN THE TEXT. PERFORMANCE TESTS WERE UNDERTAKEN TO
        ESTABLISH MAIN MOTOR OUTPUT SPEED FOR VARIOUS RUNNING CONDITIONS.
        COMPONENT INERTIA VALUES AND RELATIVE SPEED RELATIONSHIPS WERE DERIVED
        FROM DRAWINGS OF THE VARIABLE SPEED UNIT

C*** THE FOLLOWING MUST BE SUPPLIED IN THE SUBROUTINE CALL STATEMENT :-

      REV - DRAWROLL SPEED (R.P.M.)

      SRAT - SPEED RATIO OF CROSSED HELICAL MESH ( = 29/20 FOR MDT.2 & MDT.3)

      AJ1 - INERTIA OF HALF COUPLING

C*** SPECIFY COMPLEX VARIABLES & RESERVE SPACE FOR COMPLEX ARRAYS
      COMPLEX K(250),F(250),RHK(15),RHF(15),LHK(15),LHF(15),JAY,JW
C*** RESERVE SPACE FOR REAL ARRAY
      DIMENSION AJV(10)
C*** IDENTIFY VARIABLES COMMON TO SUBROUTINE AND CALLING SEGMENT
      COMMON/CROSTOP/JAY,JW,W2,F,RHK,RHF,LHK,LHF,SRAT2,NBH
     1/STIFFNESS/K
C*** SPECIFY DRIVE COMPONENT INERTIAS
      DATA AJM,AJV(1),AJV(2),AJV(3),AJV(4)/.470,.0348,.03672,.314,.0348/
C*** COMPUTE REDUCTION RATIOS OF DRIVE SYSTEM ROTATING COMPONENTS
      REVLS = REV/SRAT
      REVMOT = 1510 -.016*REV
C*** (MOTOR SPEED RELATIONSHIP DERIVED FROM PERFORMANCE TESTS)
      VSRAT = REVLS/REVMOT
      VSRAT2 = VSRAT*VSRAT
      DDBO =1.414*VSRAT*2.7559/(VSRAT+1.)/(SQRT(1.+((VSRAT-1.)/(VSRAT+1.
     1))**2))
      RATDB = DDBO/4.750
      RATDB2 = RATDB*RATDB
      REVRR = 522.2 + 539.0*VSRAT
      RATRR = REVLS/REVRR
      RATRR2 = RATRR*RATRR
C*** COMPUTE EQUIVALENT INERTIA OF VARIABLE SPEED DRIVE UNIT
      AJVSD = AJV(1)+AJV(2)/RATDB2+AJV(3)/RATRR2+AJV(4)/VSRAT2
      AJVS1 = AJVSD*32.2*12.
C*** COMPUTE DYNAMIC STIFFNESS OF COMPLETE VARIABLE SPEED DRIVE SYSTEM
      K(241) = CMPLX(-W2*(AJM + AJ1)/(VSRAT2*SRAT2),0.0)
      FFF1 = 1./840000.
C***** FFF1 = FLEXIBILITY OF COUPLING BETWEEN V.S.D. UNIT AND MOTOR
C***** FFF1 IS EQUAL TO STANDARD COUPLING FLEXIBILITY ******
      F(242) = 1./K(241) + (FFF1*VSRAT2)
      K(242) = 1./F(242)
      K(250) = K(242)+CMPLX(-W2*((AJVSD + AJ1/VSRAT2)+AJ1)/SRAT2,0.0)
C*** RETURN TO MAIN PROGRAM
      RETURN
      END
```

Appendix I

Computer Subroutine Geardata

```
      SUBROUTINE GEARDATA(NT,MAT)
C ***** SUBROUTINE GEARDATA CALCULATES THE INERTIA VALUES OF COMPONENT GEARS,
      EMPLOYED IN THE DRAWTWISTER HEADSTOCK,ACCORDING TO PLATT DRG.
       NO. MDT. 22/559-599
C ** THE FOLLOWING MUST BE SUPPLIED IN THE SUBROUTINE CALL STATEMENT :-

      NT  -  NUMBER OF TEETH ON GEAR

      MAT -  MATERIAL TYPE FACTOR (IE. MAT = 1 FOR CAST IRON GEARS AND 2 FOR
             TUFNOL GEARS)

C ** SPECIFY REAL QUANTITIES
      REAL DIAP,NT
C ** IDENTIFY VARIABLES COMMON TO SUBROUTINE AND CALLING SEGMENT
      COMMON /TMATJ/AJG,DIAP
      PI = 3.141593
C ** SPECIFY FIXED GEAR DIMENSIONS
      DIA1 = 3.250
      DIA1 = 1.875
      FW = 2.0625
      TH = 0.375
C * CALCULATE GEAR VARIABLE DIAMETERS
      DIAP = NT*7.981/60.
      DIA2 = DIAP-1.250
C * SPECIFY MATERIAL DENSITIES
      RO1 = .276
      RO2 = 0.054
      DIAP2 = DIAP*DIAP
      DIA12 = DIA1*DIA1
      DIA12 = DIA1*DIA1
      DIA22 = DIA2*DIA2
C * SELECT GEAR DESIGN ACCORDING TO SIZE AND COMPUTE INERTIA VALUE TAKING
      ACCOUNT OF MATERIAL DENSITY
      IF (NT .GT. 52.0) GO TO 620
      IF(MAT .EQ. 2)GO TO 610
      AJG = RO1*FW*PI*(DIAP2*DIA12)*(DIAP2-DIA12)/(32.*32.2*12.)
      GO TO 640
610   AJG = RO2*FW*PI*(DIAP2*DIA12)*(DIAP2-DIA12)/(32.*32.2*12.)
      GO TO 640
620   IF(MAT .EQ. 2)GO TO 630
      AJG = PI*RO1*((DIAP2*DIA22)*(DIAP2-DIA22)*FW+(DIA22*DIA12)*(DIA22-
     1DIA12)*TH+(DIA12*DIA12)*(DIA12-DIA12)*FW)/(32.*32.2*12.)
      GO TO 640
630   AJG = PI*RO2*((DIAP2*DIA22)*(DIAP2-DIA22)*FW+(DIA22*DIA12)*(DIA22-
     2DIA12)*TH+(DIA12*DIA12)*(DIA12-DIA12)*FW)/(32.*32.2*12.)
640   CONTINUE
C * RETURN TO CALLING SUBROUTINE
      RETURN
      END
```

Appendix J

Computer Program Speedplot

```
      MASTER SPEEDPLOT
C *****  SPEEDPLOT PLOTS DYNAMIC LOADS, FOR EVERY MESH, AGAINST OPERATING SPEED.
C        THE PROGRAM IS RUN IN CONJUNCTION WITH 'DT TOTAL ANALYSIS' WHICH FIRST
C        COMPUTES ALL RESULTS AND STORES THEM ON A MAGNETIC TAPE FILE.
C
C *****  RESERVE SPACE FOR ARRAYS
      DIMENSION  Y(61,10,6),X(301),XP(301),YP(301),XH(2),YH(2),XV(2),YV(
     12)
C *****  READ INPUT DATA FROM MAGNETIC TAPE FILE
      READ(4) NMK,MOD
      READ(4) NBM,NDAT
C *****  READ MIN., MAX. AND INCREMENTAL SPEEDS
      READ(4) REVL,REVH,REVI
    9 FORMAT(////15H MACHINE   MDT ,I1,2X,4HMOD ,I3//)
      WRITE(2,9)NMK,MOD
   91 FORMAT(6H NBM  ,I3,8H  NDAT  ,I3)
      WRITE(2,91)NBM,NDAT
  557 FORMAT(//8H REVL = ,F6.0,2X,8H REVH = ,F6.0,2X,8H REVI = ,F4.0/)
      WRITE(2,557) REVL,REVH,REVI
C *****  OPEN GRAPH PLOTTER FACILITY
      CALL UTPOP
C *****  READ , IN SEQUENCE, ALL DRAWROLL SPEEDS AND CORRESPONDING LOADINGS FROM
C          MAGNETIC TAPE FILE
      DO 30 I=1,NDAT
      READ(4) X(I)
      XP(I)=X(I)
      DO 20 J=1,NBM
      DO 10 K=1,6
   10 READ(4) Y(I,J,K)
   20 CONTINUE
   30 CONTINUE
      F = 1.0
      J = NBM
C *****  DRAW A SET OF LOG-LINEAR AXES FOR EACH DRAWBOX
       CALL UTP8A(1000.,4000.,1.,1.E5,6.,9.,XXT,0,YYT,0)
      K = 1
      DO 40 I=1,NDAT
   40 YP(I) = Y(I,J,K)*F
C *****  PLOT THE LOAD-SPEED GRAPH FOR DRAWROLL PAIR NO. 1
      CALL UTP8B(XP,YP,NDAT,2)
C *****  MULTIPLY FACTOR 'F' BY 10 BEFORE PLOTTING CURVE FOR NEXT MESH IN SAME
C        DRAWBOX  (THIS PROVIDES A SPACING FACTOR OF 10 LBF.-IN. BETWEEN ADJACENT
C        MESHES AND ALLOWS RESULTS FOR A COMPLETE GEARBOX TO BE PLOTTED ON ONE
C        SET OF AXES)
   50 F = F*10.
C *****  DRAW GRATING LINES ,ON GRAPH, PARALLEL TO X-AXIS
      XH(1) = 1000.
      XH(2) = 4000.
      YH(1) = 10.
      YH(2) = 10.
      DO 500 I=1,6
      CALL UTP8B(XH,YH,2,3)
      YH(1) = YH(1)*10.
      YH(2)=YH(1)
  500 CONTINUE
C *****  DRAW GRATING LINES ,ON GRAPH, PARALLEL TO Y-AXIS
      XV(1) = 1500.
      XV(2) = 1500.
      YV(1) = 1.0
      YV(2) = 1.E5
      DO 600 I=1,6
```

```
      CALL UTp8B(XV,YV,2,3)
      XV(1) = XV(1) + 500.
      XV(2)=XV(1)
  600 CONTINUE
C *****  SET FACTOR 'F' TO UNITY FOR NEXT DRAWBOX
   70 F = 1.0
C *****  CLOSE GRAPH PLOTTER FACILITY
      CALL UTpCL
C *****  IF PROGRAM RUNS SUCCESSFULLY WRITE ''PLOTTING COMPLETED''
   99 FORMAT(19H PLOTTING COMPLETED)
      WRITE (2,99)
      STOP
      END
```

Appendix K

Computer Program Histoplot

```
      MASTER HISTOPLOT
C *****  HISTOPLOT PLOTS MESH DYNAMIC LOAD DISTRIBUTIONS IN HISTOGRAM FORM FOR
C        ANY PARTICULAR RUNNING SPEED. THE PROGRAM IS RUN IN CONJUNCTION WITH
C        'DT TOTAL ANALYSIS' WHICH FIRST COMPUTES ALL RESULTS AND STORES THEM ON
C        A MAGNETIC TAPE FILE.
C
C *****  RESERVE SPACE FOR ARRAYS
      DIMENSION Y(10,6),XP(300),YP(300)
C *****  READ INPUT DATA FROM MAGNETIC TAPE FILE
      READ(4) NMK,MOD
      READ(4) NBM
      READ(4) NDAT
   10 FORMAT(1H ,//,7H NMK = ,I1,7H MOD = ,I3,7H NBM = ,I2,7H NDAT =,I2)
      WRITE(2,10) NMK,MOD,NBM,NDAT
C *****  OPEN GRAPH PLOTTER FACILITY
      CALL UTPOP
      DO 40 I=1,NDAT
C *****  READ DRAWROLL SPEED FROM MAGNETIC TAPE FILE
   15 READ(4) REV
   20 FORMAT(1H ,//,18H DRAWROLL SPEED = ,F7.1)
      WRITE(2,20) REV
      M=1
      AX1 = .14286
      XP(M) = AX1
      YP(M) = .001
      DO 30 J=1,NBM
      DO 25 K=1,6
C *****  READ ELEMENTS OF DYNAMIC LOAD ARRAY FROM MAGNETIC TAPE FILE
      READ(4) Y(J,K)
C *****  FOR A PARTICULAR SPEED CALCULATE COORDINATES FOR DYNAMIC LOADING
C        HISTOGRAM (EACH INCREMENT ON X-AXIS REPRESENTS ONE DRAWSHAFT MESH AND
C        SPACING  PROVIDED BETWEEN BOXES FOR EASE OF IDENTIFICATION)
C        STORE ALL 'X' AND 'Y' POINTS IN ARRAYS XP AND YP RESPECTIVELY
      YP(M+1),YP(M+2) = Y(J,K)
      XP(M+1) = XP(M)
      XP(M+2) = XP(M) + AX1
   25 M=M+2
      YP(M+1),YP(M+2) = .001
      XP(M+1) = XP(M)
      XP(M+2) = XP(M) + AX1
   30 M=M+2
      NPLOT = NBM+14
C *****  DRAW GRAPH AXES WITH LOGARITHMIC Y-AXIS AND LINEAR X-AXIS
      CALL UTP8A(0.,10.,1.,1.0E4,9.0,5.5,XXXX,0,YYYY,0)
C *****  PLOT HISTOGRAM ON DRAWN AXES BY JOINING ALL COORDINATES BY A STRAIGHT
C        LINE
      CALL UTP8B(XP,YP,NPLOT,3)
C *****  CONTINUE PLOTTING LOOP UNTIL HISTOGRAMS PLOTTED FOR ALL RUNNING
C        CONDITIONS OF INTEREST
   40 CONTINUE
C *****  CLOSE GRAPH PLOTTER FACILITY
      CALL UTPCL
C *****  IF PROGRAM RUNS SUCCESSFULLY WRITE ''PLOTTING COMPLETED''
   45 FORMAT(1H ,20H PLOTTING COMPLETED )
      WRITE(2,45)
      STOP
      END
```

Appendix L

Computer Program Histolimitplus

```
      MASTER HISTOLIMITPLUS
C ***** FOR SEVERAL COMPLETE SETS OF DYNAMIC LOADING RESULTS, HISTOLIMITPLUS
C       PLOTS IN HISTOGRAM FORM I-
C
C       1"  THE MAX  AND MIN. DYNAMIC TORQUE LIMITS OCCURING AT EACH MESH
C
C       2"  THE AVERAGE DYNAMIC TORQUE AT EACH MESH
C
C       THE PROGRAM IS RUN IN CONJUNCTION WITH DT TOTAL ANALYSIS WHICH FIRST
C       COMPUTES ALL RESULTS AND STORES THEM ON A MAGNETIC TAPE FILE
C
C ***** RESERVE SPACE FOR ARRAYS
      DIMENSION Y(10,6),XP(500),YH(10,6),YL(10,6),YpH(300),YpL(300)
      DIMENSION YSUM(10,6),YAV(300)
C ***** READ INPUT DATA FROM MAGNETIC TAPE FILE
      READ(4) NMK,MOD
      READ(4) NBM
      READ(4) NDAT
   10 FORMAT(1H ,//,7H NMK = ,I1,7H MOD = ,I3,7H NBM = ,I2,7H NDAT =,I2)
      WRITE(2,10) NMK,MOD,NBM,NDAT
C ***** OPEN GRAPH PLOTTER FACILITY
      CALL UTPOP
C ***** FOR EACH MESH SET ; MAX. LOAD TO ZERO ; MIN. LOAD TO INFINITY AND
C       AVERAGE LOAD TO ZERO
      DO 30 J=1,NBM
      DO 20 K=1,6
      YH(J,K) = 0.
      YL(J,K) = 1.E50
      YSUM(J,K) = 0.0
   20 CONTINUE
   30 CONTINUE
      DO 70 I=1,NDAT
C ***** READ DRAWROLL SPEED FROM MAGNETIC TAPE FILE
      READ(4) REV
   40 FORMAT(1H ,//,18H DRAWROLL SPEED = ,F7.1)
      WRITE(2,40) REV
      DO 60 J=1,NBM
      DO 60 K=1,6
C ***** READ ELEMENTS OF DYNAMIC LOAD ARRAY FROM MAGNETIC TAPE FILE.
      READ(4) Y(J,K)
C ***** SUM THE DYNAMIC LOADS FOR EACH STATION AND STORE IN ARRAY
      YSUM(J,K) = YSUM(J,K) + Y(J,K)
C ***** FOR EACH POSITION, IF STORED 'MAXIMUM' LOAD IS LESS THAN NEW LOAD,
C       DELETE THE FORMER AND REPLACE IT BY THE LATTER
      IF(YH(J,K).GT.Y(J,K)) GO TO 50
      YH(J,K) = Y(J,K)
C ***** FOR EACH POSITION, IF STORED 'MINIMUM' LOAD IS GREATER THAN NEW LOAD,
C       DELETE THE FORMER AND REPLACE IT BY THE LATTER
   50 IF(YL(J,K).LT.Y(J,K)) GO TO 60
      YL(J,K) = Y(J,K)
   60 CONTINUE
   70 CONTINUE
C ***** CALCULATE COORDINATES FOR HISTOGRAMS OF MAX.,MIN. AND AVERAGE DYNAMIC
C       TORQUES  EACH INCREMENT ON X-AXIS REPRESENTS ONE DRAWSHAFT MESH AND
C       SPACING PROVIDED BETWEEN BOXES FOR EASE OF IDENTIFICATION
      M=1
      AX1 = -14286
      XP(M) = AX1
      YPH(M),YPL(M) = .001
      YAV(M) = 001
      DO 90 J=1,NBM
```

```
      DO 80 K=1,6
      YPH(M+1),YPH(M+2) = YH(J,K)
      YPL(M+1),YPL(M+2) = YL(J,K)
      YAV(M+1),YAV(M+2) = YSUM(J,K)/NDAT
      XP(M+1) = XP(M)
      XP(M+2) = XP(M) + AX1
   80 M = M + 2
      YPH(M+1),YPH(M+2),YPL(M+1),YPL(M+2) = .001
      YAV(M+1),YAV(M+2) = .001
      XP(M+1) = XP(M)
      XP(M+2) = XP(M) + AX1
   90 M = M + 2
      NPLOT = NBM+14
C *****  DRAW AXES FOR TORQUE LIMITS GRAPH (LOG. Y-AXIS AND LINEAR X-AXIS)
      CALL UTP8A(0.,10.,1.,1.E4,9.0,5.5,XXXX,0,YYYY.0)
C *****  PLOT MAX. AND MIN. DYNAMIC TORQUE LIMITS, IN HISTOGRAM FORM , ON THE
C        SAME AXES (APPROPRIATE POINTS ARE JOINED BY STRAIGHT LINES)
      CALL UTP8B(XP,YPH,NPLOT,3)
      CALL UTP8B(XP,YPL,NPLOT,3)
C *****  DRAW AXES FOR THE AVERAGE LOADING GRAPH (LOG. Y-AXIS AND LINEAR X-AXIS)
      CALL UTP8A(0.,10.,1.,1.E4,9.0,5.5,XXXX,0,YYYY.0)
C *****  PLOT AVERAGE DYNAMIC LOADING HISTOGRAM (POINTS JOINED BY STRAIGHT
C        LINES)
      CALL UTP8B(XP,YAV,NPLOT,3)
C *****  CLOSE GRAPH PLOTTER FACILITY
      CALL UTPCL
C *****  IF PROGRAM RUNS SUCCESSFULLY WRITE ''PLOTTING COMPLETED''
  100 FORMAT(1H ,20H PLOTTING COMPLETED )
      WRITE(2,100)
      STOP
      END
```

APPENDIX M

PRINCIPLES OF MAGNETIC RECORDING

Magnetic recording depends on two electromagnetic phenomena, as follows:-

1. magnetic material can be magnetized by the application of a magnetizing force produced by the passage of an electric current through a coil,

and 2. when a magnetic field undergoes a change in space or time, an electric field is created and, as a consequence, an electric current will flow in a circuit linked with the magnetic field.

A magnetic head is essentially a wire-wound, ferro-magnetic ring which has a small air gap arranged to run across the path of a recording medium. Signals to be recorded are converted into electrical voltages, if not already in this form, and applied to the windings thereby inducing a magnetic circuit in the ring. The effect of the air gap is to produce concentrated magnetic field in the air at this point which in turn produces local microscopic orientations in the passing recording material. In the "replay" mode[/] these stored magnetic signals link the head air gap and thereby induce a magnetic circuit in the ring which in turn creates an electrical flow in the

[/] the same head may be used for both recording and replay but often in practice a separate head is used for each function.

coil. This may, for example, be arranged for audio sensing, as in the case of music and speech recording*, or visual display as in video recording for television.

Further details on basic magnetic recording (59) and industrial applications (60) may be obtained from the literature.

* film sound tracks also come into this category.

Appendix N

Computer Program Histoexptal

```
      MASTER HISTOEXPTAL
C ***
C     HISTOEXPTAL PLOTS HISTOGRAMS OF IMPACT COUNTS.OBTAINED EXPERIMENTALLY,
C     THROUGHOUT A MULTI-BOX SYSTEM. IMPACT COUNTS ARE  WEIGHTED TO RELATE TO
C     THE CHARACTERISTICS OF ONE OF THE (THREE) INSTRUMENTED GEAR PAIRS. FOR
C     EACH FULL SET OF READINGS TWO TYPES OF GRAPH ARE PRODUCED :-
C
C        1.  A HISTOGRAM OF IMPACTS PER SECOND
C
C        2.  A HISTOGRAM OF IMPACTS PER 100 REVOLUTIONS (OF DRAWROLL)
C
C     THE FOLLOWING DATA IS INPUT ON PUNCHED CARDS .
C
C      MOD  -  MACHINE MODEL  = 200 , FOR MDT. 2
C                             = 300 , FOR MDT. 3
C                             = 600 , FOR MDT. 6
C                             = 111 , FOR MULTI-BOX RIG
C
C      NBM  -  NO. OF DRAWBOXES IN MACHINE
C
C      REVDR  -  DRAWROLL SPEED AT WHICH IMPACT RECORDS TAKEN
C
C      YLEVEL  -  IMPACT COUNTING LEVEL FOR U/V RECORDER TRACES (ONLY PULSES
C                 ATTAINING THIS LEVEL ARE COUNTED)
C
C      YNO  -  NO. OF IMPACTS COUNTED ABOVE LEVEL 'YLEVEL' IN TRACE LENGTH XLEN
C
C      XLEN  -  LENGTH OF SPECIMEN RECORD (IN)
C
C      RECSP  -  PAPER SPEED EMPLOYED DURING RECORDING OF IMPACT TRACES (MM/SEC)
C
C *** RESERVE SPACE FOR ARRAYS
      DIMENSION YNO(10,6),YSECI(10,6),YREVI(10,6),YSECO(10,6),YREVO(10,6
     1),YPT(300),YPR(300),XP(300),XLEN(20),RECSP(10)
C *** SPECIFY INPUT AND OUTPUT FORMATS
   10 FORMAT(I2,2X,I3)
   20 FORMAT(1H ,//////,I2,21H BOX TEST RIG  MOD = ,I3,/)
   30 FORMAT(2F0.0)
   35 FORMAT(1H ,40H ******** NEW DRAWROLL SPEED ********** ,//)
   40 FORMAT(1H ,//,18H DRAWROLL SPEED = ,F7.1,3X,39H IMPACT COUNTING LE
     1VEL ON U/V RECORD = ,F6.1,4HCM.,/)
   46 FORMAT(1H ,/,25H INPUT DATA (TO PROGRAM) ,/)
   47 FORMAT(1H ,8H PAIR 1 ,1X,8H PAIR 2 ,1X,8H PAIR 4 ,9H LEN(INS),12H
     1REC(MM/SEC),2X,8H PAIR 3 ,1X,8H PAIR 5 ,1X,8H PAIR 6 ,9H LEN(INS),
     212H REC(MM/SEC),/)
   48 FORMAT(1H ,F6.1,3X,F6.1,3X,F6.1,3X,F8.2,3X,F6.1,5X,F6.1,3X,F6.1,3X
     1,F6.1,3X,F8.2,3X,F6.1)
   50 FORMAT(5F0.0)
   60 FORMAT(1H ,20H PLOTTING COMPLETED )
   70 FORMAT(1H ,//,40H INPUT RECORDS (EQUIV.IMPACT DENSITIES) )
   71 FORMAT(1H ,/,9H BOX NO. ,2X,9H D/R PAIR,3X,17H IMPACTS PER SEC.,3X
     1,26H IMPACTS PER 100 REV(D/R) )
   72 FORMAT(1H ,3X,I2,11X,I1,11X,F8.2,12X,F8.2)
   73 FORMAT(1H ,/,32H INPUT AVERAGE IMPACT DENSITIES )
   74 FORMAT(1H ,8H PAIR A ,F8.2,3X,8H PAIR B ,F8.2,3X,8H PAIR C ,F8.2,2
     1X,17H IMPACTS PER SEC.,/)
   75 FORMAT(1H ,8H PAIR A ,F8.2,3X,8H PAIR B ,F8.2,3X,8H PAIR C ,F8.2,2
     1X,25H IMPACTS PER 100 REV(D/R))
   80 FORMAT(1H ,////,41H OUTPUT RECORDS (EQUIV.IMPACT DENSITIES) )
C *** OPEN GRAPH PLOTTER
      CALL UTPOP
```

```
      READ(1,10) NBM,MOD
      WRITE(2,20) NBM,MOD
  100 CONTINUE
      READ(1,30) REVDR,YLEVEL
      IF(REVDR .EQ. 1111.)GO TO 190
      WRITE(2,35)
      WRITE(2,40)REVDR,YLEVEL
      J = 1
      N = 1
      WRITE(2,46)
      WRITE(2,47)
  110 CONTINUE
      READ(1,50)YNO(J,1),YNO(J,2),YNO(J,4),XLEN(N),RECSP(N)
      READ(1,50)YNO(J,3),YNO(J,5),YNO(J,6),XLEN(N+1),RECSP(N+1)
C ****** WRITE INPUT DATA (INPUT TO PROGRAM) ******
      WRITE(2,48)YNO(J,1),YNO(J,2),YNO(J,4),XLEN(N),RECSP(N),YNO(J,3),YN
     1O(J,5),YNO(J,6),XLEN(N+1),RECSP(N+1)
      J = J + 1
      N = N + 2
      IF(J .GT. NBM)GO TO 120
      GO TO 110
  120 CONTINUE
      J = 1
      N = 1
      YAT = 0.0
      YBT = 0.0
      YCT = 0.0
C ****** CALCULATE INPUT IMPACT DENSITIES PER SECOND ******
  130 A1 = RECSP(N)/(XLEN(N)*25.4)
      YSECI(J,1) = YNO(J,1)*A1
      YSECI(J,2) = YNO(J,2)*A1
      YSECI(J,4) = YNO(J,4)*A1
      N = N + 1
      A2 = RECSP(N)/(XLEN(N)*25.4)
      YSECI(J,3) = YNO(J,3)*A2
      YSECI(J,5) = YNO(J,5)*A2
      YSECI(J,6) = YNO(J,6)*A2
      J = J + 1
      N = N + 1
      IF(J .GT. NBM)GO TO 140
      GO TO 130
  140 CONTINUE
      WRITE(2,70)
      WRITE(2,71)
      DO 160 J=1,NBM
      DO 150 K=1,6
C ****** CALCULATE INPUT IMPACT DENSITIES PER 100 REVS ******
      YREVI(J,K) = YSECI(J,K)*6000./REVDR
      WRITE(2,72)J,K,YSECI(J,K),YBEVI(J,K)
  150 CONTINUE
C ****** CALCULATE AVERAGE IMPACTS PER SEC. FOR GEAR PAIRS A,B,C. ******
      YAT = YAT + YSECI(J,1) + YSECI(J,3)
      YBT = YBT + YSECI(J,2) + YSECI(J,5)
      YCT = YCT + YSECI(J,4) + YSECI(J,6)
  160 CONTINUE
      YATA = YAT/(NBM*2.)
      YBTA = YBT/(NBM*2.)
      YCTA = YCT/(NBM*2.)
C ****** CALCULATE AVERAGE IMPACTS PER 100 REVS FOR GEAR PAIRS A,B,C. **
      YARA = YATA*6000./REVDR
      YBRA = YBTA*6000./REVDR
      YCRA = YCTA*6000./REVDR
```

```
      WRITE(2,73)
C ***** WRITE AVERAGE IMPACT VALUES PER SEC. AND PER 100 REVS ******
      WRITE(2,74)YATA,YBTA,YCTA
      WRITE(2,75)YARA,YBRA,YCRA
      WRITE(2,80)
      WRITE(2,71)
      M = 1
      AX1 = .14286
      XP(M) = AX1
      YPT(M) = .001
      YPR(M) = .001
      DO 180 J=1,NBM
C ***** RELATE IMPACTS FROM GEARS B,C TO CHARACTERISTICS OF PAIR A ****
      YSECO(J,1) = YSECI(J,1)
      YSECO(J,3) = YSECI(J,3)
      YSECO(J,2) = YSECI(J,2)*YATA/YBTA
      YSECO(J,5) = YSECI(J,5)*YATA/YBTA
      YSECO(J,4) = YSECI(J,4)*YATA/YCTA
      YSECO(J,6) = YSECI(J,6)*YATA/YCTA
      YREVO(J,1) = YREVI(J,1)
      YREVO(J,3) = YREVI(J,3)
      YREVO(J,2) = YREVI(J,2)*YARA/YBRA
      YREVO(J,5) = YREVI(J,5)*YARA/YBRA
      YREVO(J,4) = YREVI(J,4)*YARA/YCRA
      YREVO(J,6) = YREVI(J,6)*YARA/YCRA
      DO 170 K=1,6
C ***** WRITE ADJUSTED IMPACT DENSITIES FOR ALL GEAR PAIR POSITIONS ***
      WRITE(2,72)J,K,YSECO(J,K),YREVO(J,K)
C ***** IDENTIFY POINTS FOR HISTOGRAM PLOTS ******
      YPT(M+1),YPT(M+2) = YSECO(J,K)
      YPR(M+1),YPR(M+2) = YREVO(J,K)
      XP(M+1) = XP(M)
      XP(M+2) = XP(M) + AX1
  170 M = M + 2
      YPT(M+1),YPT(M+2) = .001
      YPR(M+1),YPR(M+2) = .001
      XP(M+1) = XP(M)
      XP(M+2) = XP(M) + AX1
  180 M = M + 2
      NPLOT = NBM+14
C ***** DRAW AXES FOR GRAPH OF IMPACTS PER SECOND *****
      CALL UTP8A(0.,10.,1.,1.E3,9.0,5.5,XXXX,0,YYYY,0)
C ***** DRAW GRAPH OF IMPACTS PER SECOND FOR ALL D/R POSITIONS ******
      CALL UTP8B(XP,YPT,NPLOT,3)
C ***** DRAW AXES FOR GRAPH OF IMPACTS PER 100 REVS. *****
      CALL UTP8A(0.,10.,1.,1.E3,9.0,5.5,XXXX,0,YYYY,0)
C ***** DRAW GRAPH OF IMPACTS PER 100 REVS. FOR ALL D/R POSITIONS ****
      CALL UTP8B(XP,YPR,NPLOT,3)
      CONTINUE
C ***** GO TO STATEMENT 100 ,REPEAT PROCEDURE FOR NEW SPEED+DATA ******
      GO TO 100
  190 CONTINUE
C *** CLOSE GRAPH PLOTTER
      CALL UTPCL
      WRITE(2,60)
      STOP
      END
```